THE STRUCTURAL USE OF FIBROUS - CEMENT IN PARTIALLY PRESTRESSED COMPOSITE CONCRETE CONSTRUCTION

A THESIS SUBMITTED FOR THE DEGREE OF DOCTOR OF PHILOSOPHY

BY

JOHN SAUNDERS BSc

DEPARTMENT OF CIVIL ENGINEERING

THE UNIVERSITY OF SALFORD

DECEMBER 1976

SYNOPSIS

A new concept in composite construction has been developed at the University of Salford*, involving the use of fibre-reinforced cement channels, combined structurally with partially prestressed composite concrete T-beams.

The British Standards Institution Code of Practice, CP110:1972, "The Structural Use of Concrete", permits the use of Class 2 and Class 3 (partially prestressed) concrete members in structural design. The limiting design criteria for such members are usually the limit states of deflection and cracking and therefore, an improvement in their flexural behaviour would be beneficial. This improvement may be brought about by the addition of fibre-reinforcement, in the form of two or three dimensionally randomly distributed fibres. The Code of Practice, CP110:1972, does not, however, give any guidance on the use of fibres in structural members and it is also apparent that the methods outlined in the code for the calculation of the limit states are limited and can be improved.

The flexural behaviour of twenty-two partially prestressed composite concrete T-beams was investigated. Each beam consisted of a precast partially prestressed X-joist web, combined with a cast-insitu lightweight aggregate concrete flange. Alkali-resistant glass fibre-reinforced cement channels were placed at the soffits of six beams and steel fibre-reinforced concrete was used in the webs of two beams. The T-beams were subjected to short-term, long-term and fatigue loading and their structural performance was considered in terms of strength, cracking and deformation.

Theoretical relationships are derived between the applied moment and the depths of the neutral axes of stress and bending, enabling a design equation relating applied moment to the steel stress to be developed. Subsequently, design equations for the calculation of the limit states of deflection and cracking are developed, which are directly applicable to both conventional and fibre-reinforced structural members.

The use of a fibre-reinforced cement channel as an integral structural part of a concrete member results in many important advantages when compared with conventional concrete members and the test results show that they considerably improve the structural performance of the partially prestressed composite concrete T-beams.

---

* University of Salford: Improvements in or relating to constructional elements of concrete. Patent application number 49179/72, British Patents Office, London, October 1972.

A C K N O W L E D G E M E N T S

The author is grateful to Professor T. Constantine, BSc, PhD, CEng, FICE, FIMunE, Professor of Civil Engineering and Chairman of the Department of Civil Engineering at the University of Salford, for providing the research facilities.

The author wishes to express his extreme gratitude to his supervisor, Professor E. R. Bryan, MSc(Eng), PhD, DSc, CEng, FICE, CIStructE, Professor of Structural Engineering at the University of Salford, for his advice and guidance during the research work.

The author is particularly indebted to Mr D. C. O'Leary, MSc, CEng, MICE, for his general supervision and constant advice and encouragement throughout the work.

The author would also like to thank Dr N. J. Dave, MEng, PhD, CEng, AMIE, MASCE, MICE, for his help and advice during the development work.

Special and sincere thanks are due to the late Mr F. W. Simon, for his technical advice and assistance in the laboratories.

The author also wishes to thank Mr K Naylor and all the staff of the Civil Engineering Laboratories at the University of Salford, for their technical assistance during the practical work.

The author would like to acknowledge the financial support provided by the University of Salford and the Science Research Council. The author further acknowledges Mills Scaffold Company Limited, for the supply of fibrous-cement channels, National Standard Company Limited, for the supply of steel fibres, Richard Johnson and Nephew Limited, for the supply of prestressing steel, the Cement Marketing Corporation for the supply of cement and Fram Precast Concrete Limited for the initial supply of X9 flooring joists.

Finally, the author would like to sincerely thank his wife for conscientiously typing the text and for her constant support, encouragement and, above all, patience throughout the work.

CONTENTS

Page

Page

NOTATION

GENERAL

A_c	- Area of transformed concrete section
A_i	- Area of cast-insitu flange
A_p	- Area of precast web
A_{sc}	- Area of compression steel
A_{st}	- Area of tensioned steel
A_{su}	- Area of untensioned steel
A_{sf}	- Equivalent area of reinforcing steel
b	- Width of cast-insitu flange
b_w	- Width of precast web
d	- Effective depth of tension steel
d_{sc}	- Effective depth of compression steel
d_{st}	- Effective depth of tensioned steel
d_{su}	- Effective depth of untensioned steel
d_c	- Depth to centroid of compression force, C
d_{ch}	- Depth to centroid of tensile force in fibrous cement channel, T_{ch}
d_{ct}	- Depth to centroid of tensile force in concrete, T_c
d_{dc}	- Depth to centroid of compressive force at decompression
E_c	- Modulus of elasticity of concrete
E_i	- Modulus of elasticity of cast-insitu flange
E_p	- Modulus of elasticity of precast web
E_s	- Modulus of elasticity of steel
E_{sc}	- Modulus of elasticity of compression steel
E_{st}	- Modulus of elasticity of tensioned steel
E_{su}	- Modulus of elasticity of untensioned steel
e	- Eccentricity of differential shrinkage force
h	- overall depth of beam

h_f - Depth of cast-insitu flange

I_o - Second moment of area of transformed concrete section

l - Clear span

M - E_{sc}/E_i

n - A_{sc}/A_i

q - $\delta_{fst}/\delta_{fsu}$

r - A_{st}/A_{su}

t_f - Age of cast insitu flange

t_w - Age of web when flange cast

V_f - Volume fraction of fibres

x - Depth to neutral axis

x_b - Depth to neutral axis of bending

x_{cr} - Depth to neutral axis of stress at instant of first cracking

x_s - Depth to neutral axis of stress

$1/r_b$ - Curvature of beam at mid point

$1/r_x$ - Curvature of beam at point x

γ_m - Partial safety factor for materials

ϕ - Creep coefficient

DEFORMATIONS

a - Mid point deflection

a_{max} - Maximum deflection on previous cycle

a_{res} - Residual deflection

w - Crack width

W_{max} - Maximum crack width

FORCES

C - Total compressive force

C_c - Compressive force in concrete

C_s - Compressive force in steel

F - Differential shrinkage force

T - Total tensile force

T_c - Tensile force in concrete

T_{ch} - Tensile force in fibrous-cement channel

T_s - Tensile force in steel

T_{st} - Tensile force in tensioned steel

T_{su} - Tensile force in untensioned steel

MOMENTS

M - Applied moment

δM - Increase in applied moment

M_{cr} - Applied moment causing cracking

M_d - Dead load moment

M_{dc} - Applied moment causing decompression

M_l - Live load moment

M_{max} - Maximum moment on previous cycle

M_o - Total external moment at decompression

M_{ult} - Ultimate moment

M_1 - Maximum moment on precracking cycle

STRAINS

e_c - Strain in concrete

e_{ch} - Applied strain in fibrous-cement channel

e_i - Free shrinkage strain of cast-insitu flange

$\bar{e}_i$ - Apparent shrinkage of cast-insitu flange

e_p - Shrinkage plus creep strain in precast web

e_{sc} - Applied strain in compression steel

e_{st} - Applied strain in tensioned steel

e_{su} - Applied strain in untensioned steel

e_1 - Concrete strain measured at bottom of section

e_4 - Concrete strain measured at top of section

p - Differential shrinkage strain

STRESSES

f_c - Compressive stress in concrete

f_{cr} - Tensile stress in concrete at instant of cracking

f_{mr} - Modulus of rupture of precast concrete

f_s - Tensile stress in steel

f_{st} - Tensile stress in tensioned steel

f_{su} - Tensile stress in untensioned steel

δ_{fst} - Increase in stress in tensioned steel

δ_{fsu} - Increase in stress in untensioned steel

f_{stdc} - Tensile stress in tensioned steel at decompression

f_{sudc} - Tensile stress in untensioned steel at decompression

f_{sto} - Tensile stress in tensioned steel at start of test

f_{suo} - Tensile stress in untensioned steel at start of test

f_t - Hypothetical tensile stress in concrete

f_{tmax} - Maximum hypothetical tensile stress in concrete

f_1 - Differential shrinkage stresses at bottom of beam

f_{mt} - Stress in tensioned steel

f_{mu} - Stress in untensioned steel

f_{yt} - Characteristic strength of tensioned steel

f_{yu} - Characteristic strength of untensioned steel

T - Nominal tensile stress in concrete

U_t - Characteristic cube strength at transfer

U_w - Characteristic cube strength

ABBREVIATIONS

A.C.I.	- American Concrete Institute
A.S.C.E.	- American Society of Civil Engineers
B.S.	- British Standard
C. and C.A.	- Cement and Concrete Association
C.E.B.	- Committee European du Beton
C.P.	- Code of Practice
F.I.P.	- Federation Internationale de la Precontrainte
I.A.B.S.E.	- International Association of Bridge and Structural Engineers
I.C.E.	- Institution of Civil Engineers
P.C.A.	- Portland Cement Association
P.C.I.	- Prestressed Concrete Institute

L I S T O F T A B L E S

L I S T   O F   F I G U R E S

L I S T O F A P P E N D I C E S

L I S T   O F   P L A T E S

PUBLICATIONS

1. O'Leary, D.C., Dave, N.J. and Saunders, J. "Steel Fibres in Partially Prestressed Composite Concrete Beams". Proceedings of the International Symposium on Fiber Reinforced Concrete, A.C.I. Fall Convention, Ottawa, SP44-27, 1973, pp477-495.

2. Dave, N.J., O'Leary, D.C. and Saunders, J. "The Structural Use of Fibrous Cement in Composite Concrete Construction". Proceedings of the International Symposium on Fiber Reinforced Concrete, A.C.I. Fall Convention, Ottawa, SP44-29, 1973, pp511-532.

3. Dave, N.J., O'Leary, D.C., Garwood, T.G. and Saunders, J. "Partially Prestressed Concrete". Proceedings of the Research Seminar on Behaviour and Design of Structural Concrete, Fulmer, 1973, C. and C.A., pp154-160.

4. Dave, N.J., O'Leary, D.C., Al-Sanjary, K.A.A. and Saunders, J. "Asbestos and Glass Fibre Reinforced Cement Structural Concrete Composites". Proceedings of the Conference on Fibre Reinforced Concrete, Delft, September 1973, University of Delft, pp115-138.

5. Saunders, J. "Structural Use of Fibrous Cement in Partially Prestressed Composite Construction". Proceedings of Rilem Symposium on Fibre Reinforced Cement and Concrete, London, September 1975, Supplementary Volume - to be published.

CHAPTER ONE

INTRODUCTION

1.1. COMPOSITE CONCRETE CONSTRUCTION

A popular form of floor construction consists of composite concrete T-beams (figure 1.1.). Each beam consists of a precast prestressed concrete web, combined with a cast-insitu reinforced concrete flange. Composite concrete construction is an attempt to economise over prestressed concrete design and yet retain its advantages. It leads to simplification of construction on site and to savings in formwork and labour costs (101). There is also a substantial saving in the cost of steel in a composite prestressed concrete beam (102). The use of high strength concrete is restricted to the precast web, allowing lower strength concrete to be used in the cast-insitu flange, resulting in a further saving in material costs.

If properly designed and constructed, a composite beam will exhibit all the characteristics such as resilience, strength, stiffness and elasticity of conventional prestressed concrete beams (103, 104).

A composite concrete T-beam may be constructed with or without the use of temporary supports to the precast web. When temporary supports are not used, the precast web carries its own weight, the dead weight of the cast-insitu flange and the form work, whilst the composite section carries the live load only. When temporary supports are used, the composite section carries the dead load of the cast-insitu flange as well as the live load. The use of temporary supports can lead to a more economic design (105) and were therefore used during the construction of the T-beams tested in this investigation.

1.2. PARTIAL PRESTRESSING

The British Standards Institution Code of Practice CP110:1972, "The Structural Use of Concrete" (106), henceforth referred to as the Unified Code, classifies structural concrete members according to the degree of flexural tensile stress or to the degree of cracking that is permitted under design loads. The four classes of structural concrete members are:-

Class 1: Fully prestressed concrete members in which no tensile stresses are allowed in the concrete under design loads.

Class 2: Prestressed concrete members in which limited tensile stresses, but no cracks, are allowed under design loads.

Class 3: Prestressed concrete members in which cracking is allowed under design loads, although the surface width of the cracks must not exceed 0.1mm for members exposed to aggressive environments and 0.2mm for all other members.

Class 4: Reinforced concrete members. The permissible crack width is 0.1mm for members in aggressive environments and 0.3mm for all other members.

Class 2 and Class 3 structural concrete members are termed as limited or partially prestressed concrete members. Terms such as "Reinforced Prestressed Concrete Members" (107) and "Prestressed Reinforced Concrete Members" (108) have also been used. This investigation is concerned with the structural behaviour of Class 2 and Class 3 members, otherwise referred to as partially prestressed members.

Further economies in composite concrete construction can be achieved by the use of partial prestressing. The advantages of partial prestressing over full prestressing are: (109)

1. Lower cost of prestressing.

2. Reduced camber minimising difficulties in construction involving precast members.

3. Possible economy resulting from the use of smaller and therefore lighter sections.

4. Increased deflection and crack widths at loads in excess of the design load, giving adequate warning before approaching failure.

5. Increased flexibility and resilience to shock.

The quantity and type of steel required in a partially prestressed concrete member will depend upon the amount of steel required to produce the required tensile force for the ultimate load condition and the amount required to produce the effective prestress, ie, it will depend upon the magnitude of the design load and the degree of tensile stress or crack width that is permitted under that design load.

There are basically three different ways of applying the prestressing force and simultaneously providing the total quantity of steel required to ensure an adequate factor of safety against collapse, namely:-

1. The total quantity of steel required is prestressing steel, all of which is tensioned to a stress less than the maximum permitted. The degree of prestress will depend upon the effective prestress required.

2. The total quantity of steel required is prestressing steel, part of which is fully tensioned to the maximum stress permitted. The remainder of the steel is left untensioned.

3. A proportion of the required quantity of steel is prestressing steel, which is tensioned to the maximum stress permitted. The remainder of the steel is untensioned and consists of mild steel or high strength reinforcing bars.

The first method is seldom used, as it is the least practical and economic. The second method is preferable for pretensioned members where reinforcement cages are not used. In practice, a nominal stress will be applied to both the "tensioned" and "untensioned" wires in order to position them accurately in the mould. The stress in the "tensioned" wires will then be increased to the maximum stress permitted. The nominal stress is designed such that after losses, the stress in the "untensioned" wires will have reduced to zero, ie prior to the application of the external load the stress in the "untensioned" wires will be zero. The third method is preferable for post-tensioned members where reinforcement cages are required (110). The second method of partial prestressing was used during this investigation.

1.3 LIGHTWEIGHT AGGREGATE CONCRETE

The lightweight aggregates that are suitable for use in concrete are known commercially as Lytag, Leca and Aglite. The strength, durability and sound insulation properties of the concrete produced from these lightweight aggregates are, at their best, equal to those of conventional concrete, whilst other properties make them desirable and economic building materials. They are: (111)

1. Lower unit weight.
2. Increased fire resistance.
3. Increased thermal insulation.
4. Ease of construction.

In addition, in areas where natural aggregates are not available or are in short supply, lightweight aggregates provide an economic solution for the manufacture of concrete.

This investigation is concerned with the structural use of Lytag (sintered pulverised fuel ash) lightweight aggregate (Plate 1.1.) in composite concrete construction.

1.4. FIBRE REINFORCEMENT

Recent improvements in cement quality and concrete mix design methods, coupled with more efficient compacting techniques have made it possible to achieve concrete compressive strengths in excess of 100N/sq.mm. at 28 days. The tensile strengths have not, however, increased in the same proportion. Consequently, in the design of reinforced and partially prestressed concrete members, the limiting design criteria are increasingly the limit states of deflection and cracking. An improvement in the tensile characteristics of the concrete would, therefore, be beneficial to its flexural behaviour. This improvement may be brought about by the addition of fibre-reinforcement to the cement or concrete matrix.

The choice of fibres available for use as fibre-reinforcement in a cementitious matrix, covers a wide range of natural and man-made fibres. The particular fibre employed will be dependent upon the physical properties required of the composite. The primary reasons for incorporating fibres in a cement or concrete matrix are to increase the extensibility and tensile strength of the matrix before cracking, to hold the matrix together after cracking and to change the failure mechanism from a brittle to a ductile form. The fibres used for this purpose are the high modulus types of which asbestos, glass and steel are examples. The low modulus fibres, polypropylene and nylon, have been used to increase the energy absorption capacity of structural concrete subject to shock or impact loading. However, they are not suitable as a means of improving the tensile properties.

The distribution of fibres in a matrix (figure 1.2.), may be one (1D), two (2D) or three-dimensional (3D). The fibres may be continuous or discontinuous and in a 2D or 3D system, the distribution can be random or orderly. The efficiency of fibre-reinforcement in a preferred direction is 100% for a 1D distribution and may be as low as 33% and 16% for 2D and 3D random distributions, respectively (112).

This investigation is concerned with the use of two-dimensionally randomly distributed alkali-resistant glass fibres (Plate 1.2.) and three-dimensionally randomly distributed steel fibres (Plate 1.3.).

1.5. FIBROUS-CEMENT COMPOSITE CONSTRUCTION

1.5.1. Introduction

The idea for a new form of construction emerged from the desire for an economic form of floor construction that would make full use of the new provisions for partially prestressed concrete in the Unified Code (106). It has already been shown in the previous sections, that composite T-beams, incorporating a precast partially prestressed web, combined with a lightweight aggregate concrete flange, can form the basis for an extremely economic flooring system and that the addition of fibre-reinforcement to the precast web can provide for an adequate degree of serviceability. It only remains to optimise the fibre-reinforcement.

Previous work by Hannant (113), has indicated that deflections in structural members can be significantly reduced by the addition of three-dimensionally randomly distributed steel fibres. He also suggested that the use of steel fibres could be of benefit, in association with normal or high tensile reinforcement, as a means of limiting crack widths in concrete beams. However, the use of a 3D distribution is far less efficient than a 2D distribution (112). In addition, the primary reason for adding fibre-reinforcement to structural concrete is to improve its tensile strength, the inclusion in the compression zone of a member is, therefore, neither beneficial nor economic. Thus, the optimum solution is to have a 2D distribution, with the fibres concentrated in the zone of maximum tensile stress. This may be achieved by using a fibrous-cement sheet, covering all or part of the surface of the tensile zone of the structural member. Thus, the concept of a fibrous-cement/structural concrete composite was evolved. In addition, by using fibres in a cementitious matrix, a material is produced which will form a natural and complete bond with the structural concrete member cast on to it.

The fibrous-cement composite, if correctly designed and produced, will have an improved deflection and cracking performance. This improvement will be a function of the properties and thickness of the fibrous-cement sheet. The fibrous-cement sheet will act as a form of surface reinforcement to the concrete member, preventing crack initiation and propagation and thereby limiting deflections. By profiling the sheet into a channel form (Plate 1.4.), it is possible to increase the area reinforced by the fibrous-cement sheet and, therefore, surface cracks can be completely avoided up to and beyond the normally accepted design load for the member. The structural member, which may be reinforced or partially prestressed in the conventional manner, is cast in conjunction with the preformed fibrous-cement sheet, which is either placed in the mould or forms part of the mould itself. Thus a composite is formed in which the fibrous-cement sheet forms an integral part of the beam, with a natural bond being developed at the interface.

Fibrous-cement sheets, incorporating either glass or asbestos fibres, are available at present. This investigation is concerned with the use of alkali-resistant glass fibre-reinforced cement sheets, profiled into a channel section.

1.5.2. Advantages

The use of a fibrous-cement sheet as an integral part of a structural concrete member can result in the following advantages:-

1. Increased resistance to tensile stresses, resulting in delayed cracking.

2. Reduction in crack widths and the rate of crack propagation.

3. Reduction in deflections due to "increased" flexural rigidity.

4. Increased permissible working loads and stresses or a reduction in the overall dimensions of the member.

5. Reduction in cover to the reinforcement.

6. Increased use of:-
   (a) lightweight aggregate concrete
   (b) high tensile steel

7. Increase in the use of partially pre-stressed members.

8. Improved surface finish.

9. Increased fire resistance.

10. Reduction in formwork costs.

11. Reduction in shear reinforcement.

12. Potential use as anti-crack reinforcement in liquid-retaining structures.

1.6. LIMITATIONS OF THE UNIFIED CODE

The Unified Code (106), does not give any guidance on the use of fibre-reinforcement in structural members and it is also apparent that the methods outlined in the Code for the design of partially prestressed concrete members are limited in the following respects:-

1. No allowance is made for the loss of prestress in the concrete, due to the effect of creep and shrinkage on the untensioned steel.

2. No method is presented for calculating the effects of differential shrinkage in composite construction.

3. No indication is given as to the effects of using lightweight aggregate concrete in composite construction.

4. The method presented for the prediction of deflections applies to the initial loading cycle only. No allowance is made for the residual deflections and the loss of tensile strength in the concrete on subsequent loading cycles.

5. No method for predicting crack widths is given.

6. No indication is given of the effects of sustained and fatigue loading.

1.7. OBJECTIVES OF THE INVESTIGATION

In view of the limitations of the Unified Code (106), outlined in section 1.6., the investigation presented in this thesis was planned with the following objectives:-

1. To investigate the general behaviour of partially prestressed composite T-beams, with particular reference to the losses of prestress, the effects of differential shrinkage and the use of lightweight aggregate concrete.

2. To investigate the use of fibre-reinforcement in partially prestressed composite concrete construction.

3. To investigate the limit state behaviour of partially prestressed composite concrete T-beams with particular reference to the development of methods for calculating the principal limit states applicable to both conventional and fibre-reinforced concrete beams.

4. To investigate the effects of sustained and fatigue loading on partially prestressed composite concrete T-beams.

1.8. OUTLINE OF THESIS

Chapter 2 reviews the current "state of the art" in composite construction, partial prestressing and fibre-reinforcement. A brief history of their development is outlined, together with the extent of existing research work.

The principles of limit state design are described in Chapter 3, together with an outline of the methods available at present for the calculation of the principal limit states.

In Chapter 4, theoretical relationships are derived between the applied moment and the depths of the neutral axes of stress and bending, enabling a design equation, relating the stress in the steel to the applied moment to be developed. Subsequently, design equations for the calculation of the principal limit states are developed, which are directly applicable to both conventional and fibre-reinforced structural members.

Chapter 5 covers the design, manufacture and testing of the beams.

Chapter 6 deals with the analysis of the stresses in the concrete and steel. The methods used for calculating the losses of prestress by both theoretical and experimental considerations are explained. Theoretical and experimental methods of analysis for the differential shrinkage stresses are developed and the procedures for determining the stresses in the steel and the depths of the neutral axes of stress and bending from the experimental data are described.

The limit state behaviour of the test beams is discussed in Chapter 7, with particular reference to the use of fibre-reinforcement. The advantages of fibrous-cement composite construction, compared with conventional concrete construction are evaluated and the experimentally obtained results are correlated with the values predicted by the proposed design equations developed in Chapter 4.

Finally, in Chapter 8, conclusions are drawn from the tests, and suggestions for future research are indicated.

References, tables, figures, plates and appendices follow after Chapter 8.

CHAPTER TWO

STATE OF THE ART

2.1. COMPOSITE CONSTRUCTION

The first attempt at using lightweight aggregate concrete in prestressed composite construction was reported by Hasnat (201) in 1965. Prior to this, investigations had been directed to beams of conventional sand and gravel aggregate concrete (202 - 208). Hasnat tested twelve prestressed composite T-beams of lightweight aggregate concrete. The variables considered were the length of the shear span, the strength of the concrete in the insitu flange and the time interval between the casting of the web and the flange. Hasnat agreed with the earlier findings of Ahmed (208), that the natural bond between the precast and insitu concrete components was erratic and should not be relied upon for the development of the ultimate flexural strength. They also found that the bond strength was directly proportional to the strength of the insitu concrete. By contrast, Evans and Parker (205), found that the relative qualities of the concrete did not affect the bond strength, whilst Dean and Ozell (206) found that the bond was equivalent to that between concrete and steel. In addition, both Hasnat (201) and Ahmed (208), found that the differential shrinkage significantly reduced the cracking stress of composite concrete T-beams. Hasnat added that the actual reduction was significantly less in composite beams of lightweight aggregate concrete than in conventional composite concrete beams, despite the higher shrinkage of lightweight aggregate concrete, because of its lower modulus of elasticity.

In 1966, Chung (209), investigated the problems arising from the use of lightweight aggregate concrete in prestressed composite concrete construction. The design of the precast component was considered with particular reference being made to the losses of prestress and the permissible compressive stresses at transfer. In addition, the merits of various types of horizontal shear connector and the influence of sectional properties on differential shrinkage were investigated. Chung found that the losses of prestress in prestressed lightweight concrete amounted to 40% and over if the initial concrete stresses exceeded 0.3 of the cube strength at transfer. He also extended the Mörsch method of analysis for differential shrinkage to take into account the effect of the reinforcement in the cast-insitu concrete. The resulting expressions for stresses and deflections due to differential shrinkage were found to give good correlation with his experimental results.

In contrast to conventional composite construction, Taylor (210) introduced the idea of a new form of composite construction in 1971. He called this new form of construction "Composite Reinforced Concrete". A composite reinforced concrete beam consists of a deep haunched composite beam in which the steel stringer is replaced by a steel channel section. The longitudinal shear at the interface of the concrete and channel is resisted by headed stud shear connectors, welded at intervals along the channel. From tests carried out on nine of these beams, Taylor and

Burdon (211), found that this type of construction gave an economical and viable structural form and was ideally suited for the use of very high strength reinforcing steels. They also found that the combined use of high tensile reinforcement and a mild steel channel meant that reinforcement stresses over 825N/sq.mm. could be used at ultimate load, whilst the serviceability limit states would not be exceeded at the working load.

2.2. PARTIAL PRESTRESSING

The origin of partial prestressing dates back to 1939, when the Austrian engineer Emperger (212) suggested that the properties of reinforced concrete could be improved by using prestressed wires in addition to the conventional reinforcing bars. In the following year, Abeles (213) suggested that the respective merits of prestressed and reinforced concrete could be combined, if a proportion of the high tensile steel required for full prestressing was tensioned, whilst the remaining tensile steel was left untensioned. Subsequent tests by Abeles (214 - 217) substantiated this, but, however, it was 1962 before partial prestressing received full recognitition.

At the Fourth Congress of the F.I.P. (218) held in Rome and Naples in 1962, Theme 3 was concerned with the "Economics of prestressed concrete in relation to regulations, partial prestressing, lightweight concrete, etc". Various applications of partial prestressing were also reported. In the following year, Orr (219) investigated the behaviour of six rectangular beams, containing the same quantity and type of steel. He showed that, by varying the proportions of steel tensioned, considerable economy could be achieved in the use of steel. The economics of partial prestressing has also been considered by Dave (220), who carried out tests on 40 beams, most of which were pretensioned by high tensile wires. The behaviour of the beams was considered under short-term, long-term and fatigue loading, and the variables considered were the total amount of steel and the proportions of the total steel tensioned. He evolved a method for calculating the steel stresses from the experimental results and produced a theoretical method of analysis for a cracked beam. Formulae for calculating the theoretical steel stresses and crack widths were also derived, which gave good correlation with his experimental results.

In 1965, Abeles (221) tested two series of high strength concrete beams, reinforced with non-tensioned prestressing steel. These tests simulated the nominal concrete stress conditions at the tensile face of equivalent prestressed concrete beams after decompression: Subsequently, Abeles developed relationships between the nominal tensile stress in the concrete and the percentage of reinforcement for given crack widths. A crack width formula was also developed by Chandrasekhar (222), following an investigation into the effects of variations in the properties and distribution of the reinforcement on the limit state of local damage. More recently, Beeby, Keyder and Taylor (223) tested sixteen partially prestressed beams containing combinations of un-tensioned deformed bars and pretensioned wires and showed how the crack formulae for reinforced concrete could be modified and applied to partially prestressed concrete.

The proceedings of a two day Colloquium (224), held in Brussels were published in 1966. After reviewing the historical development of partial prestressing, the various classes of prestressed member were discussed and the problems involved in the calculation of the various limit states were explained. Examples of partial prestressed structures were given and the position of partial prestressing in the codes of practice of different countries was also outlined.

In the same year, Session 1 of the Fifth Congress of the F.I.P. (225), held in Paris, was devoted to "Surveys of research in prestressed concrete". Research in Europe and the U.S.S.R., the performance of partially prestressed beams and the effect of creep and shrinkage on untensioned reinforcement was referred to.

Following tests on reinforced and prestressed beams having the same ultimate moment of resistance, Hutton and Loov (226), found that significant errors could be introduced if the effect of creep and shrinkage on the untensioned steel was ignored. Abeles and Kung (227) also made a comprehensive study of the losses of prestress. They tested four types of beam, each containing different amounts of untensioned steel and they found that the greater the area of untensioned steel, the greater was the loss of prestress and hence the lower the cracking load.

Also in 1966, Veeriah (228) investigated the relative merits of mild and high tensile steel as untensioned reinforcement. Mild steel was found to give a more rigid section at service loads, whilst high tensile steel was found to give a greater resilience at loads near ultimate.

In the following year, Branson and Shaikh (229) examined the effects of untensioned steel with particular reference to camber, loss of prestress, crack formation and deflection. They tested twelve pretensioned beams containing three types of untensioned steel and developed formulae for predicting the camber, deflection and ultimate strength of the beams.

The Eighth Congress of the I.A.B.S.E. (230) was held in New York in 1968. Theme 4 was devoted to "partially prestressed members" and the papers presented were concerned with the characteristics of fully and partially prestressed concrete members with reference to tensile stresses, crack formulae and practical and economic considerations.

Also in 1968, Abeles, Brown and Woods (231), carried out static and sustained load tests on fully and partially prestressed beams of lightweight and normal weight aggregate concrete. Prestressing strands were used for both the tensioned and untensioned reinforcement. They found that although the lightweight concrete beams had a lower flexural rigidity and cracking strength, there was no substantial difference in the maximum crack widths obtained.

Fatigue tests (230, 232), were also carried out on similar beams and it was found that, even after a large number of load repetitions, the maximum crack width showed no substantial increase in size.

At the Sixth Congress of the F.I.P. (233), held in Prague in 1970, papers concerned with the fatigue and breakdown of class 3 structures and the relative merits of class 1, 2 and 3 structures on a materials cost basis were presented. The effect of fatigue loading on partially prestressed concrete beams has also been reported by Magura and Hognestad (234). Tests were carried out on four prestressed beams, two of which were pretensioned. They found that if the maximum tensile stress was limited to 2.1N/sq.mm., no cracks were observed and no deterioration in serviceability occurred. However, if the maximum tensile stress was increased to 4.8N/sq.mm., cracks were observed and the post-tensioned beams showed deterioration in both serviceability and flexural capacity. Brenneisen (235) conducted four series of tests to study the deformation, crack and failure characteristics of fully and partially prestressed concrete beams under static and fatigue loading. The eccentricity of the cables, the degree of prestress and the type of untensioned steel were varied and he found that the laws of superposition applied to beams reinforced with tensioned and untensioned steel. He also found that, although the untensioned steel was effective in controlling the distribution of cracks, it also prevented the cracks from closing completely on removal of the load.

The behaviour of Class 3 beams has been investigated by Stevens (236), Veerasubramian (237) and Garwood (238). In 1969, Stevens (236) tested thirteen beams, varying from reinforced to fully prestressed, under static and fatigue loading. The behaviour of partially prestressed beams was found to be similar to that of fully prestressed beams up to cracking and similar to that of reinforced concrete after cracking. Veerasubramian (237) in 1971, studied the effect ofthe shape of the cross-section of a beam on its flexural behaviour. He modified the crack width formula proposed by Chandrasekhar (222) and also extended his method of analysis for steel stresses in Class 3 beams so that they could be used for non-rectangular beams. In 1972, Garwood (238), presented the results of tests on seventeen I-beams, post-tensioned with Macalloy bars. The beams were designed to have the same ultimate moment, although different degrees of prestress and different types of untensioned steel were used. The beams were tested under static, long term and fatigue loading. In addition, five rectangular beams, post-tensioned with high tensile wires were tested. The relative merits of the various types of steel as untensioned reinforcement and the factors contributing to the loss of prestress were examined. He found that the use of mild steel as untensioned reinforcement, although giving the most rigid section, induced the greatest loss of prestress. A theoretical relationship between the steel stress and the applied moment for a cracked beam was developed which lead subsequently, to the development of a design equation relating the crack width to the stress in the untensioned steel. A method was also evolved, whereby deflections could be predicted, taking into account the effect of the untensioned steel. Finally, he outlined a general method of design for Class 3 beams containing untensioned steel.

2.3 FIBRE REINFORCEMENT

2.3.1. Mechanism of Fibre Reinforcement

Probably the first mechanism suggested to explain the behaviour of cement based fibre composites was the "crack arrest mechanism" of Romauldi and Batson (239, 240) as applied to continuous closely spaced wire reinforcement. This mechanism, based on linear fracture mechanics, predicts that the first crack strength is inversely proportional to the fibre spacing for a given fibre volume content.

In 1964, Romauldi and Mandel (241) attempted to apply the crack arrest mechanism to concrete reinforced by short discrete lengths of steel wire. They found that the crack arrest mechanism was still maintained, although only 41% of the total amount of reinforcement could be assumed to be effective in resisting the applied tensile stresses.

The crack arrest mechanism assumes that the stress concentrations in the vicinity of the tip of a crack are resisted by the stiffer fibres and that bond forces are set up that act to reduce the magnitude of these stresses. However, the assumption that there is perfect bond between the fibres and the matrix is not necessarily valid for discrete fibres. Kar and Pal (242) considered the bond efficiency of short fibres and extended the fibre spacing concept to fibres of different lengths and diameters and to different mix proportions. Other fibre spacing equations have been suggested by Snyder and Lankard (243) and McKee (244).

The spacing concept does not apply beyond the proportional limit and does not fully explain the mechanism of fibre-reinforcement, indeed there is much controversy as to whether the spacing of fibres is in fact an important variable. Williamson (245), Nanda (246) and Durham (247) have all reported increases in the flexural strength of steel fibre reinforced concrete with a reduction in fibre spacing, whilst Untraur and Works (248) found little increase in the cracking strength and Shah and Rangan (249) showed that wire spacing alone had little influence on the tensile strength.

The linear fracture mechanics approach has also been applied, by Chan and Patterson (250), to predict the cracking strength of glass reinforced cement. Shah and Rangan (249) have suggested another approach based on the "law of mixtures" to predict the strength and elastic properties of the composite, but the theory has not yet been satisfactorily correlated with experimental data.

For continuous fibre composites, a theory of multiple fracture (251, 252) has been applied to brittle matrices and the theoretical results show good correlation with published data for steel, glass and asbestos in a cementitious matrix. A combined mechanism of fibre pull out and fibre fracture has also been suggested for two dimensionally randomly distributed fibres in gypsum plaster (253). Most cement based composites, however, fail by fibre pull out and the currently available theories do not adequately correlate theory with experimental data.

2.3.2. Physical and Mechanical Properties

Fibres have been used to reinforce brittle materials since ancient times (254). The fibres compensate for the low tensile strength and brittle nature of the matrix and in fibre-reinforced cement and concrete, the fibres also improve the mechanical and physical properties of the composite.

One of the first applications of randomly orientated reinforcement for concrete was made by Porter (255) in 1910. He added cut nails and spikes to concrete and obtained some dramatic increases in its physical properties. In 1914, Ficklin (256) patented the idea of adding pieces of metal to concrete mixes to improve its resistance to abrasion and spalling. More recently, Romualdi (257) carried out fatigue tests on randomly reinforced concrete beams and showed that they had properties far superior to those of plain concrete.

The properties of fibrous concrete are influenced by many interdependent parameters; the fibre aspect ratio being perhaps the most critical. It influences almost all aspects of fibre reinforcement, including fibre handling, dispersion, mixing, workability, bond and strength. Romualdi and Mandel (241) reported that both the fibre aspect ratio and the water cement ratio are critical factors in preventing balling up of the fibres during mixing. Nanda (246) and Durham (247) used randomly distributed short lengths of steel wire as reinforcement for concrete and found that there was increased difficulty in mixing the fibres into the concrete as the aspect ratio was increased. They also found that the workability was reduced such that it could not be compacted by conventional techniques. Satisfactory compaction was, however, obtained by using an electric vibrating hammer. Agbin (258) and Williamson (245) also reported difficulty in mixing steel wires into the concrete.

In addition to the fibre aspect ratio, the surface treatment of fibres by such methods as chemical cleaning, galvanising and the provision of mechanical indentations can have considerable effect on bond. Improvements in flexural strength of up to 300% have been obtained (259). The bond strength of fibre reinforced composites has also been investigated by deVekey and Majumdar (260, 261) and the results show that the bond between glass fibres and cement is of the same order as that between steel fibres and cement.

Another important parameter is fibre orientation (figure 1.2.). With random fibre orientation, the orientation or efficiency factor can be as low as 16% (262, 263), although the method of compaction and the relative size of the mould to the length of fibre can influence this factor considerably. Edgington and Hannant (264) have reported that steel fibre-reinforced concrete, which is normally randomly reinforced in three dimensions, can exhibit anisotropic behaviour due to fibre orientation during compaction. They have shown that table vibration can cause the fibres to rotate and orientate themselves parallel to the table surface, resulting in a

50% to 100% increase in flexural strength. Abolitz (265) has stated that wires close to the surface of the concrete will be preferentially aligned in that plane and will, therefore, have a higher efficiency factor compared to those in the middle of the concrete. He added that scale effects are, therefore, important and the cross-sectional dimensions of specimens should be compared to the lengths of the fibres in order to see if wires at the surface or in the centre predominate. He also added that the low effectiveness of randomly distributed fibres is economically unfavourable with regard to their use in reinforced concrete beams and one way slabs, but however, they are more competitive in two way slabs.

Probably the most critical property of fibrous-cement composites is their durability. Plastic fibres such as nylon and polypropylene are known to be stable in the strongly alkaline (ph 12 to 13) environment of the hydrating cement matrix. Fibres such as cotton and rayon are, however, subject to alkaline attack and are, therefore, unsuitable as reinforcement in cementitious composites. Low alkali borosilicate glass fibres such as E-glass are also subject to corrosion (266), however, they can be utilised quite successfully in high alumina cement (267, 268) and gypsum plaster (269, 270). Corrosion resistant coatings have been used for glass fibres (271) and more recently, with relatively more success, alkali resistant glass fibres have been produced (272). Steel fibres are relatively free from corrosion, showing adequate resistance to corrosion by salt water

(273) and freeze-thaw environments (274). The available data on the long term durability of glass and steel fibres is still very limited (275, 276), however, the results do show that the use of high alumina cement and pulverised fuel ash can improve the durability of glass fibres and that alkali-resistant glass fibres have adequate strength retention properties for one to two years.

CHAPTER THREE

LIMIT STATE DESIGN

3.1. GENERAL

The British Code of Practice for Reinforced Concrete (301), permits the use of elastic and load factor analysis in the design of structural concrete members. In elastic analysis, permissible stresses are limited to a fraction of the specified strength of the materials, whilst in load factor analysis sections are designed to have ultimate strengths some multiple of the working loads, this multiple being the factor of safety or load factor.

The British Code of Practice for Prestressed Concrete (302) stipulates that the design of prestressed concrete must satisfy two requirements, one related to permissible stresses under working load conditions, and the second to the provision of a minimum load factor. The American Standard A.C.I. 318-63 (303) includes similar requirements.

These design procedures, however, when considered in view of the purpose of design and the phenomena related to it, present certain shortcomings (304): No direct account is taken of the variability of the material strengths or of the magnitudes of the loading in the finished structure. In addition, the changes in permissible stresses and load factors that have occurred in successive codes, have been introduced as a result of the satisfactory performance of the materials and the general improvement in construction techniques without giving specific indications of the resulting reduction in structural safety. Also, although deflections and crack widths effectively govern the serviceability of a structure, no detailed design procedures are given.

These problems were considered by the Russians as early as 1930 and since then various attempts have been made to overcome them (305 - 307). As a result of the early work in Russia, a new design philosophy was evolved, which was called the Limit State Approach. This approach, adopted by the Russian Code in 1954 (308), forms the basis of the recent C.E.B. - F.I.P. recommendations (309) and is evident in the revised American Standard A.C.I. 318-71 (310).

The philosophy of limit state design is based on the application of the methods of statistics to the variations that occur in the strengths of construction materials and the expected loads. The British Unified Code, CP110:1972 (311) is based on this limit state philosophy.

3.2. BASIC PRINCIPLES

A limit state is defined as that condition which renders a structure or a member unfit for the purpose for which it is required. It follows that the purpose of design may be defined as the achievement of an acceptable probability that the structure will not reach any relevant limit state during it working life.

The principal limit states to be considered are the ultimate and serviceability limit states. The ultimate limit state is concerned with the maximum load carrying capacity of the structure, whilst the serviceability limit states are concerned with the durability and deformation behaviour of the structure. The importance of a particular limit state will depend upon the function of the structure and upon the environmental conditions.

Characteristic loads and strengths are used as reference values in limit state design and are, ideally, defined in statistical terms to take into account any variations in the magnitude of the loading, which are likely to occur during the life of the building, and anticipated variations in the actual strength of the materials. At the present time, the statistical evidence required to establish characteristic loads is not available and the values used in design are taken from CP3 - Chapter 5 (312).

3.3. DESIGN PRINCIPLES

The design of a structure for a specific function is best considered in two parts:-

1. Analysis of the structure: involving an assessment of the loads acting on the structure, the provision of a suitable structural system to support those loads and a calculation of the forces and moments produced in individual members.

2. Analysis of sections: involving the provision of members which satisfy the requirements of all applicable limit states under the action of the forces and moments calculated in (1).

For each specific limit state, two partial safety factors, one on loads and one on materials, are introduced to define the design loads and material strengths relevant to that limit state. The partial safety factors are introduced to take account of any unforseen effects of the load due to inadequacies of the methods of analysis or dimensional inaccuracy in construction and possible differences between the strength of the materials in the actual structure and the strength derived from the test specimens.

This ensures a more uniform degree of safety throughout the structure and enables improvements in quality control, construction and design practices and increased knowledge of loading conditions to be incorporated more readily into the design process, to give a greater overall economy with a defined degree of safety.

3.4. CALCULATION OF THE LIMIT STATES

3.4.1. General

All relevant limit states should be considered in design so as to ensure an adequate degree of safety and serviceability. The usual approach will be to design on the basis of the most critical limit state and then check that the remaining limit states will not be reached.

Analysis of the structure for all the limit states may be based on elastic methods using the gross, transformed or concrete section, modified if required by redistribution of peak moments. Analysis of sections for the ultimate limit state must be based on inelastic methods using short term stress-strain curves appropriate to the design strength of the materials. Analysis of sections for the serviceability limit states may be based on elastic methods making suitable allowances for creep and shrinkage strains where appropriate.

The suitability of partially prestressed concrete members for limit state design has been established by many investigators, notably Abeles (313, 314). They will generally be designed to comply with the requirements of the serviceability limit states of cracking and deflection and will subsequently be checked for compliance with the ultimate limit state. It may also be necessary to consider the limit states of fatigue, vibration and fire resistance.

3.4.2. Ultimate Limit State

Many theories have been established for the calculation of the ultimate flexural strength of structural members, notably by Whitney (315), Evans (316) and Baker (317). The basic procedure is to obtain an equilibrium between the internal forces acting across the section considered by using the principles of strain compatability. A value for the ultimate concrete strain in the extreme compression fibre and a suitable stress distribution for the concrete are assumed. In addition, it is assumed that concrete resists no tension and that the strain distribution across the section is linear. Then, by a trial and error process, the neutral axis depth is adjusted until the algebraic sum of the internal forces is zero. The ultimate flexural strength is then determined by taking moments of the internal forces about a convenient point.

The assumption that concrete does not resist tension is of course untrue. However the force is so small that its effect on the ultimate moment can be neglected and provided that the beam is in the under-reinforced category, then the linear strain distribution assumption is also justified (318).

The Unified Code (311) provides design tables for calculating the ultimate flexural strength of rectangular beams. For non-rectangular beams, the use of the above analysis is recommended. The ultimate concrete compressive strain is assumed to be 0.0035 and a rectangular-parabolic stress distribution is assumed for the concrete. The design strengths for the materials used are the characteristic strengths divided by the partial safety factors for the ultimate limit state of 1.5 and 1.15 for concrete and steel, respectively. The design assumptions for the ultimate limit state are illustrated diagramatically in Figure 3.1.

3.4.3. Serviceability Limit State

3.4.3.1. Limit State of Deflection

The general approach used is to assess the curvature of sections under the appropriate moments and then to calculate the deflection from the curvatures by normal numerical integration procedures. The deflected shape of a member is related to the curvature by the equation:-

$$\frac{1}{r_x} = \frac{d^2y}{dx^2}$$

where $\frac{1}{r_x}$ is the curvature of the beam at point x.

Alternatively, the following simplified approach may be used:-

$$a = kl^2 \frac{1}{r_b}$$

where: a is the deflection

l is the effective span

k is a constant depending on the shape of the bending moment diagram

$\frac{1}{r_b}$ is the curvature of the beam at mid-span.

Existing formulae for the calculation of deflections (319 - 323) are usually derived from consideration of a bilinear moment-curvature relationship. In the first stage, the concrete is uncracked and the section behaves elastically. In the second stage, the concrete in tension is cracked and factors are introduced to account for the tension stiffening effect of the uncracked concrete in the tension zone. The Unified Code (311), however, relates the curvature of sections to the stress in the steel reinforcement at that section on the basis of the following assumptions:-

1. Plane sections remain plane.

2. The reinforcement, whether in tension or compression, is assumed to be elastic. Its modulus of elasticity is taken to be 200 KN/sq.mm.

3. The concrete in compression is assumed to be elastic. Under long term loading, an

effective modulus may be taken, having a value of $1/(1+\phi)$ times the short term modulus where ϕ is the appropriate creep coefficient.

4. Stresses in the concrete in tension may be calculated on the assumption that the stress distribution is triangular, having a value of zero at the neutral axis and a maximum value at the centroid of the tension steel of 1 N/sq.mm. instantaneously, reducing to 0.55 N/sq.mm. in the long term.

These assumptions are illustrated diagramatically in Figure 3.2..

For both the uncracked and cracked case, the curvature can be obtained from the relationships:-

$$\frac{1}{r_b} = \frac{f_c}{xE_c} = \frac{f_s}{(d-x)E_s}$$

where: $\frac{1}{r_b}$ is the curvature of the beam at mid-span

f_c is the maximum compressive stress in the concrete

x is the depth of the neutral axis

E_c is the modulus of elasticity for concrete

f_s is the stress in the steel

d is the effective depth of the tension reinforcement

E_s is the modulus of elasticity for steel.

Alternatively, the following formula may be more convenient for the uncracked case:-

$$\frac{1}{r_b} = \frac{M}{E_c I_o}$$

where: M is the applied moment,

I_o is the second moment of area of the transformed section.

The advantage of this method over many of the semi-empirical formulae developed to predict deflections is that it permits creep effects to be dealt with in a more correct way by allowing for the difference in creep behaviour between concrete in compression and in tension.

3.4.3.2. Limit State of Cracking

Formulae for the calculation of crack widths relate crack widths either to the steel stress or to the hypothetical tensile stress at the soffit of the beam. The "classical" theory of the mechanism of crack formation assumes that cracks are produced by slip of the concrete relative to the reinforcement. It also assumes that the crack spacing is governed by the bond characteristics of the steel and that at the steel level the crack is approximately uniform in width between the steel and the side of the beam. This theory has been adopted by the C.E.B. (309), Hognestad (324) and Broms (325). In contrast, the "no-slip" theory assumes that crack widths taper from a maximum at the surface of the beam to zero at the steel, implying that the bond does not breakdown. The C. and C.A. (326), whose formula is based on this theory, found that crack widths are directly proportional to the distance from the point of measurement to the surface of the nearest reinforcing bar. In both these theories, the crack width is related to the steel stress.

Abeles (327), however, from the results of tests carried out at the University of Southampton (328), devised a concept relating crack widths to the hypothetical tensile stress in the concrete. The hypothetical tensile stress in the concrete is the tensile stress at the soffit of the beam, calculated on the basis of an uncracked section, even though the tensile stress has been exceeded. Bennet and Chandrasekhar (329), Veerasubramanian (330) and Beeby and Taylor (331), have all produced similar relationships.

The Unified Code (311), adopts this latter concept and relates allowable crack widths to hypothetical tensile stresses. The allowable crack width depends upon the environmental conditions and the related hypothetical tensile stress depends upon the method of stressing and the distribution of the prestressing steel.

It must be remembered that cracking is a semi-random phenomenon and absolute crack widths cannot be predicted. Hence, the hypothetical tensile stresses are designed to give a crack width with an acceptably small chance of being exceeded.

CHAPTER FOUR

PROPOSED METHODS FOR CALCULATING THE PRINCIPAL LIMIT STATES

4.1. INTRODUCTION

In the design of partially prestressed concrete members, the two principal limit states to be considered are the ultimate and serviceability limit states, the latter comprising the limit states of deflection and cracking. For each specific limit state, two partial safety factors are introduced to define the design loads and material strengths relevant to that limit state, e.g. the design strength of a material is its characteristic strength, divided by the respective partial safety factor. It follows that in the determination of the ultimate flexural strength of a beam, for example, the value so calculated is referred to as the "design ultimate strength". If, however, the actual material strengths are known and used in the calculation, then the material partial safety factors assume a value of unity and the ultimate flexural strength is referred to as the "calculated ultimate strength".

In the following sections, the proposed methods for calculating the principal limit states relate to the calculation of "design" strengths and loads etc., whilst the sample calculations given in the appendices relate to the calculation of "calculated" strengths and loads etc.

4.2. ULTIMATE LIMIT STATE

4.2.1. Conventional Concrete Beam

The strain compatability method, outlined in Section 3.4.2., for the calculation of the design ultimate strength of a member, can be applied to beams of any shape of cross-section and to partially prestressed concrete beams containing any type and combination of tensioned and untensioned reinforcement. The method is based on certain assumptions, illustrated diagramatically in Figure 3.1., which are as follows:-

1. The strain distribution across the depth of the section is linear.

2. The maximum compressive strain in the outermost concrete fibre is 0.0035.

3. The concrete has no tensile strength.

4. The concrete in compression has a rectangular-parabolic stress distribution, i.e. at strains less than $e_c = \sqrt{U_w}/5000$, the distribution is parabolic and at strains greater than e_c the distribution is uniform.

5. The maximum compressive stress in the concrete is $0.67U_w/\gamma_m$.

6. The stress-strain curve for the reinforcement is trilinear as given in the Unified Code (401).

A graphical method (Figure 4.1.) is proposed for the actual calculation, which involves a trial and error process as follows:-

1. The effective prestrain, after losses, in the tensioned steel is calculated (Section 6.2.) and plotted on the abscissa axis to give point X.

2. The stress-strain curve for the tensioned steel (see Unified Code) is plotted, using point X as the origin.

3. The stress-strain curve for the untensioned steel is plotted using point O as the origin, i.e. the effective prestrain in the untensioned steel is assumed to be zero (Section 1.2.).

4. The levels of the centroids of the tensioned and untensioned steels are plotted.

5. A value for the ratio x/d is assumed and is plotted on the ordinate axis to give point Y.

6. A linear strain profile is drawn through point Y having the limiting strain of 0.0035 as the origin.

7. The intersection points, Z_t and Z_u, of the strain profile and the levels of the

tensioned and untensioned steels respectively are projected on to the respective stress-strain curves and the values of f_{mt}/f_{yt} and f_{mu}/f_{yu} are read off.

8. The total force, T, in the reinforcement is then calculated from:-

$$T = T_{su} + T_{st} \qquad \text{(Figure 3.1.)}$$

where: $T_{su} = A_{su} \cdot f_{mu}$

$T_{st} = A_{st} \cdot f_{mt}$

9. The total compressive force, C, is calculated from:-

$$C = C_c + C_s \qquad \text{(Figure 3.1.)}$$

where: $C_c = \frac{2}{3} \cdot \frac{U_w}{\gamma_m} (b.x - A_{sc} - \frac{b}{3} \cdot x \cdot \frac{\sqrt{U_w}}{17.5})$

$$C_s = 0.0035 \cdot A_{sc} \cdot E_{sc} \cdot \frac{(x-d_{sc})}{x}$$

10. If C = T, then the assumed value of x/d is correct, if not, steps (5) to (9) are repeated until the desired degree of accuracy is obtained.

11. The design ultimate strength of the beam, M_{ult}, is calculated by summing the moments of all the internal forces about a convenient point.

12. If the design dead load moment for the beam is given by M_d, then the design working or live load moment for the beam, M_l, is given by:-

$$M_l = \frac{M_{ult} - 1.4M_d}{1.6}$$

where the constants 1.4 and 1.6 are the partial safety factors for the ultimate limit state applied to the dead and live loads, respectively.

4.2.2. Fibre-Reinforced Concrete Beam

The primary reason for incorporating fibre-reinforcement in the tension zone of a flexural concrete member is to improve its serviceability performance before and after cracking. Any improvement in its load carrying capacity is, therefore, of secondary importance and should not be relied upon in the calculation of factors of safety against collapse due to the variability of fibre bond.

In fibrous-cement composite construction (Section 1.5.), the fibre-reinforced cement channel has an ultimate strain capacity less than that of the steel reinforcement and will therefore fail prematurely. No improvement in the load carrying capacity of the concrete is, therefore, expected. The premature and ductile failure of the channel, however, adds a further advantage to this type of composite construction in that it gives adequate warning of approaching failure or overload without any sudden decrease in serviceability.

In fibre-reinforced concrete construction, where the fibres are distributed randomly throughout the concrete section, some continuity will be provided across the cracks by the fibres (Plate 4.1.), even at high loads, and therefore some increase in the load carrying capacity of the member can be expected.

The proposed method for allowing for this increase is to substitute an equivalent area of reinforcing steel for the fibres in the strain compatability calculation (Section 4.2.1.). It has already been stated (Section 1.4.) that the efficiency of a three-dimensional random distribution of fibres is 16% and therefore the equivalent area of reinforcing steel, A_{sf}, is given by:-

$$A_{sf} = 0.16 \cdot V_f \cdot A_p \quad \ldots\ldots \quad (4.1.)$$

where: A_p is the area of the fibre-reinforced concrete section

V_f is the volume fraction of fibres.

For a steel fibre-reinforced concrete beam, a volume fraction of fibres of between 1.4% and 1.6% is generally used. The equivalent area of reinforcing steel, calculated from the above equation, is then assumed to act at the centroid of the fibre-reinforced concrete section.

4.3. SERVICEABILITY LIMIT STATE

4.3.1. Limit State of Deflection

The general method, outlined in Section 3.4.3.1., for the calculation of deflections can be applied to partially prestressed concrete beams as well as beams containing fibre-reinforcement. The equations used in the calculation are as follows:-

$$a = kl^2 \frac{1}{r_b} \quad \dots\dots\dots\dots\dots\dots \quad (4.2.)$$

where: $$\frac{1}{r_b} = \frac{f_s}{(d-x_b).E_s} \quad \dots\dots\dots\dots \quad (4.3.)$$

The actual method proposed for calculating the mid-point deflection of a beam is in two parts, the first part is applicable to beams in the uncracked condition, i.e. acting under an applied load less than the cracking load on the initial or precracking cycle and less than the decompression load on the subsequent or post-cracking load cycles. The second part is applicable to beams in the cracked condition. In addition, the formulae are extended to allow for the residual deflection at the start of the second and subsequent loading cycles.

4.3.1.1. Uncracked Beam

The uncracked beam is treated as a homogeneous elastic section and therefore the concrete and steel stresses may be calculated on the basis of a transformed concrete section.

If the concrete at the level of the tensioned steel is considered, then the increase in stress in the concrete, f_c, due to an applied moment, M, will be given by:-

$$f_c = \frac{M(d_{st} - y_2)}{I_o}$$

where: d_{st} is the depth to the tensioned steel

y_2 is the depth to the centroid of the transformed concrete section

I_o is the second moment of area of the transformed concrete section.

The corresponding increase in strain in the concrete, e_c will be given by:-

$$e_c = \frac{M(d_{st} - y_2)}{E_c \cdot I_o}$$

The corresponding increase in stress in the tensioned steel, δf_{st}, will be given by:-

$$\delta f_{st} = \frac{M.E_{st}}{E_c} \cdot \frac{(d_{st} - y_2)}{I_o} \quad \text{.....(4.4)}$$

Now, if the stress in the tensioned steel, when the applied moment is zero, is given by f_{sto} and the stress under the applied moment, M, is given by f_{st}, then the increase in stress in the tensioned steel, δf_{st}, will be given by:-

$$\delta f_{st} = f_{st} - f_{sto} \quad \text{.............. (4.5.)}$$

From equations 4.4. and 4.5.

$$f_{st} = f_{sto} + \frac{M.E_{st}}{E_c} \cdot \frac{(d_{st}-y_2)}{I_o} \quad \text{.. (4.6.)}$$

Similarly, the stress in the untensioned steel, f_{su}, will be given by:-

$$f_{su} = f_{suo} + M. \frac{E_{su}}{E_c} . \frac{(d_{su}-y_2)}{I_o} \quad ..(4.7.)$$

Now, substituting δf_{st} from equation 4.4. into the general equation 4.3. gives:-

$$\frac{1}{r_b} = \frac{M}{E_c I_o} \quad ....(4.8.)$$

Let $$E_c.I_o = k_1 \sqrt{\frac{U_w}{\gamma_m}} . I_o \quad ....(4.9.)$$

Where k_1 is a constant, depending on the type of fibre-reinforcement, if any, values of which can be determined from the slope of the load-deflection curves for the beams.

From equations 4.8. and 4.9.

$$\frac{1}{r_b} = \frac{M}{k_1.I_o} \sqrt{\frac{\gamma_m}{U_w}} \quad ....(4.10.)$$

For this investigation (section 7.2.2.2.) the following values of k_1 were obtained:-

k_1 = 5.15 for composite T-beams with a normal weight aggregate concrete flange

k_1 = 3.61 for composite T-beams with a lightweight aggregate concrete flange

$k_1 = 3.65$ for steel fibre-reinforced composite T-beams with a lightweight aggregate concrete flange

$k_1 = 3.81$ for fibrous-cement composite T-beams with a lightweight aggregate concrete flange.

Similar values of $k_1 = 5.08$ and $k_1 = 5.51$ for normal weight aggregate concrete beams are given by Beeby (402) and the Unified Code (401), respectively.

4.3.1.2. Cracked Beam

The following analysis applies for a cracked beam within its normal working range of applied loads and can be used for calculating the average stresses in the tensioned and untensioned steel. The analysis is based on the following assumptions, illustrated diagramatically in Figure 3.2. :-

1. The reinforcement, whether in compression or tension, remains within its elastic limit.

2. The concrete in compression remains within its elastic limit.

3. The concrete in tension has a triangular stress distribution.

4. After decompression at the soffit, the additional strains in the tensioned and untensioned steel are directly proportional to the respective distances of the steels from the neutral axis of stress.

The starting point for the analysis of a cracked beam is the decompression load stage (figure 4.2.). The total external moment, M_o, acting across the section is given by:-

$$M_o = M_d + M_{dc}$$

where: M_d is the dead load moment

M_{dc} is the applied moment causing decompression.

By taking moments of the steel forces about the centroid of the total compressive force, C, the moment equilibrium equation can be written as:-

$$M_d + M_{dc} = A_{st} \cdot f_{stdc}(d_{st} - d_{dc}) + A_{su} \cdot f_{sudc}(d_{su} - d_{dc}) \quad \ldots\ldots (4.11.)$$

Figure 4.2. also shows the condition at a general load stage after cracking, when the applied moment, M, has been increased by an increment, δM.

i.e. $M = M_{dc} + \delta M$

The moment equilibrium equation, for this load stage, can be written as:-

$$M_d + M = A_{st}(f_{stdc} + \delta f_{st})(d_{st} - d_c) + A_{su}(f_{sudc} + \delta f_{su})$$

$$(d_{su} - d_c) + T_c(d_{ct} - d_c) + T_{ch}(d_{ch} - d_c) \quad \ldots\ldots (4.12.)$$

where: d_c is the depth of the centroid of the total compressive force, C.

d_{ct} is the depth of the centroid of the concrete tensile force, T_c.

d_{ch} is the depth of the centroid of the tensile force in the fibrous-cement channel, T_{ch}.

The tensile force in the concrete, T_c, is a function of the nominal tensile stress in the concrete, T, at the level of the centroid of the tensile reinforcement and is introduced to allow for the tension stiffening effect of the uncracked concrete in the tension zone. The magnitude of the nominal tensile stress, T, depends upon the type of fibre-reinforcement, if any, and for this investigation (Section 6.5.3.) values of T = 1 N/sq.mm. and T = 4 N/sq.mm. were obtained for conventional and fibrous-cement composite concrete beams, respectively. A value of T = 1 N/sq.mm. is also given by the Unified Code (401) for conventional concrete beams.

Now, subtracting equation 4.11. from equation 4.12. gives:-

$$\begin{aligned} M - M_{dc} = {} & (A_{st}.f_{stdc} + A_{su}.f_{sudc})(d_{dc} - d_c) \\ & + A_{st}.\delta f_{st}(d_{st} - d_c) + A_{su}.\delta f_{su}(d_{su} - d_c) \\ & + T_c(d_{ct} - d_c) + T_{ch}(d_{ch} - d_c) \end{aligned}$$

Let:

$$A_{st} = r.A_{su}$$

$$\delta f_{st} = q.\ \delta f_{su}$$

$$T_{dc} = A_{st}.f_{stdc} + A_{su}.f_{sudc}$$

$$\begin{aligned} \therefore\quad M - M_{dc} = {} & q.r.A_{su}.\delta f_{su}(d_{st} - d_c) + A_{su}.\delta f_{su}(d_{su} - d_c) \\ & + T_{dc}(d_{dc} - d_c) + T_c(d_{ct} - d_c) + T_{ch}(d_{ch} - d_c) \end{aligned}$$

$$\therefore\ \delta f_{su} = \frac{M-M_{dc}-T_{dc}(d_{dc}-d_c)-T_c(d_{ct}-d_c)-T_{ch}(d_{ch}-d_c)}{A_{su}(\ (q.r.d_{st}+d_{su})-(1+q.r.)d_c\ )}$$

..........(4.13.)

Now, if the stress in the untensioned steel at decompression is given by f_{sudc} and the stress under the applied moment, M, is given by f_{su}, then the increase in steel stress, δf_{su}, is given by:-

$$\delta f_{su} = f_{su} - f_{sudc} \quad \text{......................(4.14.)}$$

from equations 4.13. and 4.14.:-

$$f_{su} = f_{sudc} + \frac{M-M_{dc}-T_{dc}(d_{dc}-d_c)-T_c\ (d_{ct}-d_c)-T_{ch}(d_{ch}-d_c)}{A_{su}(\ (q.r.d_{st}+d_{su})-(1+q.r.)d_c\ )}$$

..........(4.15.)

from assumption (4):-

$$q = \frac{d_{st}-x_s}{d_{su}-x_s} \cdot \frac{E_{st}}{E_{su}}$$

$$\therefore\ \delta f_{st} = \frac{d_{st}-x_s}{d_{su}-x_s} \cdot \frac{E_{st}}{E_{su}} \cdot \delta f_{su} \quad \text{..............(4.16.)}$$

from equations 4.15. and 4.16. :-

$$f_{st} = f_{stdc} + \frac{d_{st}-x_s}{d_{su}-x_s} \cdot \frac{E_{st}}{E_{su}} \cdot (f_{su}-f_{sudc}) \text{...(4.17.)}$$

From equations 4.15. and 4.17., it can be seen that the average stress in the tensioned and untensioned steel, for any given applied moment, M, can be calculated provided that the vales of T_{dc} and the depth of the neutral axis of stress are known. The value of T_{dc} depends upon the sum of the steel stresses $(f_{stdc}+f_{sudc})$ at the decompression load stage and can be calculated by substituting M_{dc} for M in equations 4.6. and 4.7. In order to determine the depth of the neutral axis of stress, x_s, for a given applied moment, M, an empirical relationship between the two variables is required. In addition, from equation 4.3. it can be seen that the increase in curvature of a beam, for a given increase in steel stress and hence applied moment, can be calculated provided that the depth of the neutral axis of bending, x_b, is known. In order to determine the depth of the neutral axis of bending, x_b, for a given applied moment, M, a second empirical relationship is required. The derivation of the two empirical relationships follows in section 4.3.1.3.

4.3.1.3. Proposed Relationships between the Applied Moment and the Depths of the Neutral Axes of Stress and Bending

For any given applied moment, M, the depth of the neutral axis of bending, x_b, is defined as the depth to the level at which the change of strain incurred between the start of the test (i.e. zero applied moment) and the given applied moment is zero. The neutral axis of bending is given by point O in Figure 4.3., where the line ABC represents the strain profile across the beam at the start of the test and the line DOBE represents the strain profile imposed due to the applied moment.

Similarly, the depth of the neutral axis of stress, x_s, is defined as the depth to the level at which the compressive stress in the concrete is zero. The neutral axis of stress is given by point B in Figure 4.3..

The proposed empirical relationships, illustrated in Figure 4.4., have a practical application since they apply forboth the precracking and postcracking load cycles and also for beams containing fibre-reinforcement. The six points defining each curve are derived as follows:-

<u>Point A</u> - decompression load stage

$M = M_{dc}$

$x_s = h$ by definition

$x_b = x_8$

where: x_8 is the depth of the centroid of the uncracked transformed concrete section.

<u>Point B</u> - initial cracking load stage

$M = M_{cr}$

$x_s = x_4 = c_1 . x_{cr}$

$x_b = x_7 = c_2 . x_8$

where: x_{cr} is the depth of the neutral axis of stress at the instant of first cracking, calculated as follows:-

Figure 4.5. shows the concrete stress distribution in a composite beam at the instant of first cracking

by similar triangles:-

$$\frac{x_{cr}-h_f}{\dfrac{M_{cr}}{Z_2}-f_2} = \frac{h-x_{cr}}{f_t}$$

rearranging:-

$$x_{cr} = \frac{\left(\dfrac{M_{cr}}{Z_2} - f_2\right) h + h_f . f_t}{\dfrac{M_{cr}}{Z_2} - f_2 + f_t}$$

The constants c_1 and c_2 are introduced to allow for the actual movement of the neutral axis of bending between decompression and the instant of first cracking which occurs in practice (the elastic theory assumes the depth of the neutral axis of bending to be constant). For this investigation values of $c_1 = 0.66$ and $c_2 = 0.88$ were obtained, which are the average values for all the beams tested.

<u>Point C</u> - load stage corresponding to the maximum applied moment on the pre-cracking cycle

$M = M_1$.

Point D - load stage on post-cracking cycle corresponding to load at which cracking first occurred

$$M = M_{cr}$$

$$x_s = x_3 = c_3 \cdot x_4$$

$$x_b = x_6 = c_4 \cdot x_7$$

where: c_3 and c_4 are constants introduced to allow for the difference in depths of the neutral axes of stress and bending, respectively, between the pre-cracking and post-cracking loading cycles.

For this investigation values of $c_3 = 0.79$ and $c_4 = 0.81$ were obtained, which are the average values for all the beams tested. A similar value of $c_3 = 0.82$ was obtained by Garwood (403).

Point E - load stage at which the increase in the applied moment, δM, is equal to half that at the ultimate load stage,

i.e. $$\delta M = \frac{M_{ult} - M_d - M_{dc}}{2}$$

$$\therefore \quad M = \frac{M_{ult} - M_d + M_{dc}}{2}$$

$$x_s = x_b = x_2$$

where: x_2 is taken to be the depth of the uncracked concrete as calculated by the traditional transformed area method for cracked beams.

Point F - ultimate load stage

$$M = M_{ult} - M_d$$

$$x_s = x_b = x_1$$

where: x_1 is taken to be the depth of the uncracked concrete obtained when calculating the ultimate moment by the strain compatability method.

For a Class 2 beam, the most significant section of the proposed relationships between the applied moment and the depths of the neutral axes of stress and bending is the line AB. This line represents the normal working range for Class 2 beams.

If a general point (M, x) is taken on AB, then by similar triangles, the depth of the neutral axis of stress, x_s, under an applied moment, M, is given by:-

$$\frac{x_s - h}{M - M_{dc}} = \frac{x_4 - h}{M_{cr} - M_{dc}}$$

rearranging:-

$$x_s = \frac{h(M_{cr}-M) + x_4(M-M_{dc})}{M_{cr}-M_{dc}} \quad \text{..........(4.18a.)}$$

Similarly, the depth of the neutral axis of bending, x_b, under an applied moment, M, is given by:-

$$x_b = \frac{x_8(M_{cr}-M)+x_7(M-M_{dc})}{M_{cr}-M_{dc}} \quad \text{...............(4.18b.)}$$

For a Class 3 beam, the line DE represents the normal working range. If a general point (M,x) is taken on DE, then by similar triangles, the depth of the neutral axis of stress, x_s, under an applied moment, M, is given by:-

$$\frac{x_s-x_3}{M-M_{cr}} = \frac{x_2-x_3}{\frac{M_{ult}-M_d+M_{dc}}{2} - M_{cr}}$$

rearranging:-

$$x_s = \frac{x_3(M_{ult}-M_d+M_{dc}-2M)+2x_2(M-M_{cr})}{M_{ult}-M_d+M_{dc}-2M_{cr}} \quad \text{..(4.19a.)}$$

Similarly, the depth of the neutral axis of bending, x_b, under an applied moment, M, is given by:-

$$x_b = \frac{x_6(M_{ult}-M_d+M_{dc}-2M)+2x_2(M-M_{cr})}{M_{ult}-M_d+M_{dc}-2M_{cr}} \quad \text{..(4.19b.)}$$

The loads represented by the line EF would be outside the normal working range for Class 3 beams and the assumptions of linear stress distributions in the concrete and steel would no longer apply.

4.3.1.4. Residual Deflection

At the start of each loading cycle, there will be a residual deflection in the beam due to the effect of the previous loading history. The residual deflection will be directly proportional to the maximum deflection on the previous cycle and inversely proportional to the degree of prestress in the beam and the duration of the recovery period between the loading cycles.

Thus, the residual deflection, a_{res}, may be calculated from:-

$$a_{res} = \frac{a_{max}}{k_2 + k_3 \dfrac{M_{dc}}{M_{max}}} \qquad \text{................(4.20)}$$

where: a_{max} is the maximum deflection,

M_{max} is the maximum applied moment on the previous loading cycle and

k_2 and k_3 are constants, depending on the recovery period and the degree of prestress.

For a Class 1 beam (fully prestressed),

$$M_{dc} = M_{max}$$

$$\therefore \quad a_{res} = \frac{a_{max}}{k_2 + k_3}$$

For a Class 4 beam (reinforced),

$$M_{dc} = 0$$

$$\therefore \quad a_{res} = \frac{a_{max}}{k_2}$$

For Class 2 and Class 3 beams (partially prestressed),

$$M_{max} > M_{dc} > 0$$

$$\frac{a_{max}}{k_2} > a_{res} > \frac{a_{max}}{k_2+k_3}$$

For this investigation (Section 7.5.1.1.) values of $k_2 = 6$ and $k_3 = 16$ were obtained, which were the average values for all the beams tested. Similar values of $k_2 = 5$ and $k_3 = 10$ were obtained by Garwood (403).

4.3.1.5. Summary of Proposed Deflection Formulae

The mid point deflection of a beam, a, acting under an applied moment, M, is given by:-

$$a = a_{res} + k.l^2.\frac{1}{r_b}$$

where $$a_{res} = \frac{a_{max}}{k_2+k_3.\frac{M_{dc}}{M_{max}}}$$

For an uncracked beam:-

$$\frac{1}{r_b} = \frac{M}{k_1 I_o}\sqrt{\frac{\gamma m}{U_w}}$$

For a cracked beam:-

$$\frac{1}{r_b} = \frac{\delta f_{su}}{(d_{su}-x_b).E_{su}}$$

where:- $$\delta f_{su} = \frac{M-M_{dc}-T_{dc}(d_{dc}-d_c)-T_c(d_{ct}-d_c)-T_{ch}(d_{ch}-d_c)}{A_{su}((q.r.d_{st}+d_{su})-(1+q.r.)d_c)}$$

and x_s and x_b are determined from the respective empirical relationships between the applied moment and the depths of the neutral axes of stress and bending.

4.3.2. Limit State of Cracking

4.3.2.1. Introduction

It was stated in Section 3.4.3.2. that existing formulae for the calculation of crack widths relate the width of a crack either to the stress in the steel or to the hypothetical tensile stress in the concrete at the soffit of the beam. Figure 4.6. illustrates the simplified curvature distribution along the span of a cracked beam acting under a symmetrical four point loading system. It can be seen that, in the constant bending moment zone, the curvature is a maximum at a crack and that between the cracks the curvature reduces to a minimum due to the stiffening effect of the uncracked concrete in the tension zone. The curvature distribution in the constant bending zone, can be further simplified by taking a mean value for the curvature and by assuming the concrete in tension to have a nominal tensile strength. This nominal tensile strength is introduced to allow for the tension stiffening effect of the uncracked concrete and its magnitude will depend on the type of fibre-reinforcement, if any.

It was shown in Section 4.3.1. that the deflection of a beam is directly proportional to the average curvature and hence the average steel stress and that the deflection formulae will, therefore be directly applicable to both conventional and fibre-reinforced beams. However, the width of a crack in a beam is a localised phenomenon and is related to the maximum curvature and hence the maximum steel stress. In the calculation of the maximum steel stress, the concrete is assumed to have no tensile strength and therefore both the concrete in the tension zone and the fibre-reinforcement is ignored. Consequently, any general crack width formulae relating the width of the crack to the maximum steel stress would not be directly applicable to both conventional and fibre-reinforced beams. A method relating the crack width to the hypothetical tensile stress in the concrete at the soffit of the beam is, therefore, adopted.

4.3.2.2. Proposed Crack Width Formulae

The proposed relationship between the crack width and the hypothetical tensile stress is illustrated diagramatically in Figure 4.7.. Point A represents the load stage at which cracking first occurs and Point O represents the decompression load stage on the post-cracking loading cycle. Point B is a general load stage applicable to both the pre-cracking and post-cracking load cycles.

For the precracking loading cycle, the proposed relationship between the crack width, w, and the hypothetical tensile stress, f_t, is given by:-

$$w = k_4(f_t - k_5) \quad \text{for } k_5 \leqslant f_t \leqslant k_7 \quad \text{.......(4.21a.)}$$

$$w = 0.2 + k_6(f_t - k_7) \quad f_t > k_7 \quad \text{.......(4.21b.)}$$

where k_4 and k_6 are constants, depending on the type of fibre-reinforcement, if any, values for which can be determined by inspection of the load versus crack width curves for the beams tested.

k_5 and k_7 are the tensile strength of the concrete and the hypothetical tensile stress in the concrete corresponding to the maximum allowable crack width, respectively. Both constants are dependent on the type of fibre-reinforcement, if any.

The Unified Code (401) states that the maximum allowable crack width for a pretensioned beam, having a characteristic cube strength greater than 50 N/sq.mm. is 0.2mm. and the corresponding hypothetical tensile stress is 5.8 N/sq.mm. For members exposed to an aggressive environment, the limiting crack width is 0.1mm. and the corresponding hypothetical tensile stress is 4.8 N/sq.mm.

Thus, for a conventional concrete beam, equation 4.21. becomes:-

$$w = 0.1(f_t - 3.8) \quad \text{for } 3.8 \leqslant f_t \leqslant 5.8$$

$$w = 0.2 + k_6(f_t - 5.8) \quad f_t > 5.8$$

For this investigation, a value of $k_6 = 0.056$ was obtained for conventional concrete composite T-beams. It was also found that the above formulae applied to beams containing steel fibre reinforcement. However, for fibrous-cement composite T-beams, it was found that for the limiting crack widths of 0.1mm. and 0.2mm., the corresponding hypothetical tensile stresses were 9.8 N/sq.mm. and 12.8 N/sq.mm., respectively.

Thus, for a fibrous-cement composite T-beam, equation 4.21. becomes:-

$$w = 0.033(f_t-6.8) \qquad \text{for } 6.8 \leqslant f_t \leqslant 12.8$$

$$w = 0.2+k_6(f_t-12.8) \qquad f_t > 12.8$$

For this investigation, a value of $k_6 = 0.028$ was obtained for fibrous-cement composite T-beams.

For the post-cracking load cycle, the proposed relationship between the crack width, w, and the hypothetical tensile stress, f_t, becomes:-

$$w = w_{max} \cdot \frac{f_t}{f_{tmax}} \qquad \text{for } f_t \leqslant f_{tmax} \quad \ldots(4.22.)$$

for values of $f_t > f_{tmax}$, equation 4.21. applies as before.

where w_{max} is the maximum crack width, and

f_{tmax} is the maximum hypothetical tensile stress on the previous loading cycle.

CHAPTER FIVE

DESIGN, MANUFACTURE AND TESTING OF THE BEAMS

5.1. GENERAL

In Chapter 1, the basis for an economic flooring system was outlined, involving the use of partially prestressed composite concrete T-beams and from this developed the concept of fibrous-cement composite construction. To substantiate the efficacy of this concept and thereby fulfil the objectives of the investigation (Section 1.7.), two pilot series of rectangular beams and four series of composite T-beams were designed and tested (Table 5.1.).

The two pilot series of rectangular beams were designed to provide information on the structural behaviour of fibrous-cement composites before full-scale tests on the composite T-beams were carried out.

Each series of T-beams was designed to have approximately the same ultimate strength when subjected to either short term, fatigue or long term loading. Variations in the magnitude of the prestressing force, the type of insitu concrete and the type of fibre-reinforcement were included in each series.

5.2. DESIGN OF TEST BEAMS

5.2.1. Rectangular Beams

In order to obtain a comparative and rapid appraisal of the concept of fibrous-cement composite construction and yet, at the same time, repeat the tests on a large number of beams, it was decided to base the pilot study on the concrete prisms used in the British Standards, Modulus of Rupture Test (501). This enabled a large number of beams to be produced, in steel moulds, from the same batch of concrete.

The pilot study was divided into two series of beams as follows:-

Series P - This series contained 15 concrete beams, 100mm x 100mm x 500mm (Figure 5.1.). Five of the beams (Group PC) contained conventional concrete, whilst five beams (Group PW) contained, in addition, 1.6% by volume of duoform steel fibres, 0.38mm diameter by 25mm long (Plate 1.3.). The remaining five beams (Group PG) contained conventional concrete cast onto alkali-resistant glass fibre-reinforced cement sheets.

Series R - In order to investigate the post-cracking behaviour, the above series of beams was repeated using 15 beams (Groups RC, RW and RG) containing, in addition, two no. 6mm. diameter mild steel bars as nominal tensile reinforcement (Figure 5.2.).

5.2.2. Composite Concrete T-beams

The composite concrete T-beams tested during this investigation, were based on the composite concrete flooring system (Figure 1.1.) used by several precast concrete manufacturers, which consists of precast partially prestressed concrete webs, combined with a cast-insitu reinforced concrete flange.

In order to give the investigation a further practical application, the design of the T-beams was based on the dimensions of a standard X-9 flooring joist, combined with a structural slab, 50mm. deep. An overall length of 5.18m. and a clear span of 4.725m. were chosen as representative of this size of composite T-beam.

A total of 21 T-beams, divided into four series, were designed as follows:-

Series X - The five composite T-beams in this series (Figures 5.3. and 5.4.) were designed to provide information on the general behaviour of partially prestressed composite concrete T-beams with particular reference to the effects of differential shrinkage and the use of lightweight aggregate concrete.

To reduce the number of variables in this series, five standard X-9 flooring joists, cast on the same bed by the long-line method, were obtained from a precast concrete manufacturer. The strength of the precast concrete and the magnitude of the prestressing force was, therefore, constant for all five beams. All five beams received cast-insitu flanges. Two of the beams (Group XN) contained conventional concrete (nominal density = 2400kg/cu.m) in the insitu flange, whilst the remaining three beams (Group XL) contained lightweight aggregate concrete (nominal density = 1600kg/cu.m) in the insitu flange. In addition, the flanges of two of the beams (Beams XN3 and XL3) were reinforced with mild steel bars (nominal yield stress - 275N/sq.mm.) and two beams (Beams XN9 and XL9) were reinforced with Kam 90 steel bars (nominal yield stress = 885N/sq.mm.). The flange of the remaining beam (Beam XL6) was reinforced with Kam 60 steel bars (nominal yield stress = 590N/sq.mm.).

The flanges of the beams were reinforced with three no. 12.7mm. diameter bars, fabricated into a 200mm. square mesh. The webs were pretensioned with eight no. 7mm. diameter helically crimped prestressing wires and were designed such that the composite concrete T-beams satisfied the design criteria for Class 3 beams in the Unified Code (502).

Series S - The eight beams in this series (Figures 5.5. and 5.6.) were designed to provide information on the limit state behaviour of partially prestressed composite T-beams, with particular reference to the development of methods for calculating the principal limit states, applicable to both conventional and fibre-reinforced concrete beams.

Each beam contained seven no. 7mm. diameter helically crimped prestressing wires and the flange consisted of lightweight aggregate concrete reinforced with 10mm. diameter mild steel bars, fabricated into a 200mm. square mesh. Four of the beams (Group S) contained conventional concrete in the web and were used as control beams, whilst two beams (Group SW) contained, in addition, 1.6% by volume of duoform steel fibres, 0.38mm. diameter by 25mm. long. The remaining two beams (Group SG) contained conventional concrete cast onto alkali-resistant glass fibre-reinforced cement channels (Plate 1.4.).

The T-beams were designed such that if all seven wires were fully tensioned to 70% of their characteristic strength, a prestress of approximately 23.4N/sq.mm. would be produced at the soffit of the beam. Taking the stress due to the self-weight of the beam to be approximately 1.5N/sq.mm. and assuming a nominal loss of prestress of 46%, the residual prestress at the soffit of the beam would be 11.8N/sq.mm. If a design load was now chosen such that the tensile stress induced at the soffit of the beam was 14.0N/sq.mm., then the resultant tensile stress at the soffit beam would be 2.2N/sq.mm. This is the allowable tensile stress for prestressed concrete in CP115:1969(503).

Now, if only six of the wires were fully tensioned and one left untensioned, a prestress of approximately 21.5N/sq.mm. would be produced at the soffit of the beam. Again, allowing for a self-weight stress of 1.5N/sq.mm. and a loss of prestress of 46%, the residual prestress would be 10.8N/sq.mm. By applying the same design load as before, the resultant tensile stress at the soffit of the beam would be 3.2N/sq.mm. This is the allowable tensile stress for Class 2 beams in the Unified Code (502) for the 50N/sq.mm. grade of concrete.

If only five wires were fully tensioned and two left untensioned, a prestress of approximately 18.5N/sq.mm^2 would be produced. Again, allowing for a self-weight stress of 1.5N/sq.mm. and a loss of prestress of 46%, the residual prestress would be 9.2N/sq.mm. By applying the same design load as before, the resultant hypothetical tensile stress at the soffit would be 4.8N/sq.mm. This is the allowable hypothetical tensile stress for Class 3 beams (crack width = 0.1mm.) in the Unified Code (502) for the 50N/sq.mm. grade of concrete.

Similarly, if only four wires were fully tensioned and three left untensioned, a prestress of approximately 16.7N/sq.mm. would be produced. Assuming the same losses and applying the same design load, the residual prestress would be 8.2N/sq.mm. and the resultant hypothetical tensile stress at the soffit of the beam would be 5.8N/sq.mm. This is the allowable hypothetical tensile stress for Class 3 beams (crack width = 0.2mm.) in the Unified Code (502).

In addition, the design of the beams was such that no additional untensioned steel was required to satisfy the ultimate limit state.

Each of the three groups of beams in the series contained one beam with six wires fully tensioned (Beams S2, SW2 and SG2) and one beam with four wires fully tensioned (Beams S3, SW3 and SG3). In addition, group S contained one beam with seven wires fully tensioned (Beam S2a) and one beam with five wires fully tensioned (Beam S3a).

Series F - The four beams in this series (Figures 5.5. and 5.6.) were designed to provide comparative information on the fatigue (repeated loading) behaviour of fibrous-cement composite T-beams.

Two of the beams (Group FG) were cast onto fibre-reinforced cement channels (Plate 1.4.) and the remaining two beams (Group F) were cast conventionally.

The beams were designed such that each group contained one Class 2 beam (Beams F2 and FG2) and one Class 3 beam (Beams F3 and FG3).

Series L - The four beams in this series (Figures 5.5. and 5.6.) were designed to provide comparative information on the long term (sustained loading) behaviour of fibrous-cement composite T-beams.

As for series F, two of the beams (Beams LG2 and LG3) were cast onto fibre-reinforced cement channels and two beams were cast conventionally (Beams L2 and L3).

5.3. MATERIALS

5.3.1. Concrete

The concrete mixes for all the beams, except the mix for the precast X-joists in Series X, were produced in the concrete laboratory at The University of Salford. The pre-cast X-joists in Series X were produced by Fram Precast Concrete Limited at their precasting yard in Wythenshawe, Manchester.

The concrete mix for the precast X-joists in Series X was designed to have a characteristic strength of $50N/mm^2$ at transfer (24 hours) and $60N/mm^2$ at 28 days. High alumina cement was used to obtain the high early strength required for a daily production cycle and the aggregate consisted of natural sand and gravel, having a maximum size of 10mm. The concrete mix for the remaining precast webs was designed to have a characteristic strength of $40N/mm^2$ at transfer (6 days) and $50N/mm^2$ at 28 days. Rapid Hardening Portland Cement was used as only a weekly production cycle was required and the aggregate consisted of natural sand and gravel as before. The latter concrete mix was also used for the rectangular beams in the pilot study.

Ordinary Portland cement was used in the design of the concrete mixes for all the insitu flanges of the T-beams to give a characteristic strength of $30N/mm^2$ at 28 days. The two conventional concrete flanges contained natural sand and gravel aggregate, having a maximum size of 10mm, while the remaining lightweight aggregate concrete flanges contained fine and coarse Lytag aggregate (sintered pulverised fuel ash), having a maximum size of 6mm.

The proportions of the concrete mixes are set out in Table 5.2. and the actual concrete strengths obtained for each mix are given in Tables 5.3. and 5.4..

The mean values for the slump and compacting factor for the nine precast concrete mixes were 50mm. and 0.96, respectively and for the twenty-one insitu concrete mixes were 57mm. and 0.89, respectively.

5.3.2. Steel

5.3.2.1. Prestressing Steel

The 7mm. diameter helically crimped prestressing wire (characteristic strength = $1570N/mm^2$) was supplied in two metre diameter coils by Richard Johnson and Nephew Limited, of Leeds. Each coil of wire was supplied with a test certificate and the actual mechanical properties of the steel are given in Table 5.5. A typical stress-strain curve for the steel is illustrated in Figure 5.7..

5.3.2.2. Reinforcing Steel

The 12.7mm. diameter mild steel bars, used as compression reinforcement in the flanges of the beams, were supplied in six metre lengths. The bars were subsequently cut to length and fabricated into a 200mm. square mesh in the laboratory. The 10mm. diameter mild steel bars used as compression reinforcement in the remaining series of beams, were supplied prefabricated in sheets (1.2m. x 5.2m.) of 200mm. square mesh. The mild steel bars had a smooth, though slightly rusted, surface and a nominal yield stress of $275N/mm^2$.

The 12.7mm. diameter Kam steel bars had a ribbed surface and were supplied in 6 metre lengths. They were also cut and fabricated into a 200mm. square mesh in the laboratory. Kam steel is manufactured in Sweden and was supplied through Welbeck (Reinforcement) Limited, of Essex. Kam 60 steel is a cold worked hard alloy steel, having a nominal yield strength of $590N/mm^2$ ($60kg/mm^2$). Kam 90 steel is produced by cold stretching Kam 60 steel by almost 5% and has a nominal yield strength of $886N/mm^2$ ($90kg/mm^2$).

The actual mechanical properties of the reinforcing bars used are given in Table 5.5. and typical stress-strain curves for the steels are illustrated in Figure 5.7.

5.3.2.3. Shear and Bond Steel

Stirrups, made from 6mm. diameter mild steel bars, were provided in the shear spans of all the series of T-beams, except Series X. The stirrups were designed to ensure that a premature shear or bond failure did not occur before the ultimate flexural capacity of the beams was reached.

The beams in Series X were tested without any stirrups in order to investigate the interface bond strength and shear capacity of the composite T-beams. As was expected, three types of premature failure occurred in these beams. They were:-

1. Bond failure - slip occurred between the tension steel and the precast concrete (Plate 5.1.).

2. Shear failure - large inclined cracks appeared in the shear span of the beams (Plate 5.2.)

3. Interface bond failure - slip occurred between the precast concrete web and the insitu concrete flange (Plate 5.3.).

To prevent these failures occurring in the remaining series of T-beams, shear reinforcement was designed in accordance with the Unified Code (502). To prevent interface bond failure, horizontal shear reinforcement was designed in accordance with the recommendations of the A.S.C.E. - A.C.I. Committee on Composite Construction (505) and to prevent bond failure, end zone reinforcement was designed in accordance with the methods proposed by Marshall

(506) and Guyon (507).

In addition, the stirrups were designed to act as chairs to support the compression reinforcement. The resultant shape and spacing of the stirrups, obtained by combining the above design criteria, is illustrated in Figures 5.5. and 5.6.

5.3.3. Fibres

5.3.3.1. Steel Fibres

The steel fibres, 0.38mm. diameter x 25mm. long were supplied by National Standard Company Limited, of Kidderminster. The fibres (Plate 1.3.) were made from carbon steel and had mechanical indentations along their length to improve their bond characteristics. The volume fraction of fibres used was 1.6% (5.18% by weight). The steel fibre concrete mix proportions were as for the conventional concrete mix (Table 5.2.) with the addition of a plasticiser (140ml. plasticiser : 50kg. cement). The fibres were premixed with the dry constituents as was the plasticiser with the water and the concrete was then mixed in the conventional manner.

5.3.3.2. Glass Fibres

The alkali-resistant glass fibre reinforced cement channels (Plate 1.4.) and the flat sheets used in Series P and R, were produced and supplied by Mills Scaffold Company Limited, of Bristol. The alkali resistance of the 25mm. long fibres is due specifically to the chemical composition of the glass from which the fibre is drawn and does not, therefore, rely upon surface coatings which could only be expected to give limited protection in the highly alkaline environment (ph 12 to 13) of the hydrating cement matrix.

The fibrous-cement sheets were produced by the spray-suction process. For the rectangular beams (Series P and R), sheets were supplied in the as-cast state (1.2m x 6m) with a nominal thickness of 6mm., which were subsequently cut to size in the laboratory. For the T-beams (Series S, F and L), the fibrous-cement sheets were cut into strips whilst still in the 'green' state. The strips were then placed over wooden formers, producing channels 200mm. wide with an upstand of 38mm. Control tests were carried out on specimens cut from the sheets, the results of which are given in Table 5.6.

5.4. MANUFACTURE OF TEST BEAMS

5.4.1. Rectangular Beams

The rectangular beams (Series P and R) were cast in steel moulds, 100mm. x 100mm. x 500mm. They were compacted on a vibrating table and subsequently cured under wet hessian for 24 hours. The moulds were then stripped and the beams recovered with the wet hessian for a further six days.

5.4.2. Composite T-Beams

5.4.2.1. Precast Web

The five pretensioned X-joist webs (Series X), produced by Fram Precast Concrete Limited, were cast in the conventional manner by the long-line process. All eight prestressing wires were fully tensioned (70% characteristic strength) and the surface of the beams was left untrowelled. The transfer of prestress was carried out after an initial curing period of 24 hours.

The remaining precast webs (Series S, F and L) were produced in the laboratory. They were cast in pairs, again using the long-line process. The stirrups were first fed onto the prestressing wires and then temporarily held in position by wooden spacing bars supported on the sides of the mould (Plate 5.4.). A nominal stress (10% characteristic strength) was then applied to both the "tensioned" and "untensioned" wires in order to position them correctly in the mould. A P.S.C. Monowire prestressing jack was used to apply the stress to the wires. The stress in the "tensioned" wires was then increased to the maximum permitted (70% characteristic strength). It should be remembered that the nominal stress in the "untensioned" wires was designed such that after losses it would have reduced to zero.

The concrete was cast in two batches and subsequently compacted using external vibrators attached to the top of the steel mould. The surface of the concrete was again left untrowelled. The beams were left to cure under wet hessian for six days before the transfer of prestress was carried out. After release from the mould, the beams were left to cure for at least a further 21 days before they were placed in the second mould ready to receive the insitu concrete (Plate 5.5.).

5.4.2.2. Insitu Flange

The wooden mould for the insitu flange (Plate 5.5.) was designed such that the precast web could be supported (Section 1.1.) at third span prior to receiving the insitu concrete. In addition, the soffit of the mould was profiled to allow for the upward camber of the beam, whilst the top of the mould was straight to allow the surface of the flange to be cast horizontal. Thus, the depth of the slab varied by an amount equal to the upward camber and had a minimum value of 50mm. at mid span. Prior to receiving the insitu concrete, which was cast in the conventional manner, the surface of the precast web was wire brushed to expose some of the aggregate. The concrete was compacted, using external vibrators and the surface of the flange was trowelled smooth. The flange was cured under wet hessian for 24 hours before the mould sides and the stop-ends were removed. The flange was then recovered with the wet hessian and cured for a further six days.

5.4.3. Concrete Control Specimens

From each batch of concrete, the following control specimens were cast:-

1. Nine 100mm. cubes
2. Three 100mm. x 100mm. x 500mm. prisms
3. Three 100mm. diameter x 300mm. long cylinders.

The control specimens were compacted on a vibrating table and subsequently cured under wet hessian for 24 hours. The moulds were then stripped and the specimens cured under wet hessian for a further six days under the same conditions as the composite T-beams themselves.

5.5. TEST PROCEDURE

5.5.1. General

All the test beams were simply supported on rollers and were loaded by a symmetrical four point loading system. The load was applied at the third points by the action of a hydraulic jack acting on a steel spreader beam.

The third point loading system was chosen because it simulates, very closely, the conditions under which a beam would normally act in practice (i.e. under a uniformly distributed load). It can be shown (508), that for a uniformly distributed load (=1.33W), producing the same maximum bending moment (=W.1/6) as the third point loading system, the difference in the mid-point deflections is less than 2%.

5.5.2. Short Term Tests

5.5.2.1. Rectangular Beams

The rectangular beams (Series P and R) were simply supported over a clear span of 406.5mm., the distance between the loading points being 135.5mm. (Figures 5.1. and 5.2.). The beams were tested in a 500kN capacity Denison universal testing machine. The load was applied in 2kN increments up to failure, the mid-point deflection being noted at each load increment.

5.5.2.2. T-beams

The composite T-beams (Series X and S) were simply supported over a clear span of 4.725m., the distance between the loading points being 1.575m. (Figure 5.8. and

Plate 5.5.). The load was applied to the beams by a 200kN capacity Denison hydraulic jack, which reacted on the cross-beam of a 250kN capacity steel portal frame. The beams were loaded through three load cycles, the first up to the calculated working load for the limit state of local damage (Appendix A.2.2.), the second to the calculated working load for the limit state of collapse (Appendix A.2.1.), and the third to failure.

The load was applied in ten increments per cycle; strains, deflections and crack widths being noted at each load increment. The beams were unloaded between each cycle in five increments, readings being taken as before. The complete loading history for the composite T-beams is illustrated in Figure 5.9.

5.5.3. <u>Fatigue Tests</u>

The composite T-beams (Series F) were initially subjected to a static load test up to the calculated working load for the limit state of local damage in a test arrangement similar to that used for the short term tests (Figure 5.8. and Plate 5.6.). Subsequently, a cyclic load was applied to the beams by a 200kN capacity hydraulic jack, activated by a Losenhausen S.B.E. 80 slow load cycling unit. The load was cycled between 50% and 100% of the calculated working load at a frequency of 50 - 60 cycles per minute. At intervals of one million cycles, the test was halted and the residual strains, deflections and crack widths were noted. The beam was then subjected to a static load test up to the calculated working load before the cyclic loading was restarted. After three million cycles, the beams were subjected to a full static load test up to failure in the testing arrangement used for the short term tests.

5.5.4. Long Term Tests

The composite T-beams (Series L) were initially subjected to a static load test up to the calculated working load for the limit state of local damage in a self-straining rig (Figure 5.10. and Plate 5.7.). The load was applied to the beams by means of steel weights acting through a system of levers (lever arm ratio = 5 : 1). Strain, deflection and crack width readings were noted after each load increment (100kg.) during the loading stage and subsequently, at increasing intervals of time for a period of 500 days. The beams were then removed from the self-straining rig and subjected to a full static load test up to failure in the testing arrangement used for the short term tests.

5.5.5. Instrumentation

5.5.5.1. Strain Measurement

As soon as the composite T-beams were removed from the mould, a "demec" grid (Figure 5.11.) with a gauge length of 200mm. was marked out on the central zone of each face of the beam. Demec discs were then fixed in the appropriate positions using an epoxy resin. The epoxy resin was allowed to harden for 24 hours before the initial "demec" readings were taken. Subsequently, at regular intervals of time up to the start of the test and at each increment of load or time during the test, the strains at each level on the "demec" grid were measured using a 200mm. "demec" gauge (demountable mechanical strain gauge).

5.5.5.2. Deflection Measurement

The mid-point deflections of the beams were measured using a dial gauge having a maximum travel of 50mm. During the short term tests on the composite T-beams, the deflections were also measured at the third points. At loads near failure, the dial gauges were removed and the deflections were obtained from a vertical scale mounted alongside the beams.

5.5.5.3. Crack Width Measurement

The crack widths were measured with a small self-illuminating hand held microscope, having a magnification of 25. The width of the cracks was measured at the soffit of the beams and, in addition, at the interface of the fibrous-cement channel and the concrete for beams in Group G.

5.5.6. Control Tests

5.5.6.1. Concrete Control Specimens

The precast and insitu concrete properties were obtained from tests carried out on control specimens generally in accordance with B.S. 1881:1970 (501). The average values of the concrete properties for each beam are given in Tables 5.3. and 5.4. and the results of the creep and shrinkage tests are given in Figure 5.12. The actual tests carried out were as follows:-

(a) Compressive Strength Tests

(i) Cube Strength

The nine 100mm. cubes cast from each batch of concrete were tested in a 1800kN capacity Avery hydraulic testing machine. For each beam, three cubes were tested at the time of transfer of prestress for specimens cast from the precast concrete mix and at an age of 7 days for specimens cast from the insitu concrete mix. Three cubes were tested at an age of 28 days and the three remaining cubes were tested immediately after failure of the beams.

(ii) Cylinder Strength

The three 100mm. diameter by 300mm. long cylinders cast from each batch of concrete were tested in a 3000kN capacity Denison universal testing machine immediately after failure of the beams. The load was applied in increments of 5kN and strain readings were taken at each load increment. Strains were measured, using a 50mm. "demec" gauge, at four points at 90° to each other around the circumference of the cylinders. The strain readings were used to obtain the modulus of elasticity of each batch of concrete.

(b) Modulus of Rupture Tests

The three 100mm. x 100mm. x 500mm. prisms were loaded at the third points over a span of 406.5mm. in a 500kN capacity Denison universal testing machine. The prisms were tested at the end of the static load cycle on the composite T-beams in which cracking first occurred.

(c) Shrinkage Tests

"Demec" reference discs were fixed on each face of the 100mm. x 100mm. x 500mm. prisms 24 hours after casting. Strain readings were measured, using a 200mm. "demec" gauge after a further 24 hours and subsequently at increasing intervals of time up to the time the prisms were tested in the Modulus of Rupture tests. During this period, the prisms were stored with the composite T-beams in the laboratory and temperature and relative humidity readings were taken at corresponding time intervals. The variations in relative humidity readings with time are illustrated diagramatically in Figure 7.34.

(d) Creep Tests

In addition to the three 100mm. x 100mm. x 500mm. prisms produced from each batch of concrete for the Modulus of Rupture and Shrinkage tests, six extra prisms were cast from the batch of concrete used for the beams in Group W (steel fibre reinforced concrete) and six extra prisms were cast from the batch of concrete used for the beams in Group SG (conventional concrete). From each group of six prisms, three were used as control specimens (free shrinkage) and three were used as creep specimens (creep plus shrinkage). The creep specimens were tested in a set of six pneumatic loading cells of the type described in detail by Bennett and Loat (509). They were subjected, at an age of seven days, to a sustained axial compressive stress of 14.2N/mm^2 (approximately one third of the concrete cube strength at the time of transfer of prestress). "Demec" reference discs were fixed on two opposite faces of the creep specimens and on all four faces of the control specimens 24 hours after casting. Strain readings were measured using a 200mm. "demec" gauge after a further period of 24 hours and subsequently at increasing intervals of time for a period of 500 days. During this period, the 12 prisms were kept in a constant temperature room, where the average temperature and relative humidity was $20^{o}C$ and 50% respectively.

5.5.6.2. Steel Control Specimens

Tensile tests were carried out on 500mm. long samples taken from all the batches of reinforcing steels used. For the prestressing steel, stress-strain curves and test certificates for each batch of wire were supplied by the manufacturers.

The tests were carried out in a 200kN capacity Denison universal testing machine and the strains were measured with Huggenberger and Baty Extensometers. The mechanical properties of the steels are given in Table 5.5. and typical stress-strain curves are illustrated in Figure 5.7.

5.5.6.3. Fibrous Cement Control Specimens

All the control tests, except for the modulus of elasticity test, were carried out by the manufacturer on samples cut from each of the flat sheets produced. The modulus of elasticity tests were carried out in the laboratory, using a 200kN capacity Denison universal testing machine. The control specimens were 100mm. x 500mm. and each had five rows of "demec" reference discs on each face. The load was applied in increments of 2kN and the strains were measured with a 50mm. "demec" gauge. The resulting stress-strain curve is illustrated in Figure 5.13. and the average values of the properties of the fibrous cement are given in Table 5.6.

CHAPTER SIX

ANALYSIS OF CONCRETE AND STEEL STRESSES

6.1. INTRODUCTION

The chapter is divided into two parts. The first part deals with the analysis of the stresses induced in the concrete and steel prior to the start of the tests (i.e. the prestresses). Allowances are made for the appropriate losses of prestress and, in addition, special attention is given to the stresses induced in the composite T-beams by differential shrinkage. Methods for calculating the stresses by both theoretical and experimental considerations are presented.

The second part of the chapter deals with the analysis of the stresses induced in the steel after the start of the tests (i.e. the applied stresses). A method is presented for calculating the steel stresses by consideration of the experimental data in which allowances are made for the tension stiffening effect of the uncracked concrete in the tension zone of both conventional and fibrous-cement composite beams. The theoretical analysis of the steel stresses has previously been presented in section 4.3.

6.2. STRESSES PRIOR TO TESTING

6.2.1. Stresses at Transfer

The stresses induced in the concrete due to the transfer of the prestressing force were calculated on the basis of the net concrete section (i.e. the total cross-sectional area of the precast concrete minus the total cross-sectional area of the tensile reinforcement).

6.2.2. Stresses due to Self-weight

The stresses induced in the concrete due to the self-weight of the beams were calculated on the basis of the transformed concrete section (i.e. the total cross-sectional area of the precast concrete plus the transformed area of all the steel and the cast-insitu concrete).

The theoretical self-weight stresses were calculated assuming the density of the conventional and lightweight aggregate concrete to be 2400kg/m^3 and 1600kg/m^3, respectively, whilst the experimental self-weight stresses were calculated using the values for the density of concrete obtained by weighing the concrete control specimens cast from each batch of concrete.

6.2.3. Losses of Prestress

6.2.3.1. Theoretical Analysis

(a) Loss due to the relaxation of the prestressing steel.

The relaxation of the 7mm diameter helically crimped prestressing wires was taken to be 4.7% of the initial tensioning stress (70% of the characteristic strength) for the "tensioned" wires and 0% of the initial tensioning stress (10% of the characteristic strength) for the "untensioned" wires. The figure of 4.7% was the figure obtained by Bennett and Dave (601), who carried out relaxation tests of 1000 hours duration on samples of similar steel and the figure of 0% is the figure given in the Unified Code (602) for an initial prestress less than or equal to 50% of the characteristic strength of the prestressing wire.

(b) Loss due to elastic deformation of the concrete.

The immediate loss of prestress in the prestressing wires due to the elastic deformation of the concrete at transfer was calculated on a modular ratio basis, using the stresses in the adjacent concrete at the respective levels of the prestressing wires. The modular ratio was based on the values of the modulus of elasticity for the concrete and steel obtained from the control tests (section 5.5.6.2.).

(c) Loss due to shrinkage of the concrete.

The loss of prestress in the prestressing wires due to shrinkage of the concrete was calculated from the modulus of elasticity of the steel (section 5.5.6.2.), assuming the value for the shrinkage per unit length of the concrete to be 500 microstrain (appendix A.1.). This figure was obtained using the method for estimating the shrinkage of concrete proposed by Evans and Kong (603). The figure given in the Unified Code (602) was not used because ... "for other ages of concrete at transfer, for other conditions of exposure or for massive structures, some adjustment to the figure (given in table 41. of the Unified Code) will be necessary". No details of the necessary adjustment are, however, given in the Unified Code.

(d) Loss due to creep of the concrete.

The loss of prestress in the prestressing wires due to the creep of the concrete was calculated from the modulus of elasticity for the steel (section 5.5.6.2.), assuming that creep is proportional to the stress in the concrete. The specific creep of the concrete was taken to be 24 micro-strain per N/mm^2. This is the figure obtained from the Unified Code (602) for pretensioned concrete at an age of one month (i.e. the age at which the insitu concrete was cast).

6.2.3.2. Experimental Analysis

Due to the method of prestressing, "demec" reference studs could not be fixed onto the precast concrete web prior to the transfer of prestress and, therefore, it was impossible to calculate the actual loss of prestress, due to elastic deformation of the concrete, by strain measurement. In addition, it was 48 hours after the transfer of prestress before the first strain readings could be taken and, therefore, it was also impossible to calculate the total loss of prestress, due to creep and shrinkage of the concrete, by strain measurement.

The actual loss of prestress in the conventional and fibre-reinforced concrete composite T-beams was, therefore, obtained by consideration of the moment equilibrium equation for the load increment immediately after cracking first occurred. The actual computation was as follows:-

(1) The sum of the external bending moments acting on the beam, due to the dead and live loads was calculated.

(2) The depths of the neutral areas of stress and bending, as defined in section 4.3.1.3., were obtained from the strain profiles using the method outlined

in section 6.4.

(3) The depths to the centroids of the compressive and tensile concrete forces were calculated using the method outlined in section 6.5.

(4) The total force in the concrete in tension was calculated using the method outlined in section 6.5.

(5) The total force in the steel in compression was calculated assuming the strain in the compression steel to be the same as that measured on the surface of the adjacent concrete (Figure 4.3.).

(6) The applied strains in the tensioned and untensioned steel were obtained from the strain profiles (Figure 4.3.).

(7) The total force in the tensioned and untensioned steel was calculated from the sum of the applied stresses and the prestresses (i.e. the stresses in the tensioned and untensioned steel at the start of the test: As a first approximation, the losses of prestress were assumed to be equal to the losses calculated theoretically).

(8) The moments of the steel (tensile and compressive) and concrete (tensile) forces about the centroid of the compressive concrete force were calculated and summed.

(9) The sum of the internal moments (step 8) was equated to the sum of the external moments (step 1).

(10) Depending on the error in the moment equilibrium equation, the value of the applied strain in the tensioned steel, e_{st}, was increased or decreased by a small increment.

(11) From the new value of e_{st}, a corresponding value of applied strain in the untensioned steel, e_{su}, was obtained, assuming that the strain in the tensioned and untensioned steel, relative to the start of the test, are directly proportioned to the respective distances of the centroids of the steel from the neutral axis of strain, x_b (i.e. assuming a linear strain distribution and identical bond conditions for the tensioned and untensioned steel).

i.e. $$e_{su} = e_{st} \frac{(d_{su}-x_b)}{(d_{st}-x_b)}$$

(12) Steps (7) to (11) were then repeated until the algebraic sum of the internal and external moments was zero.

(13) The actual applied stresses were then deducted from the final calculated stresses to give the actual prestresses in the tensioned and untensioned steel.

For the fibrous-cement composite T-beams (Group G), the above method could not be used because of the unknown magnitude of the tension stiffening effect of the uncracked concrete in the tension zone, due to the presence of the fibrous-cement channel at the soffit of the beam. The total force in the concrete in tension could not, therefore, be calculated without first calculating the unknown value of T, the tensile stress in the concrete at the level of the centroid of the tensile reinforcement, which in turn could not be calculated without knowing the loss of prestress in the steel. The loss of prestress in the fibrous-cement composite T-beams was, therefore, assumed to be the same as the loss of prestress, expressed as a percentage of the initial prestress in the conventional concrete composite T-beams. The tensile stress in the concrete, T, at the level of the centroid of the tensile reinforcement was then calculated, using the method outlined in section 6.5.2.

6.2.4. Differential Shrinkage Stresses

6.2.4.1. General

In a prestressed composite concrete T-beam, the precast web will usually be well matured by the time that the insitu flange is cast. In turn, the cast-insitu concrete will mature and in doing so will shrink relative to the precast concrete. This relative or differential shrinkage will be restrained by the precast web and internal stresses will be set up in the composite section. If the cast-insitu concrete contains compression reinforcement, then the shrinkage will be further restrained, and the differential shrinkage in the composite section will be reduced. This restraint will induce tensile forces in the cast-insitu concrete in addition to the stresses caused by the differential shrinkage. Hence, the net effect of the compression reinforcement will be to reduce the stresses in the precast web and to increase the stresses in the cast-insitu flange.

6.2.4.2. Theoretical Analysis

In the following theoretical analysis, the method according to Mörsch (604) is assumed, but further extended to account for the effect of the compression reinforcement in the cast-insitu flange. The following assumptions are made in the analysis:-

(1) Shrinkage strain is uniform across the cast-insitu flange.

(2) Shrinkage plus creep strain, developing after the insitu-flange is cast, is uniform across the precast web.

(3) The strain distribution, due to differential shrinkage, is linear across the composite section.

(4) The compression reinforcement acts at the centroid of the cast-insitu flange.

The cast-insitu flange is first considered to be separate from the precast web (figure 6.1a.). When shrinkage occurs, a tensile strain, e_c, is induced in the cast-insitu concrete due to the restraint of the compression reinforcement. The corresponding tensile stress induced in the concrete, f, is given by:-

$$f = E_i . e_c \quad \ldots\ldots\ldots\ldots\ldots\ldots\ldots\ldots\ldots\ldots \quad (6.1.)$$

Where E_i is the modulus of elasticity for the cast-insitu concrete.

Therefore, the tensile force, T_c, induced in the concrete is given by:-

$$T_c = e_c . E_i . (A_i - A_{sc}) \quad \ldots\ldots\ldots\ldots\ldots\ldots\ldots \quad (6.2.)$$

Where A_i and A_{sc} are the areas of the cast-insitu flange and the compression reinforcement, respectively.

Now, the compressive strain induced in the steel, $\overline{e}_i$, is given by:-

$$\overline{e}_i = e_i - e_c \quad \ldots\ldots\ldots\ldots\ldots\ldots\ldots\ldots\ldots\ldots \quad (6.3.)$$

Where e_i is the free shrinkage strain of the cast-insitu concrete. The term $\overline{e}_i$ is also referred to as the apparent shrinkage of the cast-insitu concrete.

Therefore, the compressive force, C_s, induced in the steel is given by:-

$$C_s = \bar{e}_i . E_{sc} . A_{sc} . \quad \ldots\ldots\ldots\ldots\ldots\ldots\ldots (6.4.)$$

Where E_{sc} is the modulus of elasticity of the compression steel.

Since the algebraic sum of the internal forces must be zero:-

$$e_c . E_i . (A_i - A_{sc}) = \bar{e}_i . E_{sc} . A_{sc}$$

Combining with equation 6.3. and rearranging gives:-

$$e_c = \frac{m.n.e_i}{1+(m-1).n} \quad \ldots\ldots\ldots\ldots\ldots\ldots\ldots (6.5.)$$

Where $m = \frac{E_{sc}}{E_i}$

and $n = \frac{A_{sc}}{A_i}$

Combining equation 6.1. and 6.5. gives:-

$$\text{Shrinkage stress, } f = \frac{E_i.m.n.e_i}{1+(m-1).n} \quad \ldots\ldots\ldots (6.6.)$$

Next, a pair of tensile forces are applied at the centroid of the cast-insitu flange such that the cast-insitu flange and the precast web are of the same length (Figure 6.1b.). The forces F, are given by:-

$$F = (\bar{e}_i - e_p).E_i.A_i \quad \ldots\ldots\ldots\ldots\ldots\ldots\ldots (6.7.)$$

Where e_p is the shrinkage plus creep strain developing in the precast web, after the insitu flange is cast.

From equations 6.3. and 6.5. :-

$$\bar{e}_i = \frac{(1-n).e_i}{1+(m-1).n} \quad \ldots\ldots\ldots\ldots\ldots\ldots\ldots\ldots \quad (6.8.)$$

Combining equations 6.7. and 6.8., the differential shrinkage force, F, is given by:-

$$F = A_i.E_i\left\{\frac{(1-n).e_i}{1+(m-1).n} - e_p\right\} \ldots\ldots\ldots\ldots\ldots \quad (6.9.)$$

$\therefore$ the differential shrinkage strain, p, is given by:-

$$p = \frac{(1-n).e_i}{1+(m-1).n} - e_p \quad \ldots\ldots\ldots\ldots\ldots\ldots\ldots \quad (6.10.)$$

The cast-insitu flange and the precast web are now bonded together and the two components act as one composite section. Finally, an equal and opposite force, F, must be applied to the composite beam, acting at the centroid of the cast-insitu flange, to obtain equilibrium (Figure 6.1c.).

Thus, the total stresses induced in the composite beam are given by:-

$$f_1 = \frac{F}{A_c} - \frac{F.e.y_1}{I_o} \quad \ldots\ldots\ldots\ldots\ldots\ldots\ldots \quad (6.11a.)$$

$$f_2 = \frac{F}{A_c} - \frac{F.e.y_2}{I_o} \quad \ldots\ldots\ldots\ldots\ldots\ldots\ldots \quad (6.11b.)$$

$$f_3 = - f - \frac{F}{A_i} + \frac{F}{A_c} - \frac{F.e.y_3}{I_o} \cdot \frac{E_i}{E_p} \ldots \quad (6.11c.)$$

$$f_4 = - f - \frac{F}{A_i} + \frac{F}{A_c} + \frac{F.e.y_4}{I_o} \cdot \frac{E_i}{E_p} \ldots \quad (6.11d.)$$

and $e = x - d_{sc}$

Where E_p is the modulus of elasticity for the precast concrete; x and d_{sc} are the depths to the neutral axes of the transformed composite section and the centroid of the compression steel, respectively; f_1 and f_2 are the stresses due to differential shrinkage at the bottom and top of the precast web, respectively; and y_1, y_2, y_3 and y_4 are the distances from the centroidal axis of the transformed composite section to the respective levels in the section.

The actual computation of the theoretical differential shrinkage stresses comprises of four steps:-

(1) Assessment of appropriate values for the free shrinkage strain of the cast-insitu concrete, e_i, and the shrinkage plus creep strain of the precast concrete, e_p.

(2) Evaluation of the differential shrinkage strain, p, using equation (6.10.).

(3) Evaluation of the shrinkage stress, f, and the differential shrinkage force, F, using equations 6.6. and 6.9. respectively.

(4) Evaluation of the differential shrinkage stresses using equation 6.11.

Values for the free shrinkage strain of the cast-insitu concrete, e_i, and the shrinkage plus creep strain of the precast concrete, e_p, were obtained from the tests carried out on the shrinkage and creep specimens (section 5.5.6.1.), the results of which are plotted in figure 5.12. The values of the differential shrinkage strain, p, were evaluated using the nomogram (figure 6.2.), derived from figure 5.12. and equation 6.10., and are given in the table 7.3. Finally, the theoretical differential shrinkage stresses were evaluated (table 7.2.).

6.2.4.3. Experimental Analysis

If the total concrete strain measured at the bottom of a composite beam is given by e_1, then:-

$$e_1 = e_p + \frac{f_1}{E_p} \quad \ldots\ldots\ldots\ldots\ldots\ldots\ldots\ldots \quad (6.12.)$$

Combining equations 6.11. and 6.12. :-

$$e_1 = e_p + \frac{F}{A_c . E_p} - \frac{F.e.y_1}{I_o . E_p} \quad \ldots\ldots\ldots \quad (6.13.)$$

Similarly, if the total concrete strain measured at the top of the composite beam is given by e_4, then:-

$$e_4 = e_i + \frac{f_4}{E_i} \quad \ldots\ldots\ldots\ldots\ldots\ldots\ldots\ldots \quad (6.14.)$$

Combining equations 6.11. and 6.14. :-

$$e_4 = e_i - \frac{f}{E_i} - \frac{F}{E_i . A_i} + \frac{F}{E_p . A_c} + \frac{F.ey_4}{E_p . I_o} \quad .. \quad (6.15.)$$

Subtracting equations 6.13. and 6.15. :-

$$e_4 - e_1 = e_i - \frac{f}{E_i} - \frac{F}{E_i . A_i} - e_p + \frac{F.e.}{E_p . I_o} (y_1 + y_4) \quad \ldots\ldots\ldots\ldots (6.16.)$$

Combining equations 6.1., 6.7. and 6.16. :-

$$e_4 - e_1 = e_i - e_c - p - e_p + \frac{A_i . E_i . P . e .}{E_p . I_o .} (y_1 + y_4) \quad \ldots (6.17.)$$

from figure 6.1. :-

$$e_i - e_c = p + e_p$$

$$\therefore \quad p = \frac{(e_4 - e_1) . E_p . I_o}{(y_1 + y_4) . E_i . A_i . e} \quad \ldots\ldots\ldots\ldots\ldots\ldots (6.18.)$$

Values for the total concrete strains, e_1 and e_4, were obtained from the strain profiles (figure 7.1. to 7.4.) plotted from the strain readings on the beams prior to the start of the load tests. The values obtained for the differential shrinkage strain, p, (table 7.3.) were then substituted in equations 6.9. and 6.11. to evaluate the experimental differential shrinkage stresses (figures 7.6. and 7.7.).

6.3. STRESSES AFTER THE START OF THE TESTS

6.3.1. Experimental Analysis

6.3.1.1. Uncracked Beam

Up to the cracking load on the first loading cycle and up to the decompression load on the second and subsequent loading cycles, it was assumed that the changes in the strain in the tensioned and untensioned steel were the same as the changes in strain measured on the surface of the adjacent concrete at the respective steel levels. The corresponding changes in stress were obtained, using the modulus of elasticity for steel obtained from the control tests (section 5.5.6.2.).

6.3.1.2. Cracked Beam

For loads greater than the cracking load on the first loading cycle and greater than the decompression load on the second and subsequent loading cycles, the stresses in the tensioned and untensioned steel were calculated, using the re-iterative process employed by Garwood (605). The process was, however, modified to take into account the tension stiffening effect of the uncracked concrete in the tension zone, as follows:-

(1) The sum of the external bending moments acting on the beam, due to the dead and live loads, was calculated.

(2) The depths of the neutral axes of stress and bending, as defined in section 4.3.1.3., were obtained from the strain profiles, using the method outlined in section 6.4.

(3) The depths to the centroids of the compressive and tensile concrete forces were calculated, using the method outlined in section 6.5.

(4) The total force in the concrete in tension was calculated, using the method outlined in section 6.5.

(5) Where applicable, the total force in the fibrous-cement channel was calculated, using the applied strain, e_{ch}, at the soffit of the beam obtained from the strain profile (figure 4.3.) and the stress-strain curve obtained for the fibrous-cement in the control tests (section 5.5.6.3.).

(6) The total force in the steel in compression was calculated assuming the strain in the compression steel to be the same as that measured on the surface of the adjacent concrete (figure 4.3.).

(7) The applied strains and hence the applied stresses in the tensioned and untensioned steel were obtained from the strain profiles (figure 4.3.).

(8) The total force in the tensioned and untensioned steel was calculated from the sum of the applied stresses.

(9) The moments of the steel (tensile and compressive), concrete (tensile) and fibrous-cement (tensile) forces about the centroid of the compressive concrete force were calculated and summed.

(10) The sum of the internal moments (step 9) was equated to the sum of the external moments (step 1).

(11) Depending on the error in the moment equilibrium equation, the value of the applied strain in the tensioned steel, e_{st}, was increased or decreased by a small increment.

(12) For the new value of e_{st}, a corresponding value of applied strain in the untensioned steel, e_{su}, was obtained, assuming that the strains in the tensioned and untensioned steel relative to the start of the test, are directly proportional to the respective distances of the centroids of the steel from the neutral axis of strain x_b.

i.e. $$e_{su} = e_{st} \cdot \frac{(d_{su} - x_b)}{(d_{st} - x_b)}$$

(13) Steps (8) to (12) were then repeated until the error in the moment equilibrium equation was less than 3%.

(14) The experimental prestresses were then deducted from the final calculated stresses to give the applied stresses in the tensioned and untensioned steel.

6.4. NEUTRAL AXIS OF STRESS AND BENDING

6.4.1. General

The positions of the neutral axes of stress and bending were obtained experimentally by consideration of the strains measured on the surface of the concrete. For the short term tests, the neutral axes of stress and bending could be obtained directly from the strain profiles. However, for the fatigue and long term tests, the neutral axis of stress had to be obtained indirectly. This was necessary because account had to be taken of the creep and shrinkage strains that occurred in the time intervals between successive strain measurements.

6.4.2. Short Term Tests

The stresses in the concrete prior to the start of the tests (i.e. the prestresses) were calculated, using the method outlined in section 6.2.3.2. and the corresponding prestrains were plotted as a strain profile. Such a strain profile is represented by the line ABC in figure 4.3. For any given applied load, the applied strains measured at each "demec" level (figure 5.11.) were averaged for the two sides of the beam and plotted as a strain profile; such a strain profile is represented by the line DOBE in figure 4.3.

The position of the neutral axis of bending, defined as the level at which the change of strain incurred between the start of the test (i.e. zero applied moment) and the given applied moment is zero, is given by the point O in figure 4.3. Similarly, the position of the neutral axis of stress, defined as the level at which the compressive stress in the concrete is zero, is given by point B in figure 4.3.

6.4.3. Fatigue and Long Term Tests

To determine the neutral axes of stress and bending for a beam that has been under load for, say T days, the prestrain profile and the instantaneous applied strain profile (i.e. at $t = 0$ days) were plotted, as for the short term tests. Such profiles are given by the lines ABB'C and DOBGE in figure 6.3. The mean strains measured at time T were also plotted as a strain profile, as given by the line D'O'B'E' in figure 6.3.

To allow for the creep and shrinkage strains occurring after the start of the test (i.e. in $t = T$days), the following assumptions were made:-

(1) The increase in compressive strain with time comprises two components, one due to creep and the other due to shrinkage.

(2) The shrinkage strain is uniform across the depth of the concrete in compression.

(3) The creep strain, in the compressive zone, is proportional to the compressive strain in the concrete.

(4) The magnitude of the shrinkage strain is given by the free shrinkage strain measured on the shrinkage specimens (section 5.5.6.1.) in time T, multiplied by a factor to take into account the difference in the volume/ surface area ratios of the composite T-beams and the shrinkage specimens. The factor

was calculated to be equal to 0.96, using the method proposed by Evans and Kong (603).

The shrinkage strain calculated above was deducted from the mean compressive strains measured at time T and the level at which the resultant increase in compressive strain was zero was defined as the neutral axis of stress. This level is given by point G in figure 6.3. The magnitude of the creep strain is not required since if, at a specific level, the increase in compressive strain with time is equal to the shrinkage strain, then the creep strain at that level must be zero (assumption 1). It follows then that the strain at that level must also be zero (assumption 3). A similar method has been proposed by Garwood (605) and Gesund (606).

The neutral axis of bending, by definition, is given by point O' in figure 6.3., which is equivalent to point O for the short term tests.

6.5. CONCRETE FORCES

6.5.1. General

The moment equilibrium equation used in the re-iterative process for the calculation of the steel stresses, requires a knowledge of the depths of the centroids of the compressive and tensile concrete forces and the magnitude of the tensile concrete force. All three variables are functions of the depth of the neutral axis of stress and the shape of the section. In addition, the magnitude of the tensile concrete force is a function of the nominal tensile stress in the concrete at the level of the centroid of the tensile reinforcement.

6.5.2. Compressive Concrete Force

The Unified Code (602) assumes a rectangular - parabolic stress-strain curve for the concrete in compression (i.e. at strains less than $e_c = \frac{\sqrt{U_w}}{5000}$ the distribution is parabolic and at strains greater than e_c, the distribution is uniform). However, in this investigation, it was assumed that for strains less than e_c, the distribution was linear. This assumption was justified by Garwood (606) who showed that it introduced an error of less than 2%.

For any given applied load, therefore, provided that the concrete strain in the extreme compression fibre did not exceed e_c, the depth of the centroid of the compressive concrete force, d_c, was calculated, assuming a linear stress distribution with the value of the depth of the neutral axis of stress, x_s, being obtained from the strain profile (section 6.4.).

It was generally found that within the range of applied loads for which the steel stresses were calculated, the value of the strain e_c was never exceeded in the extreme compression fibre due to the large cross-sectional area of the cast-insitu flange which formed the compression zone of the beam.

6.5.3. Tensile Concrete Force

The Unified Code (602) assumes a triangular stress distribution for the concrete in tension, having a value of zero at the neutral axis of stress, x_s, and a nominal tensile stress, T, at the centroid of the tensile reinforcement. The nominal tensile force in the concrete is introduced to allow for the tension stiffening effect of the uncracked concrete in the tension zone and is a function of the depth of the neutral axis of stress, the shape of the section and the magnitude of the nominal tensile stress, T. The Unified Code assumes for the nominal tensile stress, T, an instantaneous value of $1N/mm^2$, reducing to $0.55N/mm^2$ in the long term.

For this investigation, an instantaneous value of $T = 1N/mm^2$ was used for the conventional and fibre-reinforced (group W) concrete composite T-beams, whilst for the fibrous-cement composite T-beams (group G), the instantaneous value of T was obtained by consideration of the moment equilibrium equation for the load increment immediately after cracking first occurred. The actual computation was as follows:-

(1) The sum of the external bending moments acting on the beam, due to the dead and live loads was calculated.

(2) The depths of the neutral axis of stress and bending, as defined in section 4.3.1.3., were obtained from the strain profile, using the method outlined in section 6.4.

(3) The depths to the centroids of the compressive and tensile concrete forces were calculated, using the method outlined in section 6.5.

(4) The total force in the steel in compression was calculated, assuming the strain in the compression steel to be the same as that measured on the surface of the adjacent concrete (figure 4.3.).

(5) The total force in the fibrous-cement channel was calculated, using the applied strain, e_{ch}, at the soffit of the beam obtained from the strain profile (figure 4.8.) and the stress-strain curve obtained for the fibrous-cement in the control tests (section 5.5.6.3.).

(6) The applied strains and hence the applied stresses in the tensioned and untensioned steel were obtained from the strain profile (figure 4.3.).

(7) The total force in the tensioned and untensioned steel was calculated from the sum of the applied stresses and the experimental prestresses (section 6.2.3.2.).

(8) The moments of the steel (tensile and compressive) and fibrous-cement (tensile) forces about the centroid of the compressive concrete force were calculated and summed.

(9) The sum of the internal moments (step 7) were subtracted from the sum of the external moments (step 1).

(10) The residual moment was equated to the moment of the tensile concrete force about the centroid of the compressive concrete force, from which a value for the nominal tensile stress, T, was obtained.

(11) Steps (1) to (10) were repeated for all the fibrous-cement composite T-beams, for which an average value of $T = 4N/mm^2$ was obtained.

For any given applied load, therefore, the depth and magnitude of the tensile concrete force was calculated, assuming a linear stress distribution with the value of the depth of the neutral axis of stress, x_s, being obtained from the strain profile (section 6.4.) and a value for the nominal tensile stress of either $1N/mm^2$ or $4N/mm^2$. The latter value applying only to the fibrous-cement composite T-beams.

CHAPTER SEVEN

DISCUSSION AND CORRELATION OF TEST RESULTS WITH PROPOSED THEORIES

7.1. INTRODUCTION

The first part of this chapter deals with the general behaviour of partially prestressed composite concrete T-beams with particular reference to the losses of prestress, the effects of differential shrinkage and the use of lightweight aggregate concrete. In addition, information on the structural behaviour of fibrous-cement composites, obtained from the tests on the two pilot series of rectangular beams, is discussed.

Secondly, experimentally obtained values for the depths of the neutral axes of stress and bending and the steel stresses are correlated with the values obtained from the proposed relationships developed in chapters four and six.

Finally, the limit state behaviour of the partially prestressed composite concrete T-beams is discussed with particular reference to the proposed methods for calculating the principal limit states, applicable to both conventional and fibre-reinforced concrete beams, developed in chapter four.

7.2. GENERAL BEHAVIOUR OF TEST BEAMS

7.2.1. Stresses Prior to Testing

In chapter four, equations were developed for predicting the deflections and crack widths in partially prestressed composite concrete T-beams. It can be seen from these equations that the accuracy of these predictions depends, amongst other things, on an accurate assessment of the decompression moment and hence the stresses induced in the concrete prior to the application of the applied loads (i.e. the prestresses). Therefore, it is essential that all the factors affecting the stresses at the soffit of the beams should be carefully considered. The factors involved are the prestress at transfer, the dead load stresses, the losses of prestress and the differential shrinkage stresses. The prestresses developed on the soffit of the test beams are summarised in tables 7.1. and 7.2.

The prestress at transfer is the compressive stress induced in the soffit of the beams due to the application of the prestressing force and the dead load stress is the tensile stress induced due to the self-weight of the beam.

7.2.1.1. Losses of Prestress

The loss of compressive stress in the soffit of the beams (i.e. the loss of prestress) is due to the following:-

(a) loss due to the relaxation of the tensile force in the prestressing steel,

(b) loss due to the elastic deformation of the concrete at transfer,

(c) loss due to creep and shrinkage of the concrete.

The methods used for calculating these losses have previously been presented in chapter six, the results of which are given in tables 7.1. and 7.2. The figures given in table

7.2. relating to the calculated losses of prestress were obtained, assuming the specific creep of the concrete to be 24 microstrain per N/mm^2 (section 6.2.3.1.) and the shrinkage per unit length of the concrete to be 500 microstrain (section 6.2.3.1.). The calculations involved in determining the latter are given in Appendix A.1.

From tables 7.1. and 7.2. it can be seen that a good correlation between the observed and calculated values for the losses of prestress was obtained. The maximum difference was only 2% when expressed as a percentage of the prestress at transfer.

It can also be seen that, for the class 2 beams, the observed loss of prestress due to the untensioned steel is approximately $0.3N/mm^2$ or 1% expressed as a percentage of the prestress at transfer. This value is small enough to be neglected in design calculations. However, for class 3 beams, the loss is approximately $1.2N/mm^2$ or 7%. This value is of the same magnitude as the stresses induced in the soffit of the test beams due to the dead load and should, therefore, always be accounted for in design calculations.

The losses are, however, small in comparison to the losses obtained by Garwood (701) and Abeles (702), who obtained values as high as 60% when using mild steel as the untensioned steel. Furthermore, they support the opinion of Abeles (703) who has always advocated the use of high strength steel as untensioned reinforcement in partially prestressed concrete.

The introduction of fibre reinforcement (groups G and W) had no appreciable effect on the losses of prestress in either the class 2 or class 3 beams.

7.2.1.2. Differential Shrinkage Stresses

In the design of prestressed composite concrete members, differential shrinkage stresses tend to be ignored or at best only a nominal allowance is made for the consequent loss of prestress. This is evident in the current codes of practice. According to A.C.I. 318-71 (704) "the effects of creep, shrinkage and temperature need not be considered except in unusual cases". Likewise, CP110:1972 (705) states that "the effects of differential shrinkage are not generally of great importance ... and in the absence of more exact data, a value of 100 microstrain should be assumed for the differential shrinkage".

In order to evaluate the extent of differential shrinkage in prestressed composite construction, a method is presented in chapter six for calculating differential shrinkage stresses by both experimental and theoretical considerations.

Prior to the start of the load tests, concrete strains were measured on the composite test beams and the results were plotted as strain distribution profiles. Typical profiles are given in figures 7.1. to 7.4. and they clearly show the progressive change of strains that occurred as shrinkage developed at different rates in the precast web and cast-insitu flange. The distribution of strains across the composite section was found to be linear, as assumed in the theoretical analysis.

The effect of using lightweight aggregate concrete in the cast-insitu flange can be seen by comparing the strain distribution profiles for beams in series X (figures 7.1. and 7.2.). The precast webs for this series of composite T-beams were produced from the same batch of concrete and the same prestressing bed. In addition, the precast webs were at least 180 days old (table 7.3.) when the insitu concrete flanges were cast and therefore, it was assumed that the degree of creep and shrinkage that had occurred was approximately the same for all five composite beams. Any variation between the strain distribution profiles is, therefore, due to the type of cast-insitu concrete (i.e. normal or lightweight aggregate concrete) and the type of compression reinforcement (i.e. Kam 90, Kam 60 or Mild Steel). From figure 7.1., it can be seen that, at an age of 88 days, the average strains in the extreme fibres of the composite T-beams of group XN (normal weight aggregate concrete flange) were +148 microstrain and -8 microstrain. From figure 7.2., the average extreme fibre strains for group XL (lightweight aggregate concrete flange) were +253 microstrain and +126 microstrain. Although the magnitude of the shrinkage strains is less for beams of Group XN, due to the reduced shrinkage of normal weight aggregate concrete (figure 5.12.), the difference between the extreme fibre strains is greater, i.e. 156 microstrain compared with 127 microstrain. In section 6.2.4.3., it was shown that the differential shrinkage strain, p, is given by:-

$$p = \frac{e_4 - e_1}{y_1 + y_4} \cdot \frac{E_p}{E_i} \cdot \frac{I_o}{A_i . e} \quad \ldots\ldots\ldots\ldots (6.18.)$$

For groups XN and XL, the values of the ratio E_p/E_i are approximately 1 and 2 respectively (tables 5.3. and 5.4.) and the values of the differential shrinkage, p, will therefore be in the approximate ratio of 156 microstrain to 254 microstrain. From table 7.3., it can be seen that the average ratio is in fact 141:233 or 1:1. 65. This compares with a ratio of 1:2.04 obtained by Evans and Chung (706).

The type of compression reinforcement appears to have little or no effect on the differentiated shrinkage strains. This agrees with the theory, since the total area of compression steel was constant for all the beams in series X and the moduli of elasticity of the different types of steel were very similar (table 5.3.). Thus, in equation 6.18., little or no variation would occur in the term I_o, the moment of inertia of the transformed composite section.

Figures 7.3. and 7.4. show typical strain distribution profiles for class 2 and class 3 composite T-beams respectively. The insitu concrete flanges for beams of group F (beams F2 and F3) were cast when the precast webs were 56 days old (table 7.3.). From the strain profiles it can be seen that the differences in the extreme fibre strains, when the flange was 88 days old, were 155 and 150 microstrain for the class 2 and class 3 beams, respectively. When substituted into equation 6.18., the differential shrinkage strains given are 160 and 162 microstrain, respectively. For beams of group FG (beams FG2 and FG3), the precast webs were 35 days old when the insitu concrete flange was cast. When the cast-insitu flanges were 56 days old, the differences in the extreme fibre strains were 115 and 120 microstrain and the differential shrinkage strains 118 and 127 microstrain for class 2 and class 3 composite T-beams respectively. Similarly, for beams in group SW, the difference in extreme fibre strains were 135 and 140 microstrains and the differential shrinkage strains 139 and 149 microstrain respectively. Thus, the results show that the differential shrinkage strains in class 2 beams are slightly less than in class 3 beams of a comparable age. This is as expected, due to the reduced effect of creep in class 3 beams due to the lower initial prestressing force.

From the results of the creep and shrinkage tests described in section 5.5.6.1., it was found that steel fibre reinforcement had no appreciable effect on the results, compared to conventional concrete. However, from the composite T-beam results, it can be seen that the differential shrinkage strains for the beams with steel fibre reinforcement (group SW) were higher than average. This was probably due to incomplete compaction of the fibre reinforced concrete in the precast web, resulting in a poorer bond between the fibre concrete and the prestressing wires and hence a lower induced prestressing force in the concrete.

For the fibrous-cement composite T-beams (group G), the differential shrinkage strains were lower than average. This was probably due to a reduced rate of initial shrinkage in the precast web due to the fibrous-cement channel covering the soffit and part of the sides of the beam. The fibrous-cement channel having a vapour resistivity of 2MNs/gm compared to 50MNs/gm for concrete (725).

Values for the extreme fibre strains from figures 7.2. to 7.4., were substituted into equation 6.18. to give values for the differential shrinkage strain at various ages. The results of which are plotted in figure 7.5. which clearly shows the variation of differential shrinkage with time for composite T-beams with conventional precast concrete webs and lightweight aggregate concrete flanges. This figure also shows that the age of the precast web when the flange was cast, t_w, has a much greater effect on the differential shrinkage than the age of the cast-insitu flange, t_f.

e.g. for a beam of age, $t_w+t_f = 116$ days

if $t_w = 28$ days and $t_f = 88$ days, then p = 128 microstrain. However, if $t_w = 88$ days and $t_f = 28$ days, then p = 162 microstrain, i.e. an increase of 27%.

It can also be seen from figure 7.5., that the nominal value of p = 100 microstrain advocated by the Unified Code (705) is at the lower bound of the values obtained in this investigation. Thus, the code would seriously underestimate the differential shrinkage strains and hence the losses of prestress. From table 7.3., however, it can be seen that the calculated values obtained using the modified method, according to Mörsch, proposed in chapter six, gives a good correlation with the observed values.

Owing to the number of variables involved, the values of differential shrinkage vary between wide limits. However, the variation obtained in this investigation of 97 to 251 microstrain compares favourably with the variation of -300 to 240 microstrain obtained by Evans and Parker (707), 78 to 280 microstrain obtained by Branson and Ozell (708), and -100 to 260 microstrain obtained by Kajfasz, Somerville and Rowe (709).

From the values obtained for the differential shrinkage, p, the differential shrinkage stresses were calculated, using equations 6.9. and 6.11, the results of which are presented in figures 7.6. and 7.7. These stress profiles show that as the age of the web when the flange was cast, t_w, increases, the stresses induced across the section of the composite T-beams increase. For values of t_w = 28, 35, 56 and 194 days, the average differential shrinkage stresses (i.e. the losses of prestress) induced in the soffit of the beams are 0.79, 0.94, 1.35 and 1.52 N/mm^2, respectively.

When expressed as a percentage of the initial prestress in the precast web, the differential shrinkage stresses represent an average loss of prestress of 4% and 6% for class 2 and class 3 beams respectively (table 7.1.). The test results show a good correlation with those obtained theoretically (table 7.2.); the differences being an average 2% when expressed as a percentage of the initial prestress. However, the differential shrinkage stresses induced in the soffit of the composite T-beams are of a comparable magnitude to those induced by the dead load and are, therefore, high enough to justify consideration in design calculations.

The range of stresses induced in the soffits of the beams varies from 0.67 to 1.74 N/mm^2, which again, compares favourably with variations of 0.14 to 1.66 N/mm^2, obtained by Evans and Parker (707), 0.52 to 1.66 N/mm^2, obtained by Branson and Ozell (708) and 0.69 to 2.42 N/mm^2, obtained by Kajfasz, Somerville and Rowe (709).

From figures 7.6. and 7.7., it can also be seen that the tensile stress at the interface of the precast web and the insitu flange for beams in groups XL, F and L, approached that of the modulus of rupture of the cast-insitu concrete (table 5.4.). This resulted in a series of cracks being observed across the surface of the cast-insitu flanges. The cracks were regularly spaced and coincided with the positions of the compression reinforcing bars. However, these cracks had little effect on the behaviour of the composite beams, as they closed completely on application of the loads during the tests.

7.2.1.3. Residual Prestress

The residual prestress is the compressive stress remaining in the soffit of the beam after all the induced stresses have been summed. From table 7.1., it can be seen that the average residual prestresses are 58% and 54% for the class 2 and class 3 beams, respectively, when expressed as percentages of the initial prestresses. Table 7.2. shows that the theoretical methods proposed in chapter six slightly overestimate the reduction in the initial prestress. However, this is on the "safe" side and the average difference in the residual prestresses is only 3% for both the class 2 and class 3 beams when expressed as a percentage of the initial prestress.

7.2.2. Test Results for Series X

7.2.2.1. Ultimate Loads

The five composite T-beams in this series (figures 5.3. and 5.4.) were cast without stirrups in order to investigate the interface bond strength and shear capacity of the composite section. As expected, three types of premature failure occurred due to the absence of stirrups in the shear spans of the composite T-beams. In beams XN9, XL9 and XL3, bond failure occurred between the prestressing wires and the precast concrete followed almost immediately by a shear failure. This was evident by retraction of the prestressing wires into the precast web (plate 5.1.) followed by the appearance of large inclined cracks in the shear span of the beams (plate 5.2.). In beams XN3 and XL6, interface bond failure occurred between the precast web and the cast-insitu flange. This was evident by a relative displacement between the two components (plate 5.3.).

The failure loads for beams XN9, XL9 and XL3 were 108.0kN, 103.0kN and 98.5kN respectively (table 7.4.). Since the precast webs for all three beams were produced from the same batch of concrete and the same prestressing bed, it was assumed that the bond and shear strength of the precast concrete was the same for all three beams. Therefore, the average reduction of 7% in the failure load for the beams in group XL, compared to the beam in group XN, must be due to an increase in the tensile stress in the concrete. This is brought about by the lower residual prestress due to increased differential shrinkage (section 7.2.1.2.) and the lower moment of inertia of the transformed composite section.

For beams XN3 and XL6, the respective failure loads were 110.0kN and 102.0kN, a reduction of 7% for the beam in group XL. The horizontal shear force at the interface of the precast web and the cast-insitu flange is resisted by adhesion and interlocking of aggregates. Therefore, the strength of the aggregates will have a direct bearing on the strength of the joint. Owing to the relative softness of the lightweight aggregate (plate 1.1.), interlocking at the interface will be less effective when lightweight aggregate concrete is used and consequently the horizontal shear strength will be relatively lower. For beam XL6, the failure load represents a horizontal shear strength of 2.4 N/mm^2. This compares with values of 2.8 N/mm^2 obtained by Chung (710) and 3.4 N/mm^2 obtained by Hanson (711). For beams in series S, F and L (figures 5.5. and 5.6.) stirrups were introduced into the shear spans to prevent the premature failures that occurred in series X (section 5.3.2.3.). The stirrups represented a steel area of 0.24% across the interface between the precast web and the cast-insitu flange and allowed the beams to develop their full ultimate flexural strength. From the loading history for the composite T-beams (figure 5.9.) it can be seen that for beam SW3 a flexural failure load of 134.3kN was obtained. This represents a minimum horizontal shear strength of 3.0 N/mm^2 as no separation was observed anywhere along the length of the interface. This is equivalent to a minimum increase in the horizontal shear strength of 2.5 N/mm^2 per 1% of steel across the interface. This compares with values of 2.3 N/mm^2, obtained by Chung and 1.2 N/mm^2, obtained by Hanson (711). Although the figures obtained by Chung and Hanson differ slightly, for 0.24% of steel across the interface, the horizontal shear strength according to Chung and Hanson would be 3.4 N/mm^2 and 3.7 N/mm^2, respectively.

From table 7.5., it can be seen that the calculated ultimate flexural strengths of the T-beams in series X are very similar, having an average value of 130.3 kN. The ratios of observed to calculated ultimate flexural strength are given in table 7.6. and because of the premature failures, the average values for group XN and XL are 0.84 and 0.78, respectively. Nevertheless, the observed ultimate loads were still in excess of 1.8 times the calculated design loads for the limit state of local damage and 1.2 times the calculated design loads for the limit state of collapse.

7.2.2.2. Deflections

The load deflection curves for the five beams in series X are given in figure 7.8. It can be seen that the beams in group XL have a lower flexural stiffness within the elastic range than the beams in group XN. This is due to the lower modulus of elasticity of the lightweight aggregate concrete and also the differential shrinkage cracks in the cast-insitu flange (section 7.2.1.2.), both of which will give a reduced flexural rigidity for the composite section.

Now, the mid point deflection, a, of a beam is given by:-

$$a = k.l^2.\frac{1}{r_b} \quad \ldots\ldots\ldots\ldots\ldots\ldots\ldots \text{(section 3.4.3.1.)}$$

where:-

$$\frac{1}{r_b} = \frac{M}{E_c.I_o} \quad \ldots\ldots\ldots\ldots\ldots\ldots\ldots\ldots\ldots \text{(4.8.)}$$

$$\therefore \quad a = k.l^2.\frac{M}{E_c.I_o}$$

now, for a third point loading system:-

$$k = \frac{23}{216} \quad \text{and} \quad M = \frac{W.l}{6}$$

$$\therefore \quad a = \frac{23}{216}\cdot\frac{l^3}{6}\cdot\frac{W}{E_c.I_o}$$

rearranging and substituting for l = 4.725m :-

$$\frac{W}{a} = 0.534\ E_c.I_o \quad \ldots\ldots\ldots\ldots\ldots\ldots\ldots \text{(7.1.)}$$

From the slope of the load-deflection curves (figure 7.8.), the average values of W/a for groups XN and XL are 10.47 and 6.03, respectively. Therefore, the corresponding ratio of the flexural rigidities is 19.61 to 11.29. Since the mid-point deflection of a beam is inversely proportional to its flexural rigidity, the ratio of deflections for group XN to group XL will be 11.29 : 19.61, which is equivalent to a ratio of 1 : 1.74. This can be shown diagrammatically by comparing the mid-point deflections of beams in group XN (beams XN9 and XN3) with the corresponding deflections of beams in group XL (beams XL9 and XL3) for the same applied load (figure 7.9.). Within the elastic range, it can be seen that the slope of the line forming the upper limit to the envelope has a slope of 1 : 1.74. Outside the elastic range, the ratio of deflections for group XN to group XL reaches a minimum of 1 : 2.50 with an average value of 1 : 2.12.

At the calculated working load, the average mid-point deflections of the beams in groups XN and XL were 6.3mm. and 10.7mm., respectively, i.e. an increase of 70% for composite T-beams with a lightweight aggregate concrete flange. At 1.5 times the calculated working load, the respective average deflections were 19.1mm. and 30.0mm., an increase of 57%.

Now the flexural rigidity, $E_c.I_o$, of a beam is given by:-

$$E_c.I_o = k_1 \cdot \sqrt{\frac{U_w}{\gamma_m}} \cdot I_o \quad \ldots\ldots\ldots\ldots\ldots\ldots (4.9.)$$

and $$\frac{W}{a} = 0.534\ E_c.I_o \quad \ldots\ldots\ldots\ldots\ldots\ldots\ldots\ldots (7.1.)$$

combining the two equations:-

$$k_1 = \frac{W}{a} \cdot \frac{1}{0.534} \cdot \sqrt{\frac{\gamma_m}{U_w}} \quad \ldots\ldots\ldots\ldots\ldots\ldots (7.2.)$$

For beams in group XN

$$\frac{W}{a} = 10.47 \text{ and } U_w = 67.6\text{N/mm}^2$$

$$\therefore \quad k_1 = 5.15$$

Similar values of $k_1 = 5.08$ and $k_1 = 5.51$ are given by Beeby (712) and the Unified Code (705), respectively. Similarly, for composite concrete T-beams with a lightweight aggregate concrete flange (including beams in series S, F and L), a value of $k_1 = 3.61$ was obtained. Values of $k_1 = 3.65$ and $k_1 = 3.81$ were also obtained for steel fibre-reinforced composite concrete T-beams with a lightweight aggregate concrete flange and fibrous-cement composite concrete T-beams with a lightweight aggregate concrete flange, respectively.

7.2.2.3. Cracking

The crack width versus load curves for the composite T-beams in series X are given in figure 7.10. Once cracking had been initiated, the rate of crack growth was very similar for all five test beams. The average rate of crack growth being 0.016 mm/kN. This is as expected, since the concrete and steel properties for the precast web are the same (tables 5.3. and 5.5.).

The only influence that the cast-insitu concrete has is on the magnitude of the cracking load. Table 7.4. shows that the observed average cracking load for the beams in group XN is 67.5 kN and for beams in group XL it is 56.7kN, i.e. a decrease of 16% for beams with a lightweight aggregate concrete flange. The lower cracking load is due to the lower residual prestress and the lower moment of inertia of the transformed composite section.

7.2.3. Test Results for Rectangular Beams

7.2.3.1. Unreinforced Concrete Beams

The load-deflection curves for the unreinforced concrete beams in series P (figure 5.1.) are given in figure 7.11. The results, which are the average results for five beams in each group, show that within the elastic range, there is no significant difference in the flexural stiffnesses of each group of beams. This indicates that the relatively lower modulus of elasticity for the fibrous-cement sheet compared to concrete (tables 5.3. and 5.6.) does not significantly affect the pre-cracking stiffness. The lower flexural rigidity being compensated for by the inhibiting effect of the fibrous-cement sheets on the rate of growth of micro-cracks.

The conventional concrete beams (group PC) failed instantaneously at an average load of 13.80kN. The fibre-concrete beams (group PW), however, exhibited a degree of yielding before failing at an average load of 15.90kN. The ultimate load and hence the tensile strength of the fibre-concrete was on average 15% greater than that of the conventional concrete (table 7.7.).

For the fibrous-cement composite beams, a crack, originating at the interface with the fibrous-cement sheet, appeared in the concrete at a nominal load of 18.50kN. This is an increase of 34% above the failure load for the conventional concrete beams. There followed a period during which increasing deformation at almost constant load took place, ending in failure by local yielding of the fibrous-cement sheet followed by cracking of the concrete at that position.

The ultimate load for the fibrous-cement composite beams was on average 19.45kN, an increase of 22% above that for the fibre-concrete beams and 41% above that for the conventional concrete beams. The average deflection at failure of the fibrous-cement composite beams was 1.5 times the initial crack deflection and 2.7 times the deflection at failure of the conventional concrete beams, indicating the ductile nature of the post-cracking behaviour.

7.2.3.2. Reinforced Concrete Beams

Comparing the load-deflection behaviour (figure 7.12.) of the reinforced concrete beams in series R (figure 5.2.) it can be seen that the average flexural stiffnesses of the five beams in each group are substantially the same up to a load of approximately 13.80kN. This is coincident with the flexural tensile strength of the conventional concrete beams in group PC. At this point, the deflection of the reinforced conventional concrete beams (group RC) deviates from linear behaviour, with an increasing rate of deflection under increasing load, up to a failure load of 34.15 kN. However, the reinforced fibre-concrete beams (group RW) and reinforced fibrous-cement composite beams (Group RG), behaved linearly up to loads of approximately 16.0kN and 20.0kN, respectively, before yielding to failure at approximately 35.0kN (table 7.7. The failure was by yielding of the mild steel reinforcement followed by cracking of the concrete and as neither of these characteristics are affected by the addition of fibre-reinforcement, the ultimate loads were, as expected, very similar. The increase in the ultimate load over that for the conventional concrete being only 3%.

In the conventional concrete beams (group RC), the failures tended to centre around one large crack, which formed early on at a nominal load of 18.60kN, whilst the beams in groups Rw and RG exhibited several small cracks in the concrete which formed at nominal loads of 20.40kN and 26.10kN respectively. For beams in group RG, failure occurred at the crack closest to the point at which yielding of the fibrous-cement sheet had occurred.

The increase in the cracking load of the fibre-concrete beams and the fibrous-cement composite beams over that of the conventional concrete beams was 10% and 40%, respectively. After cracking, they also exhibited a greater flexural stiffness, due to the inhibiting effect of the fibre reinforcement on the rate of crack growth.

It is interesting to note that there was no significant increase in the precracking stiffness of the rectangular beams with the addition of fibre-reinforcement. Similar results have been obtained by Gunasekaran (713), Williamson (714) and Takagi (715). However, the increase in cracking load, post-cracking stiffness and the resulting reduction in deflection of the fibre-concrete and fibrous-cement composite beams was considered sufficient justification for the study of the flexural behaviour of the full size composite T-beams.

7.3. ANALYSIS OF TEST RESULTS

7.3.1. The Neutral Axes of Stress and Bending

7.3.1.1. General

When analysing the experimental data, the depth of the neutral axis of stress is required in the determination of the average stresses in the tensioned and untensioned steel (section 4.3.1.2.) and is defined as the depth to the level at which the compressive stress in the concrete is zero (section 4.3.1.3.). Similarly, the depth of the neutral axis of bending is required in the determination of the curvature and hence the deflection of a beam (section 4.3.1.) and is defined as the depth to the level at which the change of strain incurred between the start of the test and the given applied moment is zero (section 4.3.1.3.).

The positions of the neutral axes of stress and bending were obtained experimentally by consideration of the strains measured on the surface of the concrete (section 6.4.). In order to determine the depths of the neutral axes of stress and bending by theoretical considerations, two empirical relationships were developed in section 4.3.1.3. and are illustrated in figure 4.4.

7.3.1.2. Short Term Tests

For the short term tests, (series S), the neutral axes of stress and bending were obtained directly from the strain distribution profiles plotted from the strains measured on the surface of the concrete. Typical strain distribution profiles for the first loading cycle are given in figure 7.13. and 7.14. For the conventional composite T-beams, the strain distributions were found to be linear for loads less than the cracking load. Once cracking had started, the distribution of flexural tensile strains became erratic and depended upon the spacing and propagation of cracks relative to the demec grid. However, the distribution of compressive strains remained linear throughout and the strain distribution profiles were obtained by extrapolation. For the fibrous-cement composite T-beams, the distribution of compressive strains in the concrete and tensile strains in the fibrous-cement channel remained linear for loads less than the cracking load for the fibrous-cement channel, irrespective of the degree of cracking in the concrete. Cracks in the concrete, however, caused erratic results for tensile strains measured between the neutral axis of stress and the interface between the fibrous-cement channel and the concrete.

Comparing figures 7.13. and 7.14., it can be seen that the effect of introducing the fibrous-cement channel at the soffit of the composite T-beam is to reduce the strains induced in the concrete and hence increase the depth of the neutral axes of stress and bending by as much as 76%.

The two empirical relationships developed in section 4.3.1.3. relate the depths of the neutral axes of stress and bending, x_s and x_b, respectively, to the increase in applied moment, δM. To enable the results from individual beams to be directly comparable, the empirical relationships are rendered dimensionless by plotting x_s/h and x_b/h against $\delta M/(M_{ult} - M_d - M_{dc})$. Plots for the beams in series S are given in figures 7.15. to 7.18. and from these it can be seen that, in general, there is a good correlation between the experimental and theoretical relationships, especially at loads with the normal working ranges for the class 2 and class 3 beams (section 4.3.1.3.). It should be noted that in figures 7.15. and 7.16., only one theoretical line is plotted since the empirical relationships for the three beams in each class are almost coincident.

7.3.1.3. Long Term Tests

For the long term tests (series L), strain distribution profiles were plotted as for the short term tests. Typical strain distribution profiles are given in figures 7.19. and 7.20. For the conventional composite T-beams, the effect of creep during the period of the tests was to increase the depth of the neutral axes of stress and bending; with the rate of increase decreasing with time. Similar observations have been made by Hajnal Konyi (716), Hollington (717) and Garwood (701). For the fibrous-cement composite T-beams, the increase in the depth of the neutral axes of stress and bending due to creep is reduced. However, the magnitudes of the induced strains are lower and hence the overall depths of the neutral axes are greater, as for the short term tests.

7.3.1.4. Fatigue Tests

Prior to the start of the fatigue tests (series F), all four beams were subjected to a static loading cycle up to the working load for the limit state of local damage. The class 3 beams (beams F3 and FG3) were therefore cracked before the application of the dynamic load.

During the fatigue test, beam F3 failed after only 463,000 cycles. Failure occurred by the progressive enlargement of the cracks developed during the static loading cycle and the spalling of concrete around the prestressing wires until the composite section would no longer support the sustained load component of the applied load. For beam F2, which was uncracked before the application of the dynamic load, a reduction in the depth of the neutral axes of stress and bending was observed during the first million load cycles (figure 7.21.). This is in accordance with the observations of Chandrasekhar (718) and Garwood (701). During this period, cracks appeared at the soffit of the beam. For the remaining two million cycles, little or no change occurred in the depth of the neutral axes.

For the fibrous-cement composite T-beams, the reduction in the depth of the neutral axes was much smaller, however, as before the overall depths of the neutral axes of stress and bending were greater (figure 7.22.).

7.3.2. Steel Stresses

7.3.2.1. Short Term Tests

Typical steel stress versus applied load curves for the beams in series S are given in figures 7.23. to 7.25. The experimental and theoretical stresses are plotted for both the tensioned and untensioned steel. The "tensioned" steel stresses relate to the average stress in the four prestressing wires at the lowest steel level (figure 5.5.). Similarly, the "untensioned" steel stresses relate to the average stress in the single prestressing wire at the highest steel level. For simplicity, the stress in the steel at the intermediate steel level was not plotted as the steel at this level was either tensioned (class 2 beams) or untensioned (class 3 beams).

The experimental steel stresses were determined using the methods described in section 6.3. The stresses were calculated for load increments on the "virgin" loading cycle i.e. for load increments up to the working load for the limit state oflocal damage on the first loading cycle (section 5.5.2.2.), for load increments from the working load for the limit state of local damage up to the working load for the limit state of collapse on the second loading cycle and for loads greater than the working load for the limit state of collapse on the third loading cycle.

The theoretical steel stresses were calculated, using equations 4.6. and 4.7. for load increments up to the decompression load and equations 4.15. and 4.17. for load increments above the decompression load.

In general, there is a good correlation between the experimental and theoretical relationships for the tensioned steel, especially at loads within the normal working ranges for the class 2 and class 3 beams (section 4.3.1.3.). For the untensioned steel, the correlation is not so good, due to the differences between the initial stresses (i.e. the stresses at zero applied load). However, a good correlation is obtained for the rate of increase in the steel stresses (i.e. the slope of the curves) and since it is the increase in steel stress and not the actual magnitude of the steel stress that is used in the determination of the mid-point deflection of the beam (section 4.3.1.5.) the difference in magnitudes is of little consequence.

Comparing figures 7.23. to 7.25., the stresses in the tensioned and untensioned steel are less for the fibrous-cement composite T-beams (group SG) compared with the conventional concrete composite T-beams (group S) and the fibre-concrete composite T-beams (group SW). For beam SG2, the increase in stress in the tensioned steel between the start of the test and the working load for the limit state of local damage was $76N/mm^2$ compared with $92N/mm^2$ for beam S2. This represents a reduction of 17%. For beams SG3 and S3, the increase in the steel stresses were $115N/mm^2$ and $237N/mm^2$, respectively, a reduction of 51%. At the working load for the limit state of collapse, the reductions were 47% and 27% for the class 2 and class 3 beams, respectively. Similar reductions in the stress in the untensioned steel were also obtained. This reduction in the stresses in the untensioned and tensioned steel of the fibrous-cement composite T-beams follows from the reduction in the strains induced across the composite section of the fibrous-cement beams discussed in section 7.3.1.2.

7.3.2.2. Long Term Tests

As stated in section 7.3.1.3., the effect of creep during the long term tests was to increase the depth of the neutral axes of stress and bending. Hence, the lever arm for the internal tensile forces was reduced, resulting in an increase in the stress in both the tensioned and untensioned steel. The rate of increase in stress, however, reduces with time.

As for the short term tests, the stresses in both the tensioned and untensioned steel are lower for the fibrous-cement composite T-beams (Group LG) than for the conventional composite T-beams (group L).

The variation in steel stress with time for the beams under long term loading is given in figure 7.26. Similar results were obtained by Dave (719) and Garwood (701).

7.3.2.3. Fatigue Tests

Figure 7.27. shows the variation in the steel stress with the number of load cycles in both the tensioned and untensioned steel for the beams under fatigue loading. As stated in section 7.3.1.4. the effect of fatigue loading was to reduce slightly the depth of the neutral axis of stress during the first one million load cycles. Consequently, there was a slight decrease in the steel stresses during the first one million load cycles. During the remaining two million load cycles, little or no change occurred in the stresses in the tensioned and untensioned steel. Similar observations were made by Dave (719), Chandrasekhar (718) and Garwood (701).

7.4. ULTIMATE LIMIT STATE

7.4.1. Short Term Tests

The observed and calculated ultimate loads for the composite T-beams in series S are given in tables 7.4. and 7.5. The observed ultimate loads were obtained from the sum of the applied and dead loads whilst the calculated ultimate loads were obtained, using the methods described in section 4.2; an example of which is given in appendix A.2.1. for beam SG3.

For the conventional concrete composite T-beams, failure was characterised by a yielding of the prestressing wires, within the zone of constant applied bending moment, followed by crushing of the lightweight aggregate concrete flange (plate 7.1.). From table 7.6., the ratio of observed to calculated ultimate loads for the conventional concrete composite T-beams has an average value of 1.06.

The natural bond between the fibrous-cement channel and the precast concrete web in the fibrous-cement composite T-beams was maintained up to approximately 90% of the ultimate load. At this load, yielding of the fibrous-cement channel occurred together with a small degree of local bond failure at the yielded section (plates 7.2. and 7.3.). There was no noticeable increase in the deflection or crack widths when the channel failed due to the ductile form of the fibrous-cement failure and the maintenance of bond in areas adjacent to the yielded section. At failure, which was characteristically the same as for the conventional concrete composite T-beams, the fibrous-cement composite T-beams displayed a further advantage by retaining the fractured concrete in the tensile zone (plate 7.4.). From table 7.6. the ratio of observed to calculated ultimate loads for the fibrous-cement composite T-beams has an average value of 1.07. The increase in the ratio over that for the conventional concrete composite T-beams is due to the increase in the tension stiffening effect of the concrete in the tensile zone due to the fibrous-cement channel which results in a reduction in the steel stresses (section 7.3.2.1.).

Prior to the failure of the fibre-concrete composite T-beams, the concrete tended to spall in areas on either side of the cracks revealing "fibre bridges" which gave the appearance of "stitching" across the cracks (plate 4.1.). These fibre bridges gave a degree of continuity across the cracks, resulting in an increase in the tension stiffening effect of the fibre concrete in the tensile zone. The failure of the fibre-concrete composite T-beams was characterised by a sudden increase in deflection caused by a breakdown of the fibre bond and subsequent pull out of the fibres, followed by fracture of the prestressing wires and crushing of the lightweight aggregate concrete flange.

The calculated ultimate loads for the two beams in group SW are 123.3kN and 122.1kN for the class 2 and class 3 beams, respectively. The average value for the ratio of observed to calculated ultimate loads is therefore 1.09, an increase of 2% over that for the conventional concrete composite T-beams. However, it has previously been stated in section 1.4. that for three dimensionally randomly distributed fibres, the efficiency of the fibres in any one direction is 16%. To allow for this in the proposed method for calculating the ultimate load of a fibre-concrete composite T-beam, an equivalent area of reinforcing steel is introduced at the centroid of the web. Thus, for a volume fraction of fibres of 1.6%, the equivalent area of reinforcing steel would be 0.16 x 1.6% = 0.256%. Using this figure in the calculation of the ultimate loads gives values of 126.1kN and 125.1kN for beams SW2 and SW3, respectively. From table 7.6., the average value for the ratio of observed to calculated ultimate loads becomes 1.065 which is in line with the figure obtained for the conventional concrete composite T-beams.

7.4.2. Long Term Tests

The four composite T-beams in group L, having been subjected to a sustained load for a period of 500 days, were unloaded and then, after a brief rest period were loaded statically to failure. The observed and calculated ultimate loads for these beams are given in tables 7.4. and 7.5., respectively. From table 7.4., it can be seen that the observed ultimate loads for the beams in group L are less than those for the corresponding beams in group S. For group L and group S, the respective average observed ultimate loads are 119.5kN and 123.5kN; i.e. a reduction of 3%. Similarly, from table 7.6., the average ratio of observed to calculated ultimate loads for group L and group S are 1.03 and 1.07, respectively, a reduction of 4%. This is in accordance with the findings of Rimmer (720) and Gadre (721), who recorded reductions of up to 6% in the ultimate strength of beams subjected to sustained loads.

From table 7.6., the ratio of observed to calculated ultimate loads for the conventional concrete composite T-beams has an average value of 1.03, whilst for the fibrous-cement composite T-beams, the average value is 1.035. The increase in the ratio for the fibrous-cement composite T-beams is similar to that obtained in the short term tests.

7.4.3. Fatigue Tests

Of the four composite T-beams tested under fatigue loading, beam F3 failed after 463,000 load cycles. The remaining three beams completed approximately three million load cycles before being loaded statically to failure. The observed ultimate loads for the beams in group F were lower than those for the corresponding beams in group S (table 7.4.). For group F and group S the respective average observed ultimate loads were 122.7kN and 123.5kN; i.e. a reduction of 1%. It can also be seen from table 7.6. that the average ratio of observed to calculated ultimate loads for group F and group S are 1.05 and 1.07, respectively, a reduction of 2%. This compares with the results of Dave (719) and Abeles (722), who found no reduction in the ultimate strength of beams that have been subjected to fatigue loading, whereas Sawko and Saha (723) and Garwood (701) all found an increase in the ultimate strength.

As for the short term tests, the average ratio of the observed to calculated ultimate loads for the fibrous-cement composite T-beams is greater than that for the conventional concrete composite T-beams. The average ratios being 1.055 and 1.04, respectively.

7.5. SERVICEABILITY LIMIT STATE

7.5.1. Limit State of Deflection

7.5.1.1. Short Term Tests

The observed load-deflection curves for the eight beams in series S are given in figures 7.28., and 7.29., together with the theoretical curves obtained from the equations developed in section 4.3.1. Each beam was subjected to three loading cycles (section 5.5.2.2.). However, the results were plotted as two loading cycles related to the cycle on which the first crack was observed. If the beam cracked on the second loading cycle (class 2 beams) then the precracking cycle consisted of the first loading cycle plus the virgin loads on the second loading cycle and the postcracking cycle consisted of the third loading cycle. Whereas, if the beam cracked on the first loading cycle (class 3 beam), then the precracking cycle consisted of the first loading cycle and the postcracking cycle consisted of the second loading cycle plus the virgin loads on the third loading cycle. Beams SG2 and SW2 were the exceptions, however, cracking on the third and first loading cycles respectively.

It was stated in section 4.3.1.4. that the residual deflection, a_{res}, at the start of each loading cycle may be calculated from:-

$$a_{res} = \frac{a_{max}}{k_2 + k_3 \cdot \frac{M_{dc}}{M_{max}}} \quad \dots\dots\dots\dots\dots\dots \quad (4.20.)$$

now by rearranging:-

$$\frac{a_{max}}{a_{res}} = k_2 + k_3 \cdot \frac{M_{dc}}{M_{max}} \quad \dots\dots\dots\dots\dots\dots \quad (7.3.)$$

Equation 7.3. represents a straight line, having an intercept on the ordinate axis equal to k_2 and a gradient equal to k_3. In order to determine values of k_2 and k_3, the residual deflection at the start of each loading cycle for the beams in series X and S were plotted using the corresponding values of a_{max}, M_{dc} and M_{max}. From figure 7.30., values of $k_2 = 6$ and $k_3 = 16$ were obtained and substituting into equation 4.20. :-

$$a_{res} = \frac{a_{max}}{6 + 16 \cdot \frac{M_{dc}}{M_{max}}} \quad \dots\dots\dots\dots\dots\dots \quad (7.4.)$$

Similar values of $k_2 = 5$ and $k_3 = 10$ were obtained by Garwood (701).

From figures 7.28., and 7.29., it can be seen that there is a good correlation between the observed and calculated residual deflections and indeed between the observed and calculated load-deflection curves. The proposed deflection formulae, generally, overestimating the deflections slightly.

Figures 7.28. and 7.29. show that for loads less than the decompression load on the postcracking cycles, the slope of the load-deflection curves is the same as the slope of the load-deflection curves for loads within the elastic range on the precracking cycles. Thus the composite T-beams may be treated as homogeneous sections at loads less than the decompression load, even though the section may in fact be cracked. It can also be seen that the deflections at the maximum load on the precracking cycles are very similar to the deflections at the corresponding load on the postcracking cycles.

In order to give a better comparison between the deflections of the three corresponding beams in each class, the load-deflection curves for the three beams in each class were superimposed (figure 7.31.). As with the reinforced concrete beams (section 7.2.3.2.) there was no significant difference in the flexural stiffness of any of the beams prior to cracking. However, at a load of approximately 22kN, the deflections of the fibre-concrete composite T-beams (beams SW2 and SW3) deviated from linear behaviour with an increasing rate of deflection under increasing load up to a load of approximately 50kN. During this period, cracks developed at the soffit of the beams. Once a stable crack pattern had been established, the load-deflection curve became linear again, although the flexural stiffness of the beams was reduced considerably. By comparison the conventional concrete composite T-beams behaved linearly up to a load of approximately 28kN, whilst, the fibrous-cement composite T-beams reached a load of approximately 45kN before the load-deflection curves became non-linear. The fibrous-cement composite T-beams, thus showed a 100% and a 60% increase in the elastic range of the load-deflection curve compared to the fibre-concrete and conventional concrete composite T-beams, respectively. After cracking had occurred, the flexural stiffness of the conventional concrete composite T-beams was less than the flexural stiffness of the fibre-concrete composite T-beams. Therefore, although the deflections of the fibre-concrete composite T-beams were greater than those of the respective conventional concrete composite T-beams at loads less than the calculated working load for the limit state of local damage, at loads approaching the calculated working load for the limit state of collapse, the deflections were, in fact, smaller. By comparison, the fibrous-cement composite T-beams exhibited, after cracking, a flexural stiffness very similar to that of the fibre-concrete composite T-beams and therefore maintained smaller deflections throughout the static load test.

A further comparison can be made between the deflections of the three beams in each class by reference to table 7.8. In this table, the deflections of each of the beams are given at both the calculated working load for the limit state of local damage and the calculated working load for the limit state of collapse. Table 7.8. shows that the deflections of the fibre-concrete composite T-beams were on average 14% greater than the deflection of the conventional concrete composite T-beams, whereas, the deflections of the fibrous-cement composite T-beams were on average 27% less than the deflection of the conventional concrete composite T-beams and 36% less than the deflection of the fibre-concrete composite T-beams.

The Unified Code (705) states that the final deflection (including the effects of temperature, creep and shrinkage), measured below the as-cast level of the supports should not in general exceed span/250. For the tests, the composite T-beams were simply supported over a clear span of 4725mm. (figure 5.8.) and therefore the allowable deflection below the as-cast level of the supports is 18.9mm. From figure 7.31., it can be seen that at the calculated working load for the limit state of local damage, the deflections of all the beams were less than span/250, even without allowing for the initial upward camber of the beams (the term deflection, unless otherwise stated refers to the downward deflection due to the applied load measured from the position of the beam at the start of the test).

From the results of the short term tests on the composite T-beams, it was found that the flexural behaviour of the fibrous-cement composite T-beams was far superior to that of the fibre-concrete composite T-beams. In addition, the improvements in the flexural behaviour of the fibre-concrete composite T-beams did not realise their full potential as indicated in the results of the pilot study of rectangular beams. Consequently, long term and fatigue tests were not carried out on fibre-concrete composite T-beams.

Prior to the start of the long term tests (section 5.5.3.) and the fatigue tests (section 5.5.4.) each of the beams in series L and F were subjected to a static loading cycle up to the calculated working load for the limit state of local damage. By averaging the results for the corresponding beams in each series, together with the results for the corresponding beam in series S, it is possible to get a much more accurate comparison between the flexural behaviours of the fibrous-cement composite T-beams (groups G2 and G3) and the conventional concrete composite T-beams (groups 2 and 3). Figure 7.32. shows the average load-deflection curves for the three corresponding beams in each group. Prior to cracking, the average flexural stiffness of the fibrous-cement composite T-beams (group G2 and G3) is marginally greater than that for the conventional concrete composite T-beams, however, the load-deflection curves for fibrous-cement composite T-beams became non-linear at much higher loads, resulting in much lower deflections at the calculated working load. For groups G2 and G3, the average working load deflections are 8.2mm. and 8.5mm. respectively, whereas for groups 2 and 3, the respective average working load deflections are 11.3mm. and 15.3mm. This represents, for the fibrous-cement composite T-beams, an average reduction in the working load deflection of 27% and 44% for the class 2 and class 3 beams, respectively.

7.5.1.2. Long Term Tests

The observed deflection versus time curves for the four beams in series L are given in figure 7.33. All four beams exhibited a high rate of increase in deflection over the first 50 days with approximately 50% of the total increase in deflection occurring during this time. However, the rate of increase in deflection reduced with time with only 5% of the total increase in deflection occurring during the last 150 days.

Considering the ratio of final deflection to initial deflection, values of 1.60 and 1.40 were obtained for beams L2 and L3, respectively. By comparison, values of 1.94 and 2.32 were obtained for beams LG2 and LG3, respectively. The increase in magnitude for the ratios for the fibrous-cement composite T-beams is partly due to the difference in ages of the beams when the sustained load was first applied. From table 7.3., the average age of the fibrous-cement composite T-beams was 64 days, whilst the average age of the conventional concrete composite T-beams was 176 days. Since time dependant deflections are due to creep and shrinkage strains, the younger the concrete is at the time the sustained load is applied, the greater is the proportion of the ultimate shrinkage strain that has still to take place and the greater will be the creep strain that will take place. The increase in magnitude for the ratios is also due to the lower modulus of elasticity of the fibrous-cement channel compared to the concrete. This will result in larger creep strains and hence larger time dependent deflections. This is evident in that although the initial and final deflections of the fibrous-cement composite T-beams are much lower than the deflections of the conventional concrete composite T-beams, the initial differences in deflections, of comparable beams, are not completely maintained, although the differences become constant after a period of approximately 50 days. Other investigators have obtained similar values for the ratio of final deflection to initial deflection for conventional concrete beams, with Dave (719) obtaining values between 1.76 and 2.64, Garwood (701) values between 1.81 and 2.44

for a test period of 400 days and Cottingham, Fluck and Washa (724) a value of 2.73 for a test period of seven years.

Although the initial rate of increase in deflection with time was greater for the fibrous-cement composite T-beams than for the conventional concrete composite T-beams, the final deflections were still much lower (table 7.8.). For the class 2 beams, the average reduction in deflections was 8%, whilst for the class 3 beams, the average reduction was 23%. These figures compare with the average values of 27% and 44% for class 2 and class 3 beams, respectively, obtained in the short term tests (section 7.5.1.1.). Thus the effect of creep and shrinkage strains is to reduce the overall reduction in deflections by an average of 20% for both the class 2 and class 3 beams.

Comparing the long term deflections of the beams with the limiting deflection of span/250 or 18.9mm., it can be seen that the deflections of both class 3 beams were greater than the limiting deflection. However, as the limiting deflection is related to the as-cast level and the deflections plotted relate to the downward deflection of the beam from the start of the test, a further 10mm. can be added to the limiting deflection to allow for the initial upward camber in the beams due to the prestressing force. Therefore, only beam L3 fails to satisfy the limiting deflection criterion.

One other factor affecting time dependent deflections is the environmental conditions in which the deflections take place. Figure 7.34. shows the variation of deflection and relative humidity with time for the four beams in series L. It can be seen that for the conventional concrete composite T-beams, the rate of increase in deflection is inversely proportional to the relative humidity. As the relative humidity in the laboratory rose during the summer months, so the rate of increase in deflection was reduced. Similarly, as the relative humidity fell during the winter months, so there was an increase in the rate of increase in deflection. These fluctuations could lead to damage occurring in partitions and ceilings under practical conditions. The fibrous-cement composite T-beams were, however, unaffected by the variations in the environmental conditions and maintained a steady increase in deflection. This was due to the stabilising effect of the fibrous-cement channel which covered the soffit and part of the sides of the beams. The fibrous-cement, having a vapour resistivity of 2MNs/gm compared to 50MNs/gm for concrete (725).

7.5.1.3. Fatigue Tests

The observed deflection versus number of load cycles for the four beams in series F are given in figure 7.35. Apart from beam F3, which failed after 463,000 load cycles, all the beams satisfactorily completed three million load cycles. As for the long term tests (section 7.5.1.2.), the beams exhibited a high initial rate of increase in deflection with approximately 60% of the total increase in deflection occurring during the first one million load cycles. The rate of increase in deflection also reduced with time with only 10% of the total increase in deflection occurring during the last one million load cycles.

Considering the ratio of final deflection to initial deflection, a value of 1.73 was obtained for beam F2. Similar values of 1.54 and 1.64 were obtained for beams FG2 and FG3, respectively. By comparison, Dave (719) obtained values of 1.41 to 2.00 for three million load cycles, Garwood (701) values of 1.62 to 2.10 for four million load cycles and Chandrasekhar (718) values of 1.35 to 1.75 also for four million load cycles.

By contrast to the long term tests, the fibrous-cement composite T-beams showed not only a reduction in the final deflection, but also a lower initial rate of increase in deflection resulting in an average reduction in deflection of 46% for the class 2 beams (table 7.8.). The improved performance of the fibrous-cement composite T-beams was further shown by the successful completion of the fatigue test by beam FG3 compared with the fatigue failure of beam F3.

It is interesting to note that for the conventional concrete composite beams, the fatigue tests were the severest, with the class 3 beam failing and the class 2 beam showing a 73% increase in deflection compared to a 60% increase during the long term tests. Similar observations were noted by Garwood (701). However, for the fibrous-cement composite T-beams, the long term tests were the severest, with an average increase in deflection of 119% compared to 59% for the fatigue tests. The large variation in the increase in deflection for the fibrous-cement composite T-beams is largely due to the difference in ages of the beams at the end of the tests. From table 7.3., it can be seen that the average ages of the fibrous-cement composite T-beams were 538 days and 206 days for the long term and fatigue tests, respectively. Since the creep strain for the fibrous-cement will be much greater than that for the conventional concrete, it is to be expected that the age difference will have a much greater effect on the final deflection of the fibrous-cement composite T-beams than on the conventional concrete composite T-beams.

Comparing the fatigue deflection of the beams with the limiting deflection of span/250 or 18.9mm., it can be seen that the deflections of beams F2 and FG3 exceed the limiting deflection. However, by taking into account the initial upward camber of the beams of 14mm. and 10mm. for the class 2 and class 3 beams, respectively, the deflection of all three beams will fall within the limiting deflection criterion.

7.5.2. Limit State of Cracking

7.5.2.1. Short Term Tests

The observed crack width versus load curves for the eight beams in series S are given in figures 7.36. and 7.37., together with the theoretical curves obtained from the equations developed in section 4.3.2. Each beam was subjected to three loading cycles. However, as for the load-deflection curves (section 7.5.1.1.), the results were plotted as two loading cycles related to the loading cycle on which cracking was first observed. By definition (section 1.2.) class 2 beams are prestressed concrete members in which limited tensile stresses, but no cracks are allowed under working load conditions. Similarly, class 3 beams are prestressed concrete members in which limited cracking is allowed under working load conditions. It follows, therefore, that since working load conditions were attained during the first loading cycle (section 5.5.2.2.), the class 2 beams should crack on the second or third loading cycle and the class 3 beams should crack on the first loading cycle. The test results (table 7.4.) show that in fact all the class 3 beams did crack on the first loading cycle and all the class 2 beams did crack on the second or third loading cycle, except beam SW2, which cracked on the first loading cycle.

From figures 7.36. and 7.37., it can be seen that there is a good correlation between the observed and calculated crack width versus load curves, with the proposed crack width formulae, generally, overestimating the crack widths slightly.

In order to obtain a theoretical value for the cracking load, it is necessary to obtain a value for the tensile stress in the concrete at which cracking first occurs. It is generally accepted that the tensile stress at which cracking first occurs, lies between the direct tensile strength and the modulus of rupture of the concrete. Evans (726) found that microcracks developed at a stress corresponding to the direct tensile strength of the concrete, whilst Chandrasekhar (718) found that the cylinder splitting strength gave a good approximation for the tensile strength at which microcracks occurred and that the modulus of rupture gave a good approximation for the tensile stress at which cracks became visible. Garwood (701), however, found that it was more convenient to express the properties of concrete in terms of the cube strength of the concrete and that a good approximation for the tensile stress, f_{cr}, at which cracks became visible was obtained from:-

$$f_{cr} = 0.6\sqrt{U_w}$$

A similar value of:-

$$f_{cr} = 0.555\sqrt{U_w}$$ was suggested by Beeby (712).

Both of these equations give values for the tensile stress at which cracking first occurs slightly less than the modulus of rupture. For the conventional concrete composite T-beams tested in this investigation, it was found that a good approximation was obtained by using $f_{cr} = 0.46\sqrt{U_w}$, or alternatively, $f_{cr} = 0.66\ f_{mr}$, where f_{mr} is the modulus of rupture. If these relationships are applied to the fibre-concrete composite T-beams, it can be seen, from table 5.3., that if $f_{cr} = 0.46\sqrt{U_w}$ is used, then similar cracking loads for the two types of composite T-beam will be obtained. However, if $f_{cr} = 0.66 f_{mr}$, is used, then the theoretical cracking loads for the fibre concrete composite T-beams will be greater than those for the conventional concrete composite T-beams. From table 7.4., it can be seen that in fact, the cracking loads for both types of composite T-beams are similar, and, therefore, the relationship $f_{cr} = 0.46\sqrt{U_w}$ should be used. However, this relationship is not directly applicable to the fibrous-cement composite T-beams, as it does not take into account the effect of the fibrous-cement channel. A convenient way of doing this would be to relate the tensile stress, f_{cr}, to the nominal tensile stress in the concrete, T, that is introduced to allow for the tension stiffening effect of the uncracked concrete in the tension zone in the analysis of a cracked beam. From section 6.5.2., a value of $T = 1N/mm^2$ was obtained for conventional concrete and fibre concrete composite T-beams and a value of $T = 4N/mm^2$ was obtained for fibrous-cement composite T-beams.

now $\quad f_{cr} = 0.46\sqrt{U_w}$

and if $f_{cr} = f(T)$

then, by inspection of the test results:-

$$f_{cr} = 0.33\sqrt{U_w} + T$$

If this equation is used in the calculation of the cracking loads, it can be seen that a good correlation is obtained with the observed values of the cracking loads (tables 7.4. and 7.5.) and that the ratio of observed to calculated cracking load has an average value of 1.06 (table 7.6.).

In order to give a better comparison between the cracking loads and the crack widths of the three corresponding beams in each class, the crack width versus load curves for the three beams in each class were superimposed (figure 7.38.). As with the reinforced concrete beams (section 7.2.3.2.), the cracking loads for the fibrous-cement composite T-beams (table 7.4.) were greater than the cracking loads for the conventional concrete composite T-beams. The increase in the cracking load was, however, only 20% compared to the

40% increase (table 7.7.) obtained with the rectangular beams. By contrast, the fibre concrete composite T-beams showed an average reduction in the cracking load of 8%, compared to an increase of 10% obtained with the rectangular beams. Thus, the overall result was an average reduction of 19% in the increase in the cracking load of the fibre-reinforced composite T-beams, compared to that of the conventional concrete composite T-beams. A similar observation has been made by Edgington (727), who has proposed that the improvement in flexural strength of fibre-reinforced concrete is a function of the gradient of the strain profile for the member, i.e. for shallow members, the potential increase in flexural strength is greater than that for deeper beams where the stress distribution at the soffit approaches the direct stress condition.

Once cracking had been initiated, the rate of crack growth was less for the fibre-reinforced composite T-beams due to the inhibiting effect of the fibre-reinforcement on the rate of crack propagation. Therefore, although the cracks in the fibre concrete composite T-beams were initially greater than those in the corresponding conventional concrete composite T-beams, at loads greater than the calculated working load, the cracks were in fact, smaller for the class 2 beams and the same size for the class 3 beams. By comparison, the fibrous-cement composite T-beams exhibited a much smaller rate of crack growth and therefore maintained smaller crack widths throughout the test.

A further comparison can be made between the crack widths of the three beams in each class by reference to table 7.9. In this table, the crack widths in each of the beams are given at both the calculated working load for the limit state of local damage and the calculated working load for the limit state of collapse. Table 7.9. shows that the crack widths in the fibre-concrete composite T-beams were on average, only 3% less than the crack widths in the conventional concrete composite T-beams, whereas the crack widths of the fibrous-cement composite T-beams were, on average, 73% less than the crack widths in both the conventional concrete and fibre-concrete T-beams.

The Unified Code (705) states that for class 2 beams, no cracking is allowed under working load conditions. From figure 7.38., it can be seen that, of the class 2 beams, only beam SW2 was cracked under working load conditions. Similarly, the Unified Code states that for class 3 beams, the maximum allowable crack width is 0.2mm. From figure 7.38., it can be seen that beams S3 and SW3 each had a maximum crack width of 0.15mm. under working load conditions, whilst beam SG3 remained uncracked.

It should be noted that the term crack width relates to the maximum crack width measured at the soffit of the conventional concrete and fibre concrete composite T-beams. For the fibrous-cement composite T-beams, the term crack width relates to the maximum crack width measured at the interface of the fibrous-cement channel upstand and the concrete web. In all cases, these cracks propagated upwards into the precast web and not visibly downwards into the fibrous-cement channel.

From figure 7.38., it can be seen that even if the working load for both the class 2 and class 3 fibrous-cement composite T-beams was increased to 60kN, the beams would still satisfy the design criteria for crack widths. This amounts to an increase of approximately 25% in the working load capacity of fibrous-cement composite T-beams, compared to conventional concrete or fibre-concrete composite T-beams.

7.5.2.2. Long Term Tests

The observed crack width versus time curves for the four beams in series L are given in figure 7.39. The maximum crack widths in the two conventional concrete composite T-beams (group L) remained constant initially for a period of 100 days before increasing slightly over a period of approximately 200 days. The crack widths then remained constant for the rest of the test period. By contrast, the two fibrous-cement composite T-beams (group LG) showed no increase in crack width with time, the maximum crack width for beam LG3 remaining constant at 0.1mm., whilst beam LG2 remained uncracked.

Considering the ratio of final crack width to initial crack width, values of 2.0 and 1.43 were obtained for beams L2 and L3, respectively. By comparison, a value of 1.0 was obtained for both beams LG2 and LG3. Other investigators have obtained similar values for the ratio of final crack width to initial crack width for conventional concrete beams with Dave (719), obtaining a maximum value of 2.2, Chandrasekher (718) a maximum value of 2.5, and Garwood (701) values between 1.46 and 1.57.

From table 7.9., it can be seen that for the class 2 and class 3 beams, the average reduction in the crack width in the fibrous-cement composite T-beams compared to the conventional concrete composite T-beams was 100% and 75% respectively. These figures compare with the reduction of 100% obtained for the class 3 beams in the short term tests.

From table 7.4., it can be seen that the observed cracking loads for beams LG3 and L3 were 48.0kN and 37.0kN, respectively. The increase in the cracking load for the fibrous-cement composite T-beams was, therefore, 30%. This compares with the increase of 20% obtained in the short term tests.

Comparing the long term crack widths of the beams with the design criteria, it can be seen that both beams in group L failed to satisfy the design criteria. Beam L2 was cracked under the working load conditions and beam L3 had a crack width in excess of 0.2mm. By contrast, both beams in group LG satisfied the design criteria. Beam LG2 remained uncracked throughout the test and the maximum crack width measured in beam LG3 was 0.1mm.

7.5.2.3. Fatigue Tests

The observed crack width versus the number of load cycles for the four beams in series F are given in figure 7.40. Apart from beam F3, which failed after 463,000 load cycles, all the beams satisfactorily completed three million load cycles. Beam FG2 was the only beam uncracked at the start of the cyclic loading and the first crack appeared after some 1.5 million load cycles. Beam FG3 showed only a slight increase in the initial crack width, the crack width remaining constant after 1.0 million load cycles. Beam F2, which was cracked from the start of the cyclic loading, exhibited a much greater increase in crack growth as did beam F3, which failed prematurely.

From table 7.9., it can be seen that for the class 2 beams, the average reduction in the crack width in the fibrous-cement composite T-beams compared to the conventional concrete composite T-beams was 83%, compared to 100% in the long term tests.

The observed cracking loads for beams FG3 and F3 (table 7.4.) were 47.0kN and 40.0kN, respectively. The increase in the cracking load was therefore 18%. This compares with the 20% and 30% increases obtained in the short term and long term tests, respectively. The average increase in the cracking load of the three fibrous-cement composite T-beams compared to the three conventional concrete composite T-beams was, therefore, 23%. This compares with the average increase of 40%, obtained for the ten rectangular beams in the series P and R (table 7.7.).

Comparing the fatigue crack widths of the beams with the limiting design criteria, it can be seen that, as for the long term tests, both beams in group F failed to satisfy the design criteria. Beam F2 was cracked under the working load conditions and beam F3 exhibited crack widths in excess of 0.2mm. before failing. By contrast, both beams in group FG satisfied the design criteria. The maximum crack width measured in beam FG3 was 0.2mm. and beam FG2 was uncracked at the start of the test. However, cracks did appear in beam FG2 after some 1.5 million cycles, although the maximum crack width did not exceed 0.1mm.

For both the fibrous-cement composite T-beams in group F, the cracks were measured at the interface of the fibrous-cement channel upstand and the concrete web. However, unlike the cracks that appeared at the interface of the fibrous-cement composite T-beams in series S and L, the cracks did propagate down into the fibrous-cement channel as well as upwards into the concrete web. These cracks opened and closed with the cyclic loading and completely closed on removal of the sustained component of the cyclic load, as did the cracks in the conventional concrete composite T-beams. The cracks in the fibrous-cement channel, which appeared to be confined to the cement matrix and not the fibres in the composite, had no adverse effect on the deflection, cracking and ultimate load performance of the fibrous cement composite T-beams.

CHAPTER EIGHT

CONCLUSIONS

8.1. CONCLUSIONS FROM PRESENT INVESTIGATION

8.1.1. Conventional Concrete Composite Construction

8.1.1.1. Composite Construction

(1) Natural bond between the precast concrete web and the cast-insitu concrete flange is insufficient for the development of the full ultimate flexural strength.

(2) Interface bond strength may be increased by a minimum of 2.5N/mm^2 per 1% of steel across the interface.

(3) Adequately designed stirrups will prevent premature bond, shear and interface bond failures and allow the development of the full ultimate flexural strength.

8.1.1.2. Partial Prestressing

(1) General behaviour of partially prestressed beams (class 2 and class 3) is intermediate between that of fully prestressed (class 1) and reinforced (class 4) concrete beams.

(2) For loads less than the cracking load on the precracking cycle and the decompression load on the postcracking cycle, the beams behave as class 1 members with a homogeneous elastic section. Above these loads, the beams behave as class 4 members with a cracked transformed concrete section.

(3) The degree of partial prestressing has no effect on the ultimate strength of the beams.

8.1.1.3. Lightweight Aggregate Concrete

(1) The use of lightweight aggregate concrete in the cast-insitu flange reduces the horizontal shear strength, flexural rigidity, cracking strength and ultimate strength of the composite T-beams.

(2) The use of lightweight aggregate concrete increases the crack widths and deflections of the composite T-beam.

(3) Losses of prestress due to differential shrinkage are increased with the use of lightweight aggregate concrete.

8.1.1.4. Compression Reinforcement

(1) The type of compression steel has no apparent effect on the flexural behaviour of composite T-beams.

(2) The type of compression steel has no apparent effect on differential shrinkage.

(3) Compression reinforcement modifies the differential shrinkage stress distributions such that the stresses in the precast web are reduced and the stresses in the cast-insitu flange are increased.

8.1.1.5. Losses of Prestress

(1) The losses of prestress, due to the relaxation of the steel and creep, shrinkage and elastic deformation of the concrete can be adequately predicted, using the methods described in chapter six.

(2) The use of high strength steel as untensioned steel results in a negligible loss of prestress in the untensioned steel in class 2 T-beams. The loss of prestress in class 3 beams is, however, large enough to justify consideration in design calculations.

(3) The average loss of prestress in the tensioned steel is 31% and 25% for the class 2 and class 3 beams, respectively.

8.1.1.6. Differential Shrinkage

(1) Differential shrinkage stresses can be adequately predicted using the method proposed in chapter six.

(2) Differential shrinkage reduces the effective prestress and hence the cracking strength of composite T-beams. The reduction increases with the age of the cast-insitu flange and more importantly, with the age of the pre-cast web when the insitu flange was cast.

(3) Differential shrinkage stresses are large enough to justify consideration in design calculations.

8.1.1.7. Ultimate Limit State

(1) The ultimate strength can be adequately predicted using the strain-compatability method and the rectangular-parabolic stress distribution for the concrete in compression.

(2) The effect of long term and fatigue loading is to slightly reduce the ultimate strength of the composite T-beams.

(3) The ductile nature of the post-cracking behaviour gives adequate warning of approaching failure.

8.1.1.8. Serviceability Limit State

(1) The deflection and cracking of composite T-beams can be adequately predicted using the methods proposed in chapter four.

(2) The effect of long term and fatigue loading is to increase the magnitude of the deflections and crack widths.

(3) The fatigue rather than the long term tests have the severest effect on the flexural behaviour of the composite T-beams.

(4) The critical limit state is the limit state of cracking.

8.1.2. Fibre Concrete Composite Construction

(1) The addition of steel fibre reinforcement to plain or reinforced concrete increases the flexural strength of the concrete.

(2) There is no increase in the precracking stiffness of reinforced or partially prestressed concrete with the addition of steel fibre reinforcement.

(3) The improvement in the flexural strength of steel fibre reinforced concrete appears to be a function of the gradient of the strain profile for the member.

(4) Steel fibre reinforced concrete exhibits a greater post-cracking stiffness than conventional concrete.

(5) The use of steel fibre reinforcement in composite T-beam construction can result in a reduction in the deflection and maximum crack width, generally at loads greater than the working load.

(6) Failure of the steel fibre reinforced concrete was by a breakdown of the fibre bond and subsequent pull-out of the fibres.

(7) The ultimate strength of a fibre concrete composite T-beam may be calculated using a strain compatability method, assuming a 16% efficiency for the randomly distributed fibres and an equivalent area of reinforcement acting at the centroid of the section.

(8) The improvements in the flexural behaviour of the fibre concrete composite T-beams do not realise their full potential as indicated by the results of the pilot study of rectangular beams.

(9) The addition of steel fibre reinforcement to the precast web of composite T-beams has no appreciable effect on the losses of prestress or the differential shrinkage stresses.

(10) The deflection and crack widths of fibre concrete composite T-beams can be adequately predicted by the methods proposed in chapter four.

8.1.3. Fibrous-Cement Composite Construction

(1) The addition of a fibrous-cement sheet at the soffit of a reinforced or partially prestressed concrete beam substantially increases the flexural strength of the concrete beam.

(2) There is no appreciable increase in the precracking stiffness of reinforced or partially prestressed concrete.

(3) The improvement in the flexural strength appears to be a function of the gradient of the stress profile for the member and is 30% greater than that for fibre concrete composite beams.

(4) Fibrous cement composite beams exhibit a greater post-cracking stiffness than conventional concrete beams.

(5) The use of fibrous-cement channels in composite T-beams results in substantial reductions in deflections and crack widths compared to fibre concrete and conventional concrete composite T-beams.

(6) The natural bond between the fibrous cement channel and the precast concrete web was maintained up to 90% of the ultimate load, at which point, the ductile nature of the fibrous-cement failure gave adequate warning of approaching failure.

(7) The ultimate strength, deflection and crack widths may be adequately predicted using the methods proposed in chapter four.

(8) The lower vapour resistivity of the fibrous cement compared to concrete, slightly reduces the effect of differential shrinkage and eliminates the fluctuations in long term deflections due to variations in the environmental conditions.

(9) The use of fibrous-cement channels results in a reduction in the depths of the neutral axes of stress and bending and hence a reduction in the stresses in the tensioned and untensioned steel.

(10) The long term and fatigue deflections and crack widths are substantially less than those for conventional concrete composite T-beams.

(11) The fatigue and long term tests have the severest effects on the cracking and deflection behaviour, respectively.

(12) The critical limit state is the limit state of cracking, although the working load may be increased by 25% and still satisfy the design criteria in the short term.

8.2. SUGGESTIONS FOR FUTURE INVESTIGATIONS

(1) Effect of depth of beam on increase in flexural strength of fibrous cement composite beams.

(2) Effect of geometrical shape of fibrous cement channel, i.e. length of upstand and thickness of material.

(3) Effect of lower vapour resistivity of fibrous cement on shrinkage of concrete confined by channel.

(4) Study of formation of cracks in concrete confined by channel.

(5) Effect of allowing higher hypothetical tensile stresses and hence higher working loads to give the same crack widths for the limit state of cracking as obtained with conventional concrete composite T-beams.

R E F E R E N C E S

CHAPTER 1

101 Hasnat, A. "Behaviour of Prestressed Composite T-Beams of Lightweight Aggregate Concrete", PhD Thesis, University of Texas, 1965.

102 Samuely, F. "Some Recent Experiences in Composite Precast and Insitu Concrete Construction with Particular Reference to Prestressing". Proceedings of I.C.E. part 3, volume 1, August 1952, pp222-279.

103 Abeles, P.W. "Breaking Tests on Three Full Size Prestressed Concrete Bridge Beams "Structural Engineer", Volume 29, No 5, May 1951, pp149-160.

104 Revesz, S. "Behaviour of Composite T-Beams with Prestressed and Unprestressed Reinforcement". Proceedings of A.C.I., Volume 49, No 6, February 1953, pp585-592.

105 Harris, J.D. and Smith, I.C. "Basic Design and Construction in Prestressed Concrete". London 1963, pp185-204.

106 CP110:1972 "Code of Practice for the Structural Use of Concrete". British Standards Institution, London 1972.

107 Chaikes, S. "Le Beton Preconstraint Armé" Proceedings of F.I.P., Fourth Congress, Rome 1962, Theme 3, Volume 1, Paper 8, pp480-483.

108 Stevens, R.F. "Tests on Prestressed Reinforced Concrete Beams" Concrete, Volume 3, No 11, November 1969, pp457-462.

109 Dave, N.J. "Limited Prestress as a Means of Economy in Structural Concrete". PhD Thesis, University of Leeds, 1967.

110 Garwood, T.G. "Flexural Behaviour of Class 3 Post-Tensioned Prestressed Concrete Beams, using Various Types of Untensioned Steel". PhD Thesis, University of Salford 1972.

111 Zunz, G.J. "Some Examples of when and how Lightweight Concrete Should be Used" International Congress on Lightweight Concrete, London, May 1968.

112 Cox, H.L. "British Journal of Applied Physics" Volume 3, 1952, p72.

113 Hannant, D.J. "Steel Fibres and Lightweight Beams" Concrete, Volume 6, No 8, August 1972, pp39-40.

CHAPTER 2

201 Hasnat, A. "Behaviour of Prestressed Composite T-Beams of Lightweight Aggregate Concrete" PhD Thesis, University of Texas, 1965.

202 Abeles, P.W. "Breaking Tests on Three Full Size Prestressed Concrete Bridge Beams" Structural Engineer, Volume 29, No 5, May 1951, pp149-160.

203 Samuely, F.S. "Some Recent Experience in Composite Precast and Insitu Concrete Construction with Particular Reference to Prestressing". Proceedinsg of I.C.E., part 3, volume 1, 1952, pp277-279.

204 Revesz, S. "Behaviour of Composite T-Beams with Prestressed and Unprestressed Reinforcement". Proceedings of A.C.I., Volume 24, No 6, February 1953, pp585-592.

205 Evans, R.H. and Parker, A.S. "Behaviour of Prestressed Concrete Beams" Proceedings of A.C.I., Volume 51, No 9, 1955, pp861-880.

206 Dean, and Ozell, "No Shear Keys are needed Here" Engineering News Record, Volume 156, No 61, June 1956, pp61-64.

207 Hanson, N.W. "Precast Prestressed Concrete Bridges 2. Horizontal Shear Connectors" Journal of Research and Development Laboratories (P.C.A.), Volume 2, No 2, May 1960, pp38-58.

208 Ahmed, W. "Structural Behaviour Of Prestressed Concrete Beams of Composite Construction" PhD Thesis, University of Wales, 1962.

209 Chung, H.W. "Application of Lightweight Concrete to Prestressed Composite Construction" PhD Thesis, University of Leeds, 1966.

210 Taylor, R. "An Idea for a New Structural Material - Composite Reinforced Concrete" Engineering, London, Volume 211, December 1971, pp1010-1012.

211 Taylor, R. and Burdon, P. "Tests on a New Form of Composite Construction" Proceedings of I.C.E., Volume 53, part 2, December 1972, pp471-486.

212 Emperger, F.V. "Vorgespannte Ameirungszulagen in den Trag-Werken aus Eisenbeton" Deutscher Beton Verien, Volume 42, 1939.

213 Abeles, P.W. "Saving Reinforcement by Prestressing" Concrete and Constructional Engineering, Volume 35, 1940, pp328-333.

214 Abeles, P.W. "Breaking Tests on Three Full Size Prestressed Concrete Bridge Beams" Structural Engineer, Volume 29, May 1951, pp 149-160.

215 Abeles, P.W. "Some New Developments in Prestressed Concrete" Structural Engineer, Volume 29, October 1951, pp259-278.

216 Abeles, P.W. "Static and Fatigue Tests on Partially Prestressed Concrete Construction" Journal of A.C.I. Volume 51, December 1954, pp361-376.

217 Abeles, P.W. "The Condition of Partially Prestressed Concrete Structures After Three to Seven Years Use". Fifth Congress I.A.B.S.E., Portugal, 1957, p 625.

218 Proceedings F.I.P., Fourth Congress, Rome-Naples, 1962 Published by C. and C.A., 1963.

219 Orr, D.M.F. "Partially Prestressed Concrete" PhD Thesis, Trinity College Dublin, 1963.

220 Dave, N.J. "Limited Prestressing as a means of Economy in Structural Concrete" PhD Thesis, University of Leeds, 1967.

221 Abeles, P.W. "Cracking and Bond Resistance in High Strength Reinforced Concrete Beams Illustrated by Photo-elastic Coating" Journal of A.C.I., Volume 63, No 11, 1966, pp1265-1278.

222 Chandresekhar, C.S. "A Study of the Influence of the Behaviour of Beams with Limited Prestress" PhD Thesis, University of Leeds, 1970.

223 Beeby, A.W., Keyder, E. and Taylor, H.P.J. "Cracking and Deformations of Partially Prestressed Concrete Beams" C. and C.A. Technical Report, January 1972.

224 Annales des Travaux Publics de Belgique No 2, 1966, Translated by C. and C.A. 1966.

225 Proceedings F.I.P., Fifth Congress, Paris, 1966, Published by C. and C.A. 1967.

226 Hutton, S.G. and Loov, R.E. "Flexural Behaviour of Prestressed, Partially Prestressed and Reinforced Concrete Beams" Journal of A.C.I. Volume 63, No 1, December 1966, pp1401-1411.

227 Abeles, P.W. and Kung, R. "The Losses of Prestress due to Effect of Shrinkage and Creep on Non-tensioned Steel in Hot Climate" International Rilem Symposium on Concrete and Reinforced Concrete in Hot Countries, Technion Israel Institute of Technology, Haifa, Israel, 2 - 5th August 1971.

228 Veeriah, C. "Partially Prestressed Concrete Structures" All India Symposium on Ultimate Load Design of Concrete Structures, 1966, pp72-76.

229 Branson, D.E. and Shaikh, A.F. "Favourable and Unfavourable Effects of Non-Tensioned Steel in Prestressed Concrete Beams" Research Report No HR - 123 HPR 1-3, Department of Civil Engineering, University of Iowa, June 1967.

230 Report on Eighth Congress of I.A.B.S.E., New York, 1968.

231 Abeles, P.W., Brown, E.I. and Woods, J.O. "Preliminary Report on Static and Sustained Loading Tests" Journal of P.C.I., Volume 13, No 4, August 1968, pp12-32.

232 Abeles, P.W., Brown, E.I. and Morrow, J.W. "Development and Distribution of Cracks in Rectangular Prestressed Beams during Static and Fatigue Loading", Journal of P.C.I., Volume 13, No 5, October 1968, pp37-52.

233 Proceedings F.I.P. Sixth Congress, Prague 1970, Published by C. and C.A. 1971.

234 Magura, D.D. and Hognestad, E. "Tests on Partially Prestressed Concrete Girder" Journal of Structural Division, Proceedings of A.S.C.E., Volume 92, February 1966, pp327-344.

235 Brenneisen, A. "Considerations Relatives a la Deformation, a'la Fissuration et le Rupture des Poutres en Beton Precontraint et Partiellement Precontraint" Leige Universite - Centre d'Etudes de Recherches et d'Essais Scientifique du Genie Civil - Memoires No 28, November 1969, pp1-55.

236 Stevens, R.F. "Tests on Prestressed Reinforced Concrete Beams" Concrete, Volume 3, No 11, November 1969, pp457-462.

237 Veerasubramanian, N. "Effect of Shape and Cross-Section on the Flexural Behaviour of Class 3 Prestressed Concrete Beams" PhD Thesis, University of Leeds, 1971.

238 Garwood, T.G. "The Flexural Behaviour of Class 3 Post-tensioned Prestressed Concrete Beams, using Various Types of Untensioned Steel" PhD Thesis, University of Salford, 1972.

239 Romualdi, J.P. and Batson, G.B. "Behaviour of Reinforced Concrete Beams with Closely Spaced Reinforcement" Journal of A.C.I., Volume 60, No 6, June 1963, pp775-789.

240 Romauldi, J.P. and Batson, G.B. "Mechanics of Crack Arrest in Concrete" Journal of Engineering Mechanics Division, Proceedings of A.S.C.E., Volume 89, E.M.B., June 1963, pp147-168.

241 Romualdi, J.P. and Mandel, J.A. "Tensile Strength of Concrete Affected by Uniformly Distributed Closely Spaced Short Lengths of Wire Reinforcement" Journal of A.C.I., Volume 61, No 6, June 1964, pp671-675.

242 Kar, J.N. and Pal, A.K. "Strength of Fibre - Reinforced Concrete" Journal of Structural Division, Proceedings of A.S.C.E., Volume 98, S.T.5, May 1972, pp1053-1068.

243 Snyder, M.J. and Lankard, D.R. "Factors Affecting Cracking Strength of Steel Fibrous Concrete" Journal of A.C.I., Volume 69, No 2, February 1972, pp96-100.

244 McKee, D.C. "The Properties of an Expansive Cement Mortar Reinforced with Random Wire Fibres" PhD Thesis, University of Illinois, 1969.

245 Williamson, G.R. "Fibrous Reinforcement for Portland Cement Concrete" Technical Report No 2-40, U.S. Army Engineering Division, Ohio River Division Laboratories, Cincinnati, 1965.

246 Nanda, V.K. "A Laboratory Investigation of Fibre Reinforced Concretes" MSc Thesis, University of Surrey, 1968.

247 Durham, J. "The Tensile Strength of Fibre Reinforced Concrete" MSc Thesis, University of Salford, 1971.

248 Untraur, R. and Works, R.E. "Discussion of Reference 241" Journal of A.C.I., Volume 61, No 12, 1964, pp1653-1656.

249 Shah, S.P. and Rangan, B.V. "Fibre Reinforced Concrete Properties" Jornal of A.C.I., Volume 68, No 2, 1971, pp126-135.

250 Chan, H.C. and Patterson, W.A. "The Theoretical Prediction of the Cracking Stress of Glass Fibre Reinforced Inorganic Cement" Journal of Materials Science, Volume 7, 1972, pp856-860.

251 Aveston, J., Cooper, G.A. and Kelly, A. "Single and Multiple Fracture" The Properties of Fibre Composites, Conference Proceedings, National Physical Laboratory, November 1971, pp15-24.

252 Aveston, J. and Kelly, A. "Theory of Multiple Fracture of Fibrous Composites" Journal of Materials Science, Volume 8, No 3, March 1973, pp352-362.

253 Laws, V., Ali, M.A. and Nurse, R.W. "The Response to Stress of a Short Fibre Reinforced Brittle Matrix" The Properties of Fibre Composites, Conference Proceedings, National Physical Laboratory, November 1971, pp29-30.

254 Stayler, G. "Two Phase Materials" Scientific American, Volume 206, No 1, 1962.

255 Porter, A.F. "Preparation of Concrete from Selection of Materials to Final Disposition" Proceeding of National Association of Cement users, A.C.I., Volume 6, 1910, p 296.

256 Ficklin, W., British Patent No 11754, 1914.

257 Romauldi, J.P. "The Static Cracking Stress and Fatigue Strength of Concrete Reinforced with Short Pieces of Thin Steel Wire - The Structure of Concrete and its Behaviour under Load" Proceedings of International Conference, London, 1965, C. and C.A., 1968, pp190-201.

258 Agbin, C.C. "Discussion of Reference 241" Journal of A.C.I., Volume 61, No 12, 1964, pp1652-1653.

259 Mayfield, B. and Zelly, B. "Steel Fibre Treatment to Improve Bonds" Concrete, Volume 7, No 3, March 1973, pp35-37.

260 DeVekey, R.C. and Majumdar, A.J. "Determining Bond Strength in Fibre Reinforced Composites" Magazine of Concrete Research, Volume 20, No 65, December 1968, pp229-234.

261 DeVekey, R.C. and Majumdar, A.J. "International Bond Strength of Glass Fibre Reinforced Cement Composites" Journal of Material Science, Volume 5, No 2, 1970, pp183-185.

262 Cox, H.L. British Journal of Applied Physics, Volume 3, 1952, p 72.

263 Laws, V. "The Efficiency of Fibrous Reinforcement of Brittle Matrices" Journal of Applied Physics, Volume 4, 1971, p1737-1746.

264 Edgington, J. and Hannant, D.J. "Steel Fibre Reinforced Concrete" The Effect of Fibre Orientation of Compaction by Vibration" Materials and Structures, Volume 5, No 25, February 1972, pp41-44.

265 Abolitz, A.L. "Discussion of Reference 241" Journal of A.C.I., Volume 61, No 12, 1964, pp1651-1652.

266 Majumdar, A.S. and Ryder, J.F. "Glass Fibre Reinforcement of Cement Products" Glass Technology, Volume 9, No 3, June 1968, pp78-84.

267 Biryukovich, K.L., Yu, L. and D.L. "Glass Fibre Reinforced Cement" C.E.R.A. Translation No 12, Civil Engineering Research Association, London, 1965.

268 Chan, H.C. and Patterson, W.A. "Effects of Weathering and Ageing on the Tensile Strength of Glass Fibre Reinforced High Alumina Cement" Journal of Materials Section, Volume 6, No 4, April 1971, pp342-346.

269 Ali, M.H. and Grimer, F.J. "Mechanical Properties of Glass Fibre Reinforced Gypsum" Journal of Materials Science, Volume 4, No 5, May 1969, pp389-395.

270 Majumdar, A.J. and Ryder, J.F. "Reinforcement of Cement and Gypsum Plaster by Glass Fibres" Science of Ceramics, Volume 5, 1970, pp539-564.

271 Agbin, C.C. "Concrete Reinforced with Glass Fibre" Magazine of Concrete Research, Volume 16, No 49, pp195-202.

272 Steele, B.R. "Glass Fibre Reinforced Cement" Prospects for Fibre Reinforced Construction Materials, Proceedings of the International Building Exhibition Conference, November 1971, pp29-36.

273 Shroff, J.K. "The Effect of a Corrosive Environment on the Properties of Steel Fibre Reinforced Portland Cement Mortar" MSc Thesis, Clarkson College of Technology, September 1966.

274 Dixon, J. and Mayfield, B. "Concrete Reinforced with Fibrous Wire" Concrete, Volume 5, No 3, March 1971, pp73-76.

275 Cahn, D.S. et al "Durability of Fibre Glass - Portland Cement Composite" Journal of A.C.I., Volume 70, No 3, March 1973, pp187-189.

276 Hannant, D.J. "Steel Fibre Reinforced Concrete" Prospects for Fibre Reinforced Construction Materials, Proceedings of the International Building Exhibition Conference, November 1971, pp47-55.

CHAPTER 3

301 CP114:1969 "The Structural Use of Reinforced Concrete in Buildings" The British Standards Institution, London, 1969.

302 CP115:1969 "The Structural Use of Prestressed Concrete in Buildings" The British Standards Institution, London, 1969.

303 A.C.I. 318-63 "Building Code Requirements for Reinforced Concrete" Journal of A.C.I. Proceedings, Volume 59, No 2, February 1962, pp145-276.

304 "Report on Structural Safety" The Structural Engineer, Volume 33, May 1955, pp141-149.

305 Freudenthal, A.M. "Safety and Probability of Structural Failure" Paper No 2843, Transaction A.S.C.E., Volume 21, 1956, pp1337-1375.

306 Pugsley, A.G. "Design for Safety and Efficiency" The Structural Engineer, Volume 35, No 1, January 1957, pp36-40.

307 Thomas, F.G. "Basic Parameters and Terminology in the consideration of Structural Safety" C.I.B. Bulletin, No 3, 1964.

308 Gvozdev, A.A., Dmitriev, S.A. and Kalatourov, B.A. "Russian Limit State Design Method for Prestressed Concrete" Translation No 117, pp1-16, C. and C.A.

309 C.E.B.-F.I.P. Joint Committee "International Recommendations for the Design and Construction of Concrete Structures" C. and C.A., June 1970.

310 A.C.I. 318-71 "Building Code Requirements for Reinforced Concrete" Detroit Michigan 1971.

311 CP110:1972 "Code of Practice for the Structural Use of Concrete" British Standards Institution, London, 1972.

312 CP3: Chapter 5: 1967 "Code of Basic Data for the Design of Buildings" British Standards Institution, London, 1972.

313 Abeles, P.W. "The Limit States of Design in Reinforced and Prestressed Concrete" The Consulting Engineer, Volume 32, No 6, June 1968, pp57-65.

314 Abeles, P.W. "Partial Prestressing and its suitability for Limit State Design" The Structural Engineer, Volume 49, No 2, February 1971, pp67-86.

315 Whitney, C.S. "Plastic Theory of Reinforced Concrete Design" Paper No 2133, Translation A.S.C.E., Volume 107, 1942, pp251-326.

316 Evans, R.H. "The Plastic Theories for the Ultimate Strength of Reinforced Concrete Beams" Journal of I.C.E., Volume 21, No 2, December 1943, pp98-117.

317 Baker, A.A.I. "A Plastic Theory of Design for Ordinary Reinforced and Prestressed Concrete, Including Moment Redistribution in Continuous Members" Magazine of Concrete Research, No 2, June 1949, pp57-66.

318 Warwarak, J., Sozen, M.A. and Sien, P. "Strength and Behaviour in Flexure of Prestressed Concrete Beams" Engineering Experiment Station, University of Illinois, Bulletin No 464.

319 C.E.B. "Recommendations for an International Code of Practice for Reinforced Concrete" Translation by A.C.I. and C. and C.A.

320 Yu, W. and Winter, G. "Instantaneous and Long Term Deflections of Reinforced Concrete Beams under Working Loads" Journal of A.C.I. Proceedings, Volume 57, No 1, July 1960, pp29-50.

321 A.C.I. Committee 318 "Building Code Requirements for Reinforced Concrete" A.C.I. Detroit, 1963.

322 Branson, D.E. "Instantaneous and Time - Dependent Deflections of Simple and Continuous Reinforced Concrete Beams" Report No 7, Alabama Highway Research Report, Bureau of Public Roads, August 1963.

323 Beeby, A.W. "Short Term Deformation of Reinforced Concrete Members" C. and C.A. Technical Report No TRA408, March 1968.

324 Hognestad, F. "High Strength Bars as Concrete Reinforcement, Part 2, Control of Flexural Cracking" Journal of P.C.A., Bulletin D53, No 1, January 1962, pp46-62.

325 Broms, B.B. "Crack Width and Crack Spacing in Reinforced Concrete Members" Journal of A.C.I., Volume 62, No 10, October 1965, pp1237-1255.

326 Base, G.D., Beeby, A.W., Reed, J.B. and Taylor, H.P.J. "An Investigation of the Crack Characteristics of Various Types of Bar in Reinforced Concrete Beams" C. and C.A. Report No 18, parts 1 and 2, 1966.

327 Abeles, P.W. "Design of Partially Prestressed Concrete Beams" Journal of A.C.I., Volume 65, No 10, October 1967, pp669-677.

328 Abeles, P.W. "Cracking and Bond Resistance in High Strength Reinforced Concrete Beams, Illustrated by Photoelastic Coating" Journal of A.C.I. Proceedings, Volume 63, No 11, 1966, pp1265-1278.

329 Bennet, E.W. and Chandrasekhar, C.S. "Calculation of the Widths of Cracks in Class 3 Prestressed Beams" Proceedings of I.C.E., Volume 49, July 1971, pp333-346.

330 Veerasubramanian, N. "Effect of Shape of Cross-Section on the Flexural Behaviour of Class 3 Prestressed Concrete Beams" PhD Thesis, University of Leeds, 1971.

331 Beeby, A.W. and Taylor, H.P.J. "Cracking in Partially Prestressed Members" Preliminary Publication, Sixth F.I.P. Congress, Prague, 1970, Concrete Society, London.

CHAPTER 4

401 CP110:1972 "Code of Practice for the Structural Use of Concrete" British Standards Institution, London, 1972.

402 Beeby, A.W. "Short Term Deformation of Reinforced Concrete Members" C. and C.A. Technical Report No TRA408, March 1968.

403 Garwood, T.G. "Flexural Behaviour of Class 3 Post Tensioned Prestressed Concrete Beams Using Various Types of Untensioned Steel" PhD Thesis, University of Salford, 1972.

CHAPTER 5

501 British Standard 1881: 1970 "Methods of Testing Concrete" British Standards Institution, London, 1970.

502 CP110: 1972 "Code of Practice for the Structural Use of Concrete" British Standards Institution, London, 1972.

503 CP115:1969 "The Structural Use of Prestressed Concrete in Building" British Standards Institution, London, 1969.

504 Bennett, E.W. and Dave, N.J. "Test Performances and Design of Concrete Beams with Limited Prestress" The Structural Engineer, Volume 47, No 12, December 1969, pp487-496.

505 A.S.C.E.-A.C.I. Committee on Composite Construction "Tentative Recommendations for Design and Construction of Composite Beams and Girders for Buildings" Proceedings of A.S.C.E., Volume 86, No ST12, Part 1, December 1960, pp73-92.

506 Marshal, W.T. "A Theory for End Zone Stresses in Pretensioned Concrete Beams" Journal of the Prestressed Concrete Institute, Volume 11, No2, April 1966, pp45-51.

507 Guyon, Y. "Prestressed Concrete" Contractors Record Limited, London, 1953.

508 Saunders, J. "Instantaneous Deflection of Reinforced Concrete Beams" Final Year Project, University of Salford 1970.

509 Bennett, E.W. and Loat, D.R. "Shrinkage and Creep of Concrete as Affected by the Fineness of Portland Cement" Magazine of Concrete Research, Volume 22, No 71, June 1970, pp69-78.

CHAPTER 6

601 Bennett, E.W. and Dave, N.J. "Test Performance and Design of Concrete Beams with Limited Prestress" The Structural Engineer, Volume 47, No 12, December 1969, pp487-496.

602 CP110:1972 "Code of Practice for the Structural Use of Concrete" British Standards Institution, London, 1972.

603 Evans, R.H. and Kong, F.K. "Estimation of Shrinkage of Concrete in Reinforced and Prestressed Concrete Design" Civil Engineer and Public Works Review, Volume 62, May 1967, pp559-561.

604 Walley, F. "Prestressed Concrete Design and Construction" H.M.S.O. London, 1953.

605 Garwood, T.G. "Flexural Behaviour of Class 3 Post-Tensioned Prestressed Concrete Beams Using Various Types of Untensioned Steel" PhD Thesis, University of Salford, 1972.

606 Gesund, H. "Shrinkage and Creep Influence on Deflections and Moments of Reinforced Concrete Beams" Journal of A.C.I., Volume 59, No 5, May 1962, pp687-704.

CHAPTER 7

701 Garwood, T.G. "Flexural Behaviour of Class 3 Post-Tensioned Prestressed Concrete Beams Using Various Types of Untensioned Steel" PhD Thesis, University of Salford, 1972.

702 Abeles, P.W. and Kung, R. "Prestress Losses Due to the Effect of Shrinkage and Creep on Non-Tensioned Steel" Journal of A.C.I., Volume 70, No 4, January 1973, pp19-27.

703 Abeles, P.W. "The Effect of Non-Tensioned Steel in Prestressed Concrete". Reinforced Concrete Review, June 1961, pp635-642.

704 A.C.I. 318-71 "Building Code Requirements for Reinforced Concrete" Detroit, Kichigan, 1971.

705 CP110:1972 "Code of Practice for the Structural Use of Concrete" British Standards Institution, London, 1972.

706 Evans, R.H. and Chung, H.W. "Shrinkage and Deflection of Composite Prestressed Concrete Beams" Concrete, May 1967, pp157-166.

707 Evans, R.H. and Parker, A.S. "Behaviour of Prestressed Concrete Composite Beams" Proceedings of A.C.I., Volume 51, 1954, pp861-878.

708 Branson, D.E. and Ozell, A.M. "A Report on Differential Shrinkage in Composite Concrete Beams" Journal of Prestressed Concrete Institute, Volume 4, No 3, December 1959, pp61-69.

709 Kajfasz, S., Somerville, B. and Rowe, R.E. "An Investigation of the Behaviour of Composite Concrete Beams" Research Report No 15, November 1963, C. and C.A., London.

710 Chung, H.W. "Application of Lightweight Concrete to Prestressed Composite Construction" PhD Thesis, University of Leeds, 1966.

711 Hanson, N.W. "Precast - Prestressed Concrete Bridges : 2. Horizontal Shear Connections" Journal of Portland Cement Association Research and Development Laboratories, Volume 2, No 2, May 1960, pp38-58.

712 Beeby, A.W. "Short Term Deformation of Reinforced Concrete Members" C. and C.A. Technical Report No TRA408, March 1968.

713 Gunasekaran, M. and Ichikawa, Y. "The Strength and Behaviour of Steel Fiber Reinforced Lightweight Concrete Made with Regulated Set Cement and Sintered Fly-Ash Aggregates" Fiber Reinforced Concrete, SP44, A.C.I., Detroit, 1974, p 117.

714 Williamson, G.R. "The Effect of Steel Fibers on the Compressive Strength of Concrete" Fiber Reinforced Concrete, SP44, A.C.I., Detroit, 1974, p 201.

715 Takagi, J. "Some Properties of Glass Fiber Reinforced Concrete" Fiber Reinforced Concrete, SP44, A.C.I., Detroit, 1974, p 101.

716 Hajnal-Konyi, K. "Tests on Beams with Sustained Loading" Magazine of Concrete Research, Volume 15, No 43, March 1963.

717 Hollington, M.R. "A Series of Long Term Tests to Investigate the Deflection of a Representative Precast Concrete Floor Component" C. and C.A. Technical Report TRA 422, April 1970.

718 Chandrasekhar, C.S. "A Study of the Influence of the Properties and Distribution of the Reinforcement on the Behaviour of Beams with Limited Prestress" PhD Thesis, University of Leeds, 1970.

719 Dave, N.J. "Limited Prestressing as a Means of Economy in Structural Concrete" PhD Thesis, University of Leeds, 1967.

720 Rimmer, B. "A Study of Some Prestressed Concrete Beams Under Sustained and Repeated Loading" PhD Thesis, University of Leeds, 1964.

721 Gadre, A.H. "Sustained Load Tests on Prestressed Concrete Beams" PhD Thesis, University of Leeds, 1961.

722 Abeles, P.W. "Static and Fatigue Tests on Partially Prestressed Concrete Constructions". Journal of A.C.I., Volume 51, December 1954, pp361-376.

723 Sawko, F. and Saha, G.P. "Fatigue of Concrete and its Effect Upon Prestressed Concrete Beams". Magazine of Concrete Research, Volume 20, No 62, March 1968, pp21-30.

724 Cottingham, W.S., Washa, G.W. and Fluck, P.G. "Creep of Prestressed Concrete Beams" Journal of A.C.I., Volume 57, No 2, February 1961, pp929-936.

725 Clare, H.J. "Private Communication" Design Section, Cem-Fil Project, Pilkington's Research and Development Laboratories, Lathom.

726 Evans, R.H. "Extensibility and Modulus of Rupture of Concrete" The Structural Engineer, December 1946, pp636-658.

727 Edgington, J. "Private Communication" University of Surrey, 1972.

TABLE 5.1. TEST PROGRAMME

Beam	Series	Loading	Insitu Concrete	Compression Steel	Fibre	Class
PC PW PG	P	Short Term	- - -	- - -	- Wire Glass	4 4 4
RC RW RG	R	Short Term	- - -	- - -	- Wire Glass	4 4 4
XN9 XL9 XL6 XL3 XN3	X	Short Term	Norm Wt Light Wt Light Wt Light Wt Norm Wt	Kam 90 Kam 90 Kam 60 M. St M. St	- - - - -	3 3 3 3 3
S2a S2 S3a S3 SW2 SW3 SG2 SG3	S	Short Term	Light Weight	Mild Steel	- - - - Wire Wire Glass Glass	2 2 3 3 2 3 2 3
F2 F3 FG2 FG3	F	Fatigue	Light Weight	Mild Steel	- - Glass Glass	2 3 2 3
L2 L3 LG2 LG3	L	Long Term	Light Weight	Mild Steel	- - Glass Glass	2 3 2 3

TABLE 5.2. CONCRETE MIX PROPORTIONS

Material	Series P,R	Series X			Series S,F,L	
		Web	Flange		Web	Flange
			N.Wt.	L.Wt.		
H.A. Cement	-	1.0	-	-	-	-
R.H.P. Cement	1.0	-	-	-	1.0	-
O.P. Cement	-	-	1.0	1.0	-	1.0
Fine Aggregate	1.0	2.0	2.0	-	1.0	-
Coarse Aggregate	2.0	4.0	4.0	-	2.0	-
L.Wt. Fine Agg.	-	-	-	1.24	-	1.24
L.Wt. Coarse Agg.	-	-	-	1.67	-	1.67
Water	0.42	0.40	0.60	0.82	0.42	0.82

TABLE 5.3. PRECAST CONCRETE PROPERTIES

Beam or Series	Cube Strength (N/mm^2)		Cylinder Strength	Mod. of Rupture	Mod. of Elasticity	Density
	U_t	U_w	(N/mm^2)	(N/mm^2)	(kN/mm^2)	(kg/m^3)
PC, RC	-	60.7	-	5.60	-	2280
PW, RW	-	56.5	-	6.47	-	2315
PG, RG	-	60.7	-	5.60	-	2280
X	52.5	67.6	43.0	5.70	31.00	2400
S2a, F2	46.3	56.5	41.1	5.08	28.91	2280
S2, F3	46.8	58.3	40.7	5.45	30.64	2280
S3a, L2	47.8	61.3	42.3	5.45	30.64	2290
S3, L3	48.7	63.2	42.7	5.53	31.00	2315
SG2, SG3	47.0	59.8	42.8	5.48	30.64	2270
SW2, SW3	46.0	56.5	48.5	6.47	29.33	2315
FG2, LG2	59.7	72.0	43.0	5.80	31.10	2315
FG3, LG3	60.7	72.2	43.2	5.80	31.58	2315

TABLE 5.4. INSITU CONCRETE PROPERTIES

Beam Notation	Cube Strength (N/mm^2)	Cylinder Strength (N/mm^2)	Mod. of Rupture (N/mm^2)	Mod. of Elasticity (kN/mm^2)	Density (kg/m^3)
XN9	40.9	32.1	5.50	25.43	2300
XL9	38.4	27.4	3.10	13.02	1580
XL6	39.8	33.3	3.22	13.33	1600
XL3	39.5	33.3	3.22	13.42	1610
XN3	41.7	33.2	5.67	26.05	2320
S2a	42.0	36.8	3.00	14.85	1650
S2	40.8	35.5	2.60	13.51	1600
S3a	40.5	35.4	2.95	13.87	1625
S3	41.4	35.5	2.78	14.36	1625
SG2	41.8	36.7	2.65	14.98	1635
SG3	41.0	35.5	2.67	14.00	1615
SW2	44.3	38.8	2.80	14.83	1655
SW3	40.0	34.7	2.65	13.38	1615
F2	44.2	43.0	3.31	14.32	1635
F3	39.2	31.5	3.21	13.33	1600
FG2	43.3	43.0	3.07	14.88	1625
FG3	45.0	38.5	2.98	13.76	1660
L2	44.7	38.0	3.45	13.69	1635
L3	43.5	37.6	3.37	13.51	1625
LG2	40.2	36.8	2.50	13.78	1625
LG3	41.2	34.2	2.68	13.69	1615

TABLE 5.5. STEEL PROPERTIES

Beam or Series	Steel	Diameter (mm)	X-Sect Area (mm^2)	Mod. of Elasticity (kN/mm^2)	0.2% Proof Stress (N/mm^2)	Ultimate Stress (N/mm^2)
X	P/S Wire	7.0	38.5	195.0	1480	1780
X	Kam 90	12.7	126.5	197.0	845	945
X	Kam 60	12.7	126.5	197.0	674	894
X	M.St	12.7	126.5	203.0	296	426
S2a, F2	P/S Wire	7.0	38.5	201.5	1382	1690
S2, F3	"	"	"	"	"	"
S3a, L2	"	"	"	"	"	"
S3, L3	P/S Wire	7.0	38.5	207.9	1360	1651
SG2, SG3	"	"	"	"	"	"
FG2, LG2	"	"	"	"	"	"
FG3, LG3	"	"	"	"	"	"
SW2, SW3	P/S Wire	7.0	38.5	198.2	1466	1763
S, F, L	M.St.	10.0	78.5	207.0	306	442

TABLE 5.6. FIBROUS-CEMENT PROPERTIES

Beam or Series	Mod. of Elasticity (kN/mm^2)	Mod. of Rupture (N/mm^2)	Density (kg/m^3)	Glass Content (%)	Thickness of Sheet (mm)
P, R	12.8	22.4	2235	4.85	6.4
SG2, SG3	12.8	44.6	2200	5.15	6.1
FG2, FG3	12.8	20.0	2175	6.62	4.7
LG2, LG3	12.8	24.3	2165	5.11	6.0

PAGE

NUMBERING

AS ORIGINAL

TABLE 7.1.

PRESTRESSES (OBSERVED) IN SOFFIT OF BEAMS (N/mm^2)

Beam Notation	At Transfer	Dead Load	Losses: Tensioned Steel	Losses: Untensioned Steel	Differential Shrinkage	Residual Prestress	% Loss
XN9	24.80	-1.44	-8.21	-	-1.37	13.78	44
XL9	24.80	-1.33	-8.21	-	-1.57	13.69	45
XL6	24.80	-1.32	-8.21	-	-1.74	13.53	45
XL3	24.80	-1.33	-8.21	-	-1.53	13.73	45
XN3	24.80	-1.44	-8.21	-	-1.01	14.14	43
S2a	23.18	-1.26	-8.42	-	-0.67	12.83	45
S2	21.69	-1.28	-6.06	-0.26	-0.84	13.25	39
S3a	18.31	-1.29	-4.37	-0.90	-0.83	10.92	40
S3	16.80	-1.29	-4.25	-1.09	-0.69	9.48	44
SG2	24.01	-1.37	-7.68	-0.31	-0.82	13.88	42
SG3	18.60	-1.38	-4.93	-1.32	-0.78	10.19	45
SW2	21.69	-1.28	-6.63	-0.26	-0.96	12.56	42
SW3	16.80	-1.29	-4.10	-1.11	-1.00	9.30	45
F2	21.69	-1.26	-7.51	-0.27	-1.27	11.38	48
F3	16.80	-1.29	-3.72	-1.08	-1.37	9.34	44
FG2	23.46	-1.37	-7.14	-0.30	-1.05	13.60	42
FG3	18.18	-1.40	-4.66	-1.26	-1.01	9.85	46
L2	21.69	-1.30	-6.83	-0.26	-1.38	11.92	45
L3	16.80	-1.30	-4.18	-1.09	-1.37	8.86	47
LG2	24.01	-1.40	-7.46	-0.30	-0.82	14.03	42
LG3	18.60	-1.41	-4.90	-1.30	-0.86	10.13	46
Av.Loss		7%	28%	4%	5%	-	44%
Class 2		6%	31%	1%	4%		42%
Class 3		8%	25%	7%	6%		46%

TABLE 7.2.

PRESTRESSES (CALCULATED) IN SOFFIT OF BEAMS (N/mm^2)

Beam Notation	At Transfer	Dead Load	Losses: Tensioned Steel	Losses: Untensioned Steel	Differential Shrinkage	Residual Prestress	% Loss
XN9	24.80	-1.44	-8.65	-	-0.25	14.46	42
XL9	24.80	-1.33	-8.65	-	-2.54	12.28	50
XL6	24.80	-1.33	-8.65	-	-2.91	11.91	52
XL3	24.80	-1.33	-8.65	-	-2.98	11.84	52
XN3	24.80	-1.44	-8.65	-	-0.51	14.20	43
S2a	23.18	-1.26	-7.51	-	-0.75	13.66	41
S2	21.69	-1.28	-6.62	-0.34	-0.76	12.69	41
S3a	18.31	-1.29	-4.90	-1.20	-0.77	10.15	45
S3	16.80	-1.29	-4.40	-1.46	-0.78	8.87	47
SG2	24.01	-1.37	-7.92	-0.41	-1.16	13.15	45
SG3	18.06	-1.38	-5.10	-1.72	-1.51	8.89	52
SW2	21.69	-1.28	-6.65	-0.34	-1.24	12.18	44
SW3	16.80	-1.29	-4.31	-1.45	-1.27	8.48	50
F2	21.69	-1.27	-6.77	-0.34	-1.42	11.89	45
F3	16.80	-1.29	-4.26	-1.45	-1.03	8.77	48
FG2	23.46	-1.37	-7.61	-0.39	-0.54	13.55	42
FG3	18.18	-1.40	-4.88	-1.65	-0.60	9.65	47
L2	21.69	-1.30	-6.62	-0.34	-1.46	11.97	45
L3	16.80	-1.30	-4.38	-1.48	-1.32	8.32	50
LG2	24.01	-1.41	-9.03	-0.39	-0.68	13.50	44
LG3	18.60	-1.41	-5.07	-1.70	-0.76	9.66	48
Av.Loss		7%	29%	5.5%	5.5%		47%
Class 2		6%	32%	2%	5%		45%
Class 3		8%	26%	9%	6%		49%

TABLE 7.3. DIFFERENTIAL SHRINKAGE STRAINS

Beam Notation	Age of Web (days)			Differential Shrinkage (microstrain)	
	Flange Cast	Start of Test	Failure	Observed	Calculated
XN9	180	268	269	162	30
XL9	187	275	276	228	370
XL6	194	282	283	251	420
XL3	201	289	290	221	430
XN3	208	296	297	119	60
S2a	28	54	55	98	110
S2	28	54	55	122	110
S3a	28	54	55	118	110
S3	28	54	55	97	110
SG2	35	62	63	106	150
SG3	42	69	70	104	200
SW2	37	64	65	139	180
SW3	44	71	72	149	190
F2	56	179	292	189	210
F3	56	270	313	199	150
FG2	35	110	190	137	70
FG3	35	181	223	133	80
L2	56	180	746	199	210
L3	56	173	740	197	190
LG2	28	71	545	108	90
LG3	28	57	532	113	100

TABLE 7.4. OBSERVED LOADS FOR T-BEAMS (kN)

Beam Notation	Decompression Load	Cracking Load	Maximum Load		Ultimate Load
			First Cycle	Second Cycle	
XN9	46.1	65.0	60.0	75.0	108.0
XL9	41.8	55.5	"	"	103.0
XL6	41.5	60.0	"	"	102.0
XL3	42.1	55.0	"	"	98.5
XN3	47.5	70.0	"	"	110.0
S2a	40.6	53.0	48.0	60.0	126.2
S2	40.8	52.0	"	"	126.4
S3a	33.8	45.5	"	"	124.4
S3	29.4	40.0	"	"	121.6
SG2	40.3	62.5	"	"	122.0
SG3	29.3	48.0	"	"	124.0
SW2	39.6	47.0	"	"	133.2
SW3	28.9	37.5	"	"	134.3
F2	35.8	46.0	48.0	60.0	123.6
F3	28.7	40.0	"	"	-
FG2	39.9	-	"	"	121.6
FG3	28.5	47.0	"	"	123.0
L2	36.8	47.0	48.0	60.0	122.0
L3	27.3	37.0	"	"	119.0
LG2	40.1	-	"	"	118.5
LG3	28.8	48.0	"	"	118.3

TABLE 7.5. CALCULATED LOADS FOR T-BEAMS (kN)

Beam Notation	Decompression Load	Cracking Load	Working Load		Ultimate Load
			L.S.L. Damage	L.S. Collapse	
XN9	48.4	60.8	59.1	77.2	130.3
XL9	37.5	48.8	55.2	77.6	129.8
XL6	36.5	47.9	54.3	77.8	130.2
XL3	36.3	47.7	54.1	77.8	130.2
XN3	47.7	60.1	58.4	77.5	130.8
S2a	43.2	54.3	50.2	70.6	118.6
S2	39.1	49.9	48.9	70.6	118.5
S3a	31.4	42.4	46.2	70.5	118.4
S3	27.5	38.8	45.5	67.9	114.3
SG2	38.1	57.1	47.4	68.5	115.2
SG3	25.5	44.3	42.2	68.2	114.6
SW2	38.4	49.3	48.4	75.3	126.1
SW3	26.3	37.1	44.3	74.7	125.1
F2	37.4	48.4	47.5	70.9	119.0
F3	27.0	37.9	44.8	70.3	118.0
FG2	39.8	59.8	49.2	68.6	115.4
FG3	27.9	47.5	44.7	68.7	115.6
L2	36.9	48.0	46.8	70.9	119.0
L3	25.6	36.8	43.5	68.6	115.4
LG2	38.6	58.0	47.7	68.1	114.5
LG3	27.4	46.7	43.9	68.1	114.6

TABLE 7.6.

RATIO OF OBSERVED TO CALCULATED LOADS

Beam Notation	Decompression Load	Cracking Load	Ultimate Load
XN9	0.95	1.07	0.83
XL9	1.11	1.14	0.79
XL6	1.14	1.25	0.78
XL3	1.15	1.23	0.76
XN3	1.00	1.16	0.84
S2a	0.94	0.98	1.06
S2	1.04	1.04	1.07
S3a	1.08	1.07	1.05
S3	1.07	1.03	1.06
SG2	1.06	1.09	1.06
SG3	1.15	1.08	1.08
SW2	1.03	0.95	1.06
SW3	1.10	1.01	1.07
F2	0.96	0.95	1.04
F3	1.06	1.06	-
FG2	1.00	-	1.05
FG3	1.02	0.99	1.06
L2	1.00	0.98	1.03
L3	1.07	1.01	1.03
LG2	1.04	-	1.04
LG3	1.05	1.03	1.03
Average	1.05	1.06	1.05

TABLE 7.7. TEST RESULTS FOR RECTANGULAR BEAMS

Group (Average of five beams)	Cracking Load (kN)	Ultimate Load (kN)	Ratio F/C*	
			Cracking Load	Ultimate Load
PC	13.80	13.80	-	-
PW	15.90	15.90	1.15	1.15
PG	~~19.45~~ 18.50	19.45	~~1.41~~ 1.34	1.41
RC	18.60	34.15	-	-
RW	20.40	35.30	1.10	1.03
RG	26.10	35.25	1.40	1.03

*F - Fibre-Concrete
Fibrous-Cement Composite

C - Conventional Concrete

TABLE 7.8.

TEST RESULTS FOR T-BEAMS - DEFLECTIONS

Beam Notation	Deflection (mm) Calculated Working Load L.S.L. Damage	Deflection (mm) Calculated Working Load L.S. Collapse	Ratio F/C* Calculated Working Load L.S.L. Damage	Ratio F/C* Calculated Working Load L.S. Collapse
S2	8.6	26.6	-	-
SG2	7.6	15.5	0.89	0.61
SW2	10.0	30.3	1.16	1.18
S3	11.6	36.4	-	-
SG3	7.8	28.2	0.67	0.77
SW3	12.8	40.4	1.10	1.11
Group 2	11.3	-	-	-
Group G2	8.2	-	0.73	-
Group 3	15.3	-	-	-
Group G3	8.5	-	0.56	-
	Time (Days)		Time (Days)	
	50	500	50	500
L2	14.9	18.7	-	-
LG2	13.5	17.3	0.91	0.93
L3	25.6	30.8	-	-
LG3	18.5	25.3	0.72	0.82
	Load Cycles ($x10^6$)		Load Cycles ($x10^6$)	
	1	3	1	3
F2	19.0	23.3	-	-
FG2	10.0	12.6	0.53	0.54
F3	Fail	-	-	-
FG3	19.2	20.2	-	-

* F - Fibrous-Cement Composite Fibre Concrete

C - Conventional Concrete

TABLE 7.9.

TEST RESULTS FOR T-BEAMS - CRACK WIDTHS

Beam Notation	Crack Width (mm)		Ratio F/C*	
	Calculated Working Load		Calculated Working Load	
	L.S.L. Damage	L.S. Collapse	L.S.L. Damage	L.S. Collapse
S2	0	0.50	-	-
SG2	0	0.15	-	0.30
SW2	0.05	0.35	-	0.70
S3	0.15	0.50	-	-
SG3	0	0.25	0	0.50
SW3	0.15	0.60	1.0	1.20
	Time (Days)		Time (Days)	
	50	500	50	500
L2	0.10	0.20	-	-
LG2	0	0	0	0
L3	0.35	0.50	-	-
LG3	0.10	0.10	0.29	0.20
	Load Cycles ($x10^6$)		Load Cycles ($x10^6$)	
	1	3	1	3
F2	0.20	0.30	-	-
FG2	0	0.10	0	0.33
F3	Fail	-	-	-
FG3	0.15	0.20	-	-

* F - Fibrous-Cement Composite
Fibre Concrete

C - Conventional Concrete

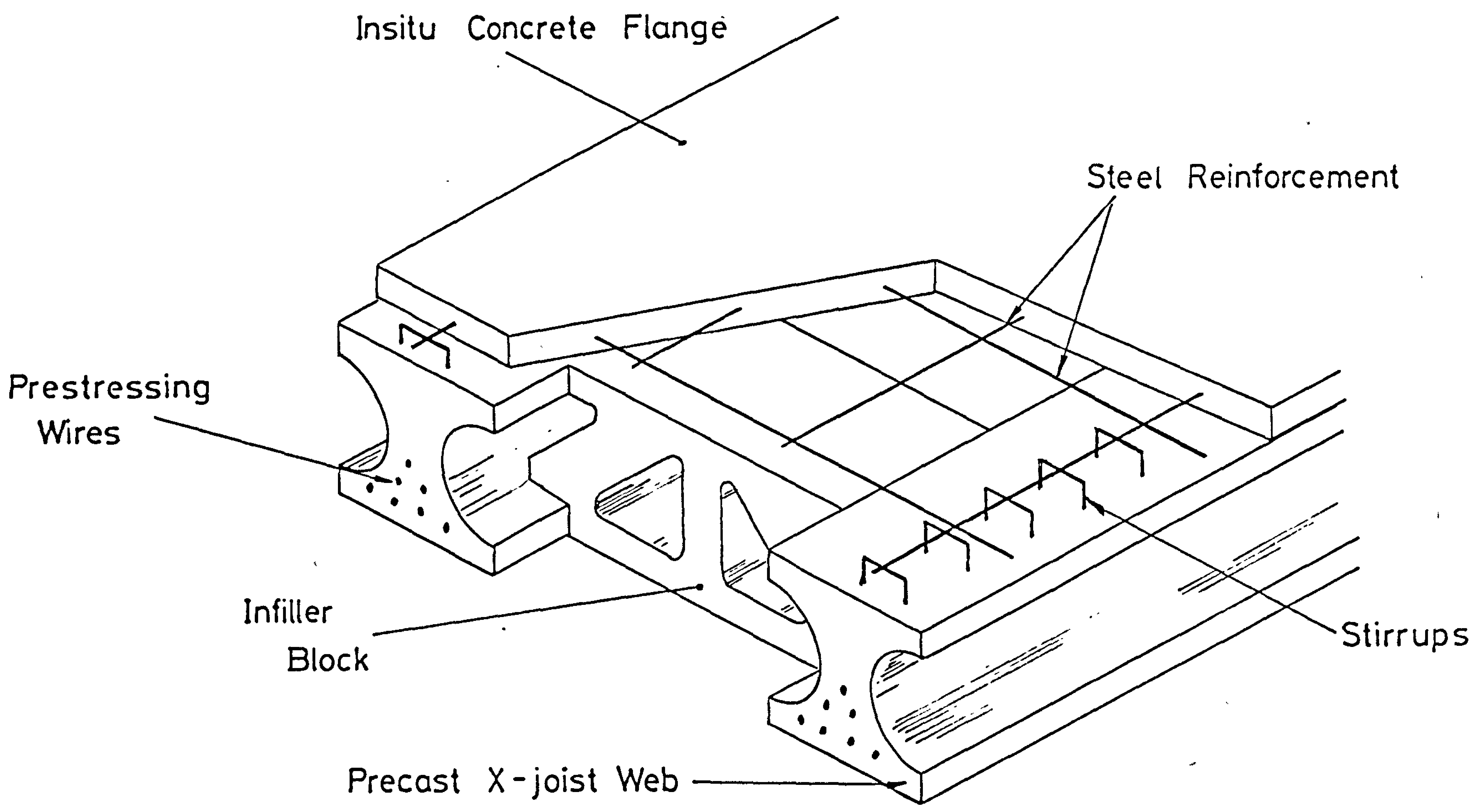

FIG. 1.1. COMPOSITE FLOOR CONSTRUCTION

FIG 1.2 FIBRE DISTRIBUTIONS

FIG. 3.1. DESIGN ASSUMPTIONS FOR ULTIMATE LIMIT STATE

FIG. 3.2. DESIGN ASSUMPTIONS FOR LIMIT STATE OF DEFLECTION

FIG. 4.1. STRAIN - COMPATABILITY CURVE

FIG. 4.2. STRESS CONDITIONS AT DECOMPRESSION & AFTER CRACKING

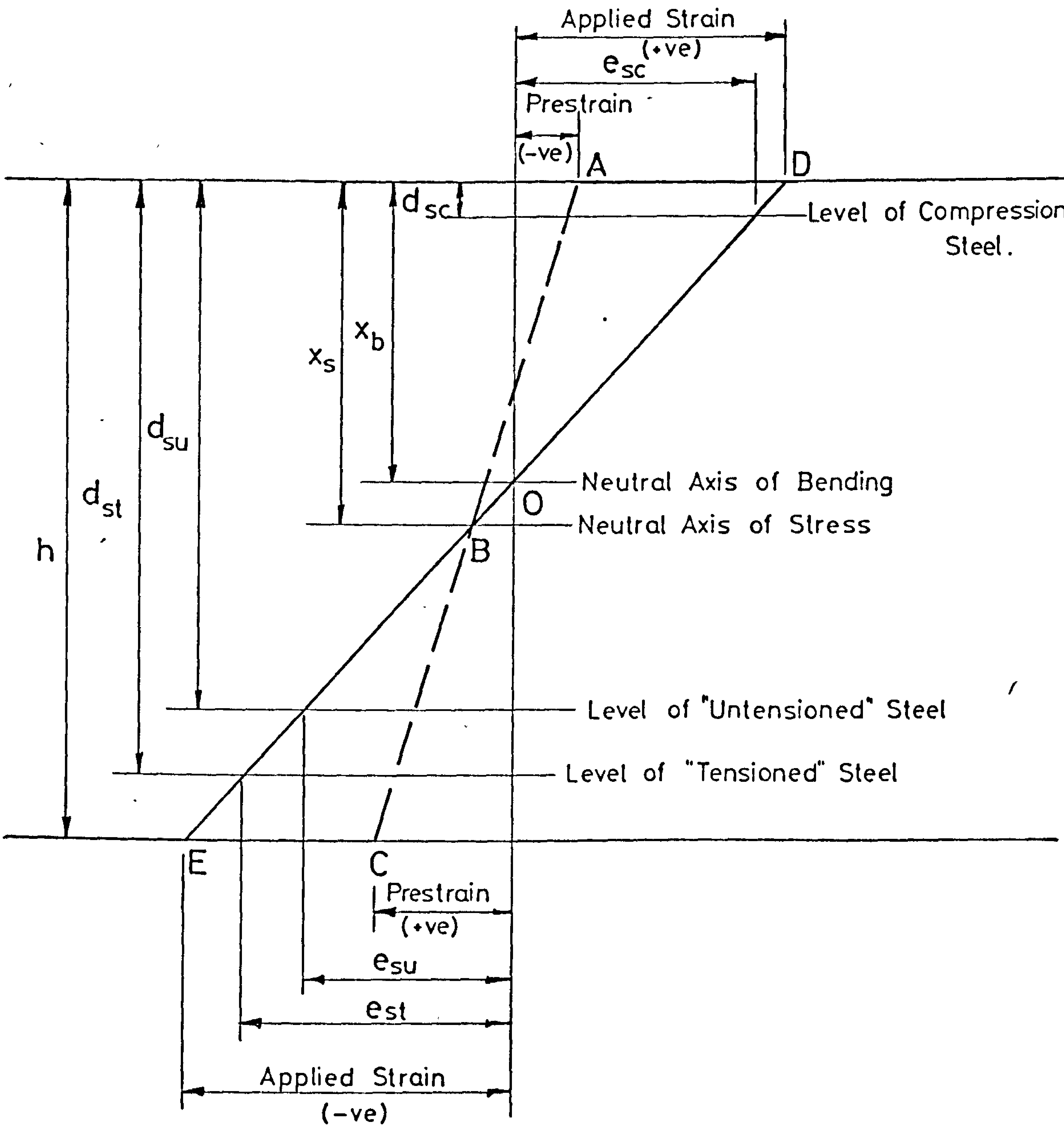

ABC - Strain Profile at Start of Test (Zero Applied Moment)

DOBE - Strain Profile due to Applied Moment

FIG. 4. 3. NEUTRAL AXES OF STRESS AND BENDING UNDER SHORT TERM LOADING

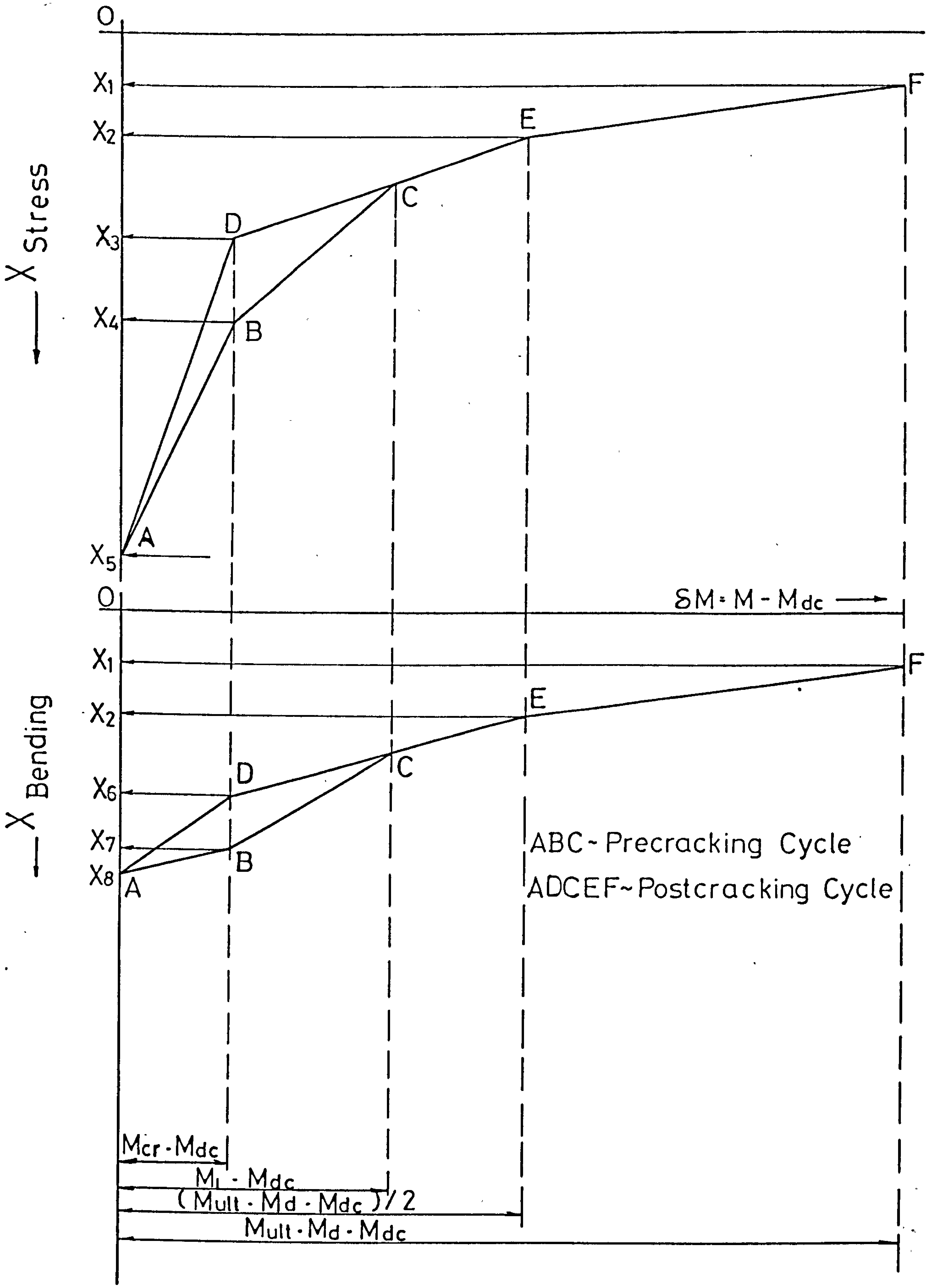

FIG. 4.4. PROPOSED RELATIONSHIPS BETWEEN THE APPLIED MOMENT & THE DEPTHS OF THE NEUTRAL AXES OF STRESS & BENDING

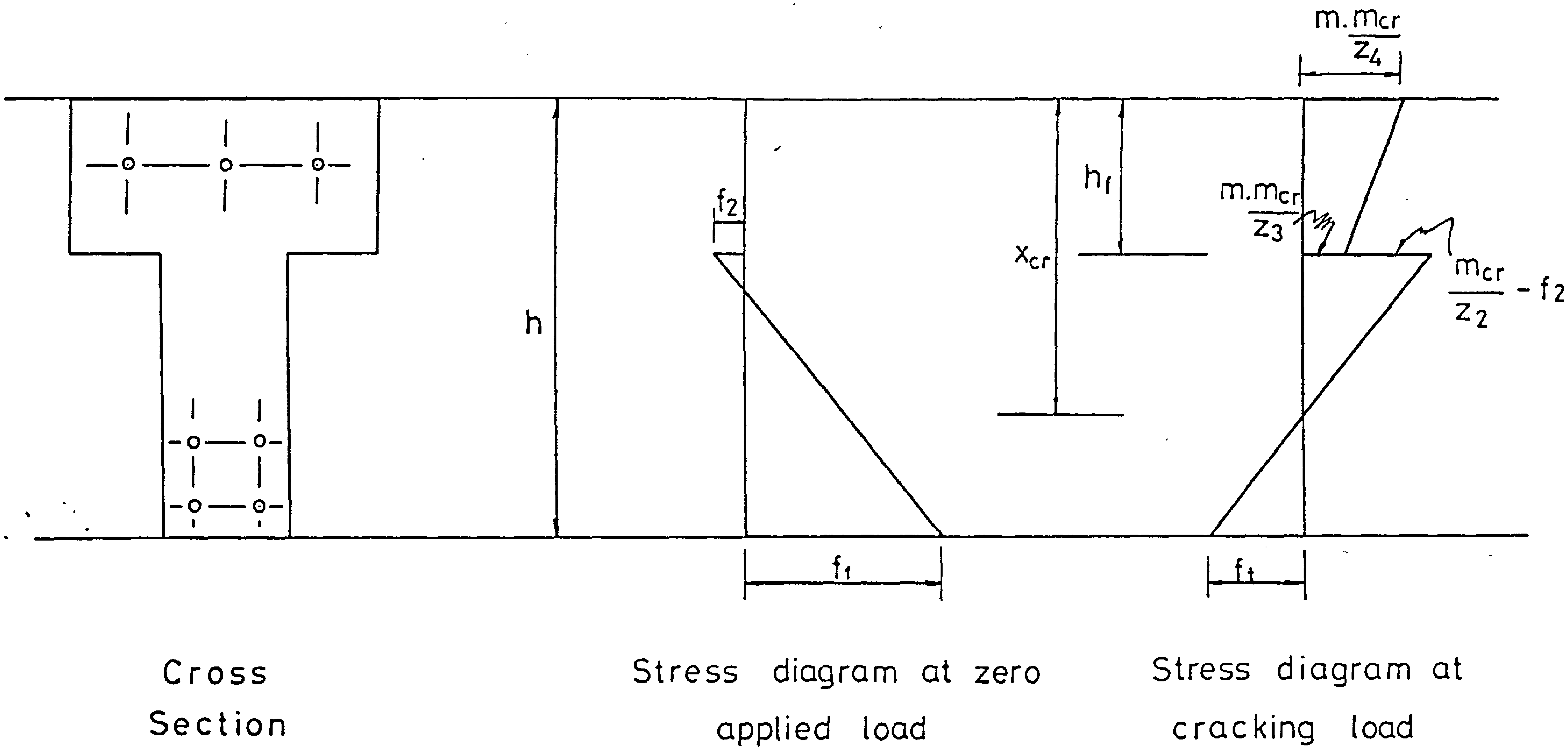

FIG. 4.5 STRESS CONDITIONS AT ZERO, APPLIED LOAD AND AT INSTANT OF CRACKING

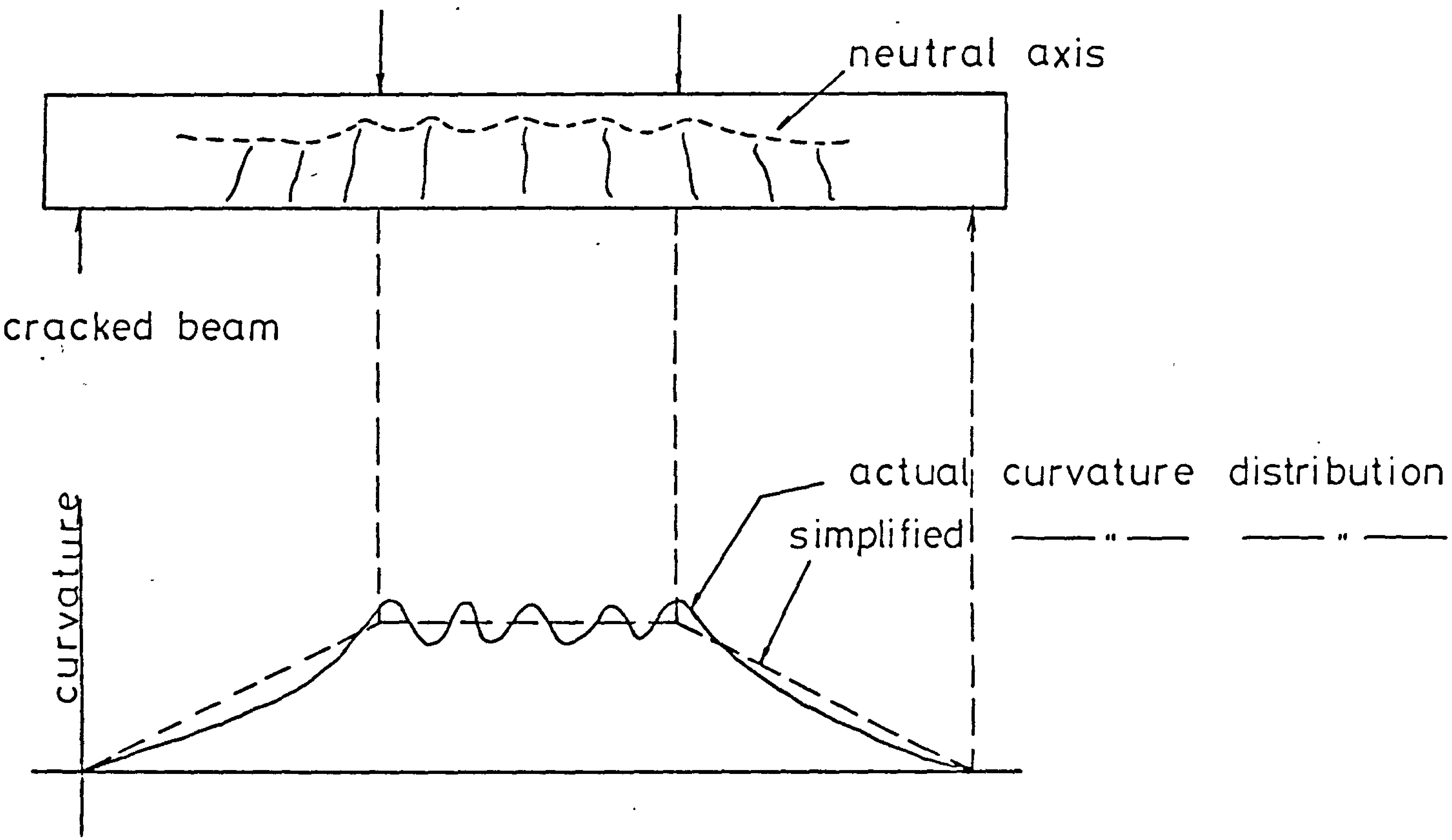

a) elevation of a cracked beam

b) curvature distribution along span

FIG. 4.6. CURVATURE DISTRIBUTION ALONG A CRACKED BEAM

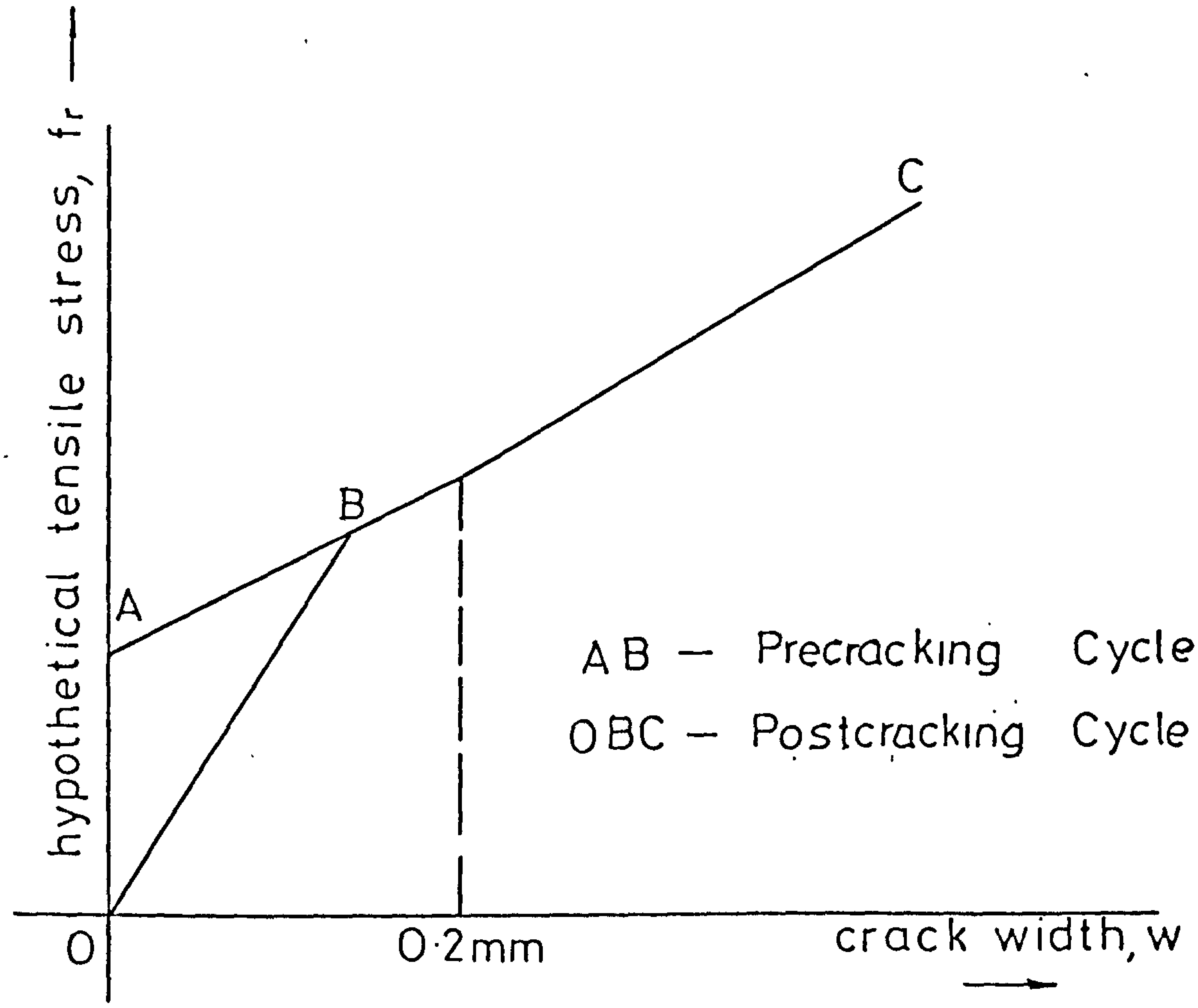

FIG. 4.7. PROPOSED RELATIONSHIP BETWEEN HYPOTHETICAL TENSILE STRESS & CRACK WIDTH

FIG.5.I. RECTANGULAR BEAM DETAILS - SERIES P

FIG. 5.2. RECTANGULAR BEAM DETAILS - SERIES R.

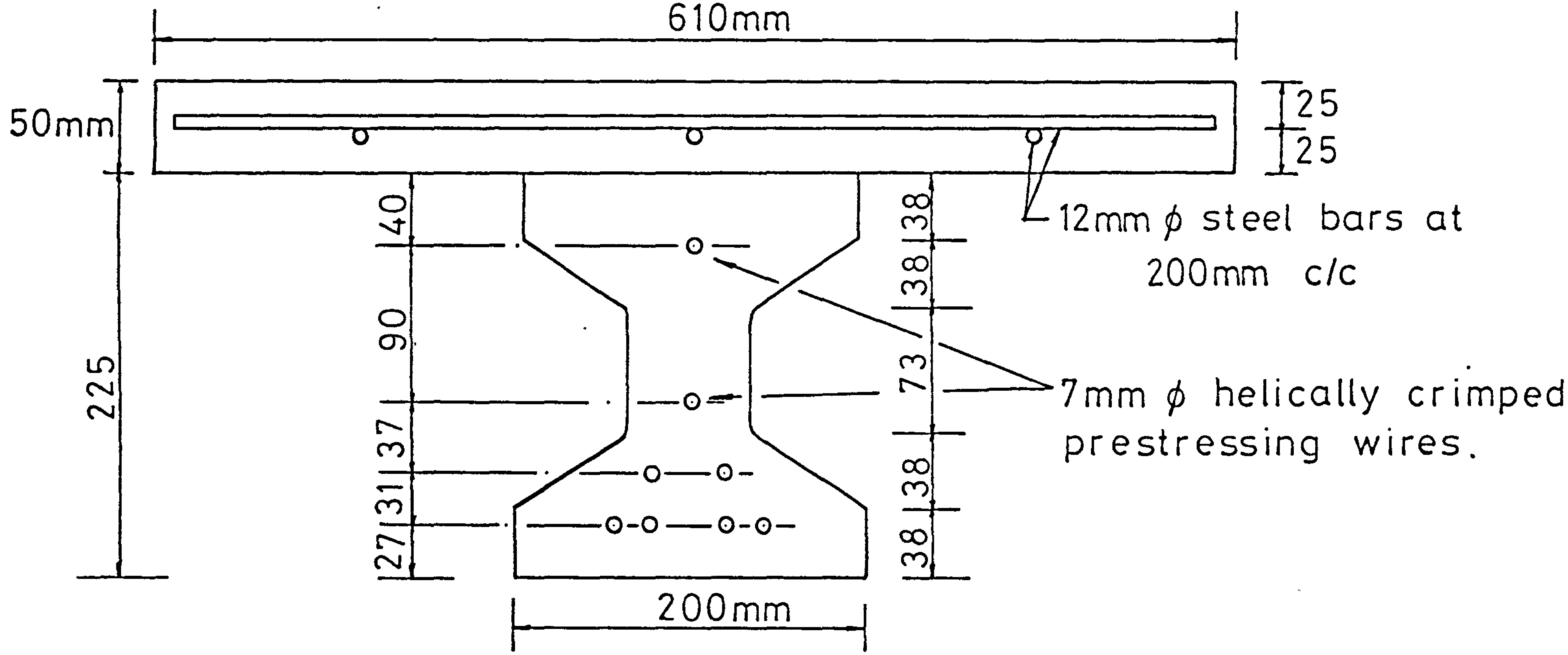

FIG. 5.3. T BEAM DETAILS - SERIES X.

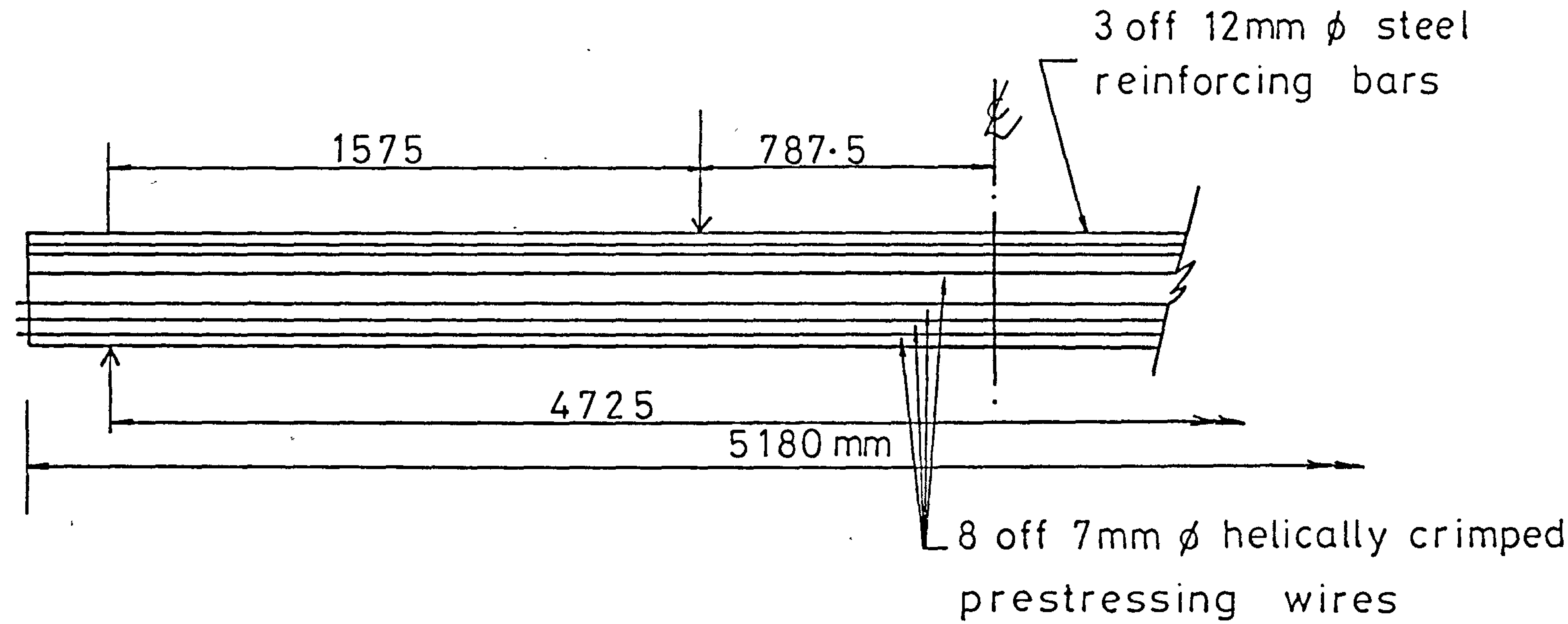

FIG. 5.4. T BEAM LONGITUDINAL SECTION - SERIES X.

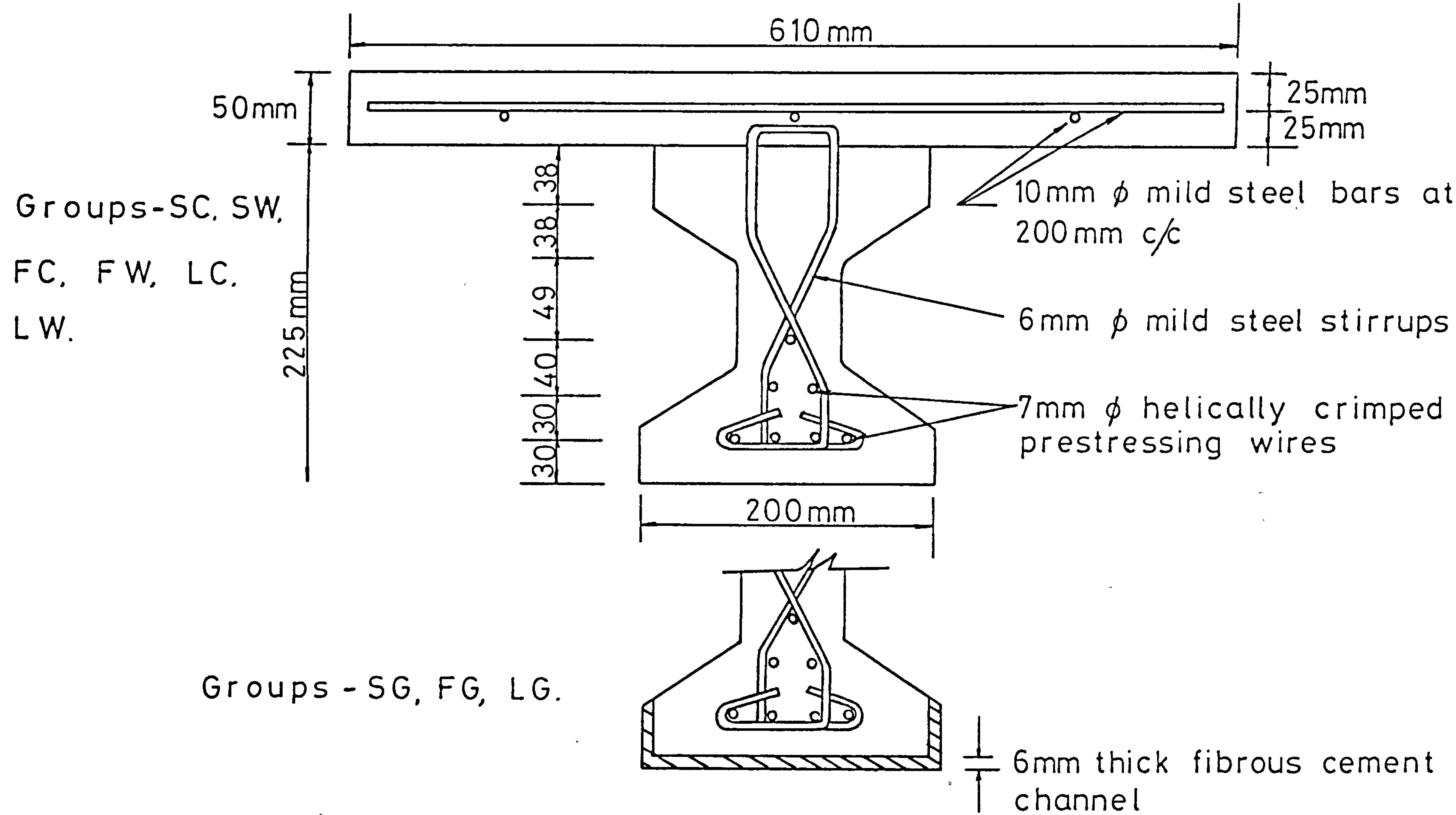

FIG. 5.5. T BEAM DETAILS - SERIES S.F. & L.

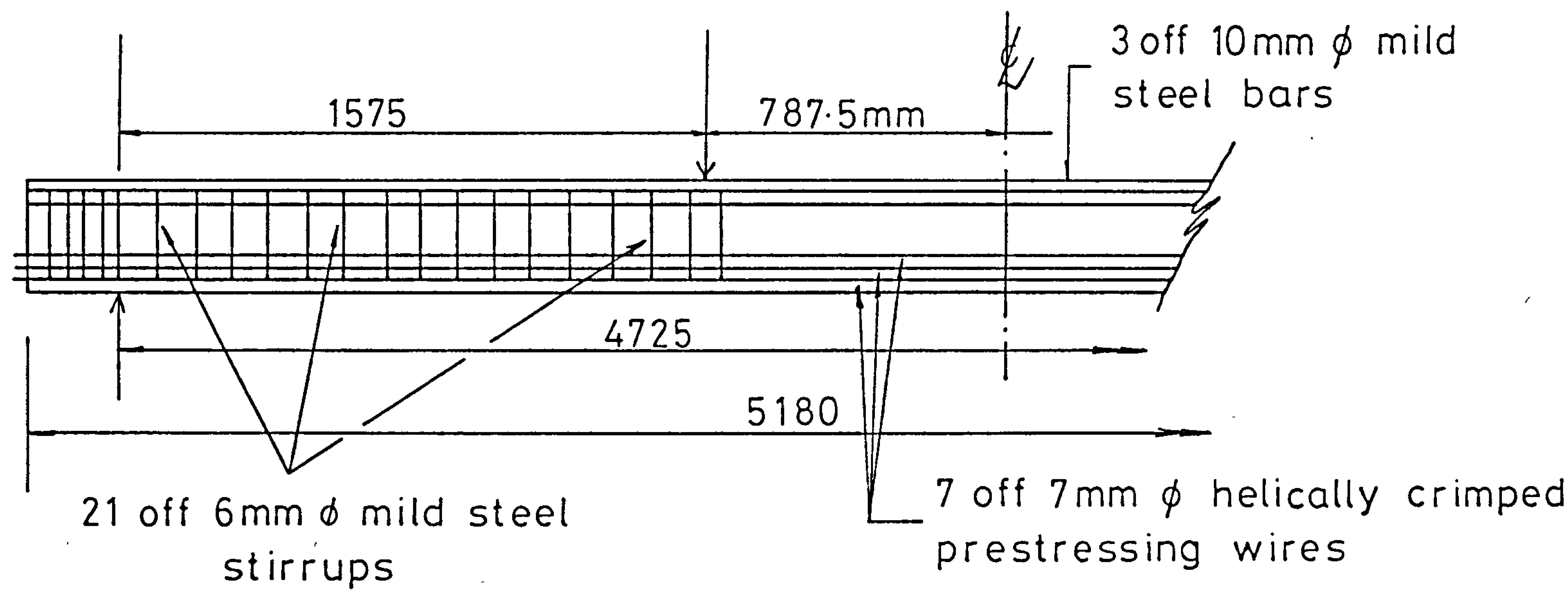

FIG. 5.6. T BEAM LONGITUDINAL SECTION - SERIES S, F & L.

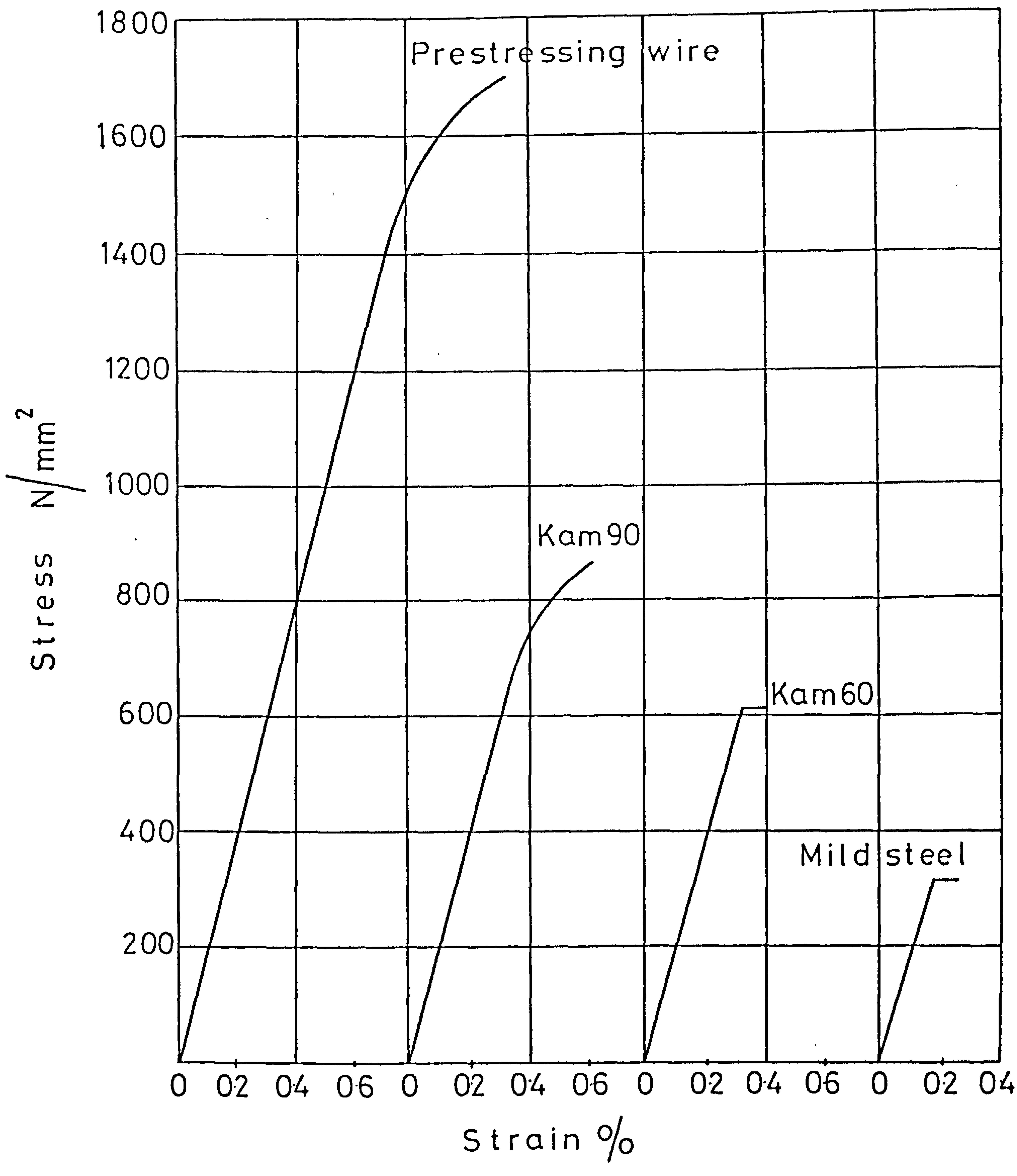

FIG 5 7 STRESS-STRAIN CURVES FOR STEEL

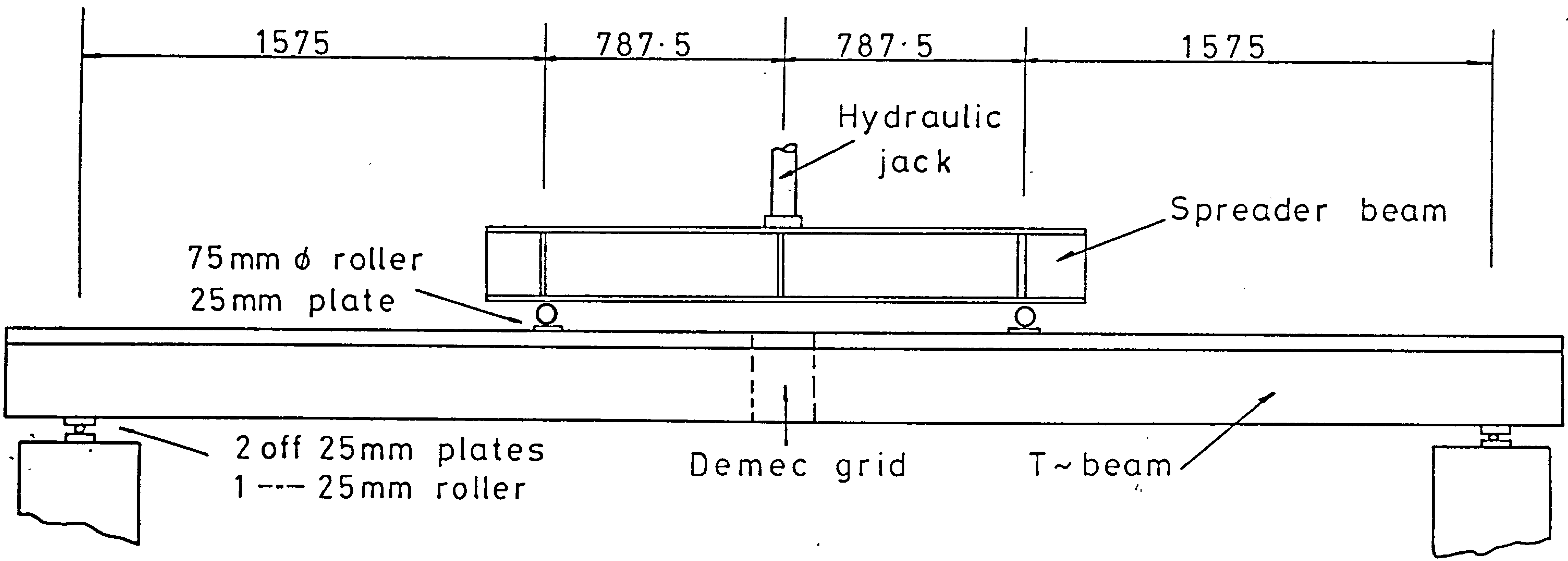

FIG. 5.8. LOADING ARRANGEMENT FOR SHORT TERM & FATIGUE TESTS

FIG. 5.9. LOADING HISTORY FOR T-BEAMS

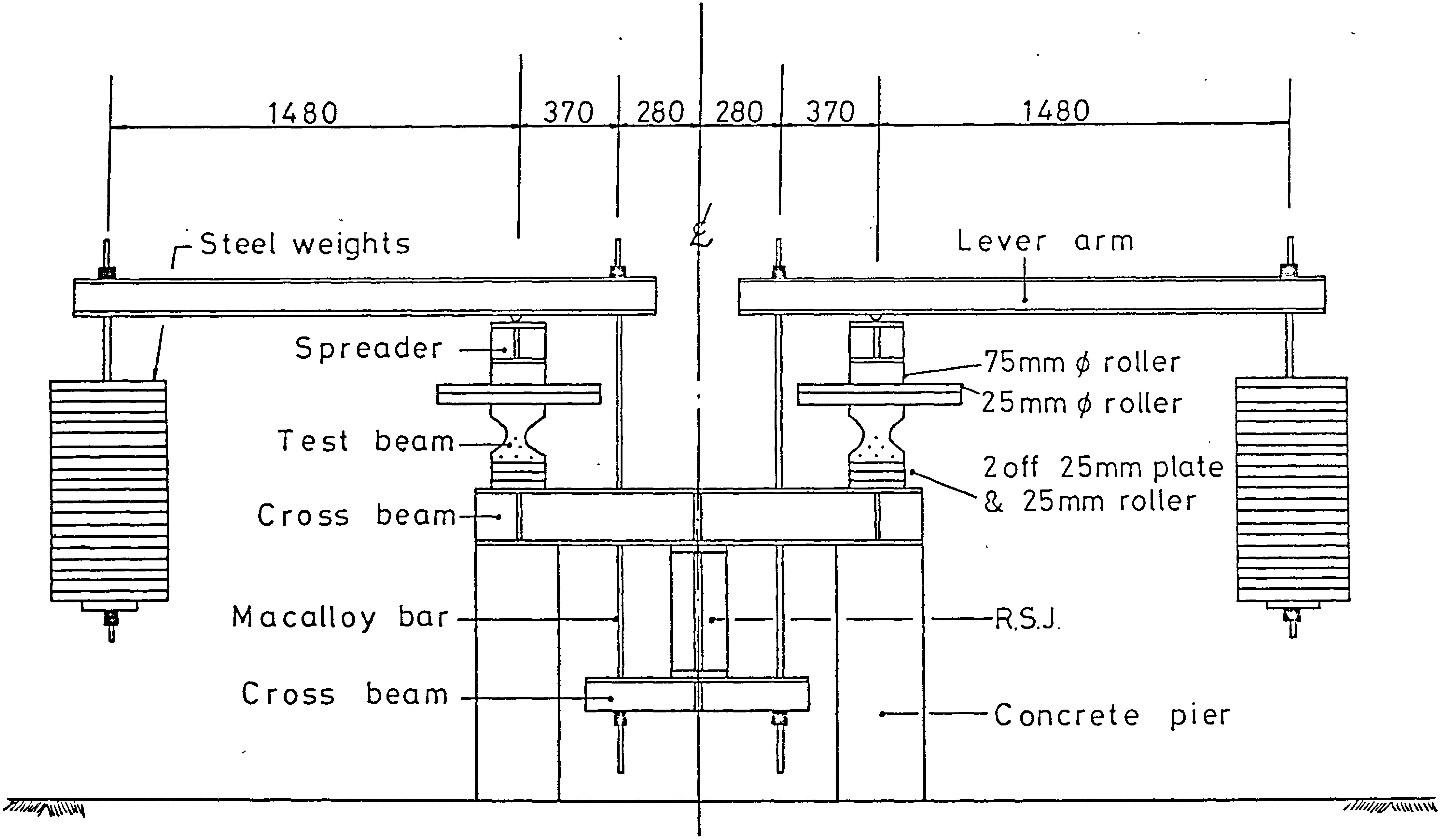

FIG. 5.10. LOADING ARRANGEMENT FOR LONG TERM TESTS

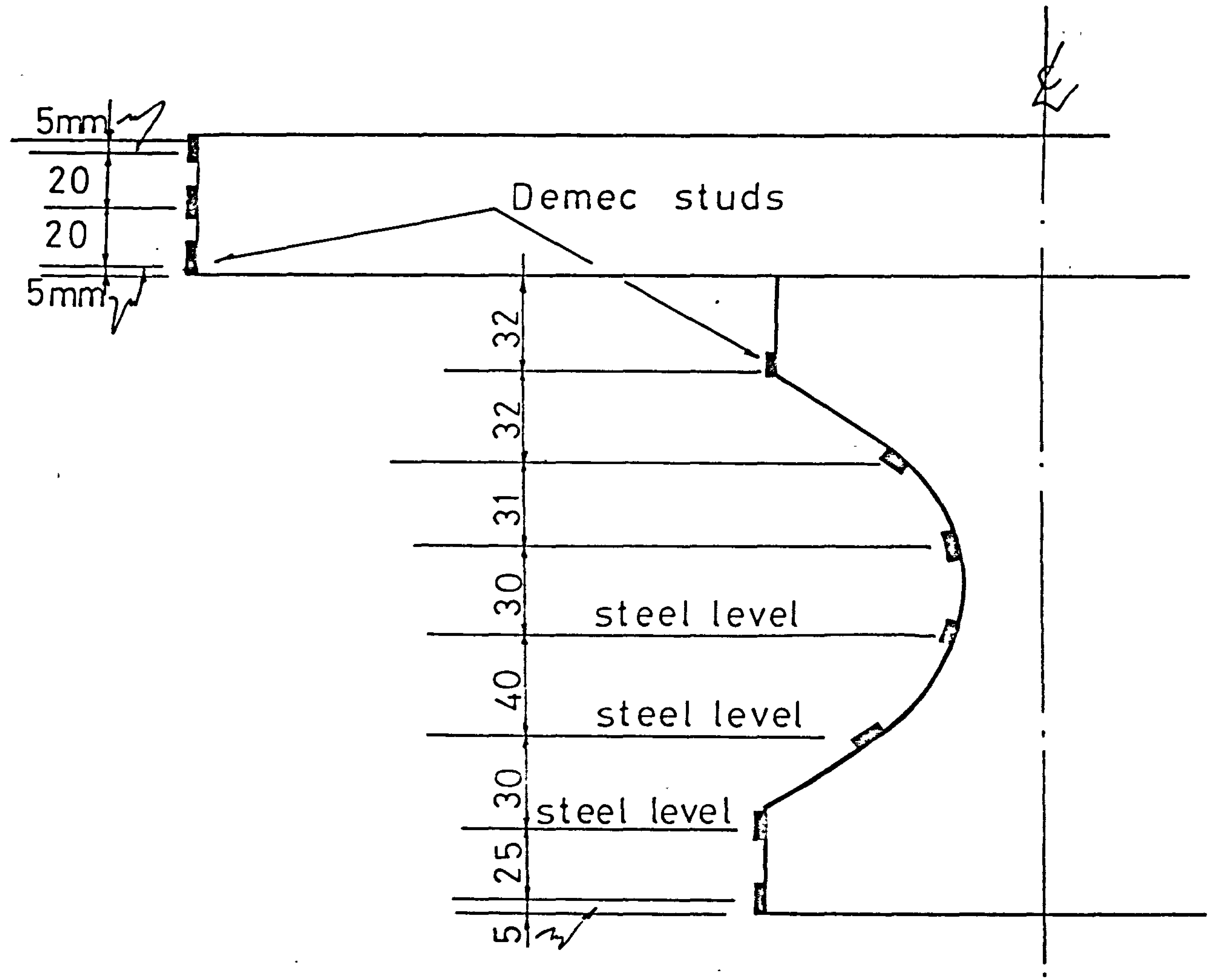

FIG. 5.11. LAYOUT OF DEMEC GRID

FIG. 5.12. SHRINKAGE & CREEP BEHAVIOUR OF CONCRETE

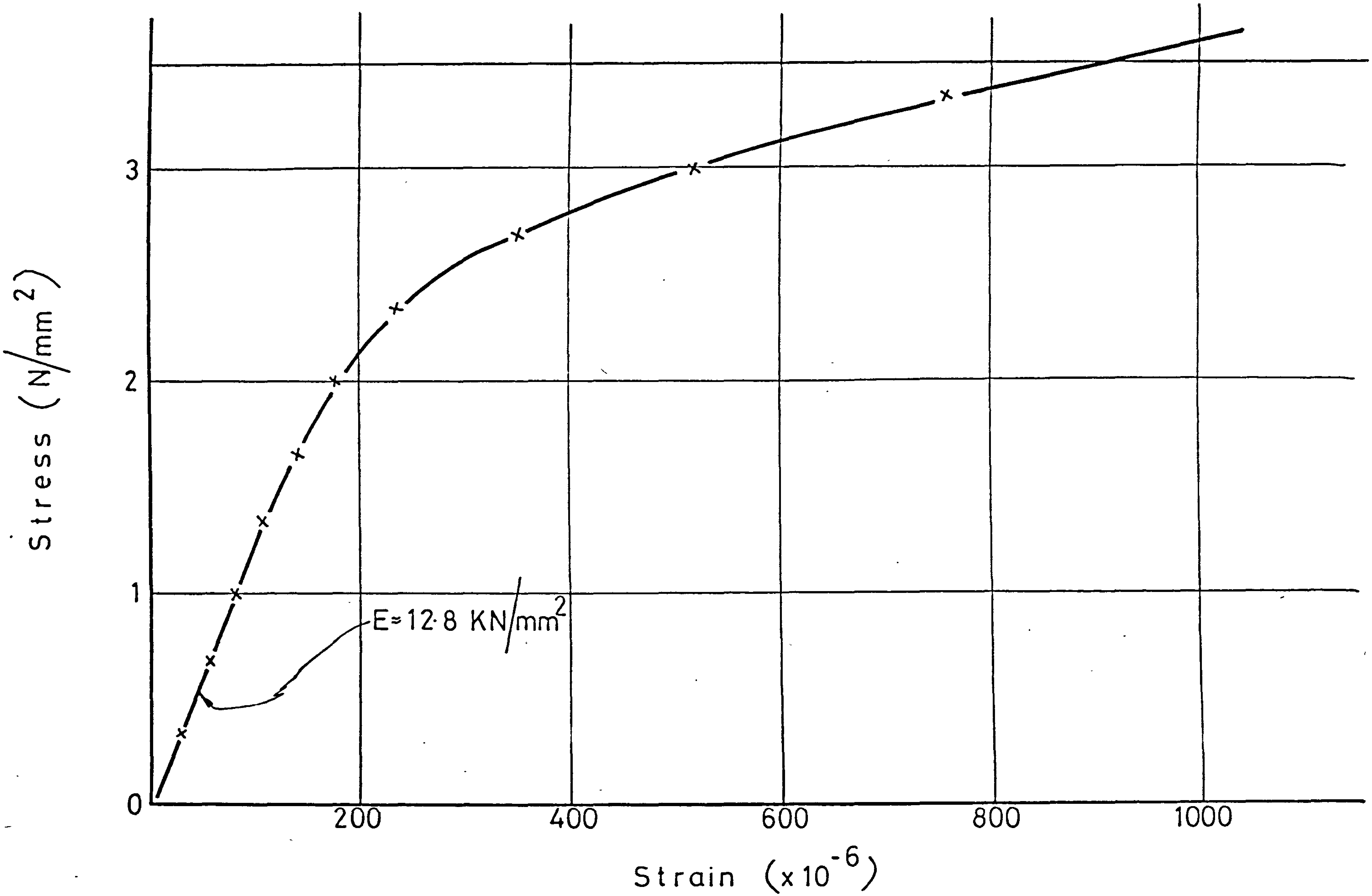

FIG. 5.13. STRESS - STRAIN CURVE, FIBROUS CEMENT

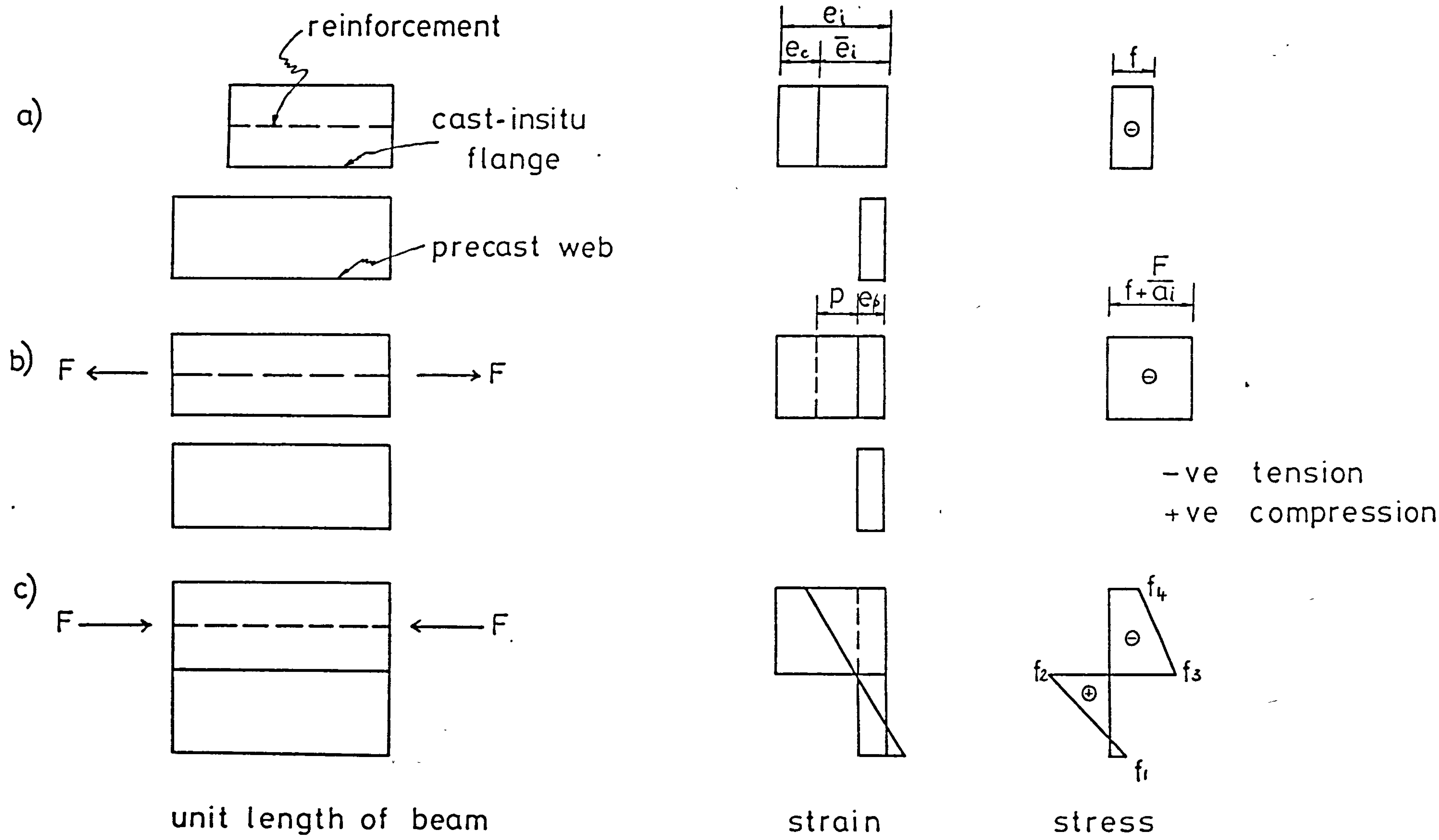

FIG. 6.1. DIFFERENTIAL SHRINKAGE STRESSES

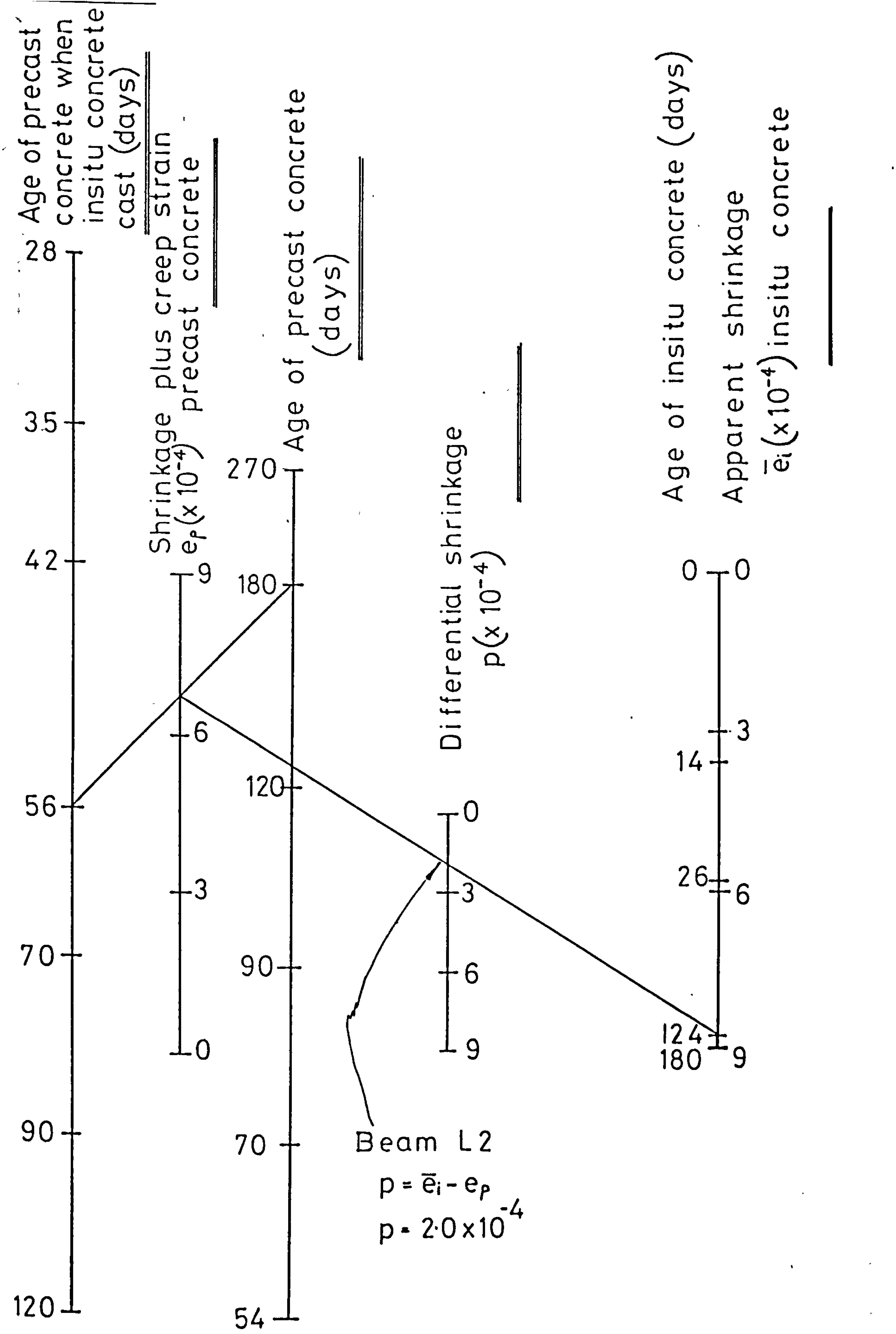

FIG. 6.2. NOMOGRAM FOR DIFFERENTIAL SHRINKAGE (SERIES S,F & L)

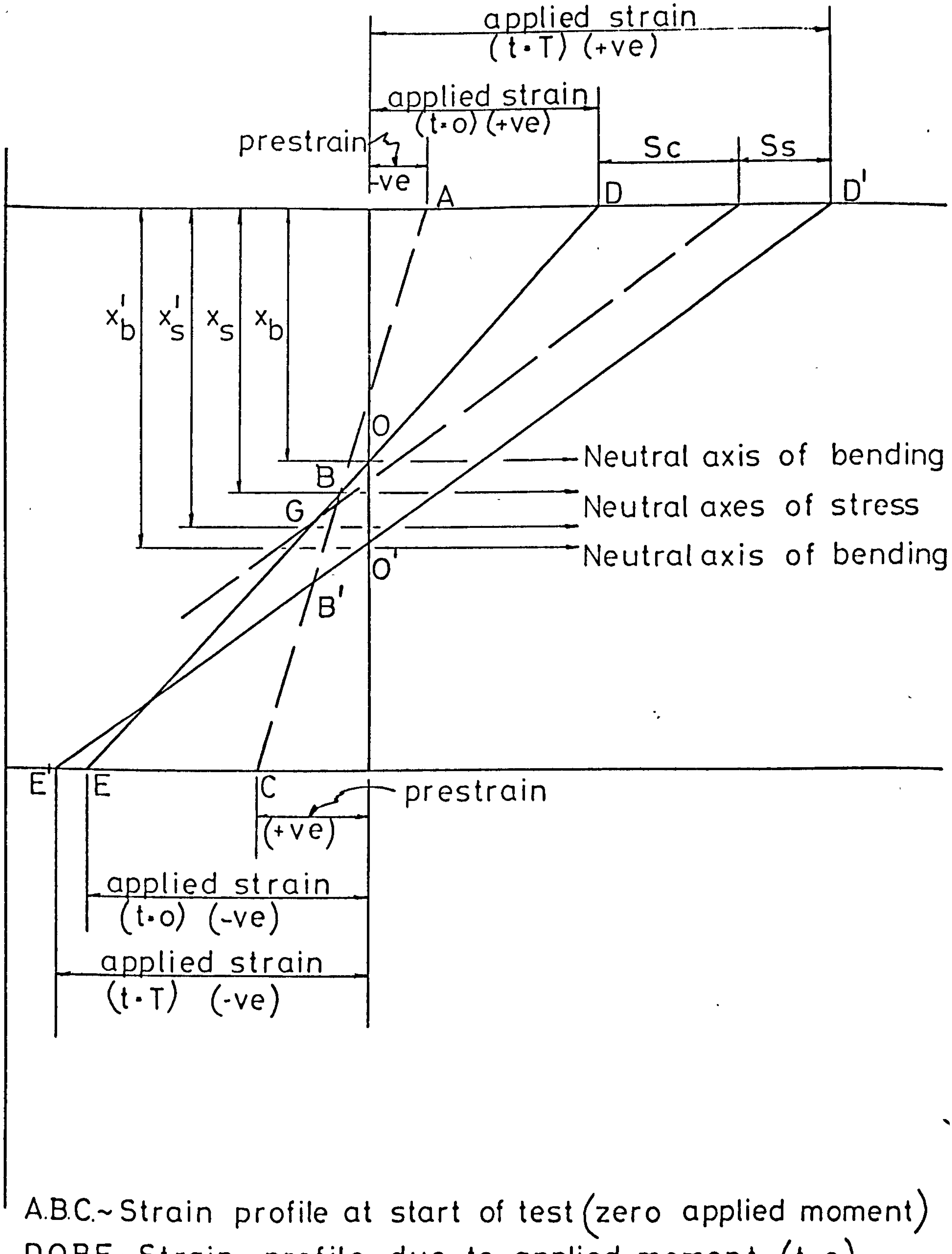

A.B.C.~Strain profile at start of test (zero applied moment)
D.O.B.E.~Strain profile due to applied moment (t·o)
D'.O'.B'E'.~Strain profile due to applied moment (t·T)

FIG. 6.3. NEUTRAL AXES OF STRESS & BENDING UNDER SUSTAINED LOADING

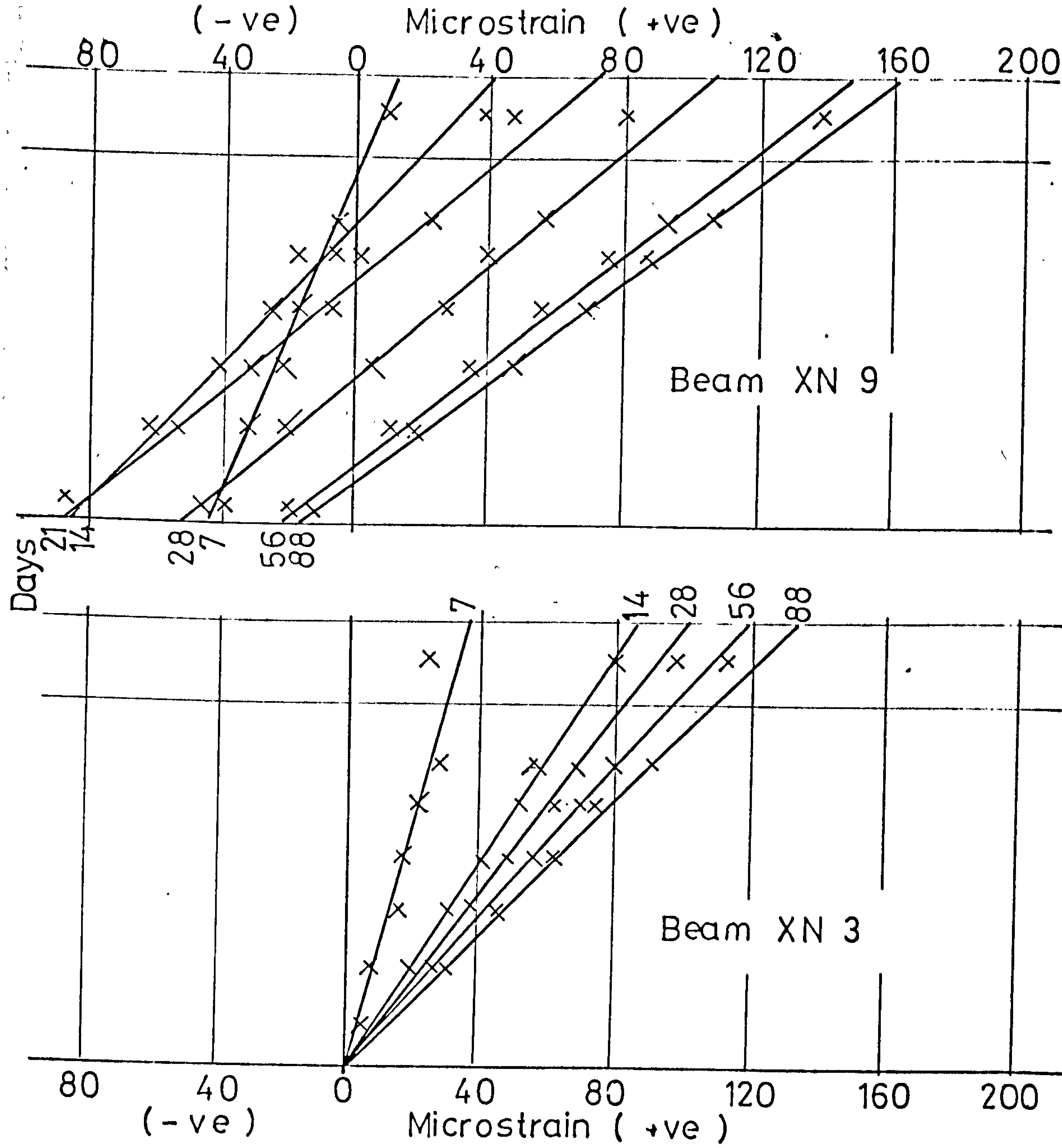

FIG. 7.1. DISTRIBUTION OF DIFFERENTIAL SHRINKAGE STRAINS — GROUP XN

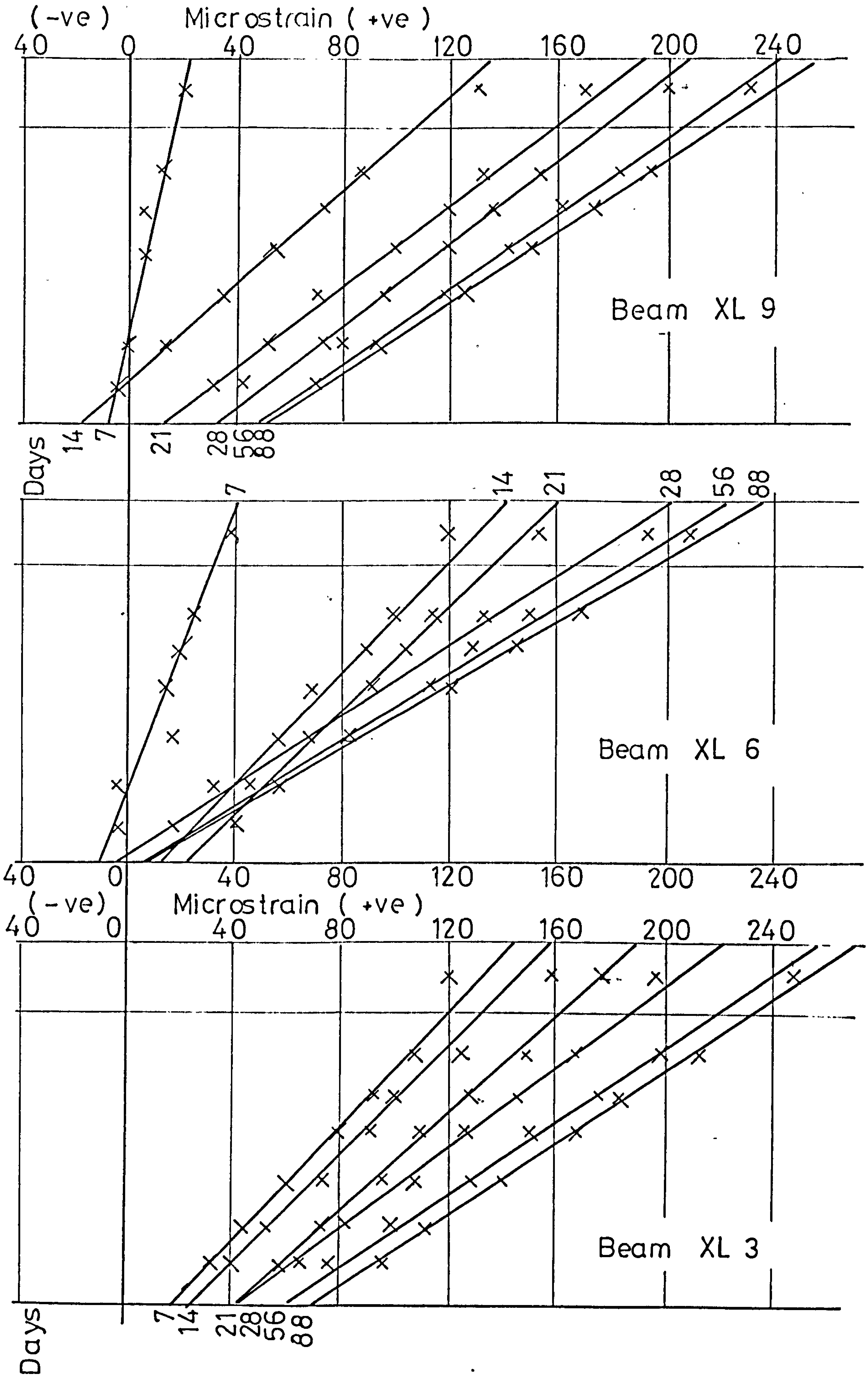

FIG. 7.2. DISTRIBUTION OF DIFFERENTIAL SHRINKAGE STRAINS —GROUP XL

FIG. 7.3. DISTRIBUTION OF DIFFERENTIAL SHRINKAGE STRAINS—CLASS 2 BEAMS

FIG. 7.4. DISTRIBUTION OF DIFFERENTIAL SHRINKAGE STRAINS—CLASS 3 BEAMS

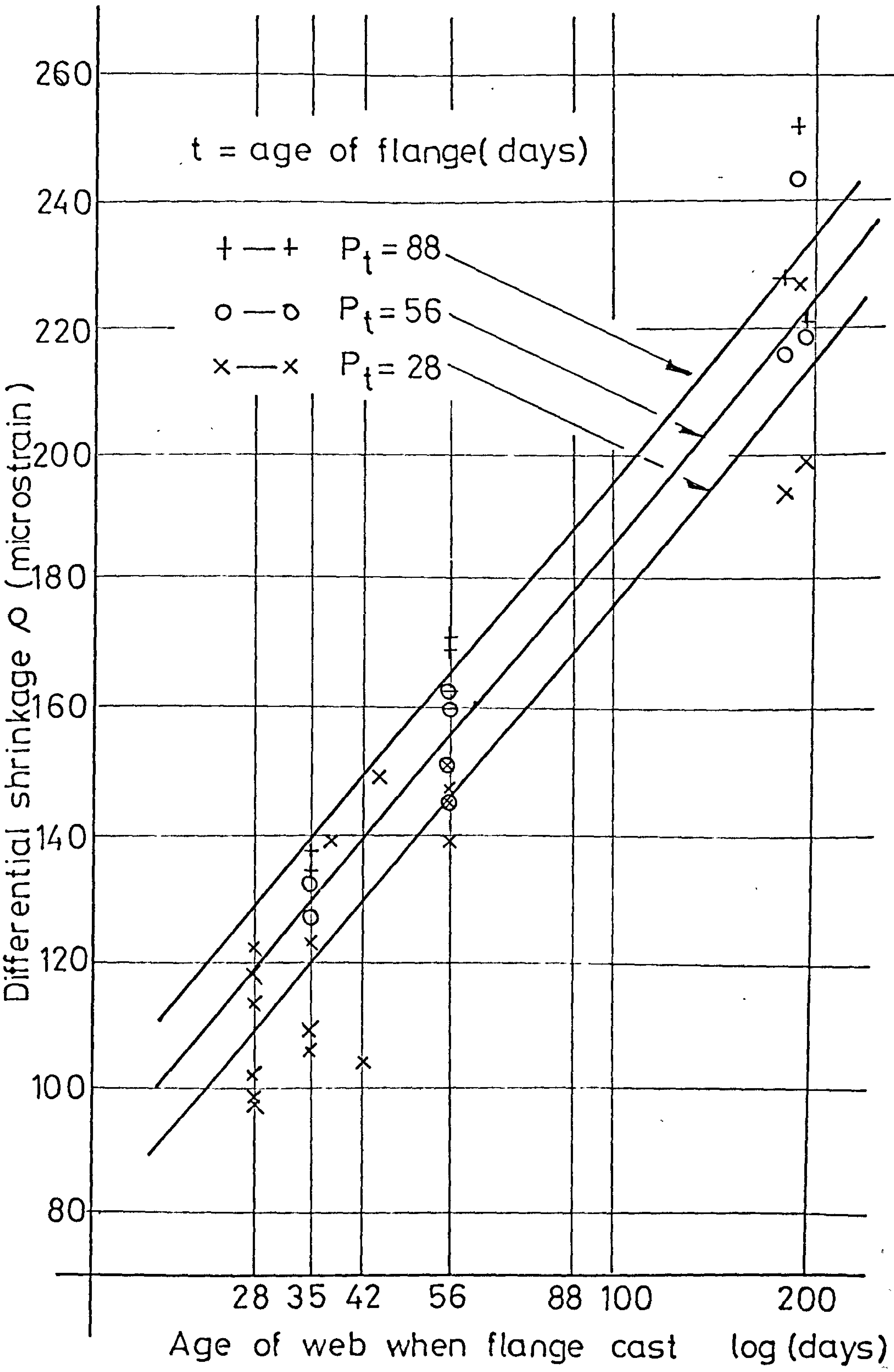

FIG. 7.5. VARIATION OF DIFFERENTIAL SHRINKAGE WITH TIME

FIG. 7.6. DIFFERENTIAL SHRINKAGE STRESSES (N/mm^2)

FIG. 7.7 DIFFERENTIAL SHRINKAGE STRESSES (N/mm^2)

FIG. 7.8. LOAD-DEFLECTION CURVES - SERIES X

FIG. 7.9 COMPARISON OF DEFLECTIONS — SERIES X

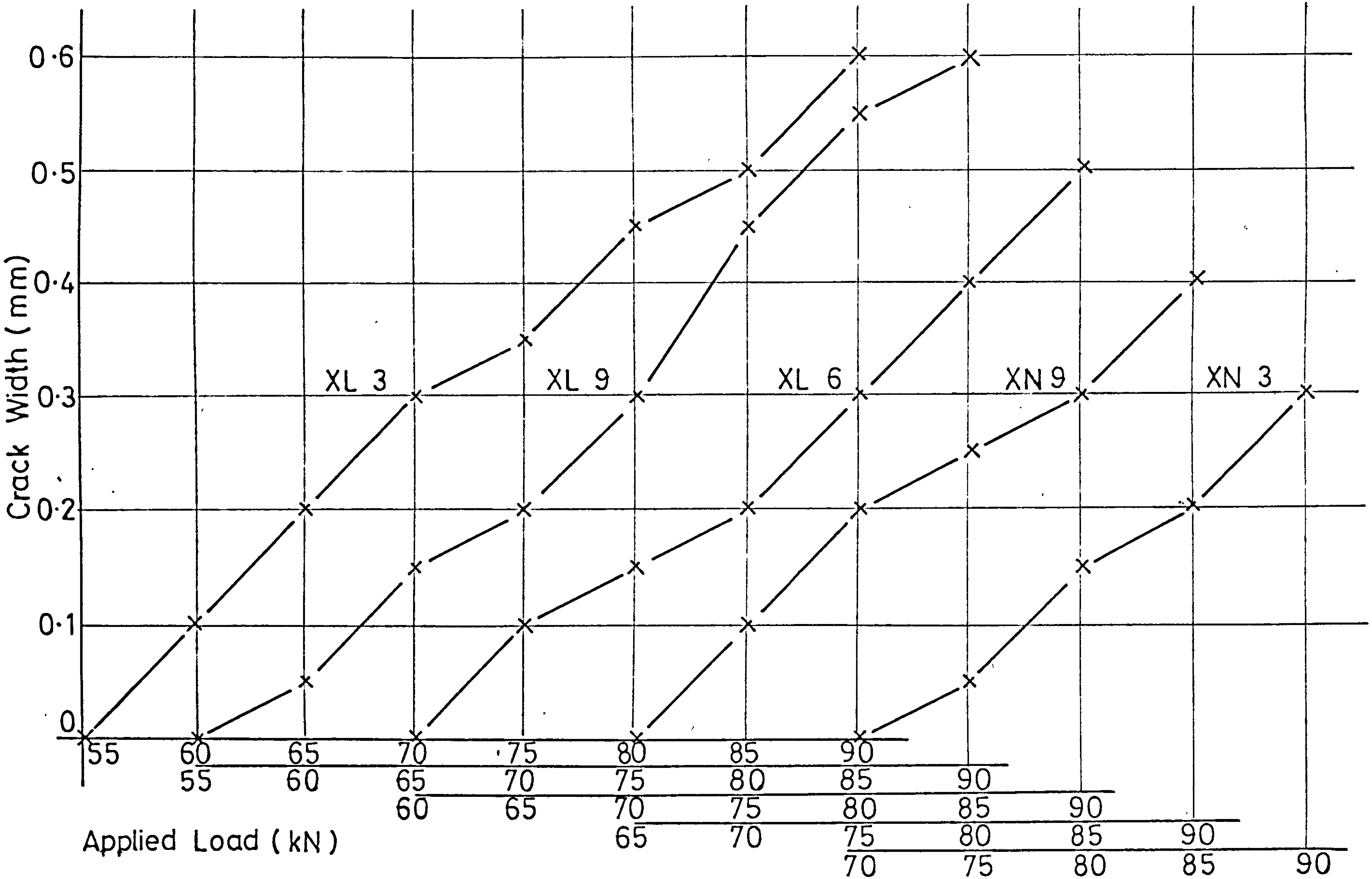

FIG. 7.10 CRACK WIDTH – LOAD CURVES – SERIES X

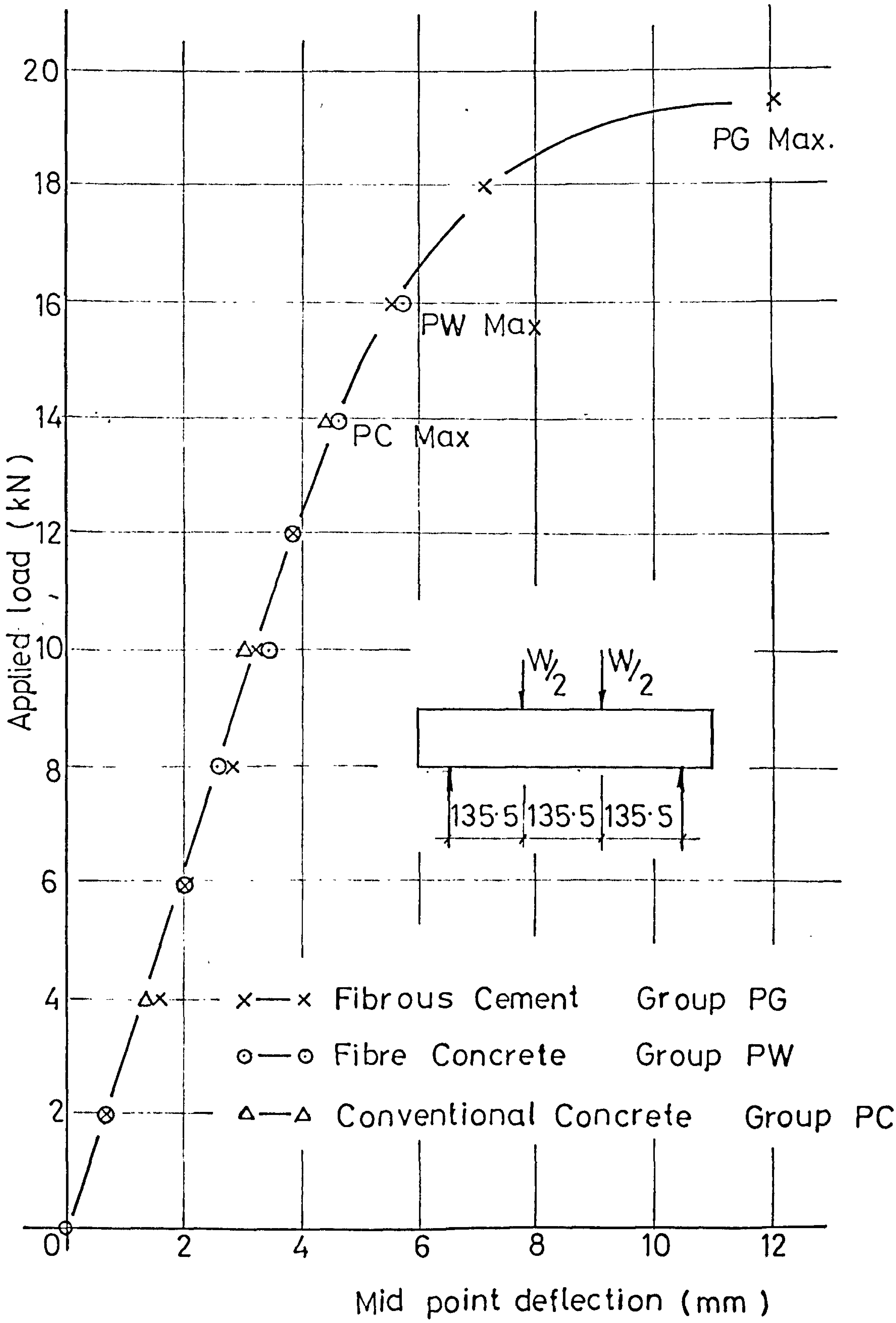

FIG. 7.11. LOAD DEFLECTION CURVES SERIES P

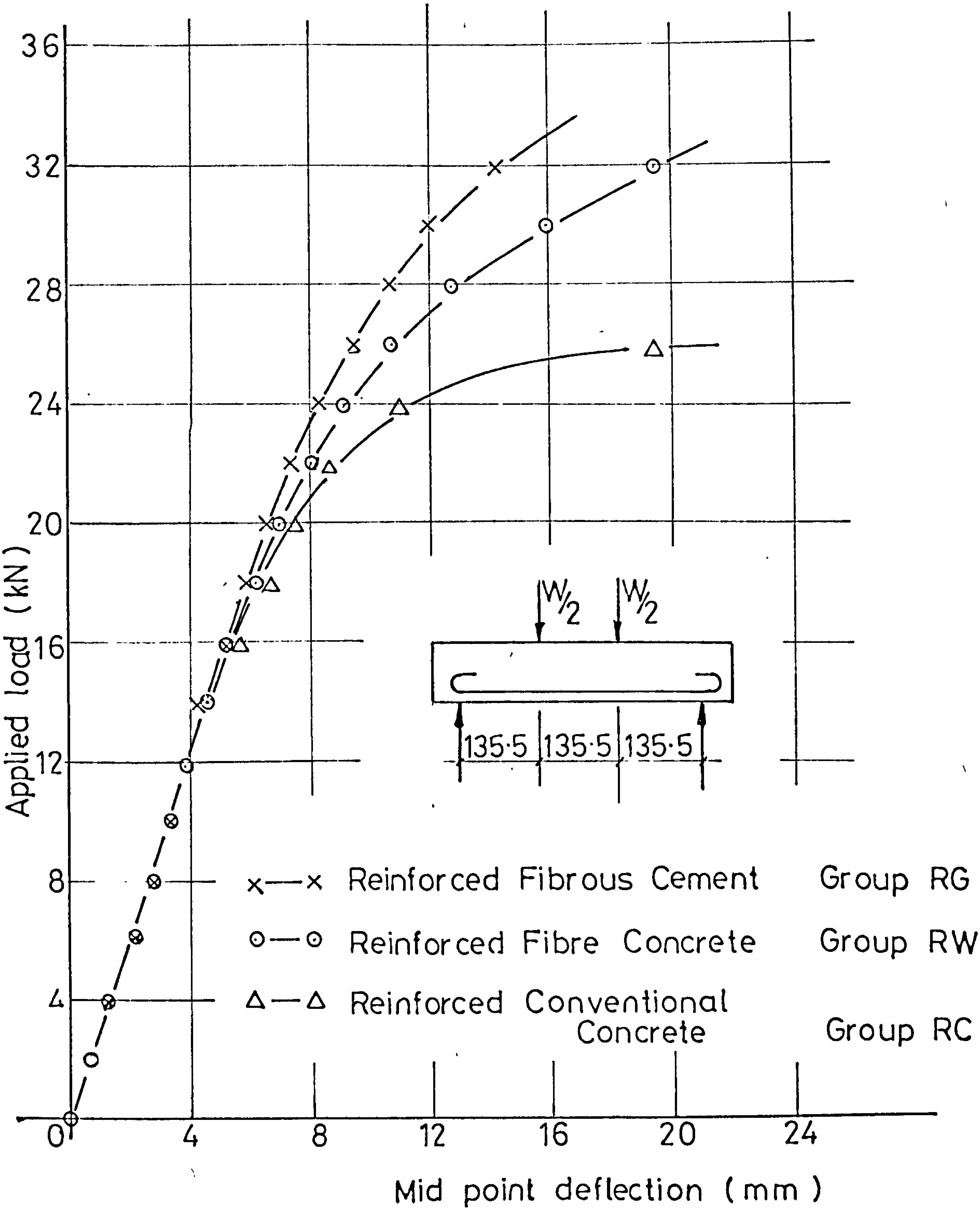

FIG. 7.12 LOAD DEFLECTION CURVES SERIES R

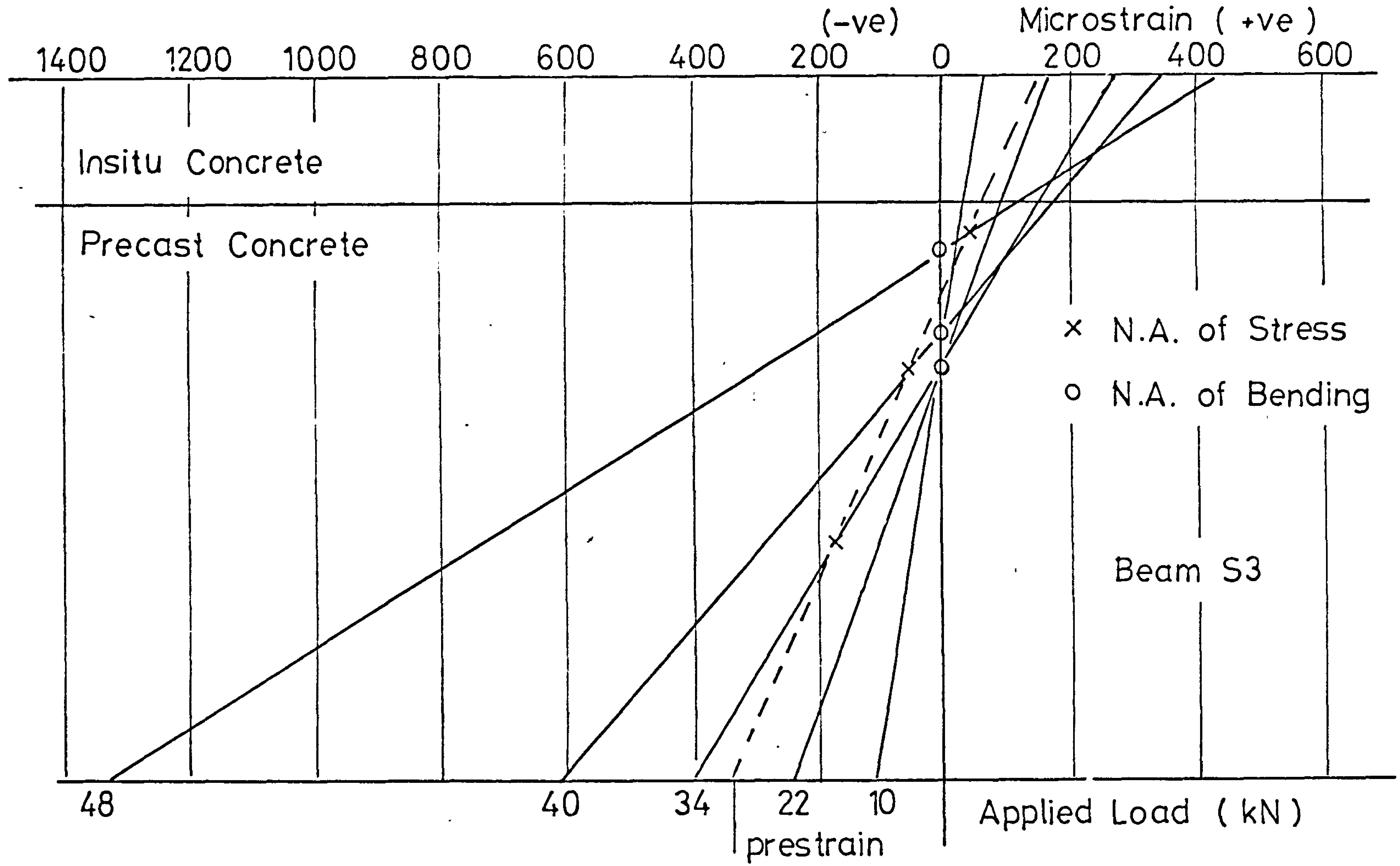

FIG. 7.13. STRAIN PROFILE -BEAM S3

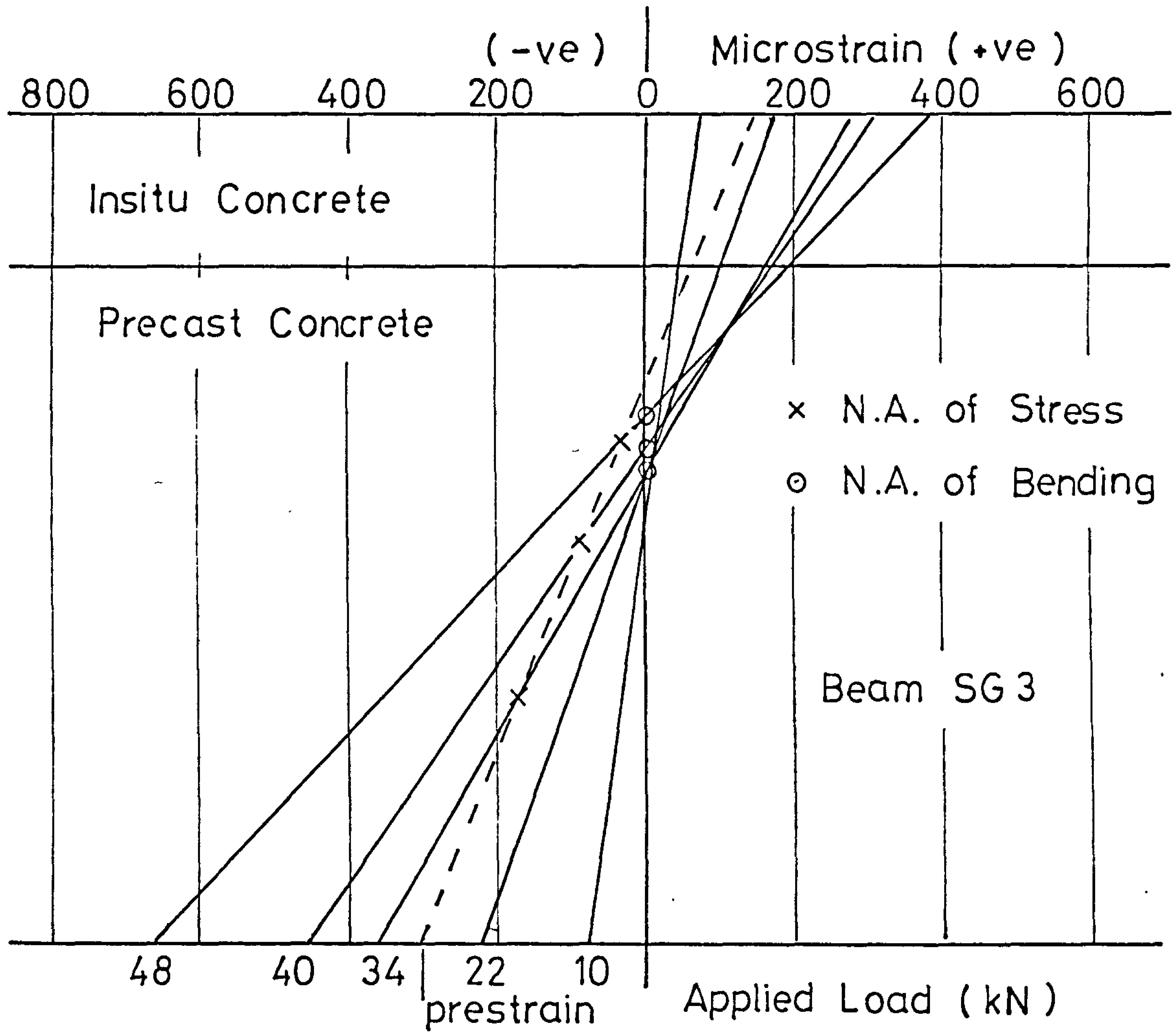

FIG. 7.14. STRAIN PROFILE BEAM SG 3

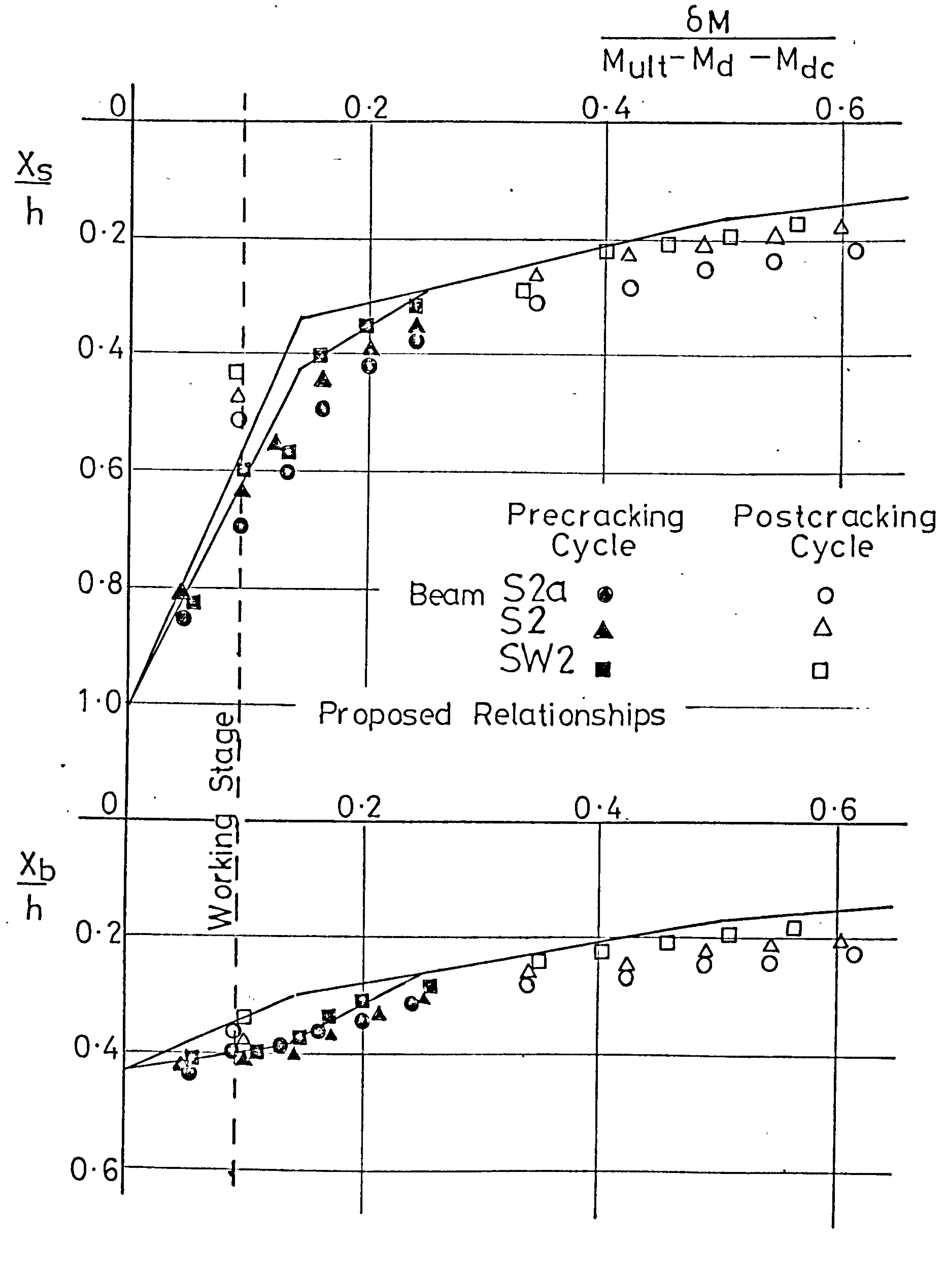

FIG: 7.15. $\frac{X}{h}$ vs $\frac{\delta M}{M_{ult} - M_d - M_{dc}}$ CLASS 2 BEAMS

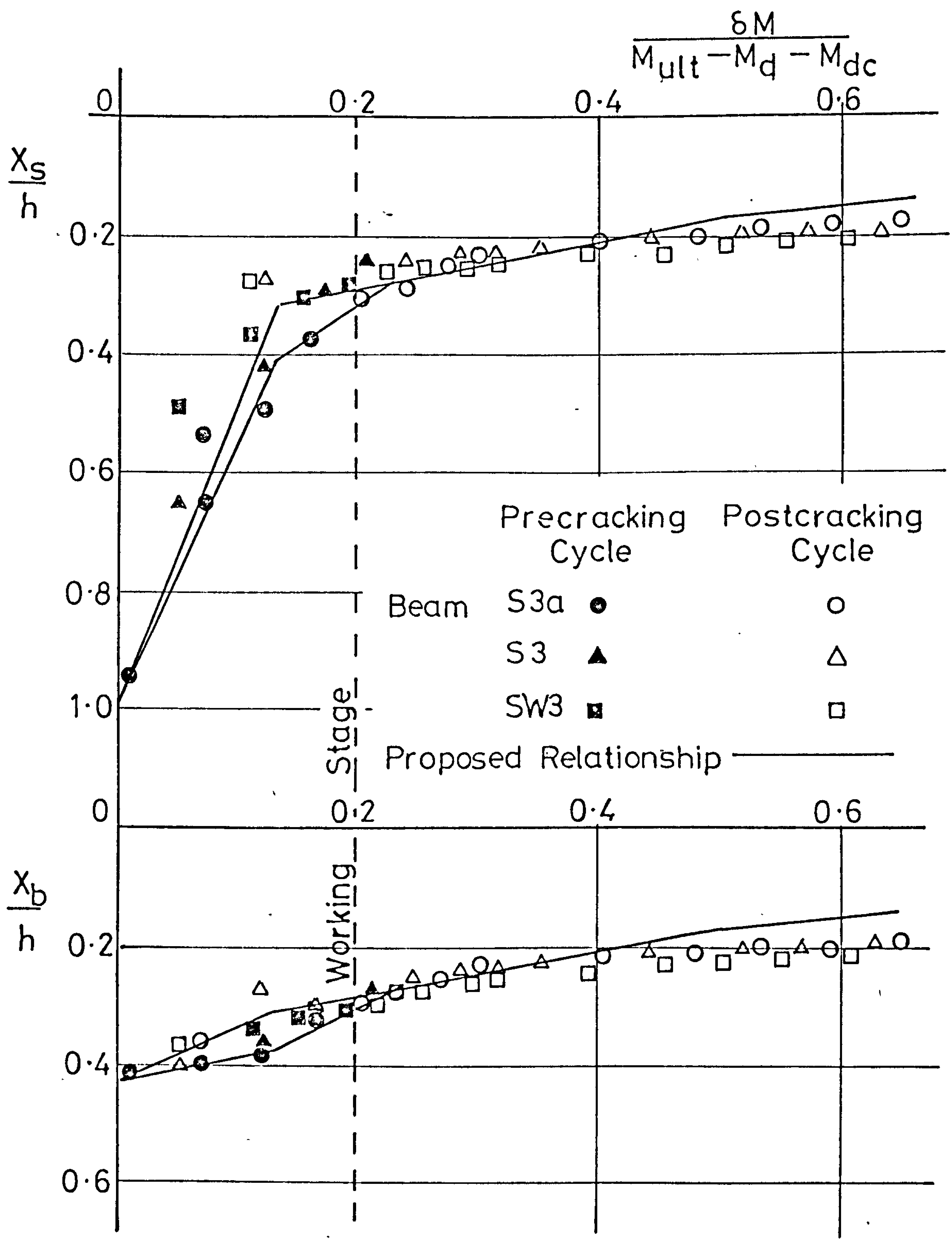

FIG. 7.16. $\frac{X}{h}$ vs $\frac{\delta M}{M_{ult} - M_d - M_{dc}}$ CLASS 3 BEAMS

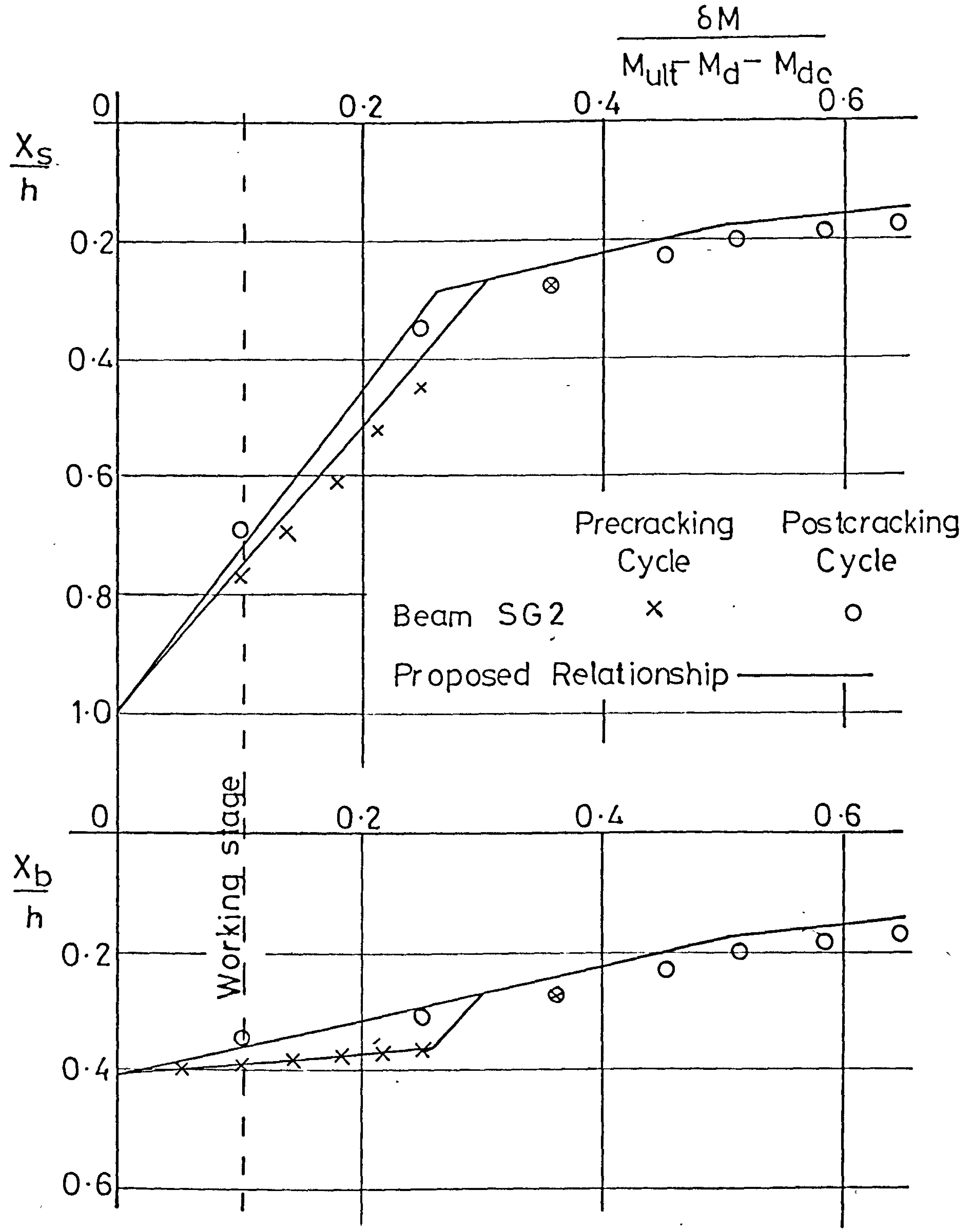

FIG. 7.17 $\frac{X}{h}$ vs $\frac{\delta M}{M_{ult} \quad M_d \quad M_{dc}}$ Beam SG2

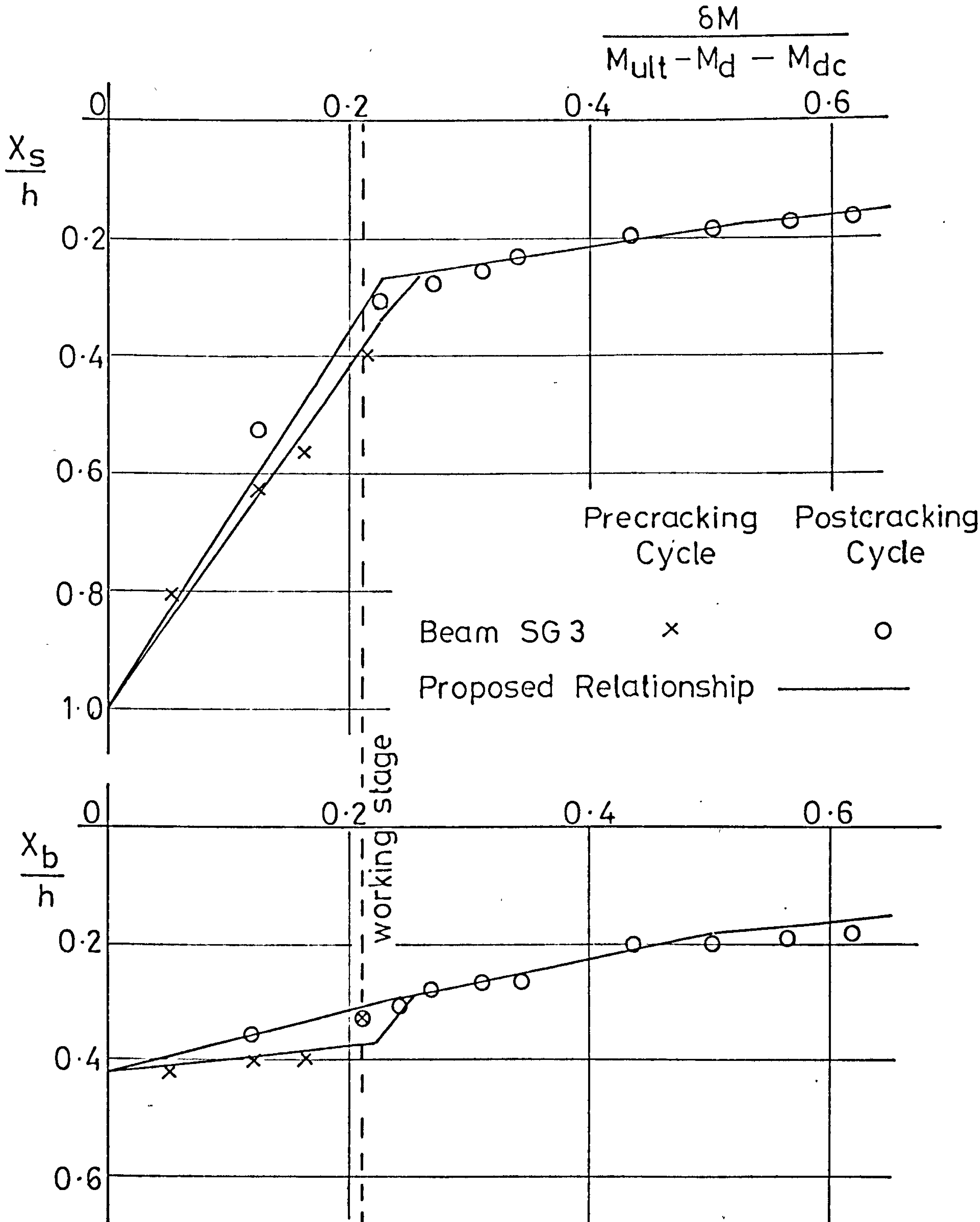

FIG. 7.18 $\frac{X}{h}$ vs $\frac{\delta M}{M_{ult} - M_d - M_{dc}}$ BEAM SG 3

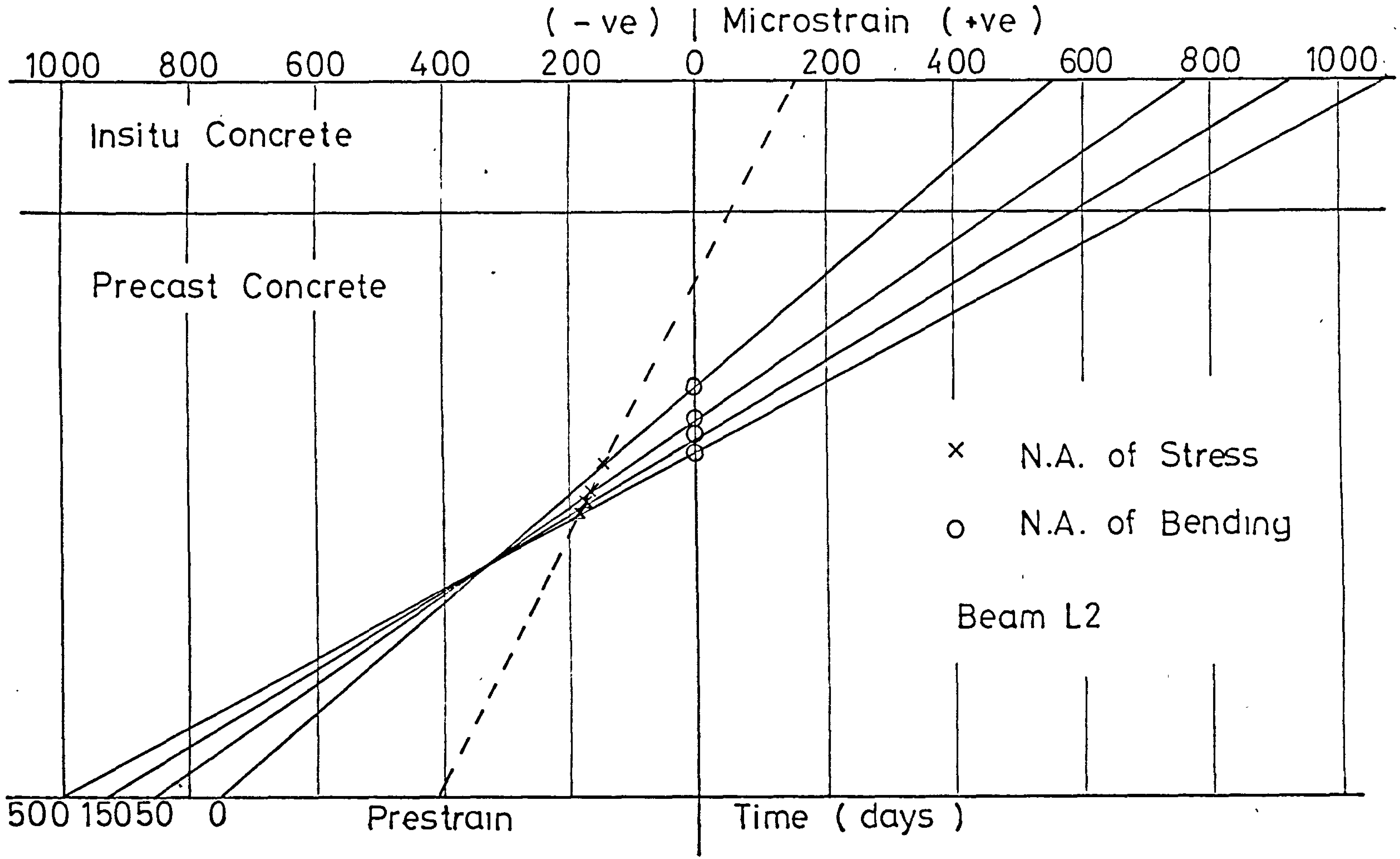

FIG. 7.19 STRAIN PROFILE BEAM L2

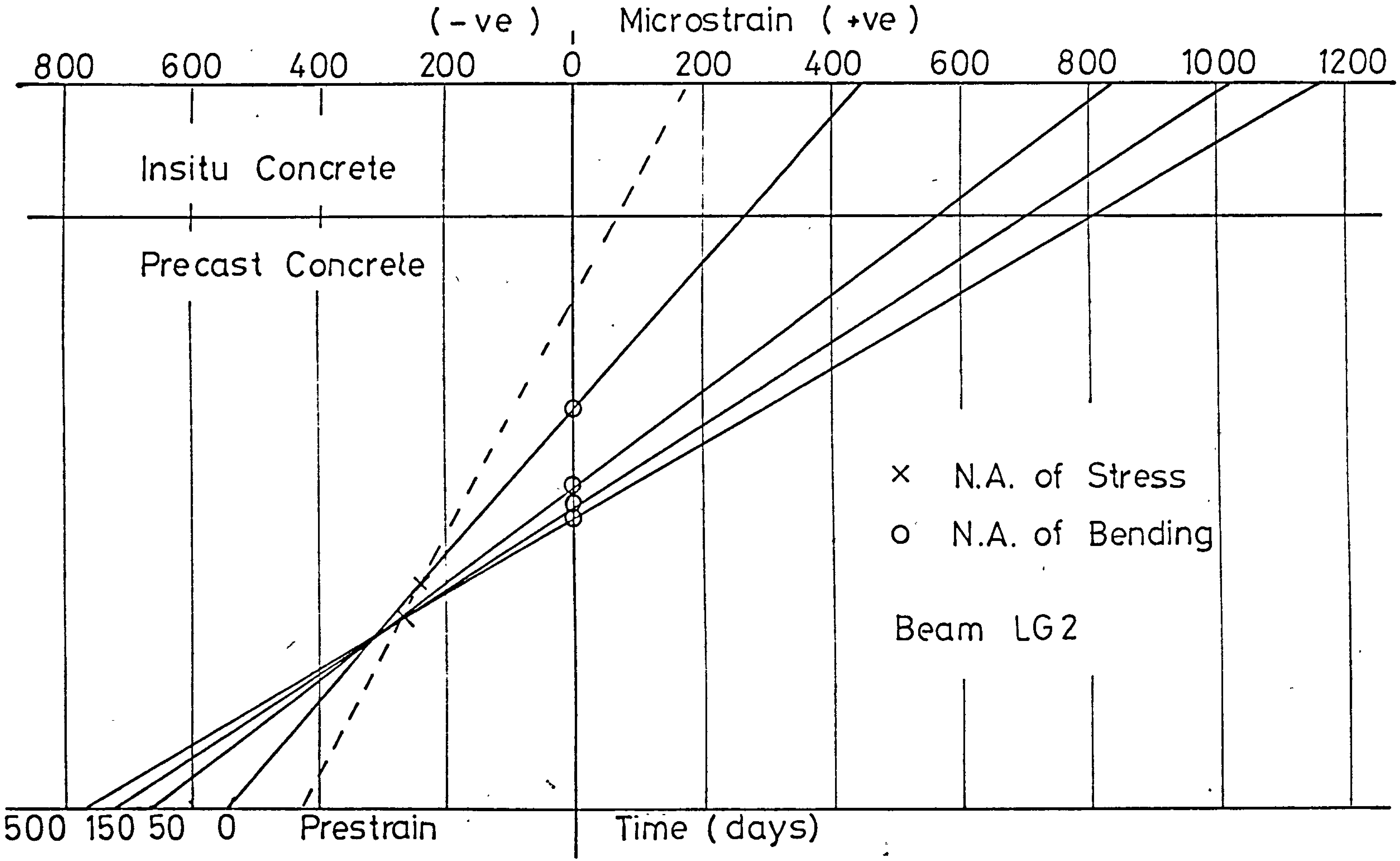

FIG. 7.20. STRAIN PROFILE BEAM LG2

FIG. 7.21. STRAIN PROFILE BEAM F2

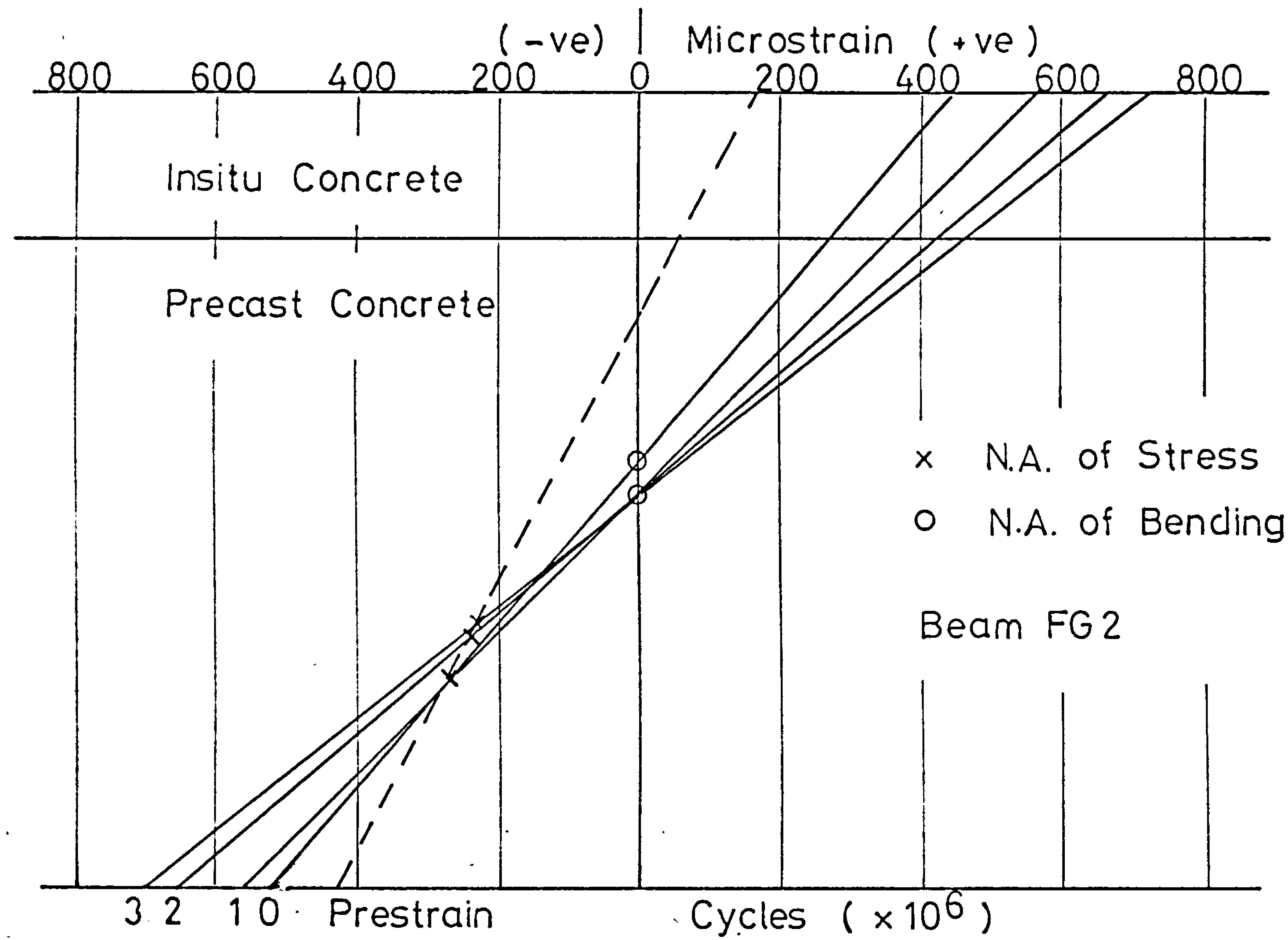

FIG. 7.22. STRAIN PROFILE — BEAM FG2

FIG. 7.23 STEEL STRESS vs LOAD - CLASS 2 BEAMS

FIG. 7.24. STEEL STRESS vs LOAD - CLASS 3 BEAMS

FIG. 7.25 STEEL STRESS vs LOAD - GROUP SW

FIG. 7.26. STEEL STRESS vs TIME — SERIES L

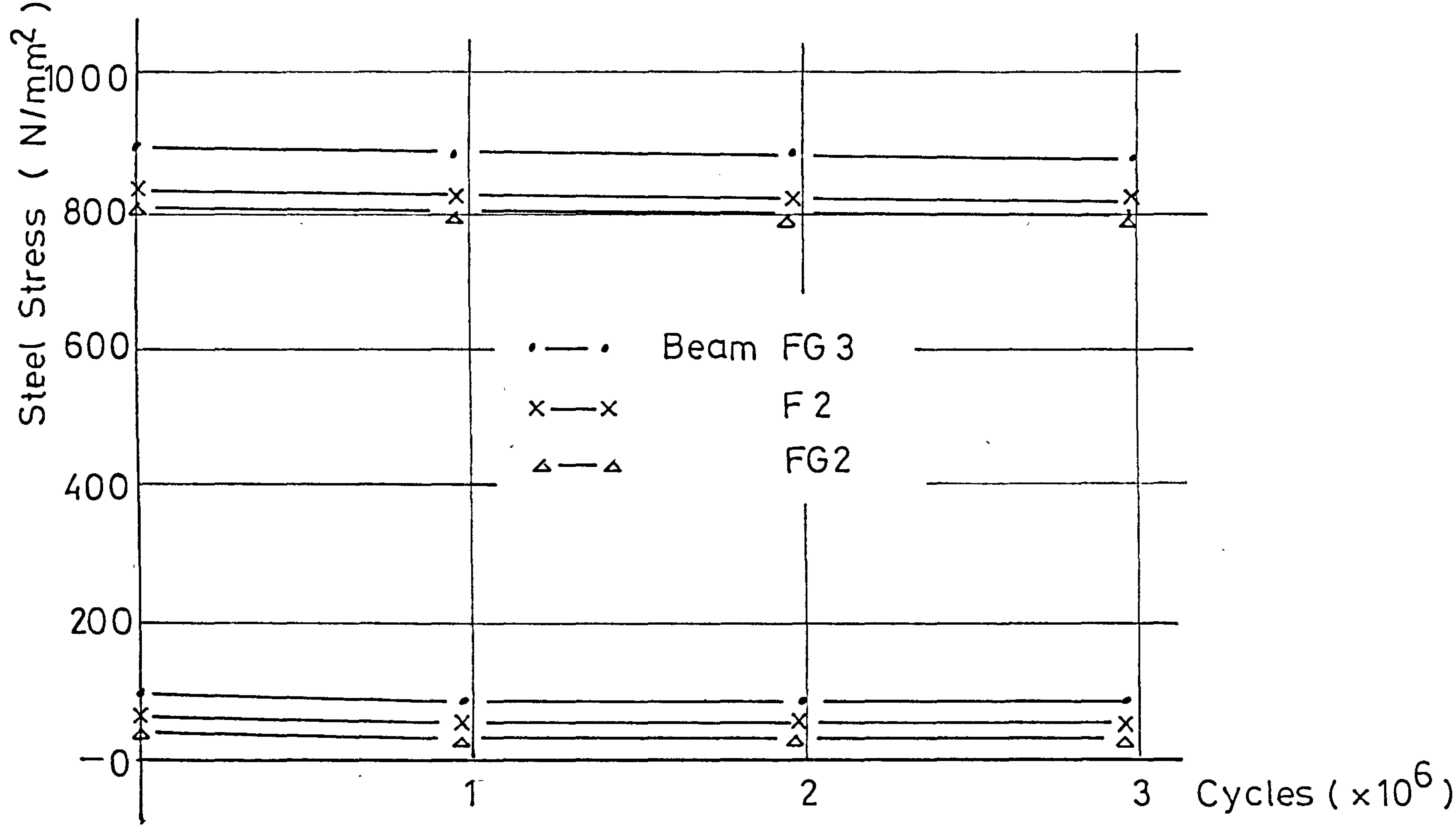

FIG. 7.27. STEEL STRESS vs LOAD CYCLES —SERIES F

FIG. 7.28 LOAD-DEFLECTION CURVES GROUPS S2 S3

FIG. 7.29 LOAD-DEFLECTION CURVES GROUPS SG, SW

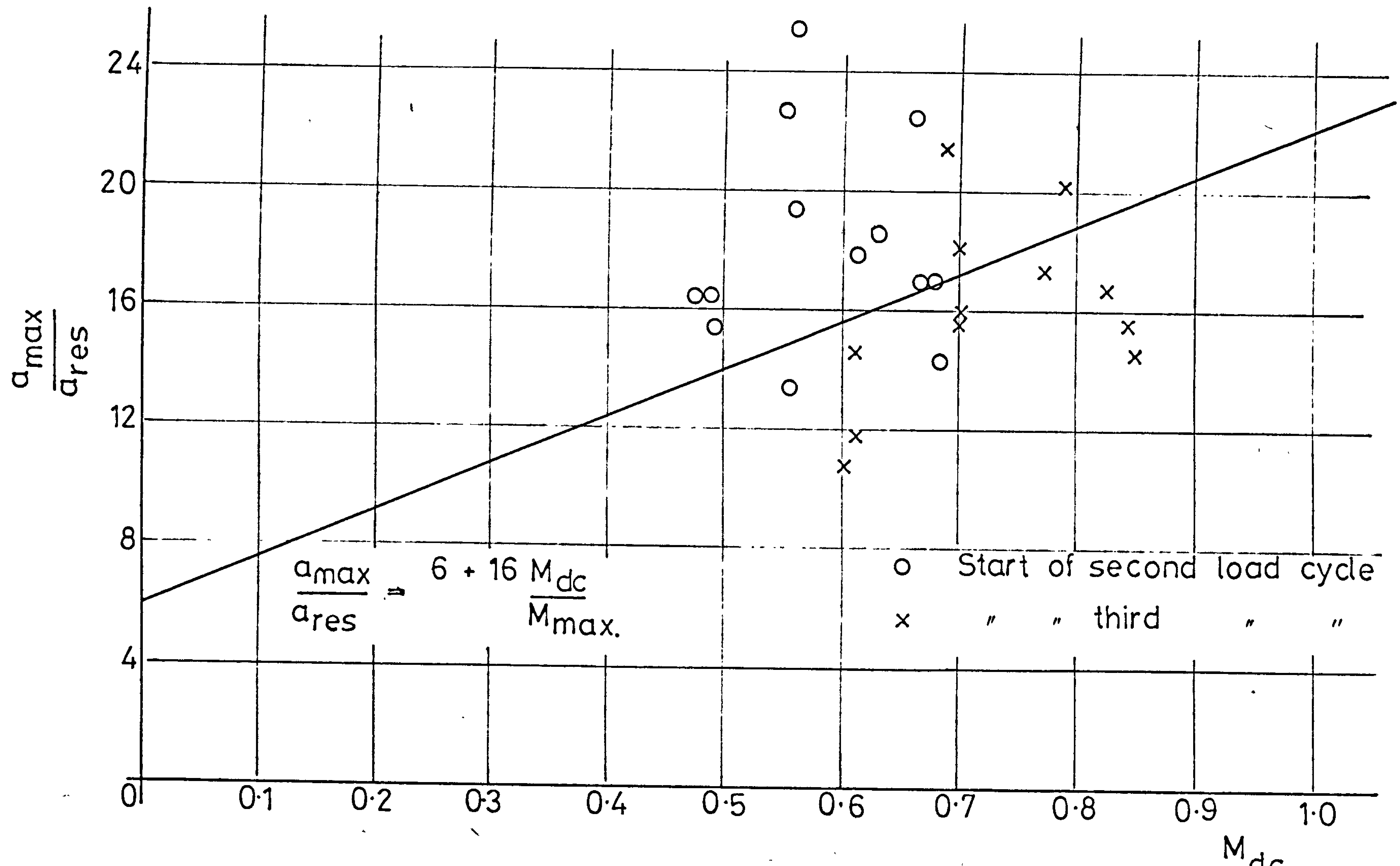

FIG.7.30 PLOT OF $\frac{a_{max.}}{a_{res}}$ vs $\frac{M_{dc}}{M_{max.}}$

FIG. 7.31 LOAD – DEFLECTION CURVES – SERIES S

FIG. 7.32 AVERAGE LOAD-DEFLECTION CURVES

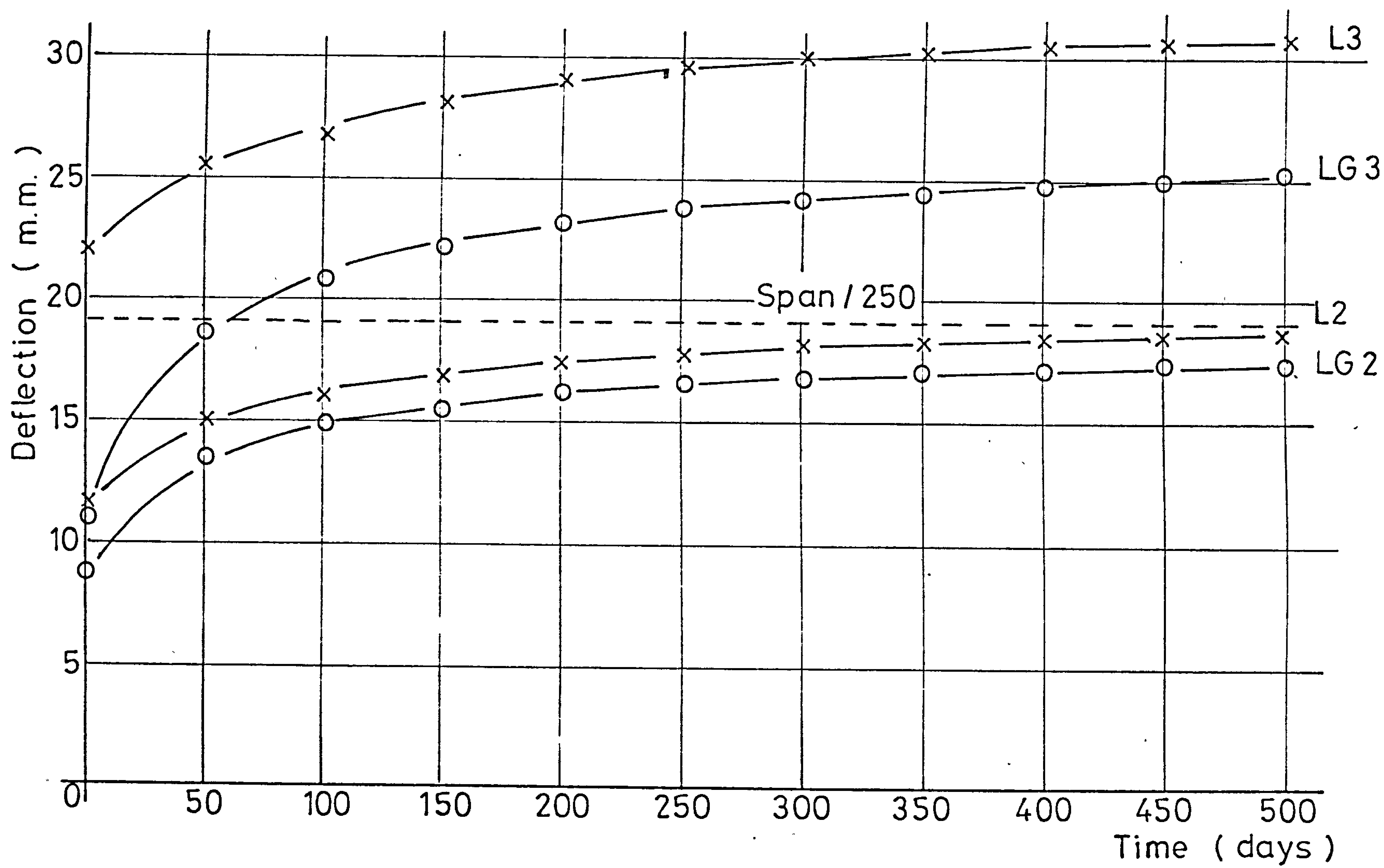

FIG. 7. 33 DEFLECTION vs TIME CURVES – SERIES L

FIG. 7.34 VARIATIONS OF DEFLECTION WITH HUMIDITY –SERIES L

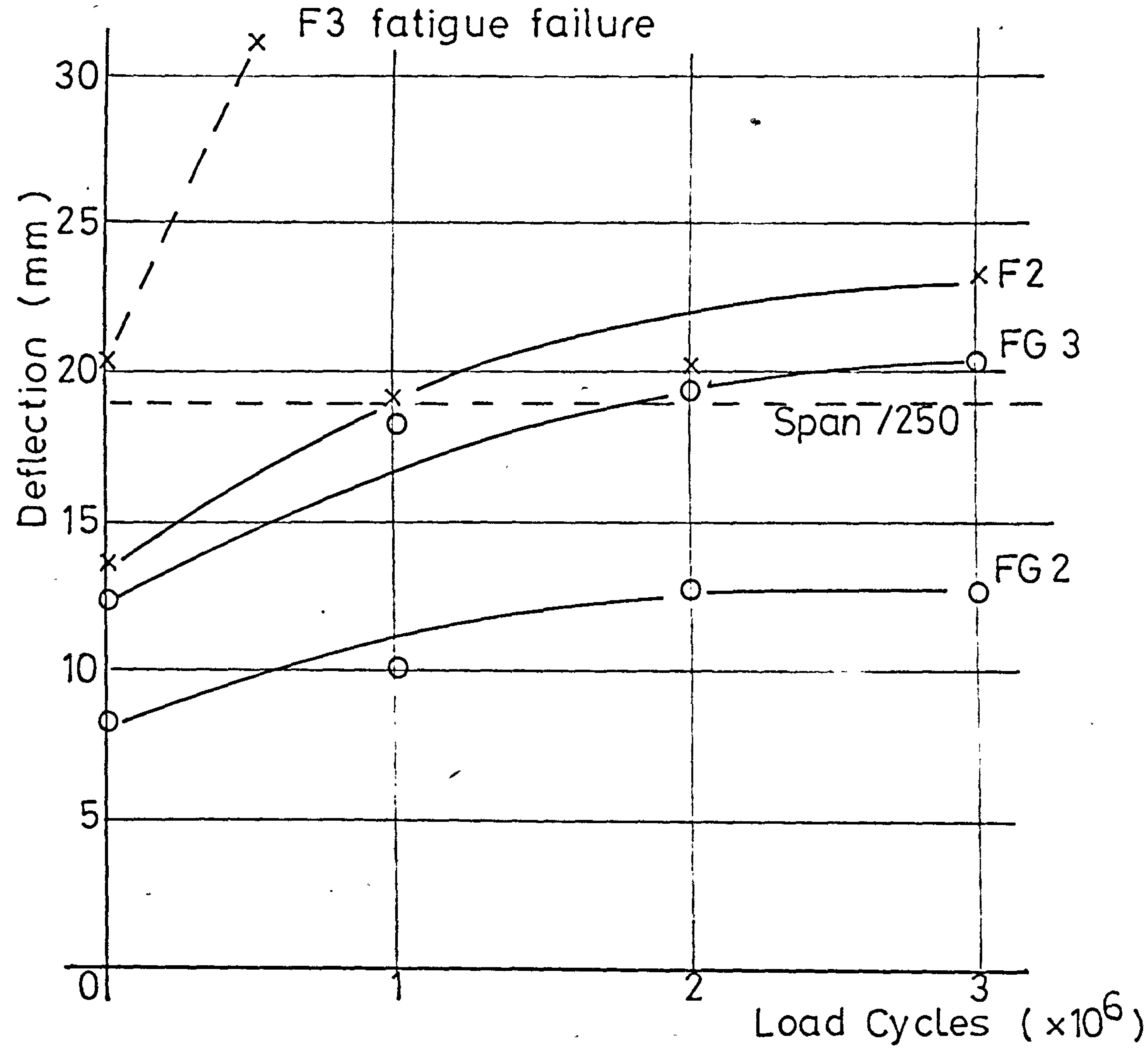

FIG. 7. 35 DEFLECTION vs LOAD CYCLES — SERIES F

FIG. 7.36 CRACK WIDTH vs LOAD CURVES-GROUPS S2 S3

FIG. 7. 37 CRACK WIDTH vs LOAD CURVES —GROUPS SG, SW

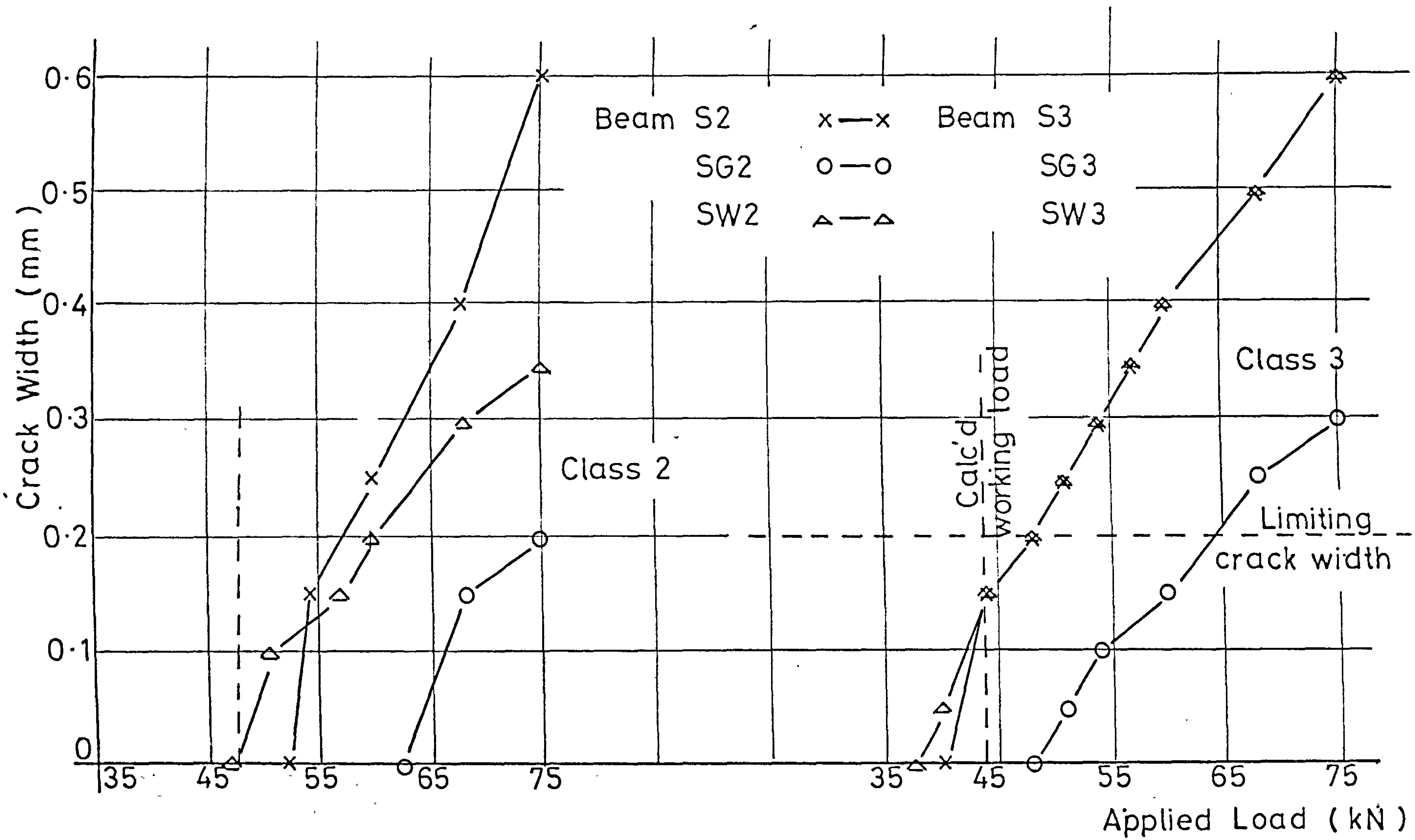

FIG. 7.38 CRACK WIDTH vs LOAD CURVES - SERIES S

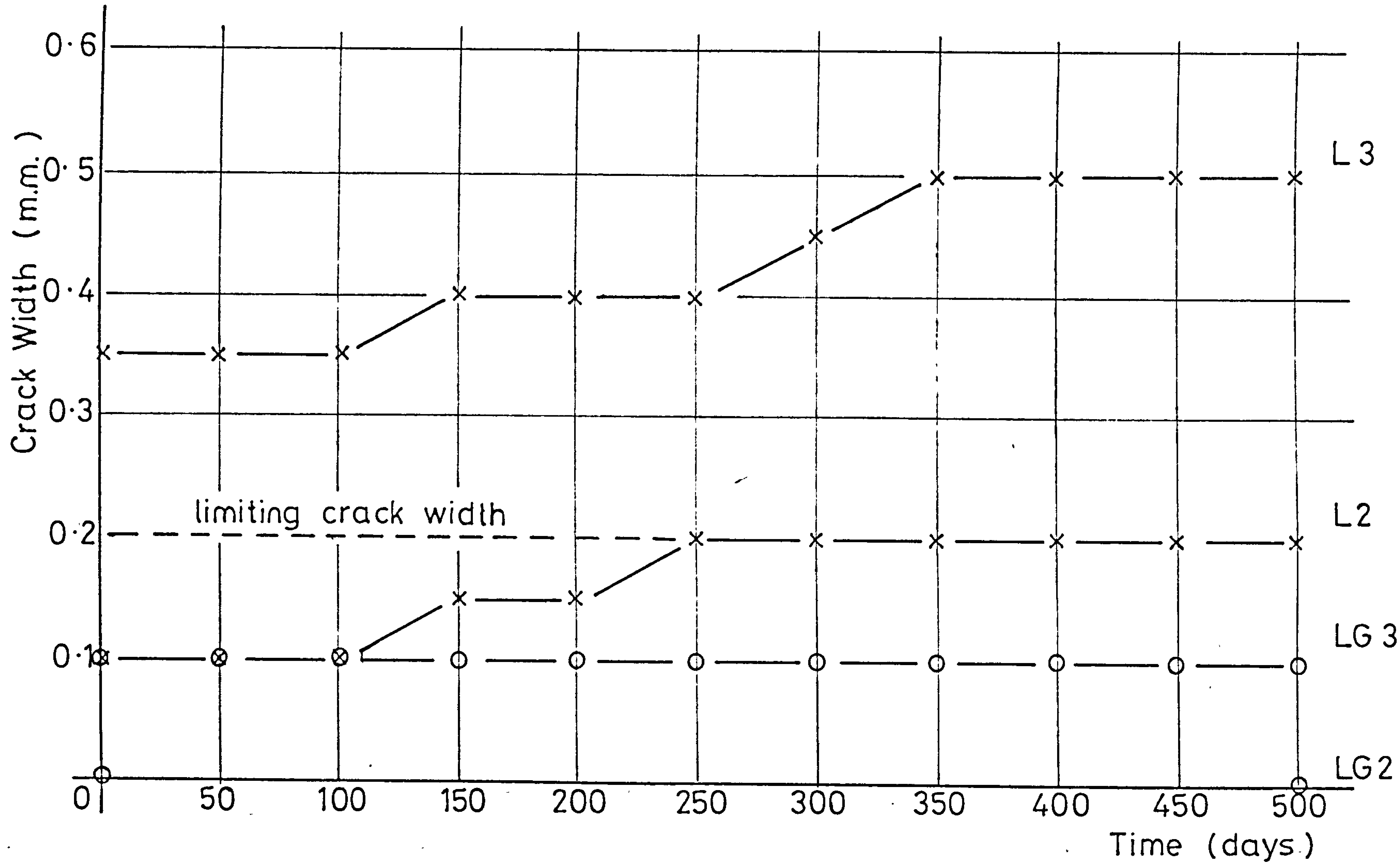

FIG. 7.39 CRACK WIDTH vs TIME CURVES – SERIES L

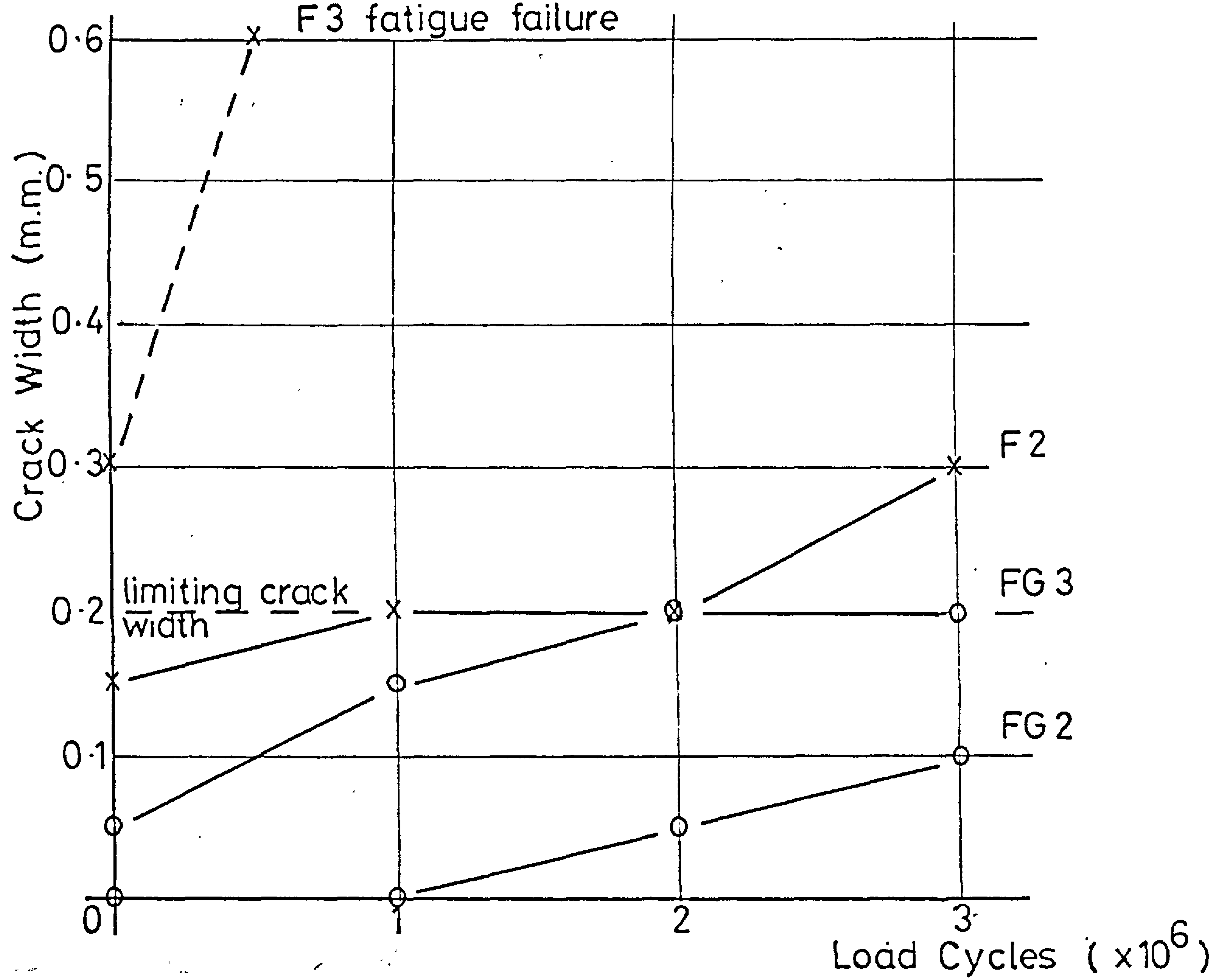

FIG. 7.40 CRACK WIDTH vs LOAD CYCLES – SERIES F

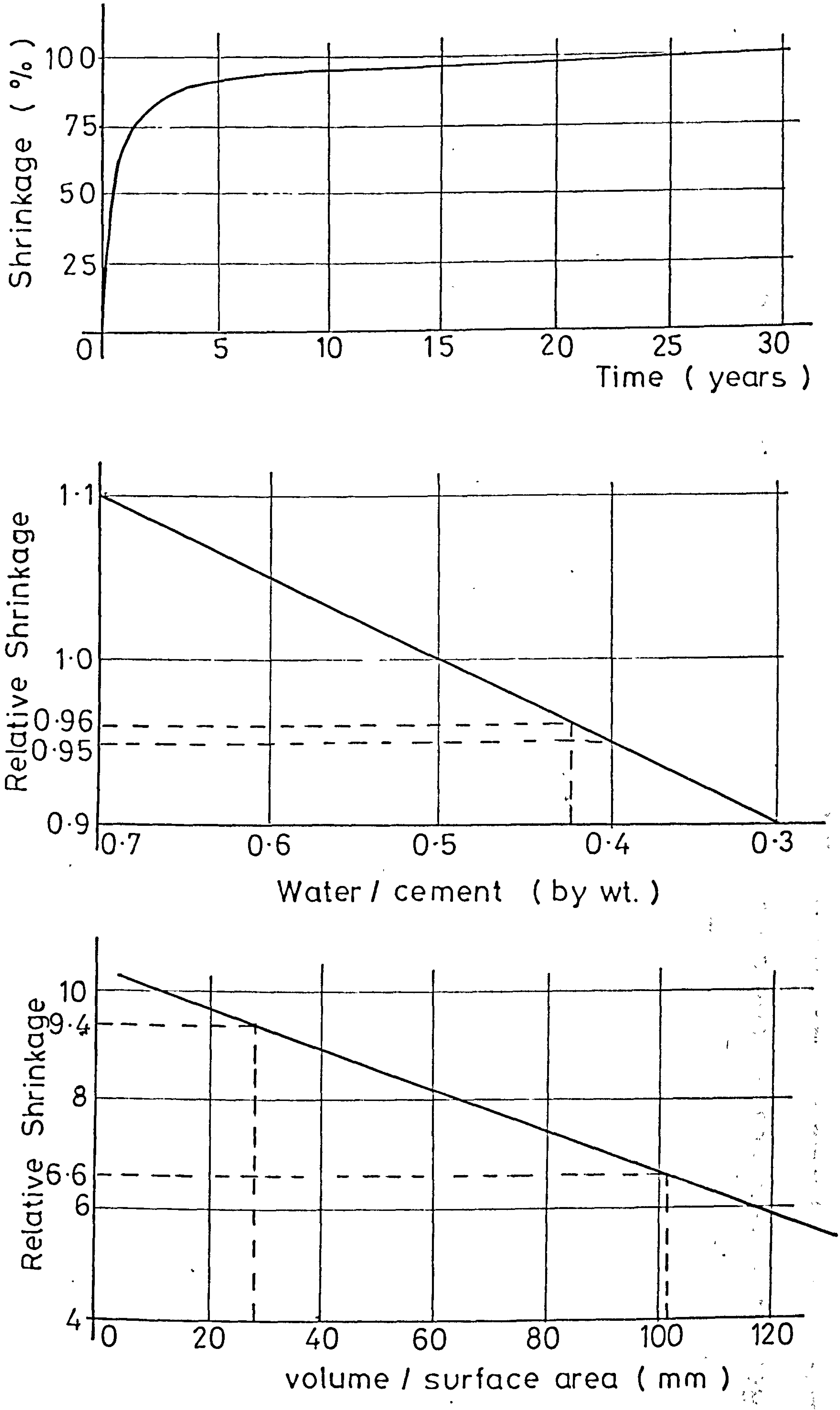

FIG. A.1. ESTIMATION OF SHRINKAGE

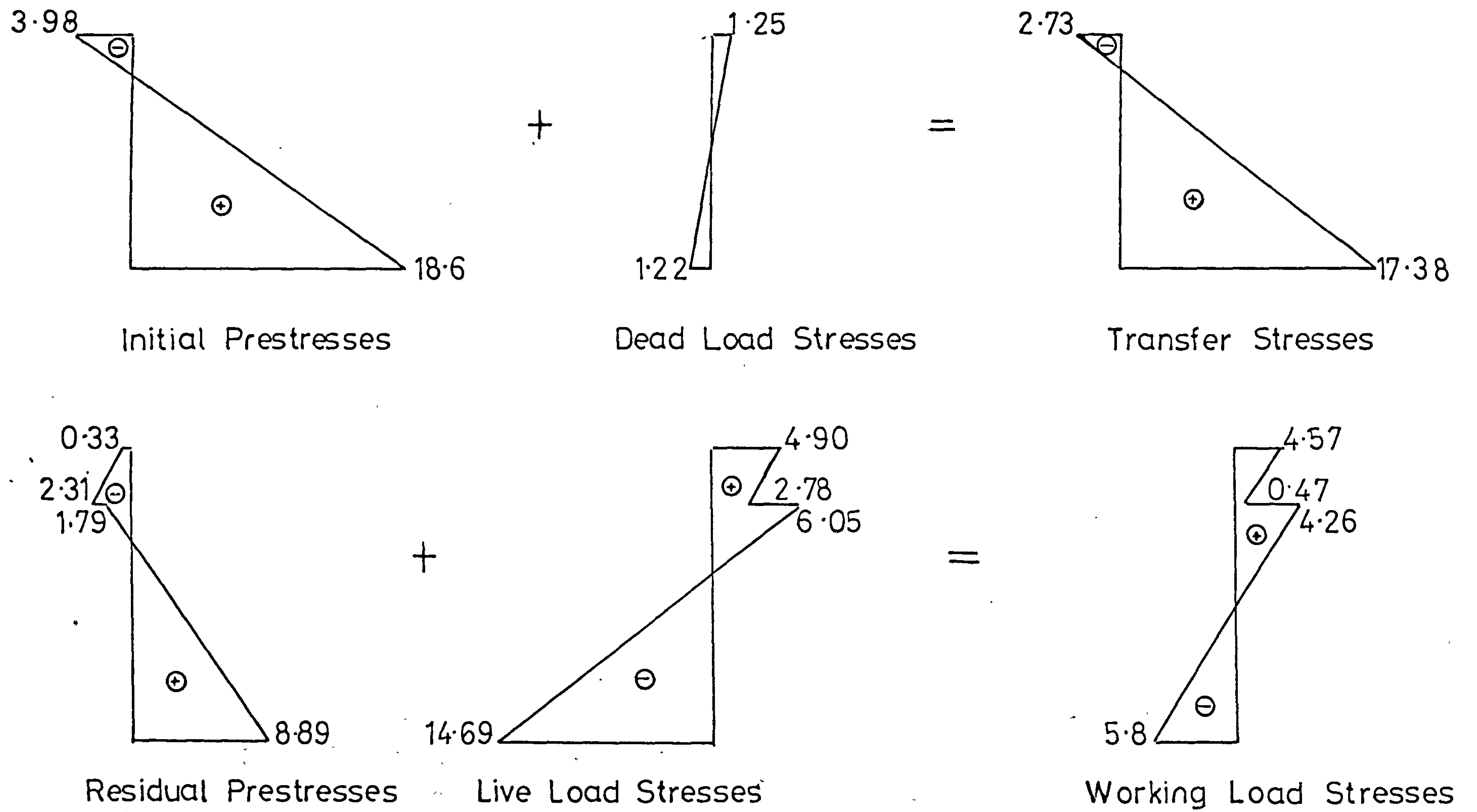

FIG. A.2. STRESS PROFILES — BEAM SG3 (N/mm^2)

A P P E N D I X

A.1. ESTIMATION OF THE SHRINKAGE OF THE PRECAST CONCRETE

In the following calculation, the method according to Evans and Kong (603) is assumed, given the following data:-

	Standard Beam	Test Beam
Mix	1:1:2/0.40	1:1:2/0.42
Cement	O.P.C.	R.H.P.C.
Volume/Surface Ratio	101.6mm.	28.4mm.
Relative Humidity	70%	63%
Temperature	60^{o}F	70^{o}F
Curing Period	30 years	22 days
Shrinkage	700 microstrain	S

The ultimate shrinkage of the standard beam exposed to the temperature and relative humidity given is 700 microstrain. The shrinkage, S, of the test beams is calculated taking into acount the effects of the following factors:-

(a) Effects of Curing Period

Figure A.1a. shows the increase in shrinkage with time for ordinary portland cement concretes under constant temperature and humidity conditions. The test beams were initially subjected to a curing period of six days under wet hesian and then a further curing period of 22 days before the insitu concrete flange was cast. It is also assumed that the length of the "wet" curing period has no effect on the magnitude of the shrinkage.

$\therefore$ the shrinkage, $S = 700 \times 0.36$ microstrain.

(b) <u>Effect of Relative Humidity</u>

Using the shrinkage at 70% relative humidity as the reference magnitude, shrinkage can be assumed to increase at the approximate rate of 2% for each per cent decrease in relative humidity and decrease at the rate of 3% for each per cent increase in relative humidity.

$$\therefore \text{ the shrinkage, } S = 700 \times \frac{100 + (70 - 63)2}{100}$$

$$= 700 \times 1.14 \text{ microstrain}$$

(c) <u>Effect of Temperature</u>

As an approximation, shrinkage can be assumed to increase or decrease at the rate of 0.5% for each one degree F. rise or fall in temperature relative to the reference temperature of 60^{o}F.

$$\therefore \text{ the shrinkage, } S = 700 \times \frac{100 + (70 - 60)0.5}{100}$$

$$= 700 \times 1.05 \text{ microstrain}$$

(d) <u>Effect of Cement Paste Content</u>

The cement paste content by volume generally lies within the range 28 to 40%. Within this range, shrinkage can be assumed to increase at the approximate rate of 7% for each per cent increase in the cement paste content by volume. Taking the specific gravity of cements to B.S. 12 as 3.15 and that of aggregates to B.S. 882 as 2.6, the cement paste content of the standard mix is 38.5% and that of the test beam is 39%.

$\therefore$ the shrinkage, $S = 700 \times \frac{100 + (39.0 - 38.5)7}{100}$

$= 700 \times 1.035$ microstrain

(e) Effect of Water/Cement Ratio

The approximate effect of the water/cement ratio on the shrinkage of cement for a given cement paste is given in figure A.1b.

$\therefore$ the shrinkage, $S = 700 \times \frac{0.96}{0.95}$ microstrain

(f) Effects of Types of Cement

For concretes of the same mix proportions but made of different types of cement, the ratio of the shrinkage of O.P.C. to R.H.P.C. to H.A.C. will be 1:1.1:1.

$\therefore$ the shrinkage, $S = 700 \times \frac{1.1}{1.0}$ microstrain

(g) Effects of Size and Shape of Concrete Member

Shrinkage varies inversely with the ratio of the volume to the surface area of a concrete member as shown in figure A.1c., i.e. for a given volume/surface ratio, shrinkage is the same irrespective of the shape of the member

$\therefore$ the shrinkage, $S = 700 \times \frac{9.4}{6.6}$ microstrain

Hence, combining the effects of all the above factors, the actual shrinkage of the test beams is given by:-

$$S = 700 \times 0.36 \times 1.14 \times 1.05 \times 1.035 \times \frac{0.96}{0.95} \times \frac{1.1}{1.0} \times \frac{9.4}{6.6}$$

$\therefore S = 500$ microstrain

A.2. DETERMINATION OF THE "CALCULATED" WORKING LOADS FOR THE VARIOUS LIMIT STATES

A.2.1. Limit State of Collapse

From the rectangular parabolic stress block given in figure 3.1. :-

$$C_c = \frac{2U_w}{3\gamma_m}\left(b.x - A_{sc} - \frac{b.x}{3} \cdot \frac{\sqrt{U_f}}{17.5}\right)$$

$$C_s = 0.0035\ A_{sc} \cdot E_{sc}\left(\frac{x - d_{sc}}{x}\right)$$

$$\beta = 1 - \alpha$$

$$\alpha = \frac{0.33 - 0.0001814\ U_f}{0.67 - 0.0127\sqrt{U_f}}$$

$$T_{su} = A_{su} \cdot f_{su}$$

$$T_{st} = A_{st} \cdot f_{st}$$

For beam SG3, the sectional and material properties were:-

U_t	=	$47.0\ N/mm^2$	U_w	=	$59.8\ N/mm^2$
U_f	=	$41.0\ N/mm^2$	γ_m	=	1.0
b	=	610 mm.	D_{sc}	=	20 mm.
A_{su}	=	$115.5\ mm^2$	A_{st}	=	$154.0\ mm^2$
A_{sc}	=	$235.5\ mm^2$	l	=	4.725 m.
E_{sc}	=	$207.0\ kN/mm^2$	E_{st}	=	$207.9\ kN/mm^2$

$$\therefore C_c = 14.64\ x - 6.44\ kN$$

$$C_s = 170.62\ \frac{(x - 20)}{x}\ kN$$

$$\alpha = 0.548$$

$$\beta = 0.452$$

Equating the compressive and tensile forces acting on the section, a trial and error process gives a value of $x = 26.6$mm. Hence:-

$$C = C_c + C_s = 383.0 + 42.3 \text{ kN}$$

$$C = 425.3 \text{ kN}$$

$$T = T_{su} + T_{st} = 181.2 + 245.4 \text{ kN}$$

$$T = 426.6 \text{ kN}$$

Compressive moment of resistance, M_{rc}, is given by:-

$$M_{rc} = C_c\,(d - \beta x) + C_s\,(d - d_{sc})$$

$$= 90.23 \text{ kNm}$$

$\therefore$ Ultimate moment of resistance, $M_u = 90.23$ kNm

Ultimate load, $W_u = \dfrac{6.M_u}{1} = 1.27\ M_u = 114.6$ kN

For beam SG3, dead load moment, $M_d = 3.12$ kNm

Working Load Moment, $M_1 = \dfrac{M_u - 1.4M_d}{1.6} = 53.66$ kNm

$\therefore$ Allowable working load, $W_1 = 1.27\ M_1 = \underline{68.2 \text{ kN}}$

A.2.2. Limit State of Local Damage

The limiting conditions are:-

(a) At Transfer: the concrete stresses must not exceed the allowable values under the deadload and the prestressing force.

Allowable compressive stress = $0.5U_t$ = 23.50N/mm^2

Allowable tensile stress = 3.2N/mm^2

(b) At Working Load: the concrete stresses must not exceed the allowable values under the dead and live loads and the prestressing force (after losses)

Allowable compressive stress = $0.33U_w$ = $19.73 N/mm^2$

Allowable tensile stress = $5.8 N/mm^2$ (Class 3)

Now, beam SG3 satisfies condition (a), figure A.2. and to satisfy condition (b), the allowable live load tensile stress = 8.89 + 5.8 = 14.69 N/mm^2

Working load moment, $M_1 = Z_1 \times f_1 = 2.267 \times 10^6 \times 14.69$

$= 33.21$ kNm

.˙. Allowable working load, $W_1 = 1.27M_1$ = 42.2kN

Best Copy Available

Variable Print Quality

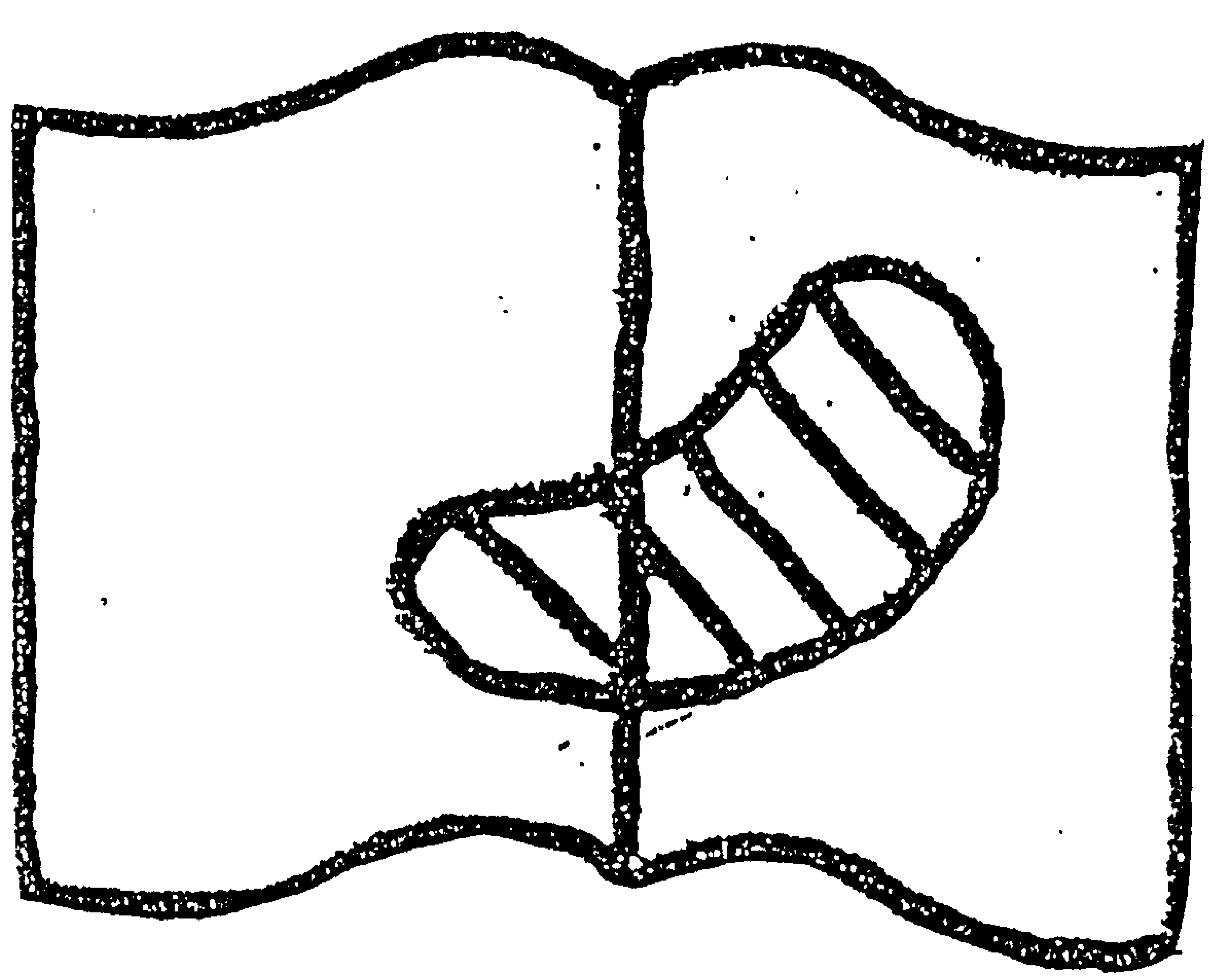

PLATE 1.1. - NORMAL WEIGHT AND LIGHTWEIGHT AGGREGATES

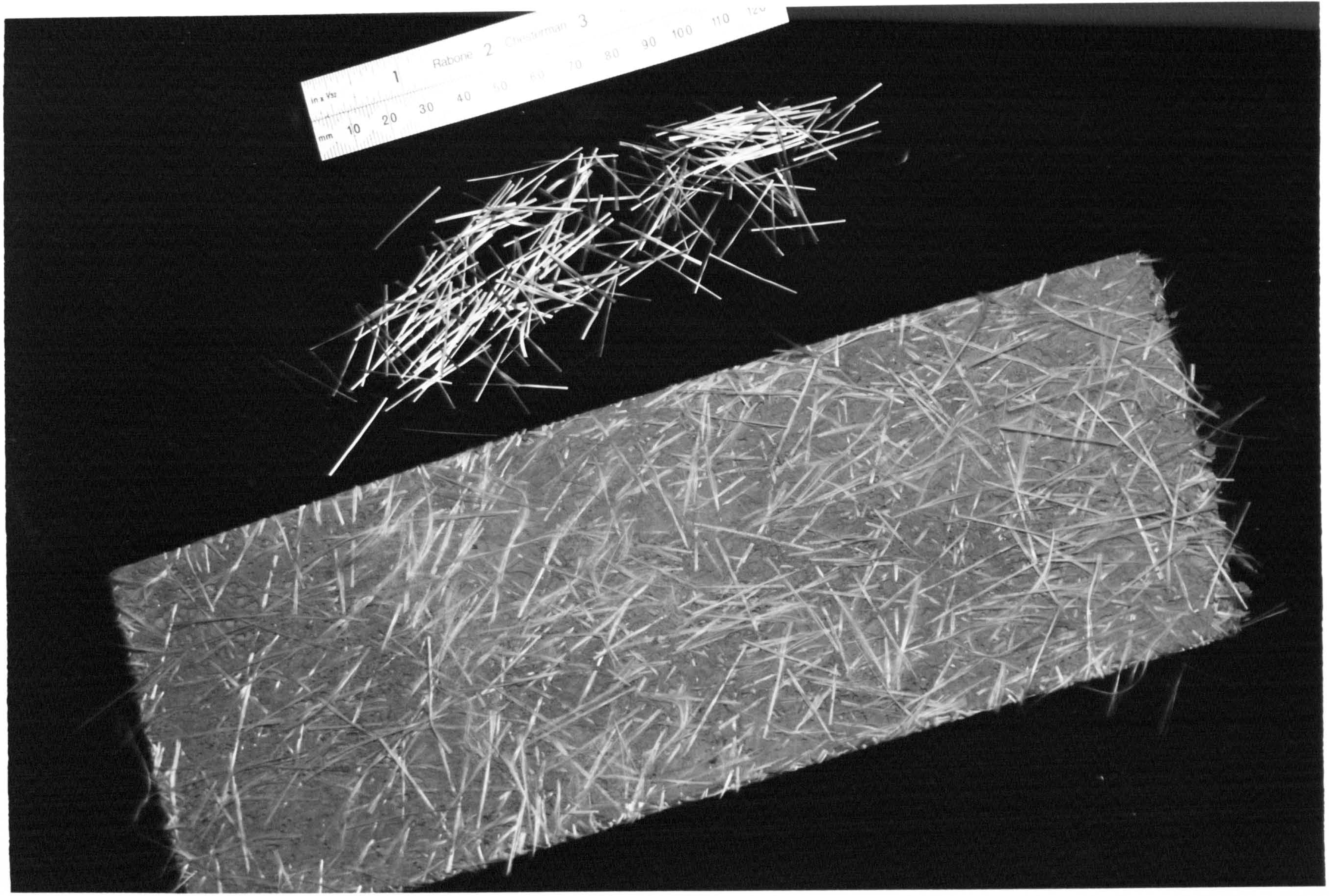

PLATE 1.2. - ALKALI-RESISTANT GLASS FIBRES

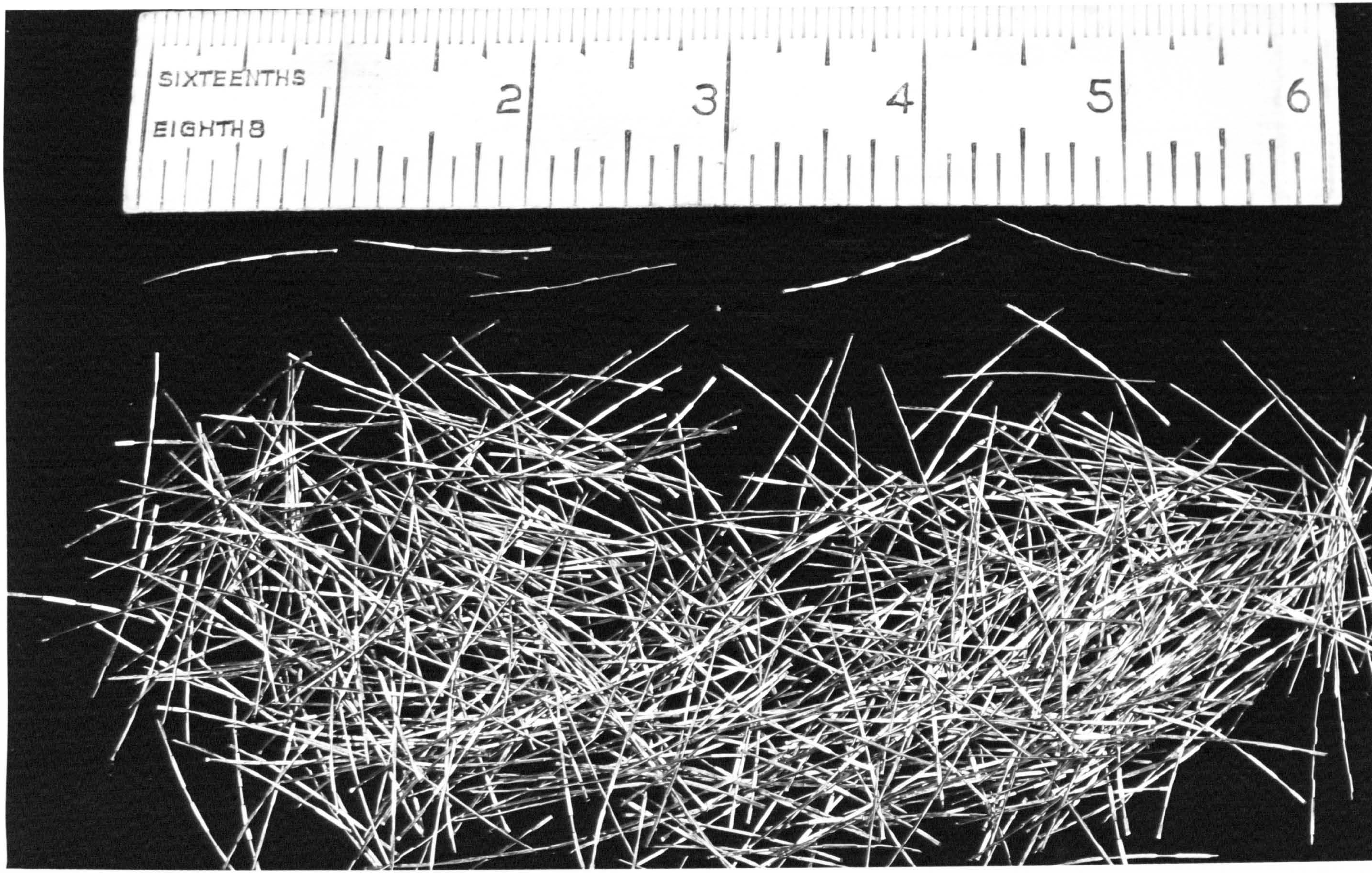

PLATE 1.3. - STEEL FIBRES

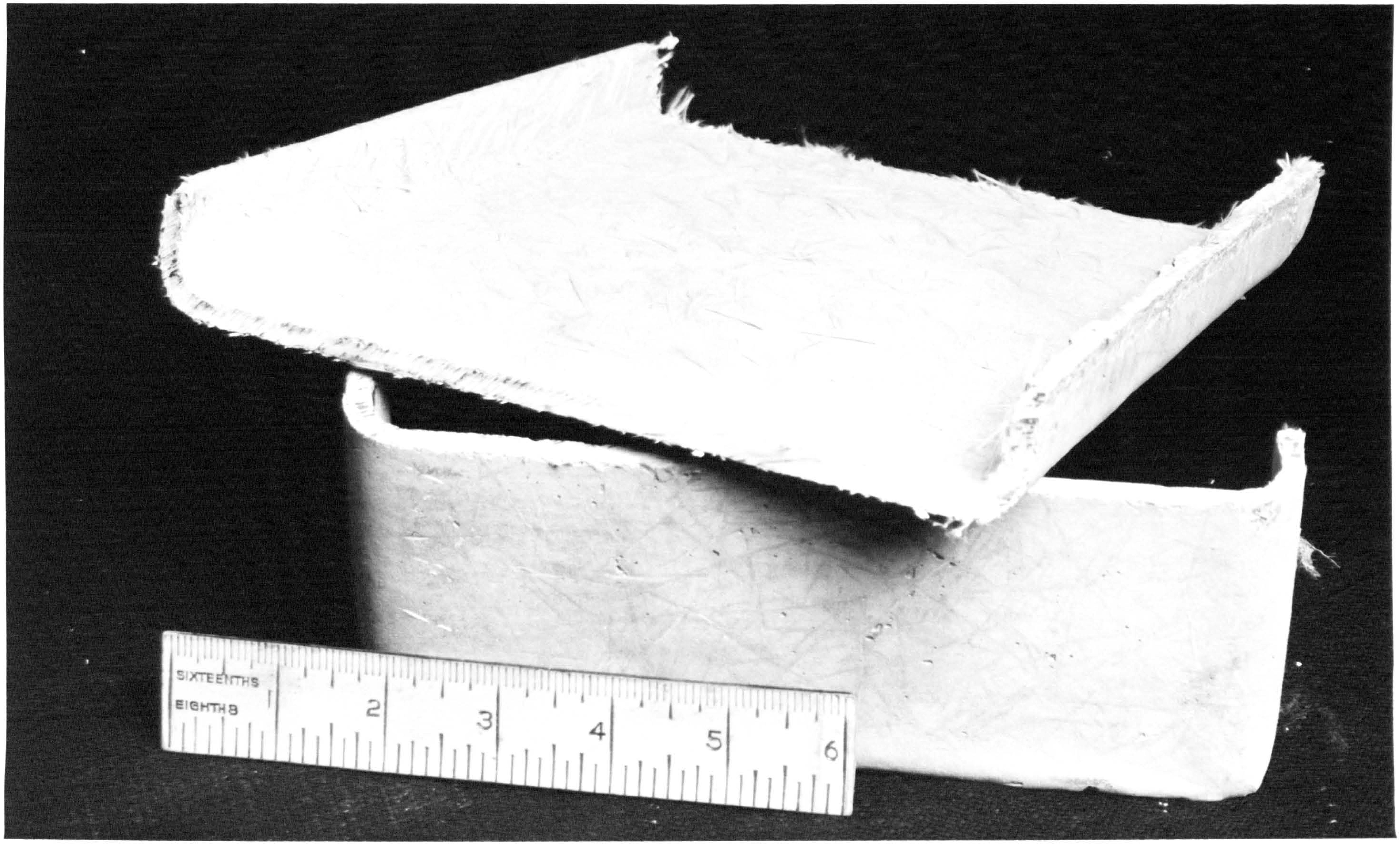

PLATE 1.4. - ALKALI-RESISTANT GLASS FIBRE REINFORCED CEMENT CHANNEL

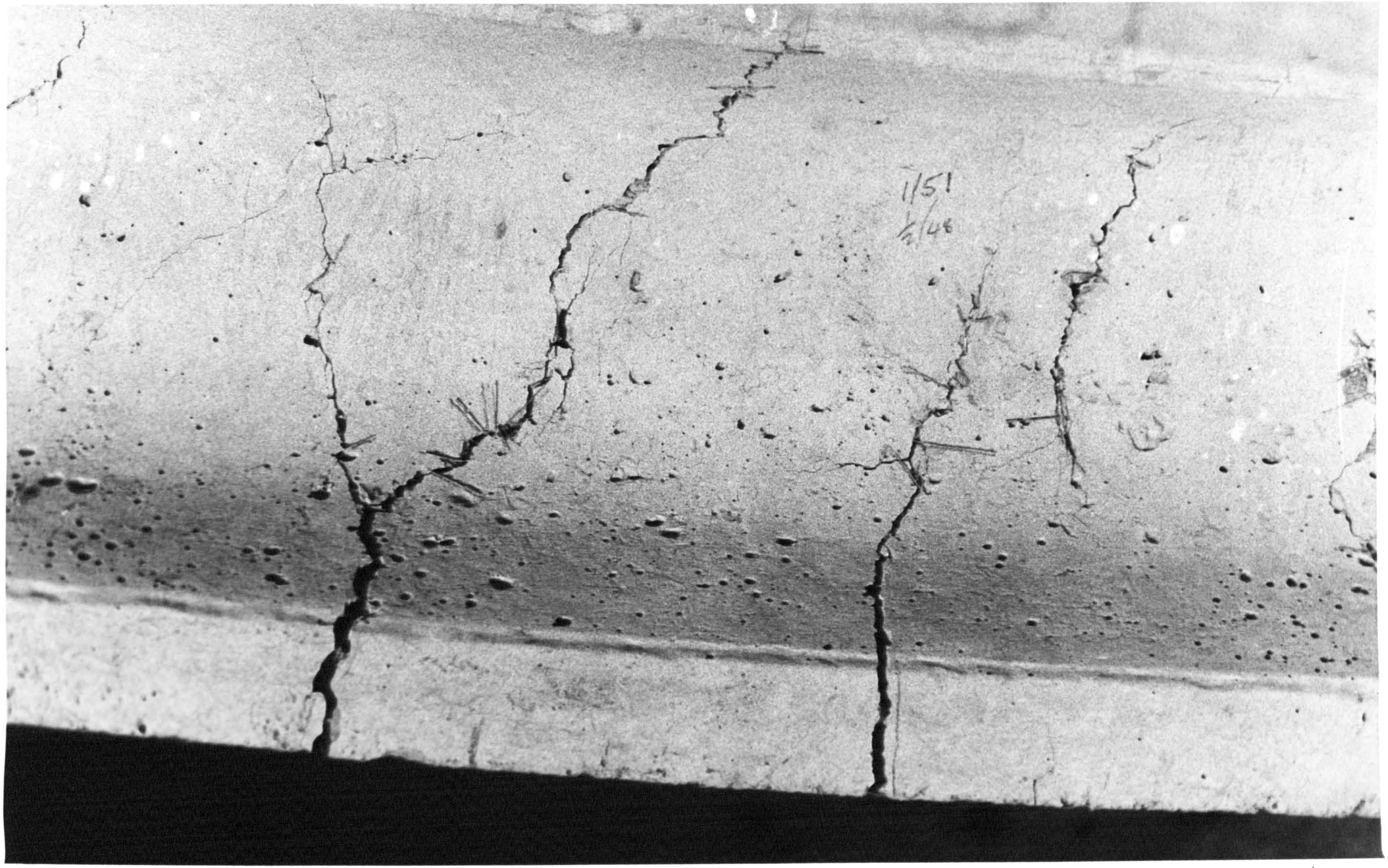

PLATE 4.1. - FIBRE "BRIDGES" ACROSS CRACKS

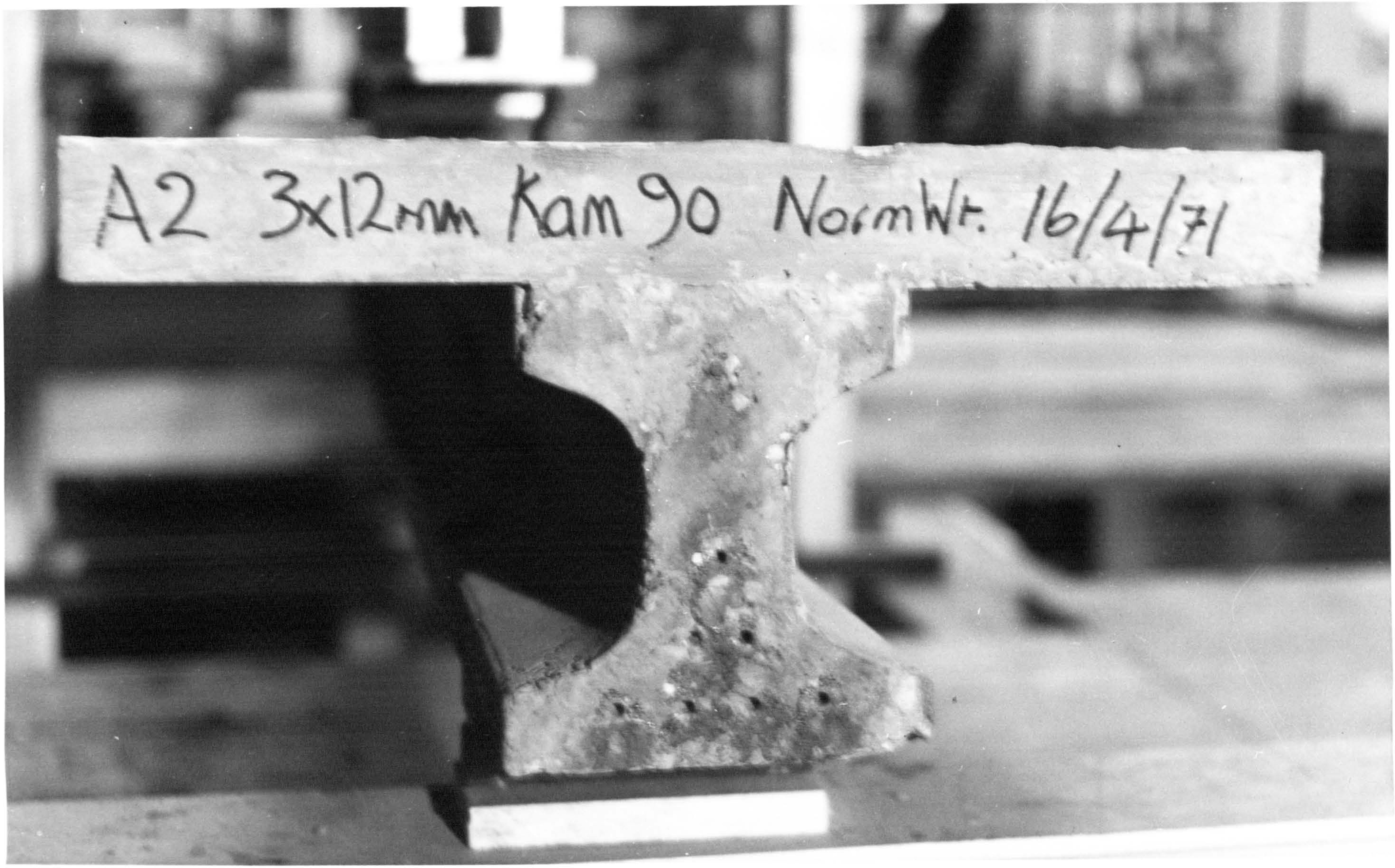

PLATE 5.1. - BOND FAILURE - SERIES X

PLATE 5.2. - SHEAR FAILURE - SERIES X

PLATE 5.3. - INTERFACE BOND FAILURE - SERIES X

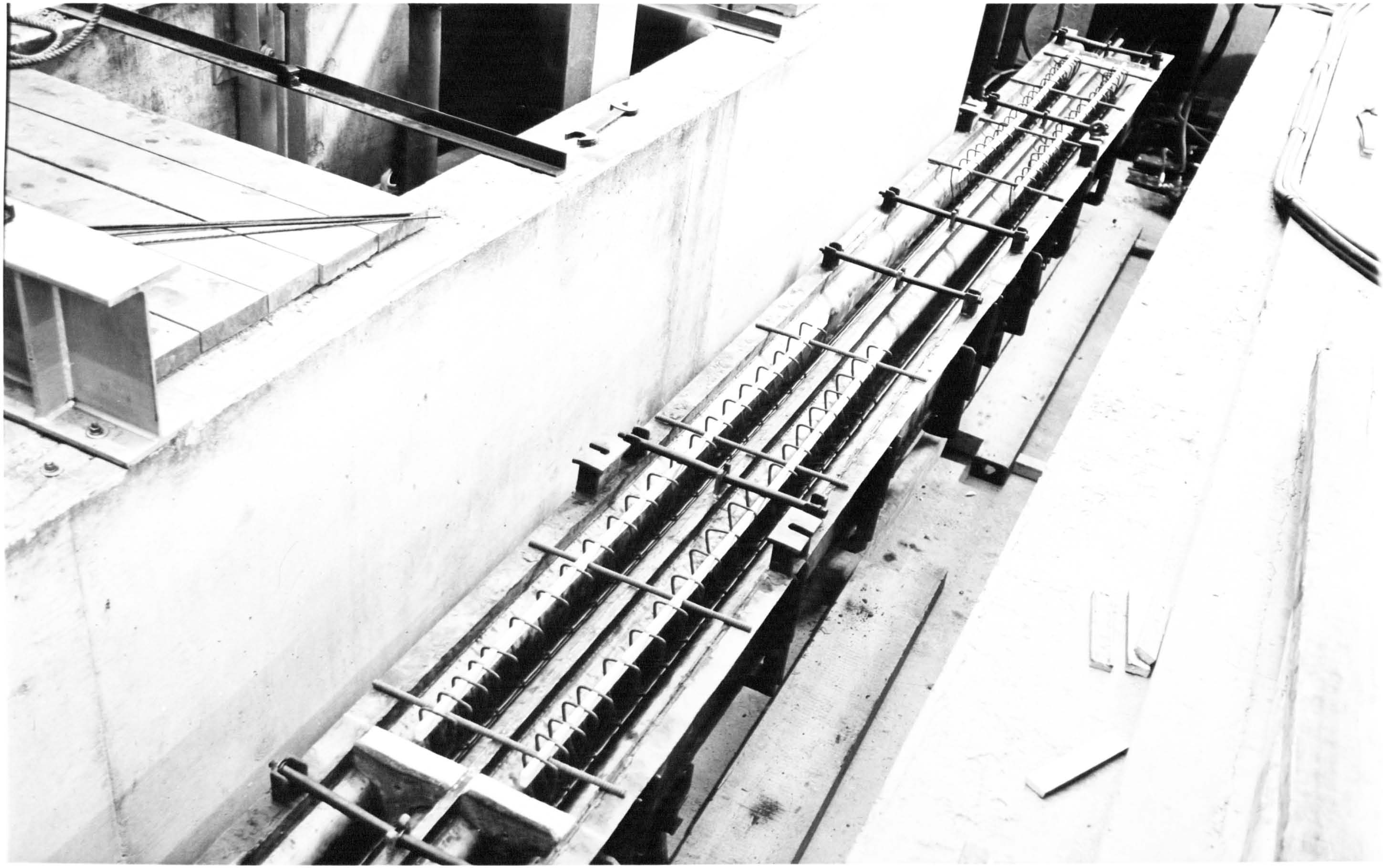

PLATE 5.4. - PRESTRESSINC MOULD

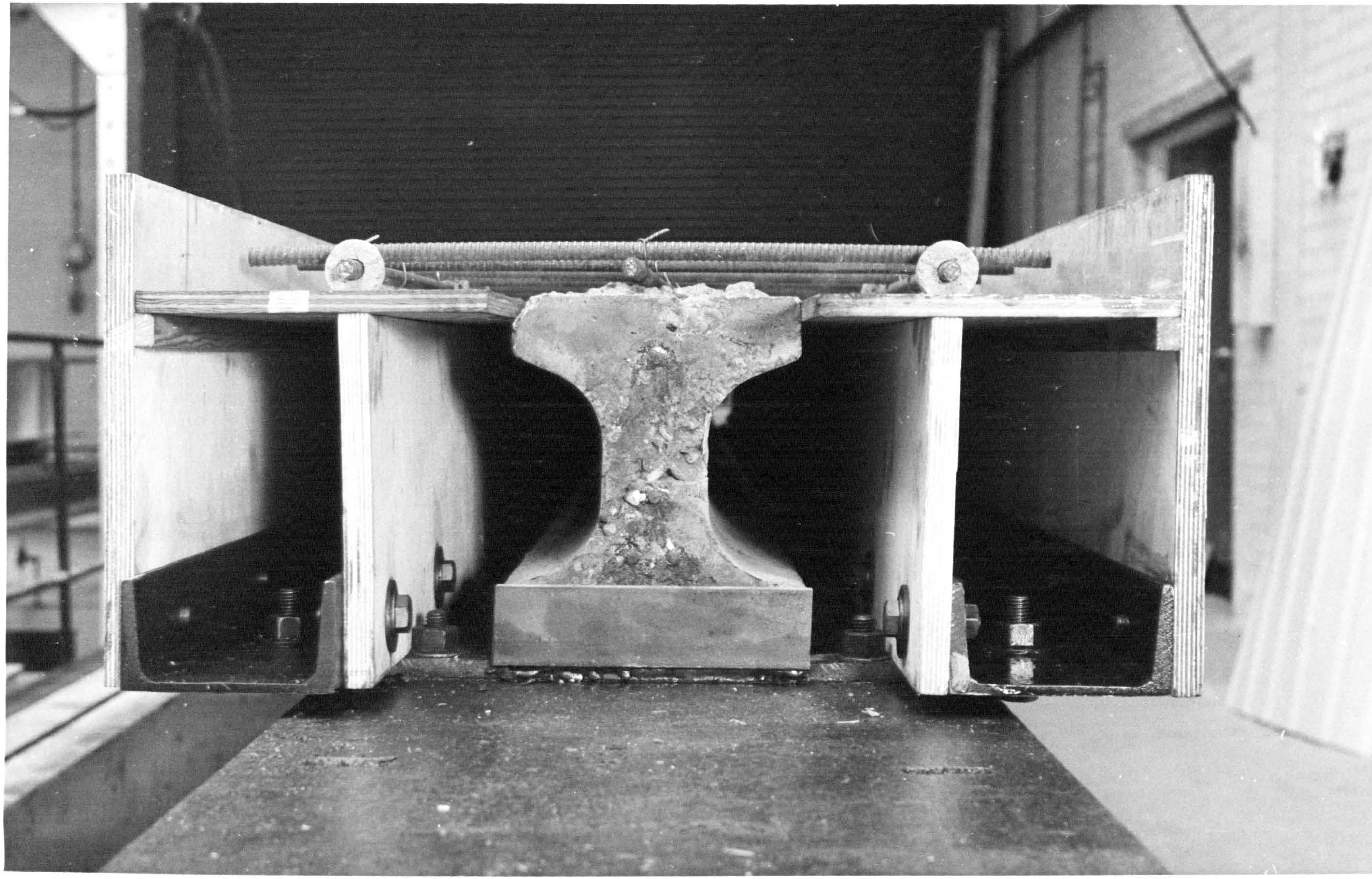

PLATE [illegible] - INSITU FLANGE MOULD

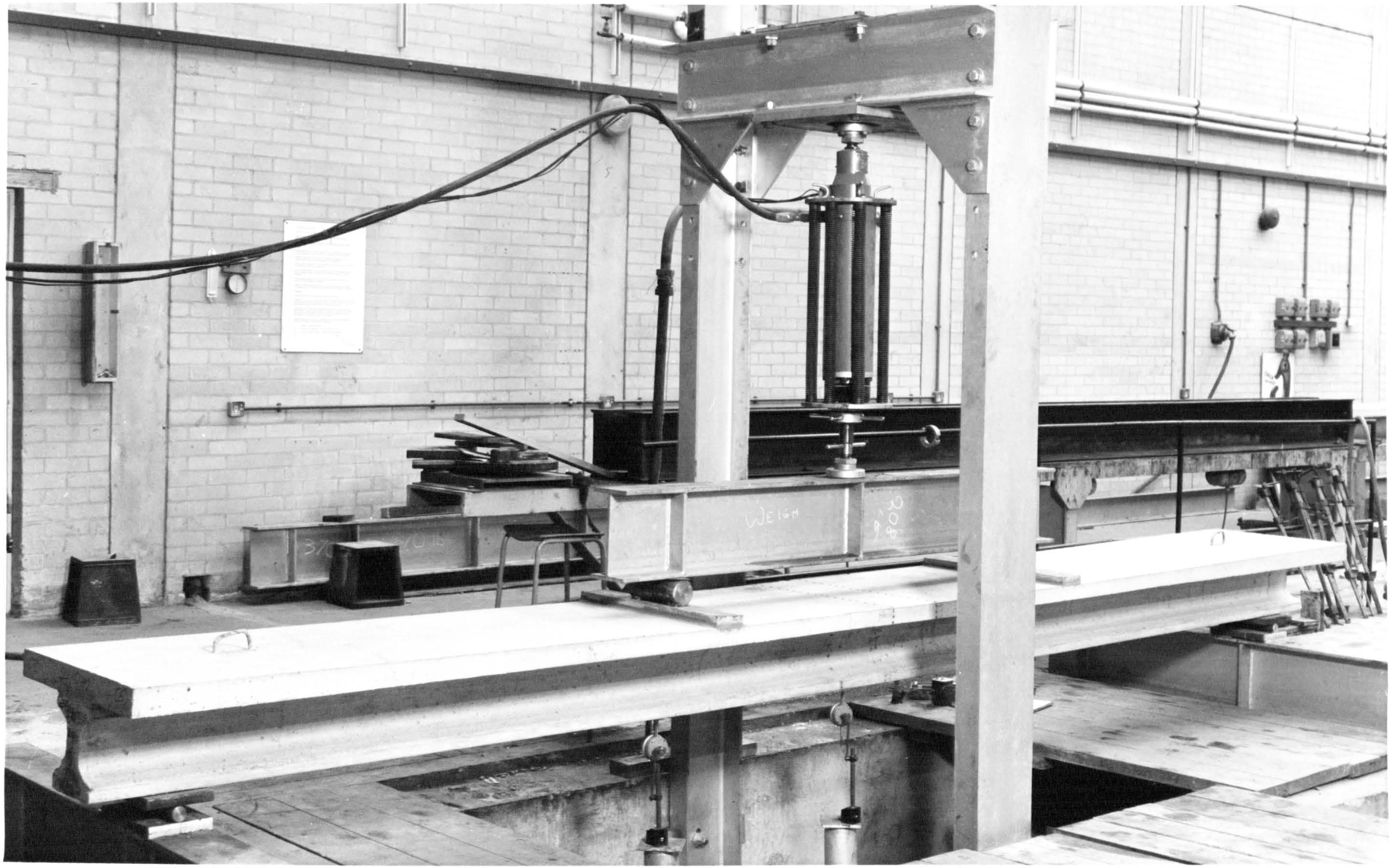

PLATE 5.6. - LOADING ARRANGEMENTS FOR SHORT TERM AND FATIGUE TESTS

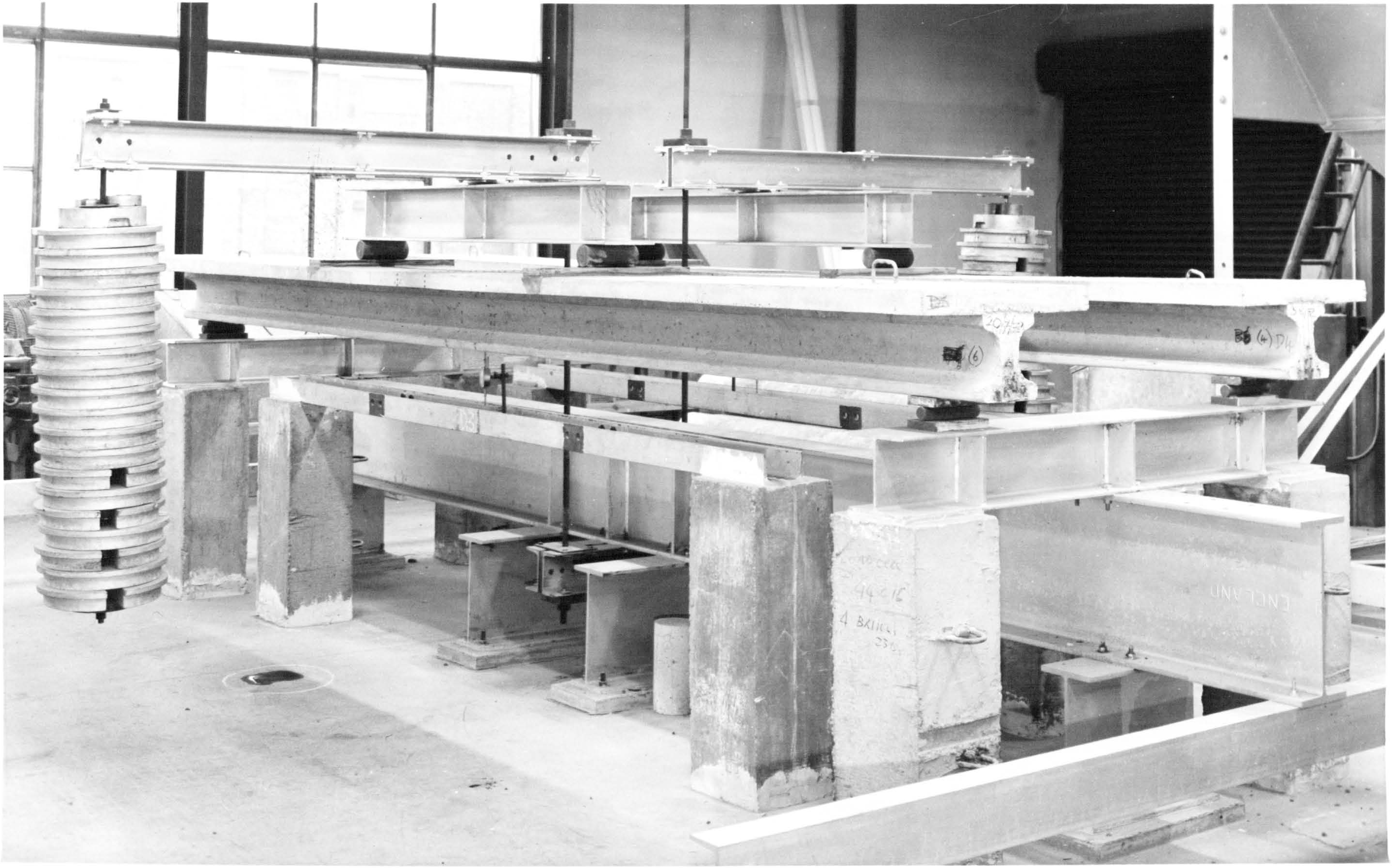

PLATE 5.7. - LOADING ARRANGEMENT FOR LONG TERM TESTS

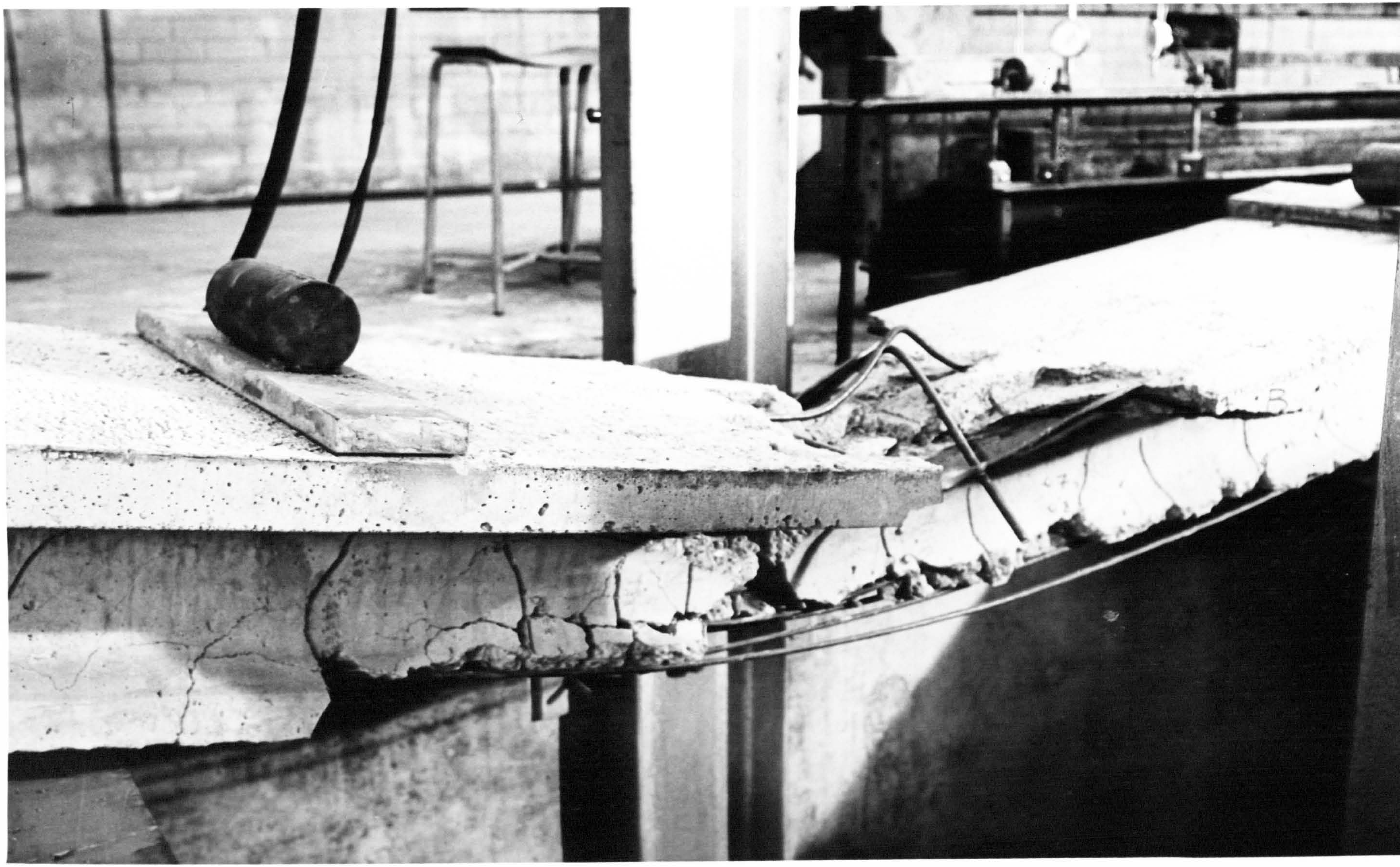

PLATE 7.1. - TYPICAL FAILURE FOR CONVENTIONAL CONCRETE COMPOSITE T-BEAM

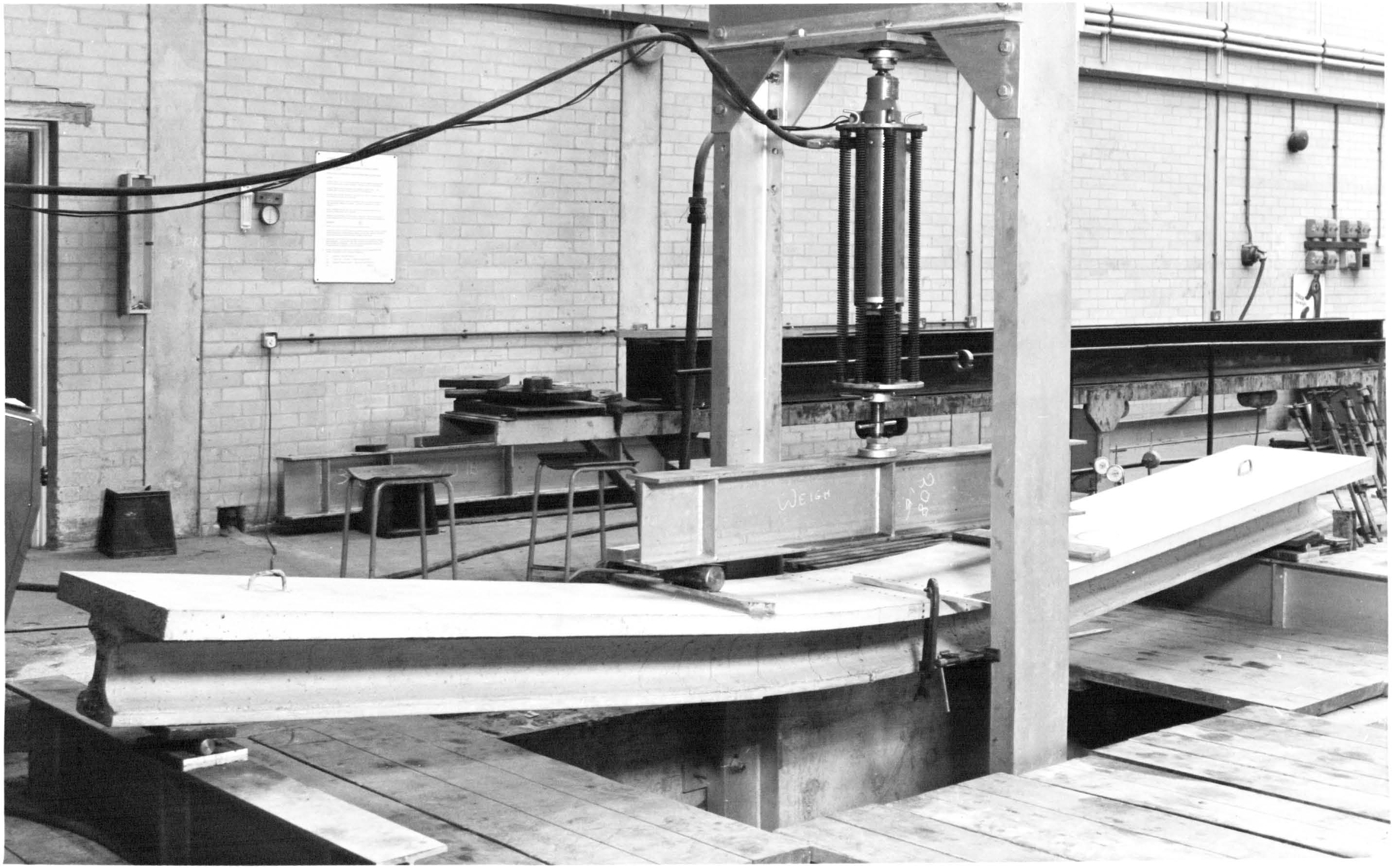

PLATE 7.2. - TYPICAL FAILURE OF FIBROUS-CEMENT CHANNEL

PLATE 7.5. - CLOSE-UP OF FIBROUS-CEMENT CHANNEL AT FAILURE